FROM SMALL MOLECULES TO NANO-SCALE ARCHITECTURES - A SUPRAMOLECULAR APPROACH

by

BENJAMIN M. T. SCOTT

B.S., The Nottingham Trent University, 2003

AN ABSTRACT OF A DISSERTATION

submitted in partial fulfillment of the requirements for the degree

DOCTOR OF PHILOSOPHY

Department Of Chemistry
College of Arts and Sciences

KANSAS STATE UNIVERSITY
Manhattan, Kansas

2008

Abstract

We have shown that supramolecular synthons can be used to construct discrete two or three component co-crystals and 1-D inorganic-organic chains and dramatically influence the arrangement of nanoparticle assemblies.

A collection of supramolecular reagents (SR's) have been designed and synthesised to carry out a systematic study into hydrogen bonding. In order to test Etter's guideline *"the best proton donor and acceptor remaining after intramolecular hydrogen-bond formation will form an intermolecular hydrogen-bond"* and to develop a hierarchy of interactions, a series of co-crystals between the supramolecular reagents and hydrogen-bond donors (carboxylic acids) have been synthesised.

Co-crystals with pyrazole benzamide SR's have demonstrated the ability to fine-tune hydrogen-bond formation. By utilising a poor hydrogen-bond acceptor (pyrazole) the incoming carboxylic acid opts to form a heteromeric acid-amide dimer via N-H•••O hydrogen bonds. Additionally, we have shown that the hydrogen-bond acceptor strength of the pyrazole can be turned up through simple covalent modifications (i.e. isomer change or addition of methyl groups to the pyrazole ring). Although the heteromeric acid-amide dimer is observed, O-H•••N hydrogen bonds to the pyrazole are also observed in cases when more than one donor site is present (i.e. di-carboxylic acids and 4-hydroxybenzoic acid).

Furthermore, co-crystals with picolyl-indazole and pyrimidine-pyrazole SR's agree with Etter's guideline. In all cases, the incoming carboxylic acid forms an O-H•••N hydrogen bond to the best acceptor (pyridine and pyrazole, respectively).

The homomeric amide-amide dimer has been used to construct inorganic-organic hybrid materials. The reaction between the pyrazole benzamide ligands with *acac* or "paddle-wheel" complex ions yielded 1-D chains. Furthermore, pyrimidine-bispyrazole and functionalised 1,3-bisbenzylpyrazole ligands have been utilised as chelating-ligands for reliable metal coordination.

Finally, the power of supramolecular synthons to control the arrangement of much larger nanoparticle assemblies has been shown. Both homomeric (acid-acid, alcohol-alcohol) and heteromeric (acid-imidazole, alcohol-imidazole) hydrogen bonding cause significant changes in nanoparticle assemblies.

FROM SMALL MOLECULES TO NANO-SCALE ARCHITECTURES - A SUPRAMOLECULAR APPROACH

by

BENJAMIN M. T. SCOTT

B.S., The Nottingham Trent University, 2003

A DISSERTATION

submitted in partial fulfillment of the requirements for the degree

DOCTOR OF PHILOSOPHY

Department of Chemistry
College of Arts And Sciences

KANSAS STATE UNIVERSITY
Manhattan, Kansas

2008

Approved by:

Major Professor
Christer B. Aakeröy

Abstract

We have shown that supramolecular synthons can be used to construct discrete two or three component co-crystals and 1-D inorganic-organic chains and dramatically influence the arrangement of nanoparticle assemblies.

A collection of supramolecular reagents (SR's) have been designed and synthesised to carry out a systematic study into hydrogen bonding. In order to test Etter's guideline *"the best proton donor and acceptor remaining after intramolecular hydrogen-bond formation will form an intermolecular hydrogen-bond"* and to develop a hierarchy of interactions, a series of co-crystals between the supramolecular reagents and hydrogen-bond donors (carboxylic acids) have been synthesised.

Co-crystals with pyrazole benzamide SR's have demonstrated the ability to fine-tune hydrogen-bond formation. By utilising a poor hydrogen-bond acceptor (pyrazole) the incoming carboxylic acid opts to form a heteromeric acid-amide dimer via N-H•••O hydrogen bonds. Additionally, we have shown that the hydrogen-bond acceptor strength of the pyrazole can be turned up through simple covalent modifications (i.e. isomer change or addition of methyl groups to the pyrazole ring). Although the heteromeric acid-amide dimer is observed, O-H•••N hydrogen bonds to the pyrazole are also observed in cases when more than one donor site is present (i.e. di-carboxylic acids and 4-hydroxybenzoic acid).

Furthermore, co-crystals with picolyl-indazole and pyrimidine-pyrazole SR's agree with Etter's guideline. In all cases, the incoming carboxylic acid forms an O-H•••N hydrogen bond to the best acceptor (pyridine and pyrazole, respectively).

The homomeric amide-amide dimer has been used to construct inorganic-organic hybrid materials. The reaction between the pyrazole benzamide ligands with *acac* or "paddle-wheel" complex ions yielded 1-D chains. Furthermore, pyrimidine-bispyrazole and functionalised 1,3-bisbenzylpyrazole ligands have been utilised as chelating-ligands for reliable metal coordination.

Finally, the power of supramolecular synthons to control the arrangement of much larger nanoparticle assemblies has been shown. Both homomeric (acid-acid, alcohol-alcohol) and heteromeric (acid-imidazole, alcohol-imidazole) hydrogen bonding cause significant changes in nanoparticle assemblies.

Table of Contents

List of Figures

List of Tables

Acknowledgements

I would like to thank my advisor Christer Aakeröy for all of his support and guidance over the past five years. I have developed both as a person and as a chemist during my time in his research group and credit must go to Christer. I couldn't have asked for a better advisor.

To the members of the Aakeröy research group, both past and present, for all the helpful advice and discussions. A special thanks to Michelle for keeping the lab an entertaining and enjoyable place to work!

I would also like to thank my committee members, Professors Eric Maatta, Paul Smith, John Tomich and David Ben-Arieh for all of their input toward writing this dissertation as well as for being so accommodating with scheduling of the final defense.

To all of my friends at Kansas State who have made my time here so memorable. I especially want to thank Jamie for being such a good friend and roommate. We have had some great times over the past five years. I also want to thank the "Brits" (Jamie, Michelle, Kris, Dipesh and Alex) for understanding the importance of a good pint!

Thanks to the various people in the department for their assistance, especially, Jim Hodgson, Tobe Eggers, Richard Bachamp, Earline Dikeman, Connie Cusimano and Kim Ross.

To Professors Ken Klabunde, Chris Sorensen, Amit Chakrabarti and Bruce Law. The input and advice you have offered regarding nanoparticle research has been invaluable and for that I thank you all.

Thanks must also go to Dr. John Desper for solving the single crystal X-ray structures, without which, most of the results in this dissertation would not have been possible, Dan Boyle for his help with TEM and Yasuaki Hiromasa for MS data.

To Mum, Dad and Peter, I couldn't have done this without your love and encouragement. I love you all and greatly appreciate everything you have done for me during my time at Kansas State.

I would also like to thank my grandmothers, aunts and uncles for all of your support over the past five years.

Finally, Jade. Your love and support over the past year has motivated me so much and for that, I am truly thankful. I love you.

Dedication

To George and Thomas

Preface

Research carried out at Kansas State University under the guidance of Christer B. Aakeröy has led to the following publications:

C. B. Aakeröy, J. Desper and B. M. T. Scott, *Chem. Commun.*, 2006, 1445.

C. B. Aakeröy, B. M. T. Scott and J. Desper, *New. J. Chem*., 2007, **31**, 2044.

CHAPTER 1 - Introduction

1.1 Supramolecular Chemistry

Supramolecular chemistry is described as *"chemistry beyond the molecule",*[1] and *supramolecular synthesis* focuses on the bringing together of molecules without making or breaking covalent bonds to form more complex species (*supermolecules*) via non-covalent interactions (e.g. hydrogen bonds, halogen bonds, van der Waals interactions and coordination bonds).

The ability to bring two (or more) molecules (*supramolecular reagents*) together via intermolecular interactions to form a supermolecule (a distinct entity independent of the individual components), is an important goal of supramolecular chemistry.

Furthermore, supramolecular chemistry strives to achieve effective control (based upon molecular recognition[1] and self-assembly[1]) over intermolecular interactions, which govern the formation of supermolecules, just like the synthetic chemist has control over the covalent bond.

1.1.1 *Molecular recognition*

Molecular recognition is defined as *"the energy and information involved in binding (with a purpose) and selection of substrate by a receptor (ligands with a purpose)".*[1]

In order to understand the concept of molecular recognition one can look to Nature, the most efficient synthetic chemist, which utilises molecular recognition within most biological systems.

A good example of natural molecular recognition is the interaction between a substrate and the receptor (active site) of an enzyme, Fig 1.1.

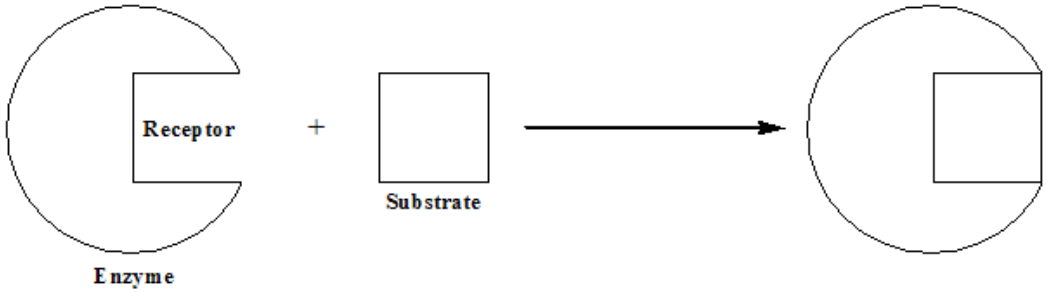

Figure 1.1 Representation of the interaction between a substrate and receptor of an enzyme.

From a more "general" point of view, molecular recognition can be considered as the *selective* binding (via non-covalent interactions) of two (or more) building blocks based on complementarity and binding strength, Figure 1.2.

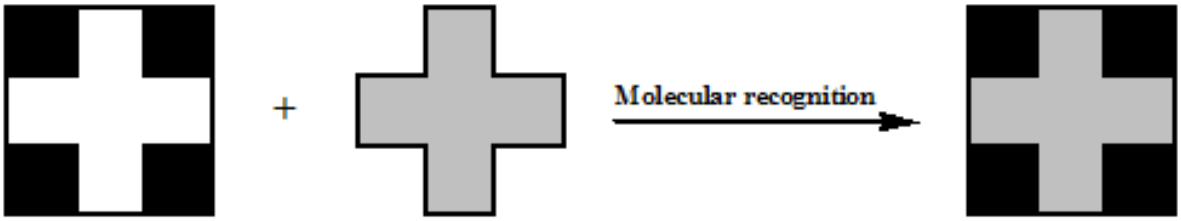

Figure 1.2 General representation of molecular recognition.

1.1.2 *Self-assembly*

Self-assembly or more specifically supramolecular self-assembly can be defined as *"recognition-directed spontaneous association of molecular components via non-covalent interactions to generate a supermolecule"*.[1]

As with molecular recognition, self-assembly is observed throughout Nature. A good example of natural self-assembly is provided by the tobacco mosaic virus, Figure 1.3.[2] Upon binding of a bilayer disk onto a RNA site, 2200 protein subunits (each weighing 18000Da) of the tobacco mosaic virus self-assemble into a helical arrangement, 300nm in length and 18nm in diameter. This clearly demonstrates the power of self-assembly with such large subunits being efficiently organised on the nanoscale.

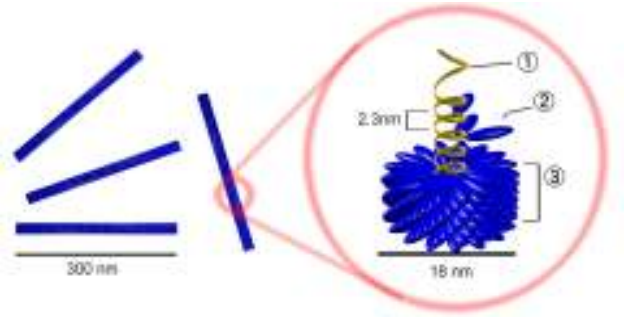

Figure 1.3 Self-assembly of the tobacco mosaic virus (1-RNA, 2-capsomer, 3-capsid).[2c]

In more general terms, self-assembly is the bringing together of building blocks in a preconceived manner (based on molecular recognition), which results in the formation of the desired supermolecule, Figure 1.4.

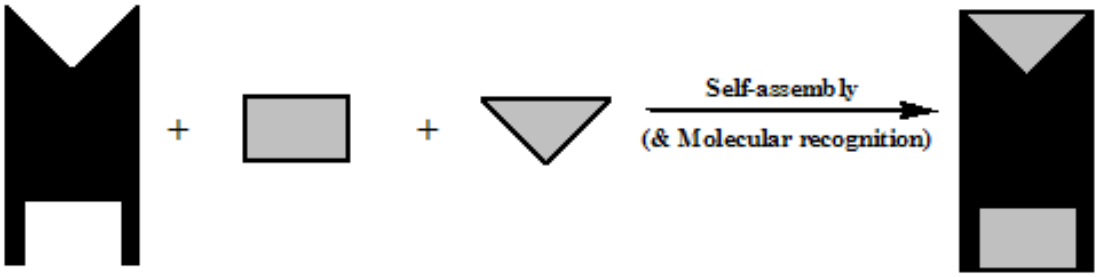

Figure 1.4 General representation of self-assembly.

Additionally, the binding preference of building blocks can be fine-tuned, thus providing a handle by which molecular recognition and self-assembly can be controlled. This allows for the tailored construction of supermolecules via simple adjustments to the individual components.

1.1.3 *Using molecular recognition and self-assembly to construct supermolecules*

This ability to utilise both molecular recognition and self-assembly principles has allowed for the construction of some very elegant supermolecules. For example, the reaction between a Zn(II) porphyrin complex and a 2,4,6-triaminopyrimidine based species demonstrates (i) selective metal coordination to the porphyrin and (ii) recognition between the hydrogen-bonding sites of the uracil functionality appended to the porphyrin and the amino-pyrimidine, Figure. 1.5.[3]

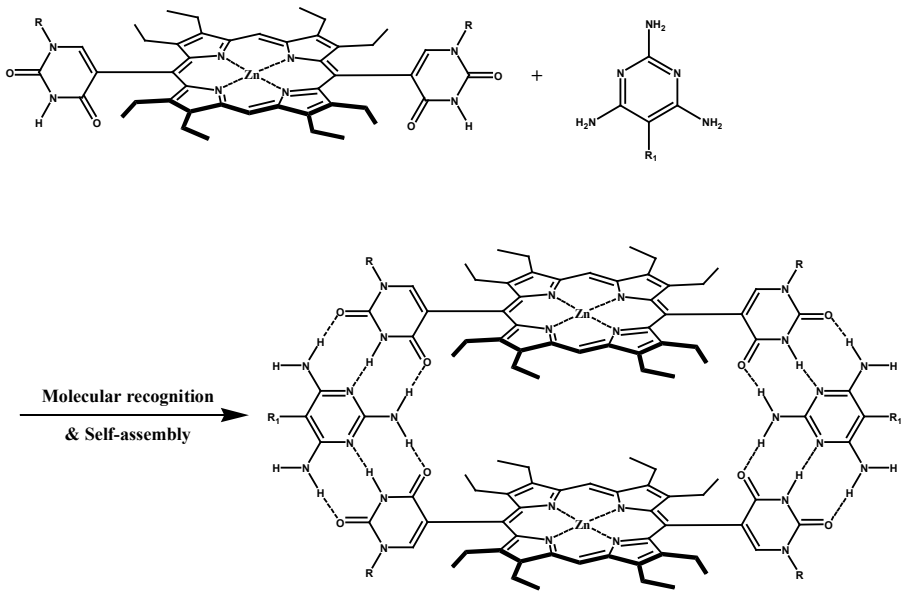

Figure 1.5 Construction of a supramolecular porphyrin cage via molecular recognition and self-assembly.[3]

1.2 Supramolecular vs. Covalent synthesis

Organic synthetic chemists have the power to construct, through the making and breaking of covalent bonds, a vast range of molecules with varying degrees of complexity via well-established synthetic procedures.[4] From the simplest small molecules to more complex natural products, Figure 1.6, the synthetic chemist has an endless number of tools that can be exploited for developing sequential multi-step synthesis, in which intermediate 'products' are isolated and purified at each step, before being subjected to further modifications in later steps. This a major advantage in covalent synthesis that allows for modifications and route changes to take place with the same final molecular goal retained.

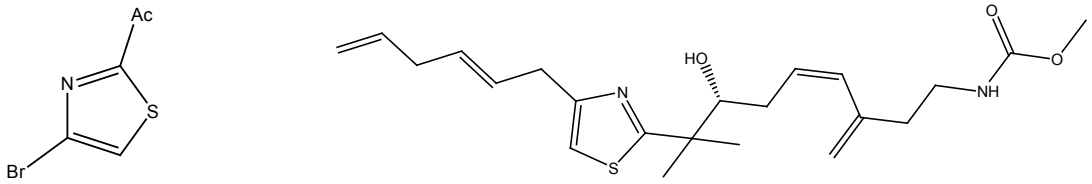

(a) (b)

Figure 1.6 From the simplest small molecules to more complex natural products. Both compounds (a) and (b) are synthesised from the same starting material via one and 18 steps, respectively.[5,6]

In contrast to synthetic chemists, the supramolecular chemist does not have a large synthetic library to consult with. Furthermore, many supramolecular syntheses are carried out as single step, one-pot, reactions with no intermediate species isolated and no additional modifications or purification steps carried out, resulting in clear limitations within supramolecular synthesis.

The principles of both synthetic chemistry and supramolecular chemistry can be combined to develop a strategy for supramolecular synthesis, in which known synthetic procedures are utilised to design and synthesise 'tunable' molecules ('receptors') via covalent modifications that possess reliable binding sites which can, via molecular recognition, combine with a complementary 'substrate' to form supermolecules.

1.3 Crystal Engineering

"One of the continuing scandals in the physical sciences is that it remains in general impossible to predict the structure of even the simplest crystalline solids from a knowledge of the chemical composition"[7]

Although supramolecular chemists still face more challenges when it comes to efficient, construction of supermolecules, significant advances have been made. The concept of crystal engineering,[8] which can be considered a sub-section of supramolecular chemistry, has allowed supramolecular chemists to go about efficiently designing crystal structures (and in a sense the desired supermolecules). Understanding how supramolecular reagents interact is key to crystal engineering and possessing such knowledge will allow for the reliable construction of supermolecules and functional materials.

1.3.1 Using crystal engineering (and supermolecules) to synthesise covalent products

An elegant example of how crystal engineering has been used is the solid-state 2+2 photodimerisation reactions carried out by MacGillivray *et al*.[9] Supermolecules capable of controlling solid-state photodimerisation reactions to produce cyclobutane-based products were targeted. In order for such photodimerisation reactions to occur the two olefins need to be parallel and within 4Å of each other.

The simple organic molecule, resorcinol, acts as a template, locking (via O-H•••N hydrogen bonds) two 4,4'-bis(ethylene)pyridine species into a suitable orientation (parallel alignment of the olefins) which meets the strict distance requirements, allowing for successful transformations to occur, Figure 1.7.

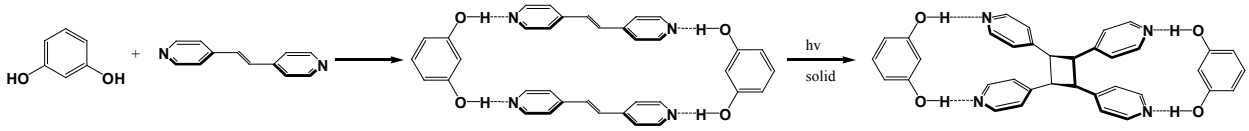

Figure 1.7 Using crystal engineering to design supermolecules for reliable covalent modifications.[9]

1.4 Hydrogen bonding as a tool for supramolecular synthesis

Arguably the most effective non-covalent interaction, *"the hydrogen bond is the most frequently encountered and hence most important non-van der Waals interaction…"*.[8] The hydrogen bond is present in some of Nature's supermolecules[10] for example nucleic acid base pairs interact via hydrogen bonds, Fig. 1.8.[11] Hydrogen bonds have also been used to carry out supramolecular synthesis with varying degrees of complexity, Fig. 1.9. [3, 12]

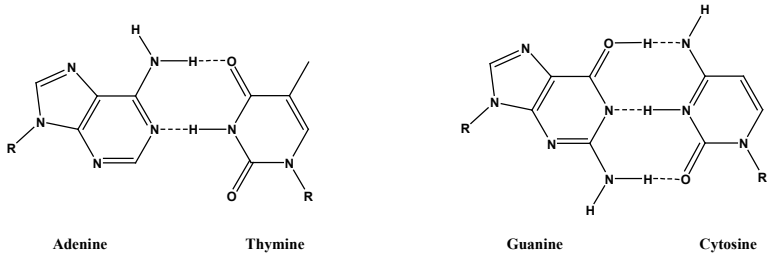

Figure 1.8 DNA base pairs interacting via hydrogen bonds.

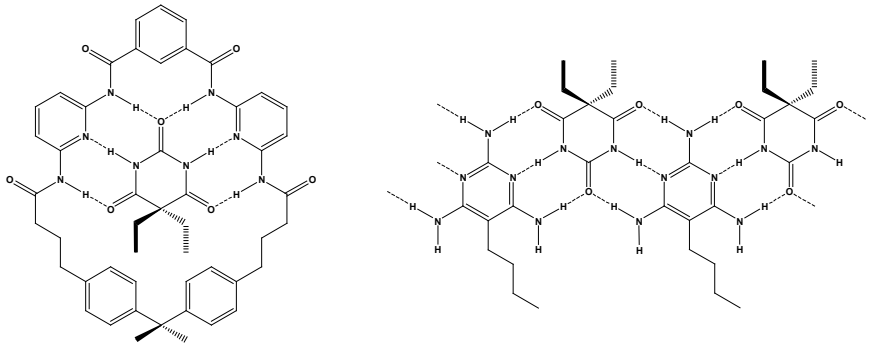

(a) (b)

Figure 1.9 Examples of supermolecules containing hydrogen bonds; (a) barbituric in a macrocycle receptor;[12a] (b) 1:1 complex of barbituric acid and 2,4,6-triaminopyrimidine.[12b]

1.4.1 Supramolecular synthons

Supramolecular synthons are defined as *"structural units within supermolecules which can be formed and/or assembled by known or conceivable synthetic operations using intermolecular interactions"*.[13] Knowing that molecules will organise themselves in a certain way in the solid-state can be exploited in the design and synthesis of supermolecules. A few examples of these powerful tools will be discussed below.

1.4.1.1 Homomeric hydrogen-bond synthons

Complementarity plays a big role within hydrogen bonding and the formation of homomeric interactions between two or more molecules of the same chemical species provides important information regarding the interactions as well as the orientation of the molecules.

Homomeric dimers are often seen between molecules containing a binding site with complementary donor and acceptor sites e.g. carboxylic acids,[14] amides[15] and amino-pyridines,[16] Figure 1.10.

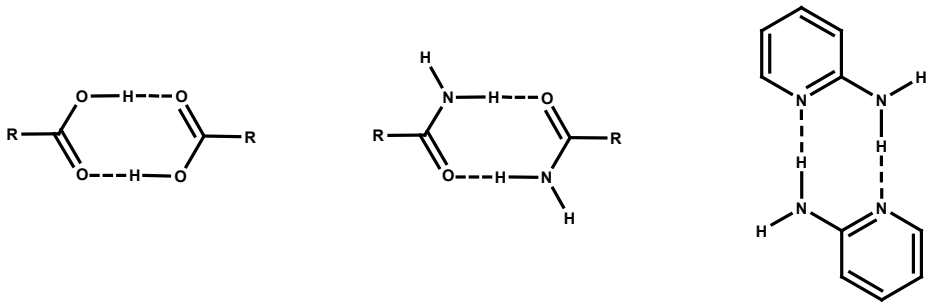

(a) (b) (c)

Figure 1.10 Examples of homomeric dimers; (a) acid-acid; (b) amide-amide and (c) aminopyridine-aminopyridine.

Homomeric dimers occur regularly throughout organic solid-state chemistry and with this continuity within families of molecules it can be applied as a reliable tool for construction of supermolecules.

There are other homomeric interactions that can take place, with chains often seen notably in secondary amides[17] and alcohols,[18] Figure 1.11.

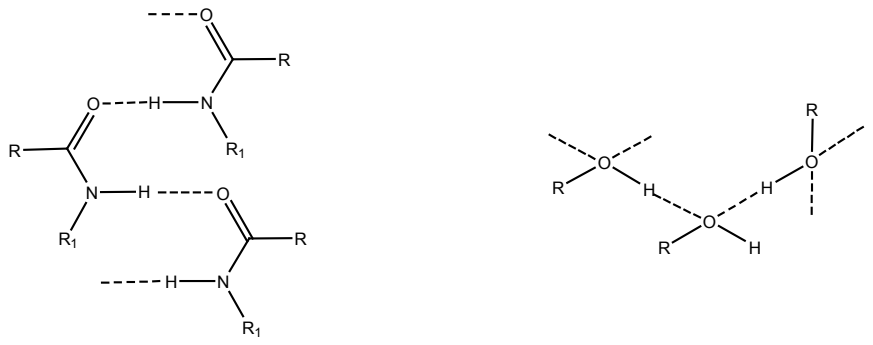

(a) (b)

Figure 1.11 Examples of homomeric chains; (a) secondary amide and (b) alcohol.

1.4.1.2 Heteromeric hydrogen-bond synthons

Reliable and recurring hydrogen bonds are also observed between two different chemical entities resulting in heteromeric synthons.[19] Dimers can be formed between two different molecules, e.g acid•••amide,[20] acid•••pyridine,[21, 20a-b] acid•••aminopyridine,[22] Figure 1.12.

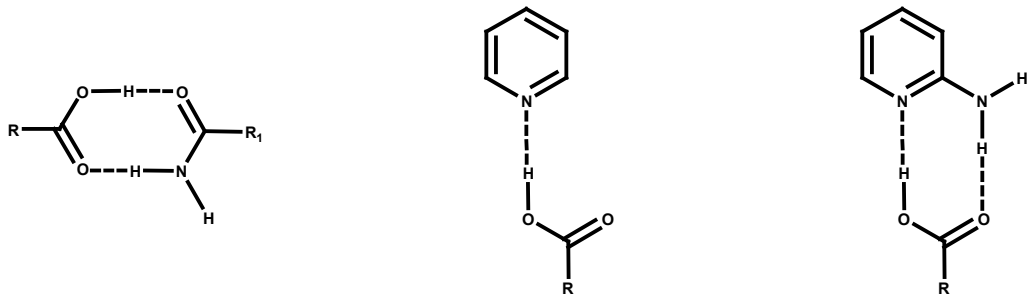

(a) (b) (c)

Figure 1.12 Examples of heteromeric hydrogen-bond synthons; (a) acid-amide; (b) acid-pyridine and (c) acid-aminopyridine.

1.4.2 Graph-set notations

Graph-set notation[23] is used to identify specific hydrogen-bonding interactions and allows for recurring trends to be identified.

The general formula, Figure 1.13, incorporates a hydrogen-bond motif (G), the number of hydrogen-bond acceptors (a), the number of hydrogen-bond donors (d) and the total number of atoms contained in the specific motif (x).

$$G_d^a(X)$$

Figure 1.13 General formula for graph-set notations.

There are four types of motifs (G) used in the assignment of graph sets, ring (R), chain (C), dimer (D) and intramolecular (S).

Graph sets are broken down into levels, N_x, where "x" is the number of different hydrogen bonds involved. The first level (N_1) considers each hydrogen bond individually, the second level (N_2) incorporates two different hydrogen bonds, N_3 involves three different hydrogen bonds etc.

For example, benzoic acid,[14i-k] Figure 1.14, has two equivalent O-H•••O hydrogen bonds present and consequently N_1 is assigned $R_2^2(8)$ (a ring motif with two hydrogen-bond donors, two hydrogen-bond acceptors and a total of eight atoms in the ring).

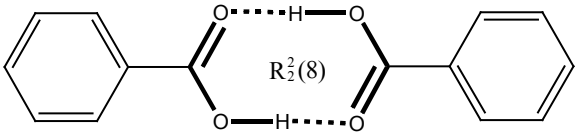

Figure 1.14 $R_2^2(8)$ graph-set notation for benzoic acid.

Benzamide,[15j-m] Figure 1.15, however, has two different N-H•••O hydrogen bonds and consequently has two levels of graph sets. N_1 for benzamide is $R_2^2(8)$; $C_1^1(4)$ and N_2 is $R_4^2(8)$.

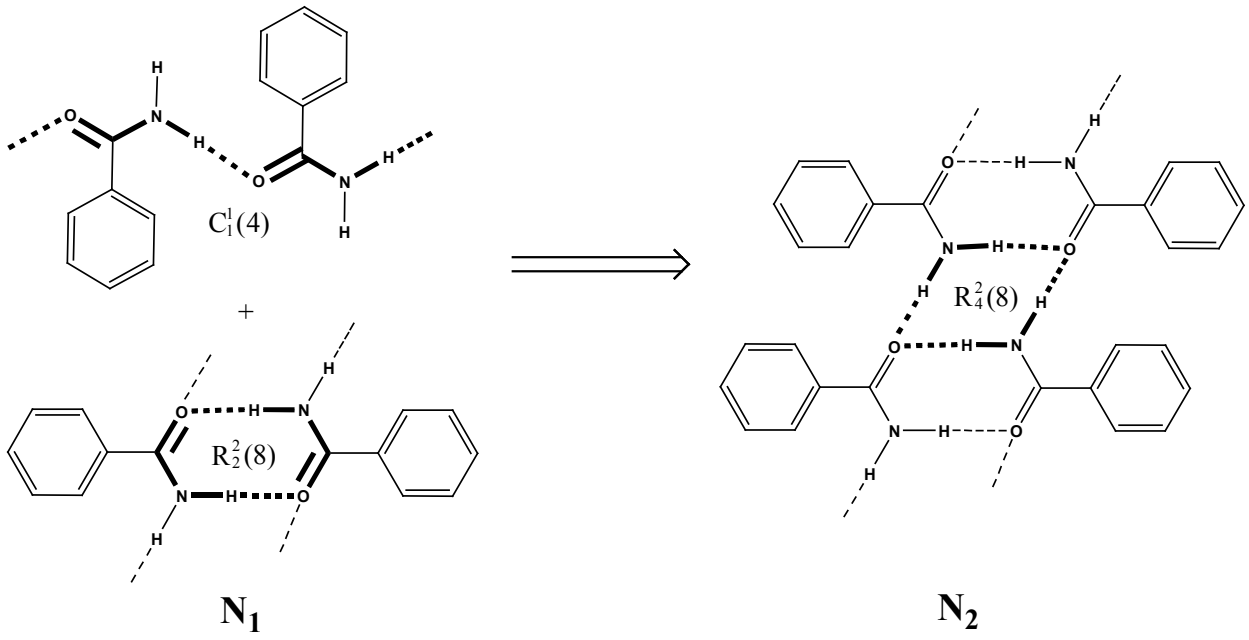

Figure 1.15 Graph sets for benzamide.

1.4.3 Etter's guidelines

Having guidelines in place to confidently assess hydrogen bonding in supramolecular synthesis is essential and provides a deeper understanding of which hydrogen bonds will form. This has been developed over the past twenty years and began with Etter[23c-d] introducing the idea of systematically looking at hydrogen-bond patterns (identified by graph-set notations) in molecular aggregates. An extensive study of the Cambridge Structural Database (CSD),[24] led to a family of guidelines that can be followed when attempting to design and synthesise supermolecules;

1) All proton donors and acceptors will participate in hydrogen bonding
2) A six-membered intramolecular arrangement will form if possible
3) The best proton donor and acceptor remaining after intramolecular hydrogen-bond formation will form an intermolecular hydrogen-bond

1.4.4 Co-crystals

Co-crystals are the result of controlled, predictable supramolecular synthesis that utilise both homomeric and heteromeric synthons. Defined as *"structurally homogeneous crystalline materials that contain two or more neutral building blocks (that are solids under ambient conditions) that are present in definite stoichiometric amounts"*,[25] co-crystals have gained attention due to their ability to control the inherent properties of simple organic compounds (including active pharmaceutical ingredients) via non-covalent interactions.[26]

Co-crystals are generally formed via solution-based "reactions" (although solid-state grinding,[27] melting,[28] and vapour digestion[27e, 29] are also suitable methods for co-crystal synthesis) in which a solution containing stoichiometric amounts of each component is allowed to evaporate in an attempt to form the single solid form. The general process is very similar to recrystallisation techniques that are used extensively (A Sci-Finder search for the term "recrystallisation" yielded 26905 hits) in synthetic chemistry to obtain pure products, Figure 1.16.

How then do co-crystallisation reactions prevail when the probability of forming the heteromeric (co-crystal) product is much lower than forming the homomeric (recrystallisation) product? With the odds stacked against co-crystal formation, the chemical species have to be

tailored to drive the reaction toward the heteromeric interaction. This can be achieved by considering the guidelines that have been put in place (i.e. Etter's guidelines and Deiraju's synthons) which provide valuable tools for driving the formation of a co-crystal instead of the homomeric recrystallisation product.

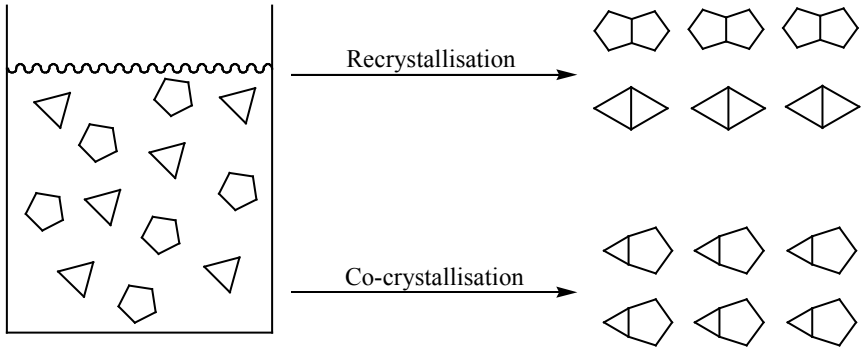

Figure 1.16 Recrystallisation vs. co-crystallisation.

1.4.4.1 Examples of co-crystals

Many binary (two component) co-crystals have been synthesised, which agrees with Etter's third guideline "*the best proton donor and acceptor remaining after intramolecular hydrogen-bond formation will form an intermolecular hydrogen bond"* [23c-d] and demonstrates the reliability of 'heterosynthons'.[19] Heteromeric acid-acid dimers have been observed, Figure 1.17a,[20b, 30] along with acid-amide heterodimers, Figure 1.17b[20] and more complex systems featuring a carboxylic acid interacting with an N-heterocycle, Figure 1.17c.[20a-b, 21, 31]

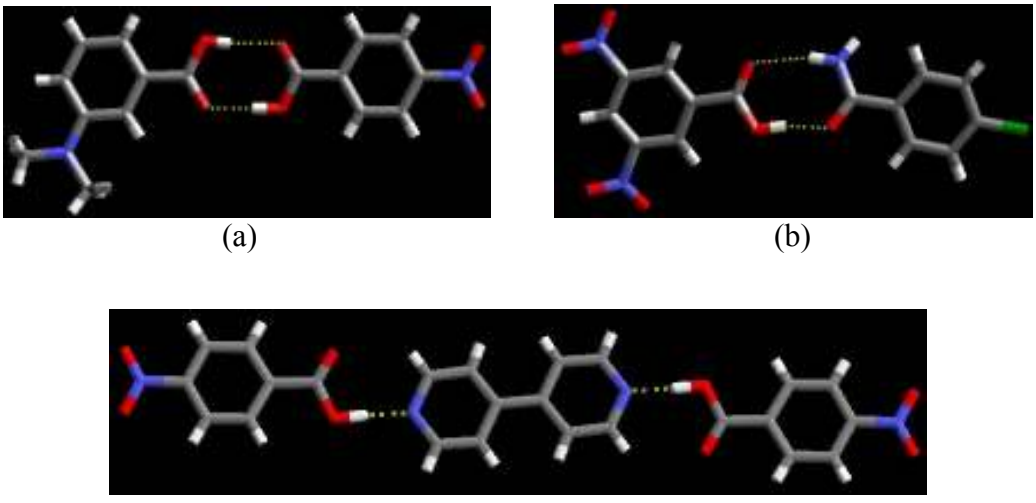

(a) (b)

(c)

Figure 1.17 Examples of binary heteromeric co-crystals – (a) acid-acid heterodimer; [20b] (b) acid-amide heterodimer; [20a] (c) acid-pyridine. [21c]

In some instances, both homomeric and heteromeric interactions are observed.[20b] For example, the binary co-crystal between isonicotinamide and 4-fluorobenzoic acid possesses both the homomeric amide-amide dimer as well as the heteromeric O-H•••N acid-pyridine interaction, Figure 1.18.

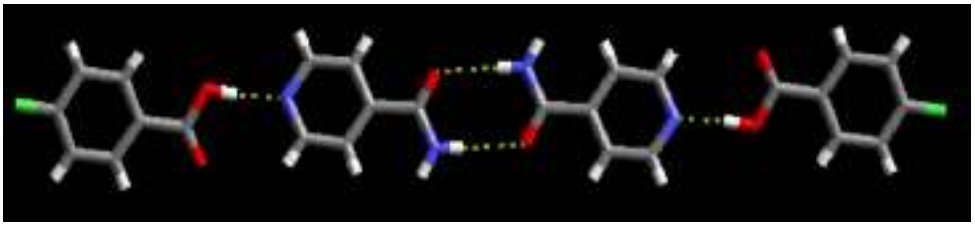

Figure 1.18 Binary 1:1 co-crystal of isonicotinamide and 4-fluorobenzoic acid.

Homo- and heteromeric interactions have also been combined to increase the level of complexity of co-crystals to the ternary (three component) level.[21d] Isonicotinamide was utilised as a primary hub for ternary co-crystallisations having two different binding sites (the pyridine and the amide). Two different carboxylic acids form heteromeric hydrogen bonds (acid-amide dimer via N-H•••O and O-H•••O hydrogen bonds and acid-pyridine via an O-H•••N hydrogen bond) to the different binding sites, Figure 1.19. These ternary co-crystals agree with Etter's guideline "*the best proton donor and acceptor remaining after intramolecular hydrogen-bond formation will form an intermolecular hydrogen bond"*.[23c-d]

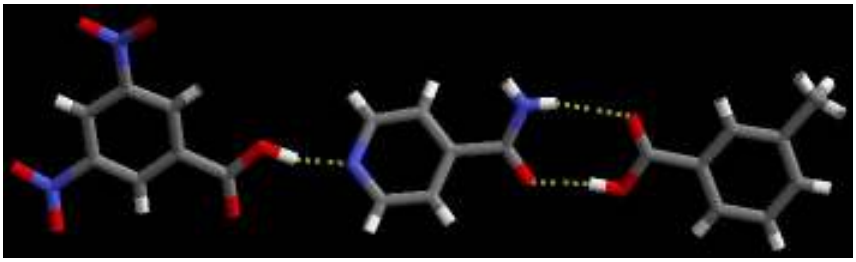

Figure 1.19 Ternary 1:1:1 co-crystal of isonicotinamide, 3,5-dinitrobenzoic acid and 3-methylbenzoic acid.[21d]

1.4.5 What do molecules want?

The complexity and difficulty surrounding the formation of 1:1:1 ternary co-crystals is demonstrated by the limited number of structures (there are only seven 1:1:1 ternary co-crystals in the CSD). Although it seems relatively straightforward, reliable supramolecular synthesis is

restricted at present due to a limited understanding of "what molecules want" with regards to non-covalent interactions.

Considering a system that possesses three different binding sites capable of accepting or donating a hydrogen bond, Figure 1.20. How do we design a hub, such that three incoming species will recognise and selectively bind to the desired site?

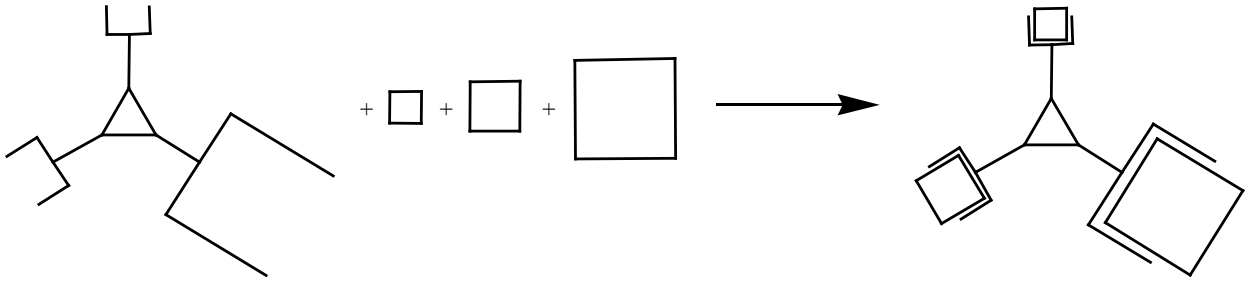

Figure 1.20 General representation of selective binding.

Previous work has utilised supramolecular synthons to construct supermolecules of varying size and complexity, Figure 1.21. From 1:1 binary[20, 21, 26a, 30, 31b-c] and 1:1:1 ternary[21d, 31a] co-crystals to inorganic-organic hybrid materials[32] to heteromeric capsules.[33] The ability to control assembly over a range of $30nm^3$ to $180nm^3$ demonstrates the robustness of supramolecular synthons and ultimately leads to the question "can supramolecular synthons be used to control even larger assemblies (e.g. nanoparticles)?"

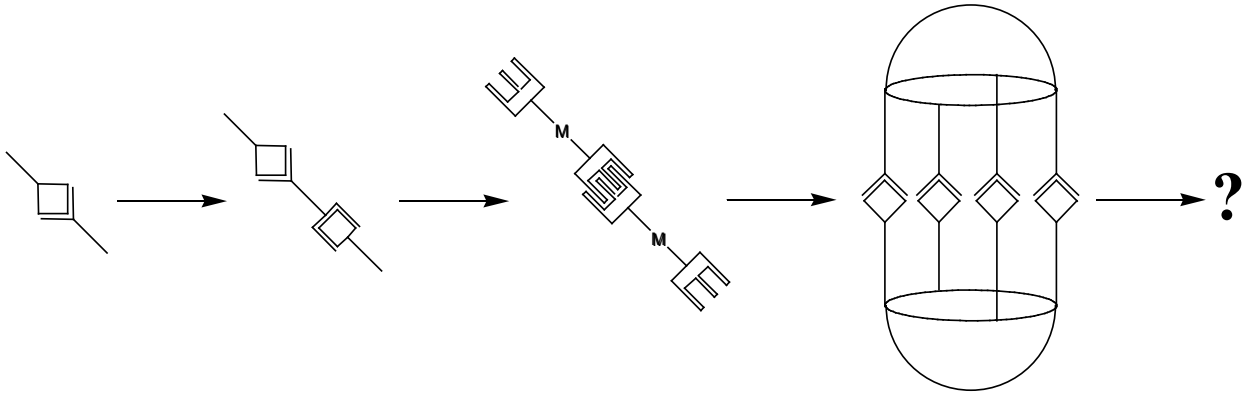

Figure 1.21 Using supramolecular synthons to construct a variety of supermolecules.

1.5 Goals

Supramolecular synthons can be used to construct supermolecules, however, the uncertainty surrounding non-covalent interactions still provides a challenge to reliable and robust synthetic strategies.

A hierarchy of non-covalent interactions needs to be developed. If a level of consistency can be attained for supramolecular synthesis similar to that for covalent synthesis (i.e when "A" is reacted with "B" the product is always "C"), then construction of supermolecules becomes far more reliable.

Consequently, the goals of this thesis are to:

I. Develop a hierarchy of reliable hydrogen-bond interactions via co-crystallisation reactions

In order to test Etter's guideline[23c-d] *"the best proton donor and acceptor remaining after intramolecular hydrogen-bond formation will form an intermolecular hydrogen-bond"* and to continue developing a hierarchy of interactions, a collection of supramolecular reagents will be designed and synthesised. Subsequent co-crystallisation reactions between supramolecular reagents and hydrogen-bond donors will allow for a systematic study into hydrogen-bond preference to be carried out.

II. Build inorganic-organic hybrid materials using non-covalent interactions

The robustness of the amide-amide dimer will be tested in the presence of potentially disruptive forces (e.g. solvent, counter-ions) by attempting to construct 1-D inorganic-organic hybrid materials. Additionally, reliable chelating ligands (*acac*, "paddle-wheel", pyrimidine-pyrazole and 1,3-bisbenzylpyrazole) will be utilised to control unpredictable metal coordination.

III. Test the synthetic capability of supramolecular synthons on a much larger scale by studying hydrogen-bond effects on nanoparticle assembly

Nanoparticles functionalised with hydrogen-bond terminated ligands will be synthesised. The structure of homomeric (acid-acid; alcohol-alcohol) and heteromeric (acid-imidazole; alcohol-imidazole) hydrogen-bond assemblies will be compared to assemblies with non hydrogen bonding (methyl and imidazole) terminated ligands, thus providing information regarding the influence of hydrogen bonding (or more specifically, supramolecular synthons) on such a large scale.

References

1. J. –M. Lehn, *Supramolecular Chemistry*, VCH, Weinheim, 1995.
2. (a) G. Lebeurier, A. Nicolaieff and K. E. Richards, *Proc. Natl. Acad. Sci. USA*, 1977, **74**, 149; (b) P. J. G. Butler and A. Klug, *Nat. New Biol.*, 1971, **229**, 47; (c) http://en.wikipedia.org/wiki/Tobacco_mosaic_virus.
3. C. M. Drain, R. Fischer, E. G. Nolen and J. –M. Lehn, *J. Chem. Soc., Chem. Commun.,* 1993, 243.
4. K. C. Nicolaou and E. J. Sorensen, *Classics in total synthesis,* Wiley-VCH, Weinhein, 1996.
5. J. Gebauer, S. Arseniyadis and J. Cossy, *Org. Lett.*, 2007, **9**, 3425.
6. A. Le Flohic, C. Meyer and J. Cossy, *Org. Lett.*, 2005, **7**, 339.
7. J. Maddox, *Nature*, 1988, **335**, 11.
8. G. Desiraju, *Crystal Engineering-The Design of Organic Solids*, Elsevier, Amsterdam, 1989.
9. L. R. MacGillivray, *CrystEngComm,* 2002, **4**, 37.
10. G. A. Jeffrey and W. Saenger, *Hydrogen Bonding in Biological Structures*, Springer-Verlag, Berlin, Heidelberg, New York, 1991.
11. (a) S. Fujita, A. Takenaka and Y. Sasada, *Biochemistry*, 1985, **24**, 508; (b) T. Ise, D. Shiomi, K. Sato, T. Takui, *Chem. Commun.*, 2006, 4832; (c) E. J. O'Brien, *Acta Crystallogr.*, 1967, **23**, 92; (d) S. Fujita, A. Takenaka and Y. Sasada, *Bull. Chem. Soc. Jpn.*, 1984, **57**, 1707.
12. (a) S. –K. Chang, D. Van Engen, E. Fan and A. D. Hamilton, *J. Am. Chem .Soc.*, 1991, **113**, 7640; (b) J. –M. Lehn, M. Mascal, A. DeCian and J. Fischer, *J. Chem. Soc., Chem. Commun.*, 1990, 479.
13. G. R. Desiraju, *Angew. Chem. Int. Ed.*, 1995, **34**, 2311.
14. (a) C. L. Nygren, C. C. Wilson and J. F. C. Turner, *J. Phys. Chem. A*, 2005, **109**, 2586; (b) K. Ohkura, S. Kashino and M. Haisa, *Bull. Chem. Soc. Jpn.*, 1972, **45**, 2651; (c) C. C. Wilson, X. Xu, A. J. Florence and N. Shankland, *New J. Chem.*, 2006, **30**, 979; (d) M. Kubota and S. Ohba, *Acta Crystallogr., Sect. B*, 1992, **48**, 849; T. F. Lai and R. E. Marsh, *Acta Crystallogr.*, 1967, **22**, 885; (e) M. Tonogaki, T. Kawata, S. Ohba, Y. Iwata and I. Shibuya, *Acta Crystallogr., Sect. B*, 1993, **49**, 1031; (f) P. Prince, F. R. Fronczek and R. D. Gandour; *Acta*

Crystallogr., Sect. C, 1991, **47**, 895; (g) V. R. Thalladi, M. Nusse and R. Boese, *J. Am. Chem. Soc*., 2000, **122**, 9227; (h) A. L. Bednowitz and B. Post, *Acta Crystallogr.*, 1966, **21**, 566; (i) G. Bruno and L. Randaccio, *Acta Crystallogr., Sect.B*, 1980, **36**, 1711; (j) R. Feld, M. S. Lehmann, K. W. Muir and J. C. Speakman, *Z. Kristallogr., Kristallgeom., Kristallphys., Kristallchem.*, 1981, **157**, 215; (k) C. C. Wilson, N. Shankland and A. J. Florence, *J. Chem. Soc., Faraday Trans.*, 1996, **92**, 5051.

15. (a) M. Kubota and S. Ohba, *Acta Crystallogr., Sect. B*, 1992, **48**, 849; (b) A. Schonleber, P. Pattison and G. Chapuis, *Z. Kristallogr.*, 2003, **218**, 507; (c) Y. Takaki, K. Nakata, T. Taniguchi and K. Sakurai, *Acta Crystallogr., Sect. B*, 1978, **34**, 2579; (d) T. Taniguchi, N. Nakata, Y. Takaki and K. Sakurai, *Acta Crystallogr., Sect. B*, 1978, **34**, 2574; (e) T. Hayashi, K. Nakata, Y. Takaki and K. Sakurai, *Bull. Chem. Soc. Jpn.*, 1980, **53**, 801; (f) K. Nakata, Y. Kato, Y. Takaki and K. Sakurai, *Mem. Osaka Kyoiku Univ. Ser. 3*, 1971, **20**, 93; (g) K. Nakata, S. Ono and K. Sakurai, *Mem. Osaka Kyoiku Univ. Ser. 3*, 1979, **27**, 117; (h) C. C. Seaton and M. Tremayne, *Chem. Commun.*, 2002, 880; (i) M. Hospital, *Acta Crystallogr., Sect. B*, 1971, **27**, 484; (j) B. R. Penfold and J. C. B. White, *Acta Crystallogr.*, 1959, **12**, 130; (k) C. C. F. Blake and R. W. H. Small, *Acta Crystallogr., Sect. B*, 1972, **28**, 2201; (l) Q. Gao, G. A. Jeffrey, J. R. Ruble and R. K. McMullan, *Acta Crystallogr., Sect .B*, 1991, **47**, 742; J. R. Ruble and A. Galvao, *Acta Crystallogr., Sect. B*, 1995, **51**, 835; (m) K. Kobayashi, A. Sato, S. Sakamoto and K. Yamaguchi, *J. Am. Chem. Soc.*, 2003, **125**, 3035; (n) N. Blagden, R. Davey, G. Dent, M. Song, W. I. F. David, C. R. Pulham and K. Shankland, *Cryst. Growth Des.*, 2005, **5**, 18.
16. (a) Å. Kvick, R. Thomas and T. F. Koetzle, *Acta Crystallogr., Sect. B*, 1976, **32**, 224; (b) Å. Kvick and J. Noordik, *Acta Crystallogr., Sect.B*, 1977, **33**, 2862; (c) M. Chao, E. Schempp and R. D. Rosenstein, *Acta Crystallogr., Sect. B*, 1975, **31**, 2922; (d) K. Goubitz, E. J. Sonneveld and H. Schenk, *Z. Kristallogr.*, 2001, **216**, 176; (e) S. Goswami, S. Dey, H. –K. Fun and S. Chantrapromma, *Acta Crystallogr., Sect. E*, 2006, **62**, o3225; (f) J. Oszust, Z. Talik, A. Pietraszko, M. K. Marchewka and J. Baran, *J. Mol. Struct.*, 1997, **415**, 53.
17. (a) D. R. Coghlan, C. J. Easton and E. R. T. Tiekink, *Aust. J. Chem.*, 2000, **53**, 551; (b) L. Leiserowitz and M. Tuval, *Acta Crystallogr., Sect. B*, 1978, **34**, 1230; (c) K. F. Bowes, C. Glidewell, J. N. Low, J. M. S. Skakle and J. L. Wardell, *Acta Crystallogr., Sect. C*, 2003, **59**,

o1; (d) P. Nimmanpipug, K. Tashiro, Y. Maeda and O. Rangsiman, *J. Phys. Chem. B*, 2002, **106**, 6842.

18. (a) D. R. Allan, S. J. Clark, A. Dawson, P. A. McGregor and S.Parsons, *Acta Crystallogr., Sect. B*, 2002, **58**, 1018; (b) M. Perrin and A. Thozet, *Cryst. Struct. Commun.*, 1974, **3**, 661; (c) I. D. H. Oswald, D. R. Allan, W. D. S. Motherwell and S. Parsons, *Acta Crystallogr., Sect. B*, 2005, **61**, 69; (d) M. Perrin, S. Rantsordas and A. Thozet, *Cryst. Struct. Commun.*, 1978, **7**, 59; (e) K. Merz, *Cryst. Growth Des.*, 2006, **6**, 1615.
19. R. D. Bailey Walsh, M. W. Bradner, L. A. Fleishman, D. Moulton, N. Rodriquez-Hornedo and M. J. Zaworotko, *Chem. Commun*., 2003, 186.
20. (a) C. B. Aakeröy, A. M. Beatty, B. A. Helfrich and M. Nieuwenhuyzen, *Cryst. Growth. Des.*, 2003, **3**, 159; (b) C. B. Aakeröy, J. Desper and B. A. Helfrich, *CrystEngComm*, 2004, **6**, 19; (c) L. S. Reddy, A. Nangia and V. M. Lynch, *Cryst. Growth Des.*, 2004, **4**, 89; (d) L. S. Reddy, P. M. Bhatt, R. Banerjee, A. Nangia and G. J. Kruger, *Chem. Asian J.*, 2007, **2**, 505; (e) W. Jankowski, M. Gdaniec and T. Polonski, *Acta Crystallogr., Sect. C*, 2006, **62**, o492; (f) P. Holy, J. Zavada, I. Cisarova and J.Podlaha, *Tetrahedron Asymm.*, 2001, **12**, 3035.
21. (a) C. B. Aakeröy, A. M. Beatty and B. A. Helfrich, *J. Am. Chem. Soc.*, 2002, **124**, 14425; (b) T. Sugiyama, J. Meng and T. Matsuura, *J. Mol. Strcut.*, 2002, **611**, 53; (c) J. R. Bowers, G. W. Hopkins, G. P. A. Yap and K. A. Wheeler, *Cryst. Growth. Des.*, 2005, **5**, 727; (d) C. B. Aakeröy, A.M. Beatty and B. A. Helfrich, *Angew. Chem. Int. Ed.*, 2001, **40**, 3240; (e) B. R. Bhogala, S. Basavgu and A. Nangia, *CrystEngComm.*, 2005, **7**, 551; (f) P. Vishweshwar, A. Nangia and V. M. Lynch, *Cryst. Growth Des.*, 2003, **3**, 783.
22. (a) D. E. Lynch, G. Smith, D. Freney, K. A. Byriel and C. H. Kennard, *Aust. J. Chem.*, 1994, **47***,* 1097; (b) D. E. Lynch, T. Latif, G. Smith, K. A. Byriel, C. H. L. Kennard and S. Parsons, *Aust. J. Chem.*, 1998, **51***,* 403.
23. (a) J. Bernstein, R. E. Davis, L. Shimoni and N. –L. Chang, *Angew. Chem. Int. Ed.*, 1995, **34**, 1555; (b) M. C. Etter, J. C. MacDonald and J. Bernstein, *Acta Crystallogr. Sect. B,* 1990*,* **46**, 256; (c) M. C. Etter, *Acc. Chem. Res.,* 1990, **23**, 120; (d) M. C. Etter, *J. Phys. Chem*., 1991, **95**, 4601; (e) J. Bernstein, M. C. Etter and J. C. MacDonald, *J. Chem. Soc. Perkin Trans. 2*, 1990, 695.
24. F. H. Allen*, Acta Crystallogr. Sect. B,* 2002*,* **58**, 380.

25. (a) C. B. Aakeröy and D. J. Salmon, *CrystEngComm.*, 2005, **7**, 439.
26. (a) C. B. Aakeröy, I. Hussain and J. Desper, *Cryst. Growth. Des.*, 2006, **6**, 474; (b) S. Motherwell and W. Jones, *Intl. J. Pharm.*, 2006, **320**, 114; (c) Ö. Almarsson and M. J. Zaworotko, *Chem. Commun.*, 2004, 1889.
27. (a) T. Frisic, L. Fabian, J. C. Burley, W. Jones and S. W. D. Motherwell, *Chem. Commun.*, 2006, 5009; (b) T. Frisic, A. V. Trask, W. Jones and S. W. D. Motherwell, *Angew. Chem. Int. Ed.*, 2006, **45**, 7546; (c) A. V. Trask, J. van de Streek, S. W. D. Motherwell and W. Jones, *Cryst. Growth Des.*, 2005, **5**, 2233; (d) A. V. Trask and W. Jones, *Topics in Current Chemistry*, 2005, **254**, 41; (e) A. V. Trask, W. D. S. Motherwell, W. Jones, *Chem. Commun.*, 2004, 890; (f) D. Braga, S. L. Giaffreda, F. Grepioni, A. Pettersen, L. Maini, M. Curzi and M. Polito, *Dalton Trans.*, 2006, 1249.
28. (a) C. C. Seaton, A. Parkin, C. C. Wilson and N. Blagden, *Cryst. Growth Des.*, 2008, **8**, 363; (b) L. S. Reddy, P. M. Bhatt, R. Banerjee, A. Nangia and G. J. Kruger, *Chem. Asian. J.*, 2007, **2**, 505.
29. D. Braga, S. L. Giaffreda, F. Grepioni, M. R. Chierotti, R. Gobetto, G. Palladino and M. Polito, *CrystEngComm*, 2007, **9**, 879.
30. (a) K. A. Byriel, D. E. Lynch, G. Smith and C. H. L. Kennard, *Aust. J. Chem.*, 1991, **44**, 1459; (b) C. V. K. Sharma, K. Panneerselvam, T. Pilati and G. R. Desiraju, *Chem. Commun.*, 1992, 832; (c) M. Gdaniec, W. Jankowski, M. J. Milewska and T. Polonski, *Angew. Chem. Int. Ed.*, 2003, **42**, 3903.
31. (a) C. B. Aakeröy, J. Desper and J. F. Urbina, *Chem. Commun.*, 2005, 2820; (b) C. B. Aakeröy, J. Desper, B. Leonard and J. F. Urbina, *Cryst. Growth Des.*, 2005, **5**, 865; (c) C. B. Aakeröy, J. Desper and J. F. Urbina, *Cryst. Growth Des.*, 2005, **5**, 1283.
32. (a) C. B. Aakeröy, N. Schultheiss and J. Desper, *Dalton. Trans.*, 2006, 1627; (b) C. B. Aakeröy, N. Schultheiss and J. Desper, *CrystEngComm*, 2006, **9**, 421; (c) C. B. Aakeröy, N. Schultheiss and J. Desper, *Inorg. Chem.*, 2005, **44**, 4983; (d) C. B. Aakeröy, J. Desper and J. V. -Martínez, *CrystEngComm*, 2004, **6**, 413; (e) C. B. Aakeröy, A. M. Beatty and K. R. Lorimer, *J. Chem. Soc., Dalton Trans.*, 2000, 3869, (f) C. B. Aakeröy, A. M. Beatty, D. S. Leinen and K. R. Lorimer, *Chem. Commun.*, 2000, 935; (g) C. B. Aakeröy and A. Beatty, *Cryst. Eng.*, 1998, **1**, 39; (h) C. B. Aakeröy and A. Beatty, *Chem. Commun.*, 1998, 1067; (i)

C. B. Aakeröy; J. Desper; M. M. Smith and J. F. Urbina, *Dalton Trans.*, 2005, 2462; (j) C. B. Aakeröy, J. Desper and J. Valdés-Martínez, *CrystEngComm.*, 2004, **6**, 413; (k) C. B. Aakeröy, A. M. Beatty and D. Leinen, *J. Am. Chem. Soc.*, 1998, **120**, 7383; (l) C. B. Aakeröy, A. M. Beatty and D. Leinen, *Angew. Chem. Int. Ed.*, 1999, **38**, 1815; (m) J. K. Bera, T. –T. Vo, R. A. Walton and K. R. Dunbar, *Polyhedra*, 2003, **22**, 3009; (n) C. B. Aakeröy, A. Beatty, J. Desper, M. O'Shea and J. Valdés-Martínez, *Dalton Trans.*, 2003, 3956; (o) B.Kozlevcar, I.Leban, I.Turel, P.Segedin, M.Petric, F.Pohleven, A.J.P.White, D.J.Williams and J.Sieler, *Polyhedra*, 1999, **18**, 755; (p) D.Chakrabarty, H.Nagase, M.Kamijo, T.Endo and H.Ueda, *Anal. Chem. Scand.*, 1992, **46**, 29; (q) A.S.Antsyshkina, T.V.Koksharova, G.G.Sadikov, I.S.Gritsenko, V.S.Sergienko and O.A.Egorova, *Zu. Neorg. Khim.*, 2006, **51**, 972; (r) B. Kozlevcar, N. Lah, I. Leban, I. Turel, P. Segedin, M. Petric, F. Pohleven, A. J. P. White, D. J. Williams and G. Giester, *Croat. Chem. Acta.*, 1999, **72**, 42

33. (a) C. B. Aakeröy and N. Schultheiss and J. Desper, *Org. Lett.*, 2006, **8**, 2607; (b) C. B. Aakeröy and N. Schultheiss and J. Desper, *CrystEngComm.*, 2006, **8**, 502.

CHAPTER 2 - How robust is the hydrogen-bonded amide 'ladder' motif?

2.1 Introduction

The way in which discrete molecules equipped with a variety of functional groups interact, bind and communicate with each other through non-covalent intermolecular forces[1] is central to the understanding of biological chemistry as well as to many areas of materials science (pharmaceutical compounds,[2] polymers,[3] liquid crystals,[4] organogelators,[5] and lithographic plates[6]). On a fundamental level it is important to be able to identify patterns of behavior of functional groups but not just in terms of their chemical reactivity. We also need to acquire an improved understanding of non-covalent interactions in order to reliably predict molecular organization, assembly, and connectivity in the solid state as this ultimately controls many physical properties of the bulk materials.[7] In this context, single-crystal structural data have offered invaluable information regarding recurring intermolecular motifs, supramolecular synthons,[8] and interactions involving specific chemical functional groups, with the concept of synthons becoming key to advancing all practical manifestations of crystal engineering.[9]

The structural chemistry of the amide moiety has received considerable attention partly due to the self-complementary nature of its hydrogen-bond donors/acceptors, but also because of the abundance of amide moieties in biological systems.[10] The amide is, on its own, frequently associated with an infinite ladder-like motif typically composed of two pairs of symmetry related N-H•••O hydrogen bonds.[11] The ladder is the result of a self-complementary, $R_2^2(8)$ homomeric amide•••amide dimer, Figure 2.1a, accompanied by N-H•••O interactions between the *anti* hydrogen atom of the $–NH_2$ group and the carbonyl oxygen of an adjacent amide moiety (producing an $R_2^2(8)$ motif). This intermolecular arrangement satisfies both hydrogen-bond donors (the $–NH_2$ hydrogen atoms) and the two hydrogen-bond acceptor sites (the lone-pairs) on the carbonyl oxygen atom, Figure 2.1b.

Complications may arise, however, if additional hydrogen-bond acceptors are present on the same molecule as the amide. For example, in one of the polymorphs of 4-nitrobenzamide, the $–NO_2$ moiety disrupts the ladder-motif by acting as a hydrogen-bond acceptor for the $–NH_2$ *anti* hydrogen atom of the amide.[12]

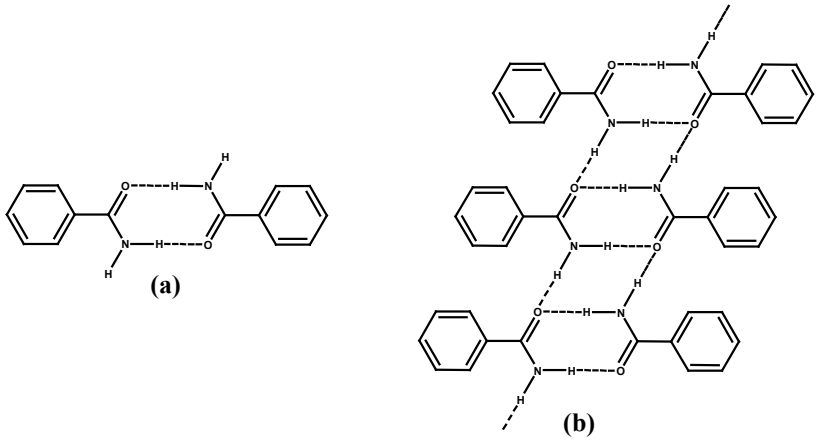

Figure 2.1 (a) Homomeric amide dimer and (b) Extended ladder.

In order to address this challenge, we have carried out a systematic structural study of a family of new compounds comprising an amide moiety and an N-heterocyclic fragment, Figure 2.2. The relative basicity, and thus ability to form hydrogen bonds, of the N-heterocycle can be varied through simple covalent modifications, which offer a practical tool for establishing correlations between molecular structure/function and supramolecular assembly/organization.

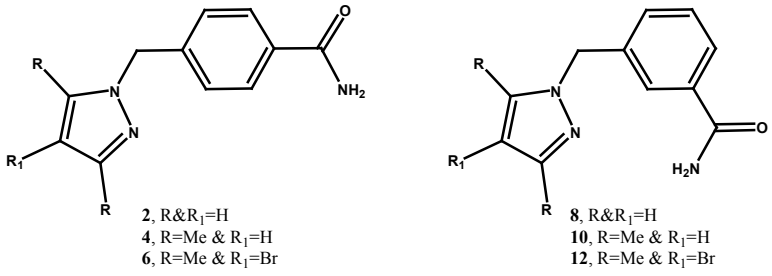

Figure 2.2 Target ligands.

We have also supplemented the new structural information with relevant data obtained from the CSD.[13] The literature search was confined to (a) compounds containing a benzamide-type fragment accompanied by an additional functional group capable of acting as a hydrogen-

bond acceptor only (such as –NO_2,-OMe -CN, -Cl, -Br), and (b) compounds comprising a N-heterocyclic fragment substituted with an amide moiety, Figure 2.3.

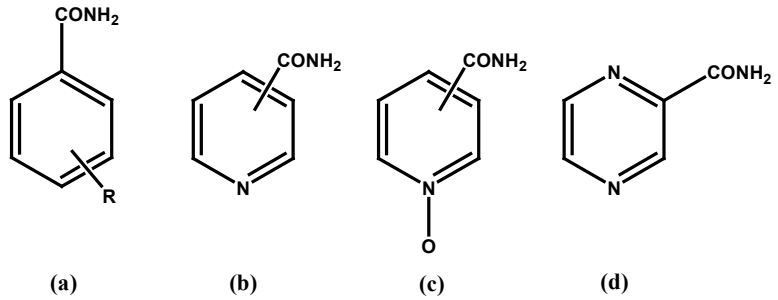

Figure 2.3 CSD search parameters; (a) substituted benzamides; (b) isonicotinamide and nicotinamide; (c) N-Oxide of isonicotinamide and nicotinamide; (d) pyrazine amide).

The combination of our new structural data with relevant information from the CSD produces a sufficiently large number of structures to enable us to explicitly address three questions:

I. How reliable is the amide ladder in the organic solid state if competing hydrogen-bond sites are present?

II. How reliable is the amide•••amide dimer in the presence of competing hydrogen-bond acceptors?

III. Is it possible to rank different functional groups according to how likely they are to disrupt the ladder by interacting with the amino *anti* hydrogen atom of the amide moiety?

2.2 Experimental

2.2.1 Synthesis

All chemicals were purchased from Aldrich and Fischer and used without further purification. 4-Bromo-3,5-dimethylpyrazole was synthesised via a previously published procedure.[14] Melting points were determined on a Fisher-Johns melting point apparatus and are uncorrected.

2.2.1.1 Synthesis of 4-[(pyrazol-1-yl)methyl]benzonitrile, 1

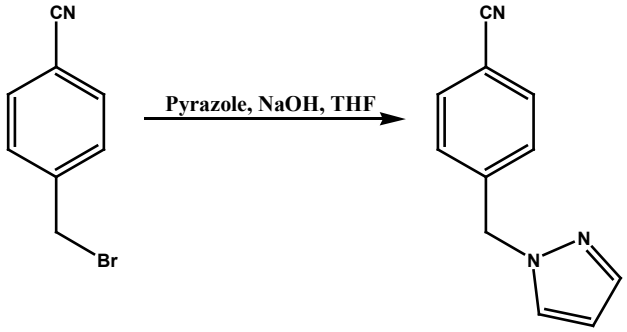

To a round bottom flask, pyrazole (1.50g, 22.1mmol) and THF (80mL) were added. To this solution, NaOH pellets (8.82g, 221mmol) were added and the reaction was stirred at room temperature for 2 hours. On completion of the stir, α-bromo-*p*-tolunitrile (4.32g, 22.1mmol) in THF (80mL) was added and the reaction mixture stirred at room temperature overnight. On completion, water was added to dissolve any excess NaOH, the organic layer was separated off, dried over $MgSO_4$ and the solvent removed under vacuum to yield **1** as a white solid (3.36g, 83.3%). Mp: 71-73^oC. ^1H NMR (δ_H; 400MHz, $CDCl_3$): 5.39 (s, 2H), 6.34 (t, J = 2.2Hz, 1H), 7.24 (d, J = 8Hz, 2H), 7.45 (s, 1H), 7.58 (s, 1H), 7.62 (d, J = 8.4Hz, 2H), Figure B.1; IR (KBr pellet): υ 3112, 2939, 2223, 1620, 1501, 1448, 1388, 1275, 1076, 1036, 950, 824, 745 cm^{-1}.

2.2.1.2 Synthesis of 4-[(pyrazol-1-yl)methyl]benzamide, 2

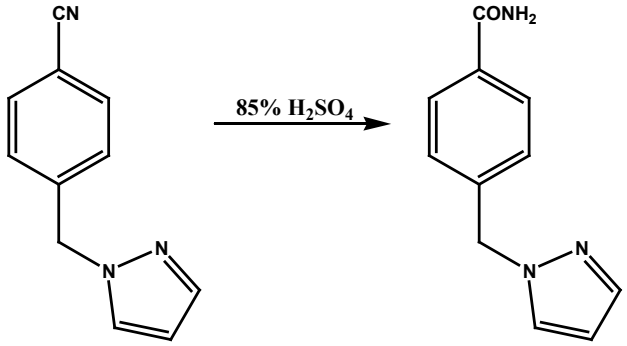

To a round bottom flask, 4-[(pyrazol-1-yl)methyl]benzonitrile (2.86g, 15.6mmol) and 85% H_2SO_4 (12mL) were added. The mixture was heated to 80^oC and stirred for 4 hours. On completion, the solution was poured slowly over ice and the resulting brown solution was adjusted to basic pH using 5M NaOH. The aqueous solution was washed with $CHCl_3$ and the organic extracts were separated, dried over $MgSO_4$ and reduced to yield **2** as a white solid (2.63g, 83.7%). Colourless plates suitable for X-ray diffraction were obtained via slow

evaporation of ethanol. Mp: 135-137°C. ^{1}H NMR, (δ_H; 400MHz, $CDCl_3$): 5.39 (s, 2H), 5.79 (s, 1H), 6.12 (s, 1H), 6.32 (t, *J* = 2 Hz, 1H), 7.25 (d, *J* = 8Hz, 2H), 7.43 (d, *J* = 2.4Hz, 1H), 7.58 (d, *J* = 1.6Hz, 1H), 7.78 (d, *J* = 4.4Hz, 2H), Figure B.2a; ^{13}C NMR, (δ_C; 100MHz, $CDCl_3$): 55.42, 106.30, 127.64 127.91, 129.46, 133.03, 139.95, 140.91, 168.65, Figure B.2b; IR (KBr pellet): *υ* 3370, 3171, 3019, 2926, 1660, 1408, 1302, 1143, 924, 758 cm^{-1}. MS: *m/z* = 201.983.

2.2.1.3 Synthesis of 4-[(3,5-dimethylpyrazol-1-yl)methyl]benzonitrile, 3

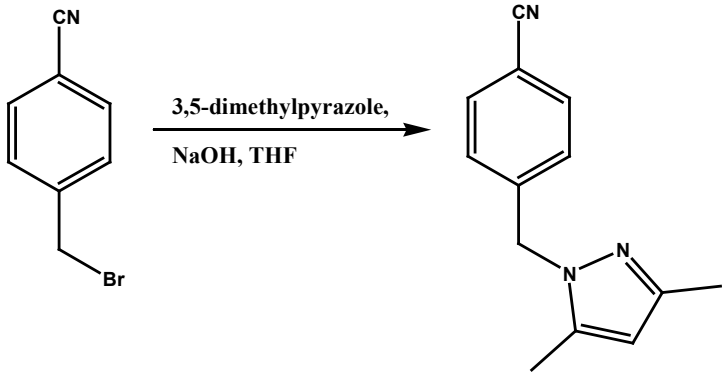

To a round bottom flask, 3,5-dimethylpyrazole (0.500g, 5.20mmol) and THF (25mL) were added. To this solution, NaOH pellets (2.10g, 52.0mmol) were added and the reaction was stirred at room temperature for 2 hours. On completion, α-bromo-*p*-tolunitrile (1.04g, 5.20mmol) in THF (25mL) was added and the reaction mixture stirred at room temperature for 3 days. On completion, water was added to dissolve any excess NaOH, the organic layer was separated off, dried over $MgSO_4$ and the solvent removed under vacuum to yield **3** as a white solid (0.936g, 85.0%). Mp: 63-65°C. ^{1}H NMR (δ_H; 400MHz, $CDCl_3$): 2.14 (s, 3H), 2.22 (s, 3H), 5.26 (s, 2H), 5.88 (s, 1H), 7.14 (d, *J* = 8.4Hz, 2H), 7.54 (d, *J* = 8.4Hz, 2H) , Figure B.3; IR (KBr pellet): *υ* 3053, 2909, 2233, 1603, 1557, 1306, 1030, 810, 769, 549 cm^{-1}.

2.2.1.4 Synthesis of 4-[(3,5-dimethylpyrazol-1-yl)methyl]benzamide, 4

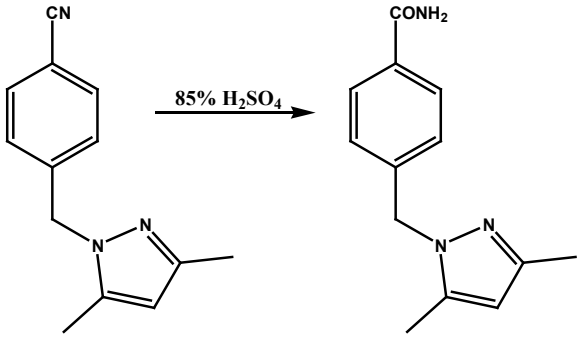

To a round bottom flask, 4-[(3,5-dimethylpyrazol-1-yl)methyl]benzonitrile (11.0g, 52.1mmol) and 85% H_2SO_4 (100mL) were added. The mixture was heated to 80°C and stirred for 4 hours. On completion, the solution was poured slowly over ice and the resulting brown solution was adjusted to basic pH using 5M NaOH. The aqueous solution was washed with $CHCl_3$ and the organic extracts were separated, dried over $MgSO_4$ and reduced to yield **4** as a white solid (5.99g, 50.0%). Colourless plates suitable for X-ray diffraction were obtained via slow evaporation of ethanol. Mp: 172-175°C. ^{1}H NMR, (δ_H; 400MHz, $CDCl_3$): 2.14 (s, 3H), 2.25 (s, 3H), 5.24 (s, 2H), 5.87 (s, 1H), 6.54 (s, 2H), 7.09 (d, J = 8.4Hz, 2H), 7.74 (d, J = 8.4Hz, 2H) , Figure B.4a; ^{13}C NMR, (δ_C; 100MHz, $CDCl_3$): 11.26, 13.60, 52.26, 106.07, 126.93, 128.06, 132.70, 139.70, 141.62, 148.09 169.41, Figure B.4b; IR (KBr pellet): υ 3447, 1680, 1644, 1414, 1383, 1306, 1117 cm^{-1}. MS: m/z = 230.022.

2.2.1.5 Synthesis of 4-[(4-bromo-3,5-dimethylpyrazol-1-yl)methyl]benzonitrile, *5*

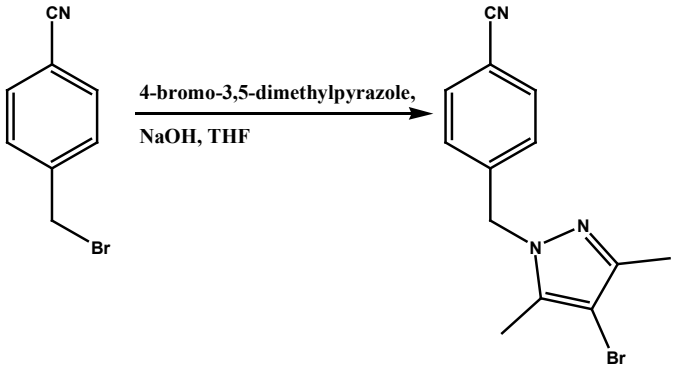

To a round bottom flask, 4-bromo-3,5-dimethylpyrazole (0.500g, 2.86mmol) and THF (25mL) were added. To this solution, NaOH pellets (1.14g, 28.6mmol) were added and the reaction was stirred at room temperature for 2 hours. On completion, α-bromo-*p*-tolunitrile (0.560g, 2.86mmol) in THF (25mL) was added and the reaction mixture stirred at room temperature for 2 days. On completion, water was added to dissolve any excess NaOH, the organic layer was separated off, dried over $MgSO_4$ and the solvent removed under vacuum to yield **5** as a white solid (2.08g, 81.5%). Mp: 76-79°C. ^{1}H NMR (δ_H; 400MHz, $CDCl_3$): 2.17 (s, 3H), 2.27(s, 3H), 5.33 (s, 2H), 7.19 (d, J = 16.4Hz, 2H), 7.63 (d, J = 16.8Hz, 2H) , Figure B.5; IR (KBr pellet): υ 3068, 2919, 2238, 1603, 1547, 1511, 1465, 1414, 1347, 1281, 1214, 1055, 810, 543 cm^{-1}.

2.2.1.6 Synthesis of 4-[(4-bromo-3,5-dimethylpyrazol-1-yl)methyl]benzamide, 6

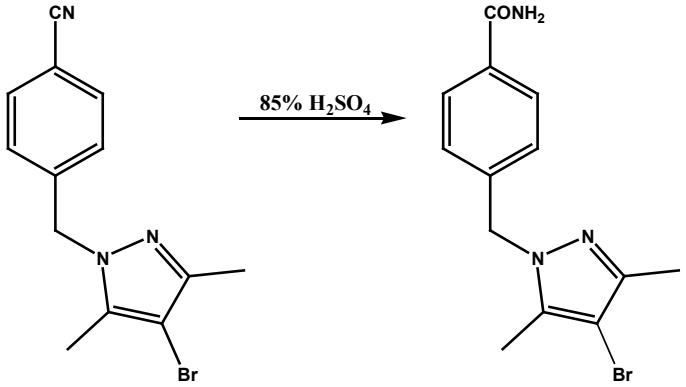

4-[(4-Bromo-3,5-dimethylpyrazol-1-yl)methyl]benzonitrile (2.08g, 8.57mmol) and 85% H_2SO_4 (20mL) were added to a round bottom flask,. The mixture was heated to 80°C and stirred for 4 hours. On completion of the stir, the solution was poured slowly over ice and the resulting brown solution was adjusted to basic pH using 5M NaOH. The aqueous solution was washed with ethyl acetate and the organic extracts were separated, dried over $MgSO_4$ and reduced to yield **6** as a white solid (1.49g, 69.0%). Colourless prisms suitable for X-ray diffraction were obtained from slow evaporation of acetonitrile. Mp: 195-198°C. ^{1}H NMR, (δ_H; 400MHz, $CDCl_3$): 2.15 (s, 3H), 2.25 (s, 3H), 5.28 (s, 2H), 5.84 (s, 1H), 5.98 (s, 1H), 7.15 (d, J = 8Hz, 2H), 7.77 (d, J = 8Hz, 2H) , Figure B.6a; ^{13}C NMR, (δ_C; 100MHz, DMSO-d^6): 9.95, 12.04, 52.53, 93.27, 126.80, 127.85, 133.55, 137.27, 140.26, 144.88, 167.56, Figure B.6b; IR (KBr pellet): υ 3339, 3186, 1670, 1624, 1388, 1071, 717, 692, 646 cm^{-1}. MS: m/z = 307.969, 309.968.

2.2.1.7 Synthesis of 3-[(pyrazol-1-yl)methyl]benzonitrile, 7

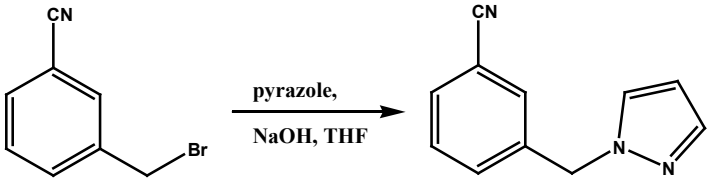

To a round bottom flask, pyrazole (1.50g, 22.1mmol) and THF (80mL) were added. To this solution, NaOH pellets (8.82g, 221mmol) were added and the reaction was stirred at room temperature for 2 hours. On completion, α-bromo-*m*-tolunitrile (4.32g, 22.1mmol) in THF (80mL) was added and the reaction mixture stirred at room temperature overnight. On completion, water was added to dissolve any excess NaOH, the organic layer separated off, dried over $MgSO_4$ and the solvent removed under vacuum to yield **7** as a yellow oil (3.42g, 84.7%).

^{1}H NMR (δ_H; 400MHz, $CDCl_3$): 5.20 (s, 2H), 6.18 (t, *J* = 4Hz, 1H), 7.26 (s, 1H), 7.28 (d, *J* = 2.8Hz 2H), 7.36 (t, *J* = 2.2Hz 1H), 7.38 (d, *J* = 4.4Hz, 1H), 7.43 (d, *J* = 2Hz, 1H), Figure B.7; IR (KBr pellet): *υ* 3119, 2930, 2231, 1583, 1511, 1434, 1395, 1291, 1089, 1055, 974, 685 cm^{-1}.

2.2.1.8 Synthesis of 3-[(pyrazol-1-yl)methyl]benzamide, 8

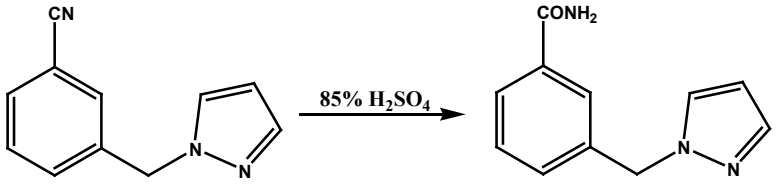

To a round bottom flask, 3-[(pyrazol-1-ylmethyl)]benzonitrile (2.59g, 14.1mmol) and 85% H_2SO_4 (10mL) were added. The mixture was heated to 80^{o}C and stirred for 4 hours. On completion of the stir, the solution was poured slowly over ice and the resulting brown solution was adjusted to basic pH using 5M NaOH. The aqueous solution was washed with $CHCl_3$ and the organic extracts were separated, dried over $MgSO_4$ and reduced to yield **8** as a pale yellow solid (1.24g, 44.0%). Colourless blocks suitable for X-ray diffraction were obtained via slow evaporation of ethanol. Mp: 117-120^{o}C. ^{1}H NMR (δ_H; 400MHz, $CDCl_3$): $CDCl_3$, 5.37 (s, 2H), 5.87 (s, 1H), 6.18 (s, 1H), 6.31 (t, *J* = 2Hz, 1H), 7.36 (d, *J* = 7.6Hz, 1H), 7.42 (d, *J* = 8Hz, 1H), 7.44 (s, 1H), 7.57 (s, 1H), 7.70 (s, 1H), 7.73 (d, *J* = 7.6Hz, 1H), Figure B.8a; ^{13}C NMR, (δ_C; 100MHz, $CDCl_3$): 55.43, 106.30, 126.68, 126.97, 129.16, 129.58, 131.08, 133.94, 137.25, 139.76, 168.93, Figure B.8b; IR (KBr pellet): *υ* 3327, 3149, 1684, 1388, 1046, 769, 762 cm^{-1}. MS: *m/z* = 201.983.

2.2.1.9 Synthesis of 3-[(3,5-dimethylpyrazol-1-yl)methyl]benzonitrile, 9

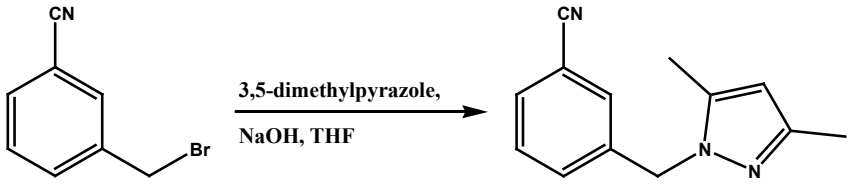

To a round bottom flask, 3,5-dimethylpyrazole (5.00g, 52mmol) and THF (125mL) were added. To this solution, NaOH pellets (21.0g, 520mmol) were added and the reaction was stirred at room temperature for 2 hours. On completion, α-bromo-*m*-tolunitrile (10.4g, 52mmol) in THF (125mL) was added and the reaction mixture stirred at room temperature for 3 days. On completion, water was added to dissolve any excess NaOH, the organic layer was separated off,

dried over $MgSO_4$ and the solvent removed under vacuum to yield **9** as a white solid (10.58g, 96.3%). Mp: 33-35°C. ^{1}H NMR (δ_H; 400MHz, $CDCl_3$): 2.17 (s, 3H), 2.25 (s, 3H), 5.24 (s, 2H), 5.89 (s, 1H), 7.30 (d, *J* = 15.2Hz, 2H), 7.43 (t, *J* = 15.2Hz, 1H), 7.54 (d, *J* = 14.8, 1H) , Figure B.9; IR (KBr pellet): *υ* 3112, 2939, 2223, 1620, 1501, 1448, 1388, 1275, 1076, 1036, 950, 824, 745 cm^{-1}.

2.2.1.10 Synthesis of 3-[(3,5-dimethylpyrazol-1-yl)methyl]benzamide, 10

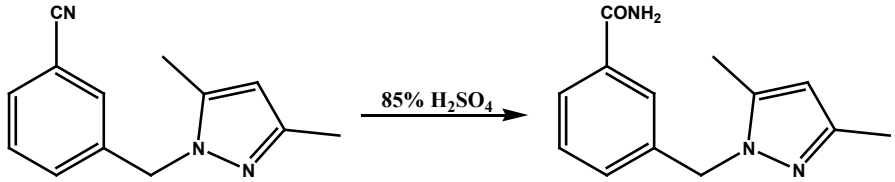

3-[(3,5-dimethylpyrazol-1-yl)methyl]benzonitrile (0.300g, 1.42mmol) and 85% H_2SO_4 (3mL) were added to a round bottom flask,. The mixture was heated to 80°C and stirred for 4 hours. On completion of the stir, the solution was poured slowly over ice and the resulting brown solution was adjusted to basic pH using 5M NaOH. The aqueous solution was washed with $CHCl_3$ and the organic extracts were separated, dried over $MgSO_4$ and reduced to yield **10** as a white solid (0.203g, 62.4%). Colourless plates suitable for X-ray diffraction were obtained via slow evaporation of ethanol. Mp: 158-161°C. ^{1}H NMR, (δ_H; 400MHz, $CDCl_3$): 2.15 (s, 3H), 2.24 (s, 3H), 5.24 (s, 2H), 5.86 (s, 1H), 5.95 (s, 1H), 6.21 (s, 1H), 7.20 (d, *J* = 8Hz, 1H), 7.38 (t, *J* = 7.6 Hz, 1H), 7.57 (s, 1H), 7.69 (d, *J* = 7.6Hz, 1H) , Figure B.10a; ^{13}C NMR, (δ_C; 50MHz, $CDCl_3$): 11.17, 13.54, 52.17, 105.83, 125.70, 126.54, 129.13, 130.25, 133.86, 138.11, 139.38, 147.97, 169.00, Figure B.10b; IR (KBr pellet): *υ* 3355, 3288, 3140, 2919, 1680, 1603, 1547, 1455, 1373, 784, 707 cm^{-1}. MS: *m/z* = 230.033.

2.2.1.11 Synthesis of 3-[(4-bromo-3,5-dimethylpyrazol-1-yl)methyl]benzonitrile, 11

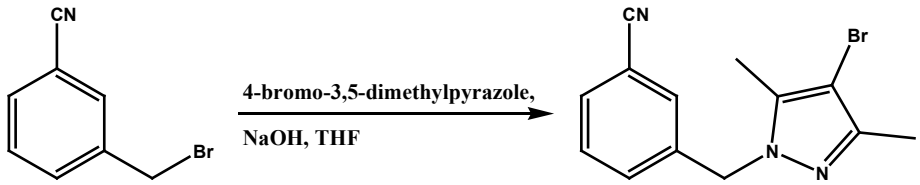

To a round bottom flask, 4-bromo-3,5-dimethylpyrazole (1.50g, 8.57mmol) and THF (25mL) were added. To this solution, NaOH pellets (3.43g, 85.7mmol) were added and the reaction was stirred at room temperature for 2 hours. On completion, α-bromo-*m*-tolunitrile

(1.68g, 8.57mmol) in THF (25mL) was added and the reaction mixture stirred at room temperature for 2 days. On completion, water was added to dissolve any excess NaOH, the organic layer was separated off, dried over $MgSO_4$ and the solvent removed under vacuum to yield **11** as a white solid (2.25g, 90.5%). Mp: 72-75^oC. ^1H NMR (δ_H; 200MHz, $CDCl_3$): 2.17 (s, 3H), 2.22 (s, 3H), 5.27 (s, 2H), 7.35 (d, *J* = 7.8Hz, 2H), 7.44 (t, *J* = 7.4Hz, 1H), 7.55 (d, *J* = 7.8Hz, 1H), Figure B.11; IR (KBr pellet): *υ* 3027, 2925, 2228, 1542, 1470, 1265, 1070, 907, 804, 702 cm^{-1}.

2.2.1.12 Synthesis of 3-[(4-bromo-3,5-dimethylpyrazol-1-yl)methyl]benzamide, *12*

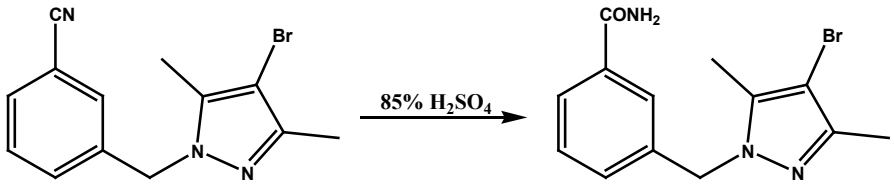

To a round bottom flask, 3-[(4-bromo-3,5-dimethylpyrazol-1-yl)methyl]benzonitrile (0.300g, 1.03mmol) and 85% H_2SO_4 (3mL) were added. The mixture was heated to 80^oC and stirred for 4 hours. On completion, the solution was poured slowly over ice and the resulting brown solution was adjusted to basic pH using 5M NaOH. The aqueous solution was washed with chloroform and the organic extracts were separated, dried over $MgSO_4$ and reduced to yield **12** as a white solid (0.125g, 39.0%). Colourless plates suitable for X-ray diffraction were obtained from the co-crystallisation reaction with fumaric acid via slow evaporation of acetonitrile. Mp: 133-136^oC. ^1H NMR, (δ_H; 200MHz, $CDCl_3$): 2.150 (s, 3H), 2.22 (s, 3H), 5.24 (s, 2H), 6.51 (s, 2H), 7.19 (d, *J* = 7.8Hz, 1H), 7.28-7.40 (m, *J* = 8Hz, 1H), 7.64 (s, 1H), 7.70 (d, *J* = 7.8Hz, 1H) , Figure B.12a; ^{13}C NMR, (δ_C; 50MHz, $CDCl_3$): 10.41, 12.32, 53.40, 94.78, 126.00, 126.74, 129.15, 130.25, 134.06, 137.20, 137.42, 146.49, 169.31, Figure B.12b; IR (KBr pellet): *υ* 3355, 3165, 2919, 1660, 1409, 1296, 1066, 805, 738, 661. MS: *m/z* = 307.985, 309.985 cm^{-1}.

2.3 Results

All hydrogen bond geometries are listed in Table 2.1. A summary of the crystallographic information for each compound is displayed in Tables A.1-A.6.

Table 2.1 Hydrogen bond geometries for **2**, **4**, **6**, **8**, **10** and **12.**

Compound	D-H···A	D-H / Å	H···A / Å	D···A / Å	<(DHA) / °
2[i]	N(17)-H(17A)...O(17)#1	0.97(2)	1.93(2)	2.899(2)	176.4(17)
	N(17)-H(17B)...O(17)#2	0.86(2)	2.09(2)	2.938(2)	167(2)
4[ii]	N(17)-H(17A)...O(17)#1	0.85(2)	2.08(2)	2.913(2)	168.3(19)
	N(17)-H(17B)...N(22)#2	0.91(2)	2.23(2)	3.112(2)	162.7(17)
6[iii]	N(27)-H(27A)...O(27)#1	0.819(17)	2.137(17)	2.9488(15)	171.0(16)
	N(27)-H(27B)...N(12)#2	0.808(17)	2.249(17)	3.0341(15)	163.9(16)
8[iv]	N(27)-H(27A)...O(27)#1	0.901(15)	2.018(15)	2.9183(11)	177.2(13)
	N(27)-H(27B)...N(12)#2	0.857(15)	2.208(15)	3.0580(12)	170.9(14)
10[v]	N(17)-H(17A)...O(17)#1	0.914(15)	2.002(15)	2.9033(12)	168.4(12)
	N(17)-H(17B)...N(22)#2	0.921(14)	2.110(14)	2.9997(12)	161.9(12)
12[vi]	N(27)-H(27A)...N(32)	0.88	1.85	2.709(7)	164.9
	N(47)-H(47A)...N(12)#1	0.88	1.83	2.671(6)	160.1

i) #1 -x,-y+1,-z, #2 x,-y+1/2,z+1/2; ii) #1 -x,-y+2,-z, #2 x,y+1,z; iii) #1 -x,-y+1,-z, #2 x-1/2,-y+3/2,z-1/2; iv) #1 -x+2,-y,-z+1, #2 -x+1,-y+1,-z+1; v) #1 -x+2,-y+1,-z+1, #2 -x+1,-y+1,-z+1; vi) #1 x,y+1,z-1

2.3.1 MEP surface calculations

In order to rank the hydrogen bonding capability of the N-heterocyclic compounds included in this study, we also calculated molecular electrostatic potential (MEP) surfaces for all compounds,[15] Table 2.2 and Figure 2.4. It has previously been shown[16] that such an approach is feasible even if the calculations are performed at a relatively low level of theory (AM1), which makes this a versatile and readily accessible tool.

Table 2.2 Molecular electrostatic surface potential calculations.

Ligand	*E*(N) kJ/mol
Isonicotinamide	-247
Nicotinamide	-255
Pyrazine	-237 & -178
3-[Benzimidazol-1-yl) methyl]-benzamide	-285
3-[(2-Chlorobenzimidazol-1-yl)methyl]-benzamide	-277
4-[(2-Methylbenzimidazol-1-yl)methyl]-benzamide	-303

Ligand	$E(N_{PZ})$ kJ mol^{-1}
2	-236
4	-246
6	-229
8	-255
10	-262
12	-239

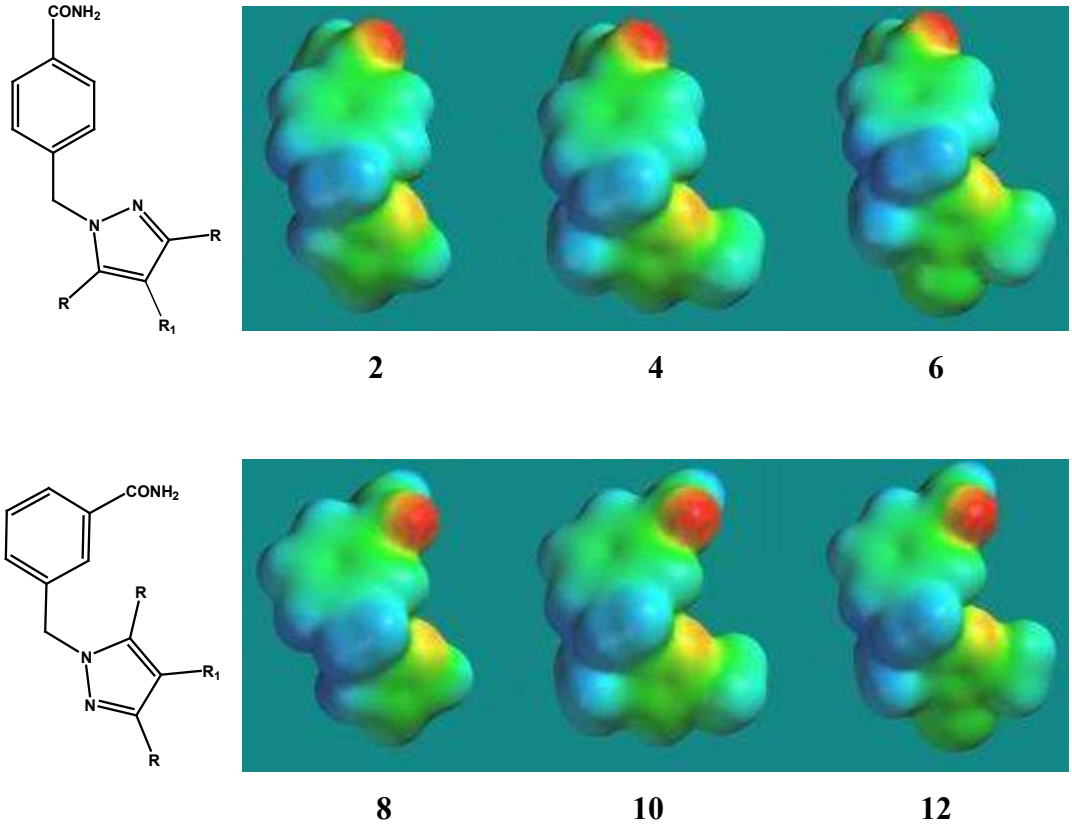

Figure 2.4 Molecular electrostatic potential surfaces for (pyrazol-1-yl)methyl benzamide ligands.

2.3.2 Crystal structure of 4-[(pyrazol-1-yl)methyl]benzamide, 2

The primary intermolecular motif in the crystal structure of **2** is an amide-amide dimer constructed from two symmetry related N-H•••O hydrogen bonds (2.899(2)Å). These dimers are subsequently linked into an infinite 1-D chain via secondary N-H•••O interactions (2.938(2)Å)

between the *anti* amide hydrogen atom and the carbonyl oxygen of an adjacent amide, Figure 2.5.

Although a 'classic' ladder is not formed, the same hydrogen-bond interactions are present in the structure of **2**, as those that combine to form a ladder motif. The potentially competing hydrogen-bond acceptor, the pyrazole moiety, does not participate in any strong hydrogen bonds.

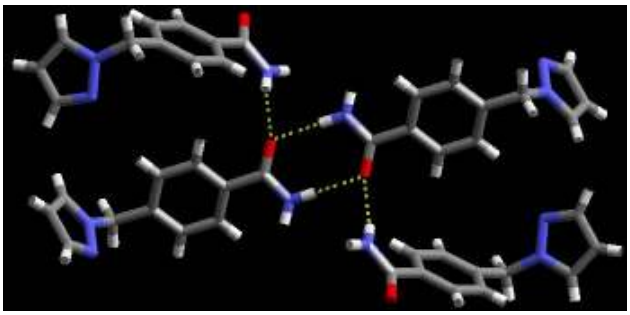

Figure 2.5 The dominating intermolecular hydrogen bonds observed in the crystal structure of **2**.

2.3.3 Crystal structure of 4-[(3,5-dimethylpyrazol-1-yl)methyl]benzamide, 4

The crystal structure of **4** again shows the formation of the symmetry related homomeric amide:amide dimer via N-H•••O hydrogen bonds (2.913(2)Å), Figure 2.6. The network is extended via secondary N-H•••N interactions (3.112(2)Å) between the *anti* amide hydrogen atom and the pyrazole nitrogen of an adjacent ligand which demonstrates how the ladder can be disrupted by a suitably competitive acceptor.

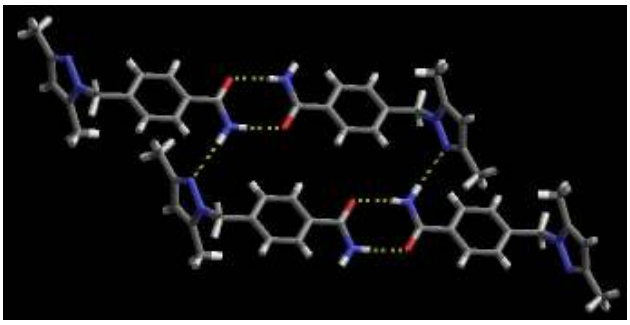

Figure 2.6 Hydrogen-bond dimers (constructed from an amide•••amide synthon) observed in the crystal structure of **4**. Dimers are interconnected via N-H•••N interactions.

2.3.4 Crystal structure of 4-[(4-bromo-3,5-dimethylpyrazol-1-yl)methyl]benzamide, 6

The crystal structure of **6** contains homomeric dimers between two amide moieties via N-H•••O hydrogen bonds (2.9488(15)Å), Figure 2.7. Again, the *anti* hydrogen atom of the amide forms a N-H•••N hydrogen bond (3.0341(15)Å) to an adjacent pyrazole moiety. The bromo substituent on the pyrazole is not participating in any specific or directional non-covalent interactions.

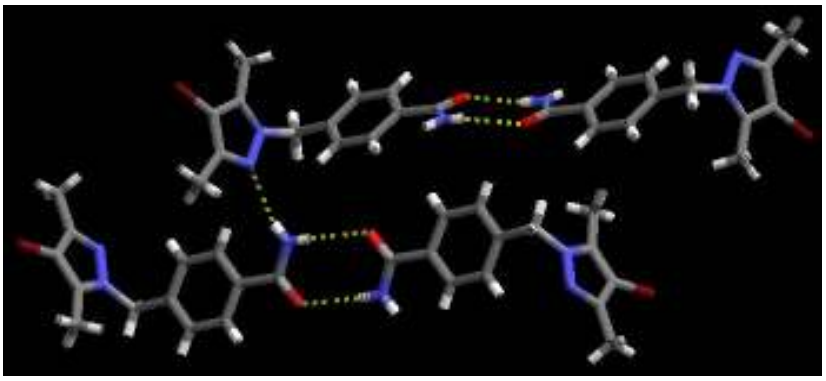

Figure 2.7 Homomeric amide•••amide dimer observed in the crystal structure **6**. Dimers are extended via N-H•••N hydrogen bonds.

2.3.5 Crystal structure of 3-[(pyrazol-1-yl)methyl]benzamide, 8

The N-H•••O hydrogen bond (2.9183(11)Å) is again observed in the crystal structure of **8** resulting in a homomeric amide synthon, Figure 2.8. Dimers interact via secondary N-H•••N interactions (3.0580(12)Å) between the *anti* amide hydrogen atom and an adjacent pyrazole site. The result is a 1:1 cyclic motif, which, combined with the amide•••amide dimer, leads to an extended 1-D motif.

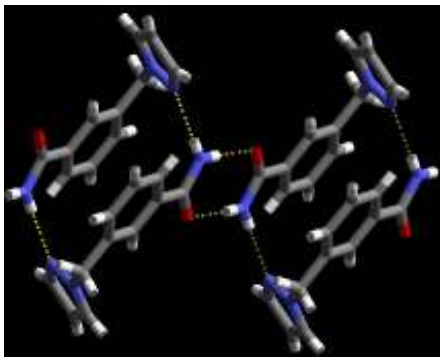

Figure 2.8 Hydrogen-bond dimers (constructed from an amide•••amide synthon) observed in the crystal structure of **8**. Dimers are interconnected via N-H•••N interactions.

2.3.6 Crystal structure of 3-[(3,5-dimethylpyrazol-1-yl)methyl]benzamide, 10

The crystal structure of **10** shows the same type of arrangement observed in **8** with the formation of the self-complementary amide•••amide dimer via N-H•••O hydrogen bonds (2.9033(12)Å), Figure 2.9. The network is extended into the cyclic type arrangement via secondary N-H•••N interactions (2.9997(12)Å) between the *anti* amide hydrogen atom and the pyrazole nitrogen of an adjacent ligand.

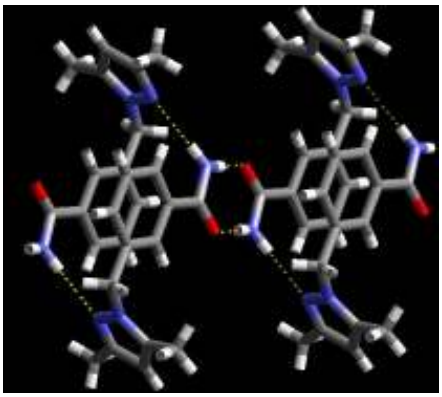

Figure 2.9 Hydrogen-bond dimers (constructed from an amide•••amide synthon) observed in the crystal structure of **10**. Dimers are interconnected via N-H•••N interactions.

2.3.7 Crystal structure of 3-[(4-bromo-3,5-dimethylpyrazol-1-yl)methyl]benzamide, 12

The crystal structure of **12** is quite different from the other compounds in this study demonstrating how simple changes in molecular conformation and structure can play a major role in determining the overall arrangement in the solid-state structure. The primary motif in **12**, is a 1-D chain resulting from N-H•••N hydrogen bonds between the *syn* amide hydrogen atom and the pyrazole nitrogen, Figure 2.10. Each ligand possesses two different N-H•••N interactions with distances of 2.709(7)Å and (2.671(6)Å, respectively. The carbonyl moiety and the *anti* hydrogen atom of the amide functionality both interact with aromatic C-H groups and, as was the case in **6**, the bromo substituent on the pyrazole is not participating in any specific non-covalent interaction.

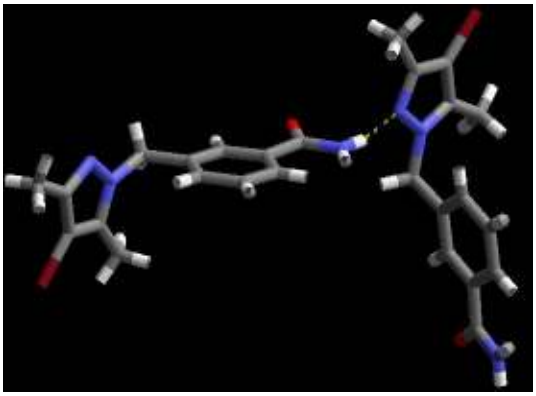

Figure 2.10 1-D chain via N-H•••N hydrogen bonds observed in the crystal structure of **12**.

2.4 Discussion

Although the new structures presented here offer some insight into the structural consequences of having the amide moiety presented with potentially disruptive hydrogen-bond moieties, it was necessary to complement our data with existing crystallographic information from the CSD[13] in order to identify structural patterns and trends. All compounds included in this search are listed in Tables 2.3 and 2.4, accompanied by their graph-set notation.[17]

Ten of the seventeen benzamides (59%) decorated with a weak hydrogen-bond acceptor (such as a halogen, nitro, cyano or methoxy substituent), contain the 'classic' $R_2^2(8)$ $R_4^2(8)$ ladder. It seems that moieties belonging to this group of relatively weak hydrogen-bond acceptors compete reasonably effectively for the *anti* hydrogen atom of the amide moiety leading to a disruption of the ladder. The amide•••amide dimer, on the other hand, is present in thirteen of the seventeen structures (76%).

Table 2.3 Graph-set notations for substituted benzamides (CSD codes in parentheses).

Ligand	N_1	N_2	N_3	N_4
2-Fluorobenzamide **(BIGSUF)**	$2\,C_1^1(4)$ 2D	$4C_2^2(4)\ R_2^2(8)$	$4C_3^2(7)$	$R_4^2(8)$
2-Chlorobenzamide #1 **(CLBZAM10)**	$C_1^1(4)\ R_2^2(8)$	$R_4^2(8)$	N/A	N/A
2-Chlorobenzamide #2 **(CLBZAM11)**	$2C_1^1(4)$	$C_2^2(8)$	N/A	N/A
2-Iodobenzamide **(IBNZAM)**	$C_1^1(4)\ R_2^2(8)$	$R_4^2(8)$	N/A	N/A
3-Fluorobenzamide **(BENAFM10)**	$C_1^1(4)\ R_2^2(8)$	$R_4^2(8)$	N/A	N/A
3-Bromobenzamide **(BRBZAM)**	$C_1^1(4)$	N/A	N/A	N/A
3-Iodobenzamide **(DUMNUU)**	$C_1^1(4)\ R_2^2(8)$	$R_4^2(8)$	N/A	N/A
4-Fluorobenzamide **(BENAFP01)**	$C_1^1(4)\ R_2^2(8)$	$R_4^2(8)$	N/A	N/A
4-Bromobenzamide #1 **(BBEZAM)**	$C_1^1(4)\ R_2^2(8)$	$R_4^2(8)$	N/A	N/A
4-Bromobenzamide #2 **(BBEZAM01)**	$C_1^1(4)\ R_2^2(8)$	$R_4^2(8)$	N/A	N/A
4-Iodobenzamide **(IOBZAM)**	$C_1^1(4)\ R_2^2(8)$	$R_4^2(8)$	N/A	N/A
2-Nitrobenzamide **(ONBZAM)**	$C_1^1(4)\ R_2^2(8)$	$R_4^2(8)$	N/A	N/A
3-Nitrobenzamide **(JACYOB)**	$C_1^1(4)\ R_2^2(8)$	$C_3^2(8)$	N/A	N/A
4-Nitrobenzamide #1 **(NTBZAM01)**	$C_1^1(4)\ R_2^2(8)$	$C_4^4(18)$	N/A	N/A
4-Nitrobenzamide #2 **(NTBZAM11)**	$C_1^1(4)\ 2C_1^1(9)$	$R_1^2(4)\ 2R_4^4(24)$	$C_3^3(22)$	N/A
3-Cyanobenzamide **(WUKHUF)**	$R_2^2(8)\ R_2^2(16)$	$C_4^4(20)$	N/A	N/A
2-Methoxybenzamide **(RECQIA)**	$2C_1^1(4)$	$C_2^2(8)$	N/A	N/A

#1-polymorph 1; #2-polymorph 2

However, the introduction of a more competitive hydrogen-bond acceptor, such as an N-heterocyclic moiety does create major disruptions to amide•••amide interactions, Table 2.4.

When an N-heterocyclic compound (or the corresponding N-oxide) is present on the same molecular backbone as the amide itself, the ladder does not survive in any of the eighteen

cases examined in this study. Instead, in eleven of eighteen structures, neighboring amide•••amide dimers are connected into a chain-like motif and in the remaining seven cases, not even the amide•••amide dimer survives.

Table 2.4 Graph-set notations for N-heterocycles (CSD codes in parentheses).

Ligand	N_1	N_2	N_3	N_4
Isonicotinamide #1 **(EHOWIH01)**	$C_1^1(4)\ R_2^2(8)$	$C_4^3(12)$	N / A	N / A
Isonicotinamide #2 **(EHOWIH02)**	$2\,C_1^1(4)\ 2\,C_1^1(7)$	$2R_4^4(20)$	N / A	N / A
Nicotinamide **(NICOAM01)**	$C_1^1(4)\ C_1^1(6)$	$R_4^4(18)$	N / A	N / A
Pyrazine carboxamide #1 **(PYRZIN02)**	$R_2^2(8)$	N / A	N / A	N / A
Pyrazine carboxamide #2 **(PYRZIN01)**	$C_1^1(4)\ R_2^2(8)$	$C_4^3(12)$	N / A	N / A
Pyrazine carboxamide #3 **(PYRZIN15)**	$R_2^2(8)\ R_2^2(10)$	$C_4^4(14)$	N / A	N / A
Isonicotinamide N-Oxide **(MEGDAE)**	$2\,C_1^1(8)$	$C_4^4(32)$	N / A	N / A
Nicotinamide N-Oxide **(MEGDEI)**	$C_1^1(7)\ R_2^2(14)$	$C_4^3(18)$	N / A	N / A
Pyrazine carboxamide N-Oxide **(MEGDUY)**	3D	$2\,R_4^2(8)\ R_4^4(28)$	$C_5^5(32)$	N / A
3-[Benzimidazol-1-yl) methyl]-benzamide **(WANBUJ)**	4D	$2C_4^4(24)\ 2C_4^4(28)$ $R_2^2(8)\ R_2^2(20)$	$2\,C_4^3(18)$	$R_4^4(26)$
3-[(2-Chlorobenzimidazol-1-yl)methyl]-benzamide **(WANCEU)**	4D	$2C_4^4(24)\ 2C_4^4(28)$ $R_2^2(8)\ R_2^2(20)$	$2\,C_4^3(18)$	$R_4^4(26)$
4-[(2-Methylbenzimidazol-1-yl)methyl]-benzamide **(WANCAQ)**	$C_1^1(4)$	$C_1^1(11)$	N / A	$C_4^4(26)$
2	$C_1^1(4)\ R_2^2(8)$	$C_4^3(12)$	N / A	N / A
4	$C_1^1(10)\ R_2^2(8)$	$R_4^4(24)$	N / A	N / A
6	$C_1^1(10)\ R_2^2(8)$	$R_4^4(24)$	N / A	N / A
8	$R_2^2(8)\ R_2^2(18)$	$C_4^4(22)$	N / A	N / A
10	$R_2^2(8)\ R_2^2(18)$	$C_4^4(22)$	N / A	N / A
12	2D	$C_4^4(36)$	N / A	N / A

#1-polymorph 1; #2-polymorph 2; #3-polymorph 3

We are now in a position to provide answers to the questions posed at the beginning of this study.[18] The ladder is shown to persist in 10 of the 35 structures (29%) examined herein, whereas the amide•••amide dimer is present in 24 of the 35 structures (69%). There is a dramatic difference to the way in which weak and strong hydrogen-bond acceptors influence the outcome in structures containing an amide moiety. For weak acceptors (such as $-NO_2$,-OMe -CN, -Cl, -Br), the frequency of ladder and amide disruption is 41% and 23% respectively.

However, with stronger hydrogen-bond acceptors (N-heterocycles and N-oxides thereof), the corresponding numbers are 100% and 39%, respectively. It is noteworthy that it is possible to provide a more detailed ranking of the hydrogen-bond accepting capability within the latter group even further. The calculated MEP values for the heterocycles included in this study, Table 2.2, indicate that pyrazine, pyrazole, and pyridine are expected to be less competitive than the benzimidazole/N-oxide acceptors. In fact, the dimer is broken 3/12 (25%) times for the former group, and 4/6 (67%) for the latter group. The hydrogen-bond acceptor strength as determined by calculated MEPs, which is consistent with reported pK_{HB} data,[19] is directly translated into structural consequences in these structures.

References

1. (a) L. MacGillivray, *Cryst. Eng. Comm.*, 2004, **6**, 77; (b) J. –M. Lehn, *Science*, 2002, **295**, 2400; (c) M. C. Etter, *J. Phys. Chem.*, 1991, **95**, 4601; (d) B. Moulton and M. J. Zaworotko, *Chem. Rev.*, 2001, **101**, 1629; (e) L. Pauling, The Nature of the Chemical Bond, Cornell University Press: Ithaca, NY, 1939; (f) J. –M. Lehn, *Angew. Chem. Int. Ed. Engl.*, 1990, **29**, 1304; (g) J. –M. Lehn, *Supramolecular Chemistry*, VCH, Weinheim, 1995. (h) J. W. Steed and J. L. Atwood, *Supramolecular Chemistry*, John Wiley and Sons Ltd, Chichester, 2000.
2. (a) S. Kim, K. Takeda and S. Sasatani, *Eur. Pat. Appl*., 1988; (b) B. T. Flatt, X. H. Gu, R. Martin, R. Mohan, B. Murphy, M. C. Nyman, W. C. Stevens, T. L. Wang and L. C. Bannen, *PCT Int. Appl.*, 2007.
3. D. A. P. Delnoye, R. P. Sijbesma, J. A. J. M. Vekemans and E. W. Meijer, *J. Am. Chem. Soc.*, 1996, **118**, 8717.
4. R. Kleppinger, C. P. Lillya and C. J. Yang, *J. Am. Chem. Soc*., 1997, **119**, 4097.
5. (a) H. Yu, H. Mizufune, K. Uenaka, T. Moritoki, K. Tatsuya and H. Koshima, *Tetrahedron*, 2005, **61**, 8932; (b) M. George, S. L. Snyder, P. Terech, C. J. Glinka and R. G. Weiss, *J. Am. Chem. Soc*., 2003, **125**, 10275; (c) R. E. Melendez, A. J. Carr, B. R. Linton and A. D. Hamilton, *Structure and Bonding*, 2000, **96**, 31.
6. M. Cavallini, F. Biscarini, S. Leon, F. Zerbetto, G. Bottari and D. A. Leigh, *Science*, 2003, **299**, 531.
7. (a) J. Bernstein, *J. Phys D: Appl. Phys.*, 1993, **26**, B66; (b) J. Bernstein, *Organic Solid State Chemistry*, G. R. Desiraju Ed. Elseveir: New York, 1987, **32**, 471.
8. G.R. Desiraju, *Angew. Chem. Int. Ed. Engl.*, 1995, **34**, 2311.
9. (a) G. R. Desiraju, *Crystal Engineering The Design of Organic Solids*, Elsevier: New York, 1989 54; (b) G. R. Desiraju, *Acc. Chem. Res.*, 2002, 35, 565; (c) C. B. Aakeröy and D. J. Salmon, *Cryst. Eng. Comm.*, 2005, **7**, 439.
10. G. A. Jeffrey and W. Saenger, *Hydrogen Bonding in Biological Structures*, Springer-Verlag: Berlin, Heidelberg, New York, 1991.
11. (a) L. Leiserowitz and A. T. Hagler, *Proc. Soc. R. Lond. A*, 1983, **388**, 133; (b) S.S. Kuduva, D. Bläser, R. Boese and G. R. Desiraju, *J. Org. Chem.*, 2001, **66**, 1621.

12. (a) M. Tonogaki, T. Kawata, S. Ohba, Y. Iwata and I. Shibuya, *Acta Crystallogr. Sect .B*, 1993, **49**, 1031; (b) F. di Rienzo, A. Domenicano and E. Foresti Serantoni, *Acta Crystallogr. Sect. B*, 1977, **33**, 3854; (c) P. G. Jones, H. Thonnessen, R. Schmutzler and A. K. Fischer, *Acta. Crystallogr.,Sect.E*, 2002, **58**, o1436.
13. Cambridge Structural Database version 5.28 (November 2006).
14. A. Osawa, T. Kaiho, T. Ito, M. Okada, C. Kawabata, K. Yamaguchi and H. Igeta, *Chem. Pharm. Bull*., 1988, **36**, 3638.
15. Molecular structures for **1-6** were constructed using Spartan '06 (Wavefunction, Inc. Irvine, CA). All six molecules were optimized using AM1, with the maxima and minima in the electrostatic potential surface (0.002 e/au isosurface) determined using a positive point charge in the vacuum as a probe.
16. C. A. Hunter, *Angew. Chem. Int. Ed*, 2004, **43**, 5310-5324.
17. (a) J. Bernstein, R. E. Davis, L. Shimoni and N.-L. Chang, *Angew. Chem. Int. Ed. Engl.*, 1995, **34**, 1555; (b) M. C. Etter, J. C. MacDonald and J. Bernstein, *Acta Crystallogr. Sect. B,* 1990, **46**, 256; (c) M. C. Etter, *Acc. Chem. Res.,* 1990, **23**, 120.
18. C. B. Aakeröy, B. M. T. Scott and J. Desper, *New. J. Chem*., 2007, **31**, 2044.
19. C. Laurence and M. Berthelot, *Persp. Drug Disc. Des.*, 2000, **18**, 39-60.

CHAPTER 3 - Breaking the amide•••amide homomeric dimer

3.1 Introduction

In supramolecular synthesis, desired products are typically held together by reversible intermolecular interactions, and therefore synthetic procedures normally have to take place in one-pot reactions.[1] For such reactions to be effective, a modular assembly process based upon a hierarchy of intermolecular hydrogen-bond interactions needs to be put in place.

A suitable starting point for developing a modular process is isonicotinamide, Figure 3.1, which has been shown[2] to be a reliable tool for the construction of binary co-crystals.

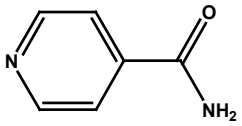

Figure 3.1 Isonicotinamide.

In 1:1 co-crystals of isonicotinamide and a carboxylic acid, the most commonly observed synthons are i) an acid-pyridine interaction via an O-H•••N hydrogen bond and ii) an amide-amide homomeric dimer via N-H•••O hydrogen bonds, Figure 3.2. A CSD[3] search revealed 96% of 1:1 binary co-crystals between isonicotinamide and a carboxylic acid contain these interactions. The consistency can be attributed to Etter's "best donor-best acceptor"[4] guideline as well as a need to satisfy all possible hydrogen-bond interactions. First, the pyridine nitrogen is the best hydrogen-bond acceptor and the carboxylic acid -OH is the best hydrogen-bond donor and consequently they have a preference toward each other. Second, the amide-amide dimer will form to satisfy the remaining hydrogen-bond donor/acceptors.

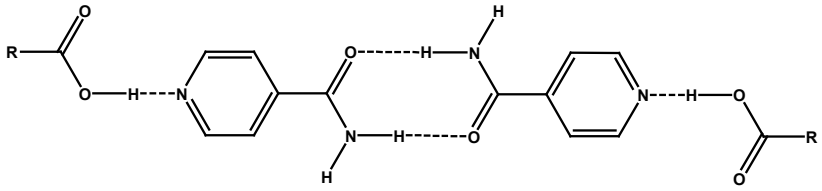

Figure 3.2 Typical 1:1 binary co-crystal of isonicotinamide and a mono carboxylic acid.

The hierarchy observed with co-crystals of isonicotinamide needs further investigation in order to establish if such a "ranking" has any real value. Unfortunately, isonicotinamide is not a suitable system in this context because it is not possible to modify one binding site without tampering with the other (i.e. adjusting the hydrogen-bond acceptor ability of the pyridine nitrogen through covalent modifications will also affect the nature of the amide site). Consequently, uncoupled amide-heterocycle supramolecular reagents (SR's), Figure 3.3 need to be constructed that will allow for electrostatic tuning of the heterocycle without affecting the amide functionality.

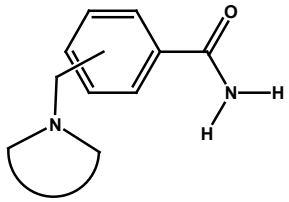

Figure 3.3 General design of decoupled amide-heterocycle species.

Uncoupled amide-heterocycle SR's were first developed using benzimidazole,[5] providing a system that has a better hydrogen-bond acceptor, based on molecular electrostatic potential (MEP) surfaces,[6] than isonicotinamide, Figure 3.4.

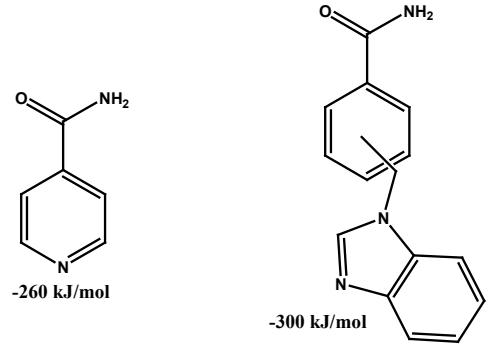

Figure 3.4 Isonicotinamide and benzimidazol-1-yl benzamide with MEP surface values.[7]

The 1:1 binary co-crystals of benzimidazol-1-yl benzamide and a carboxylic acid show the same connectivity as isonicotinamide co-crystals, with the carboxylic acid interacting (via an O-H•••N hydrogen bond) with the benzimidazole and the amide forming a self-complementary dimer, Figure 3.5.

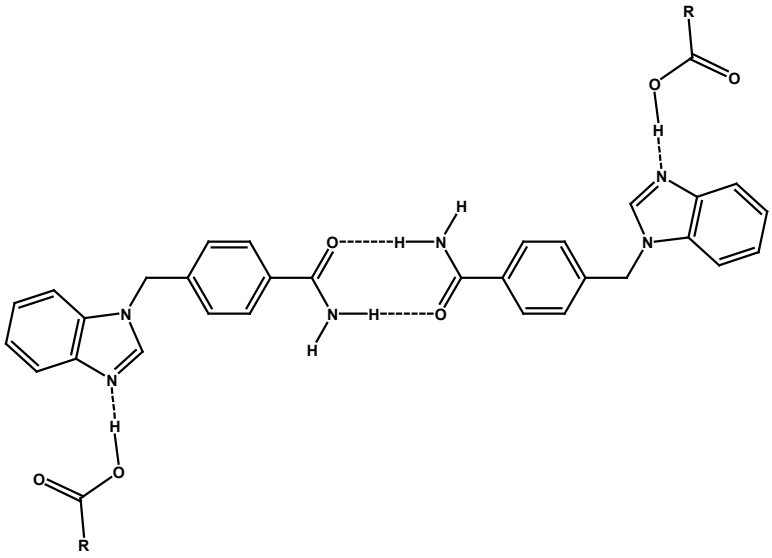

Figure 3.5 1:1 binary co-crystal of benzimidazol-1-yl benzamide and a carboxylic acid.

The benzimidazole systems provide information regarding connectivity within co-crystals that utilise a better hydrogen-bond acceptor than isonicotinamide, however, in order to demonstrate the validity of this hierarchical approach, it should be possible to move an acid from the N-heterocycle to the amide if a sufficiently weak hydrogen-bond acceptor is used.

Consequently, this chapter will address two questions:

I. Can the hydrogen-bond acceptor ability (based on MEP surfaces) be lowered such that the incoming acid will form a heteromeric acid-amide heteromeric dimer via O-H•••O and N-H•••O hydrogen bonds?

II. Can the hydrogen-bond acceptor ability (based on MEP surfaces) be fine-tuned through minor covalent modifications to "turn up" the acceptor strength of the N-heterocycle?

With this in mind, the pyrazol-1-ylbenzamide SR's discussed in Chapter 2, Figure 3.6, lend themselves well to this study due to their lower hydrogen-bond acceptor ability compared to isonicotinamide. It is also worth noting, that through simple covalent modifications (adding electron donating methyl groups to the heterocycle ring or changing the isomer from *para*- to *meta*-) a range of heterocycle acceptor strengths can be obtained.

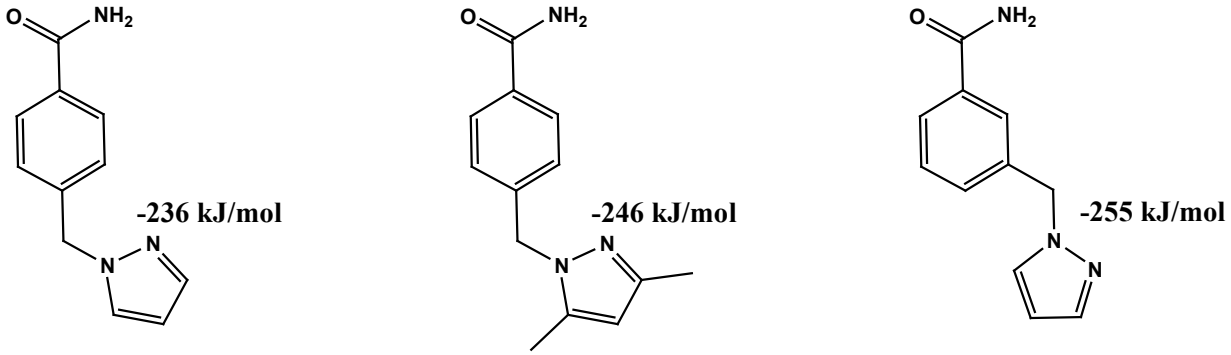

Figure 3.6 Pyrazol-1-ylbenzamide SR's and MEP surface values (in kJ/mol).

Within these SR's, there are two potential sites for the incoming carboxylic acid, Figure 3.7. Consequently, through a series of co-crystallisation reactions between pyrazol-1-ylbenzamide SR's and a range of carboxylic acids, it will be possible to probe the connectivity via single crystal X-ray crystallography.

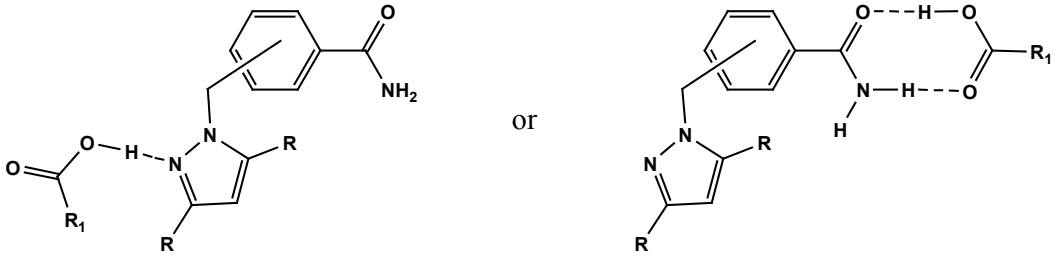

Figure 3.7 Potential interactions in co-crystals between pyrazol-1-ylbenzamide (R=H or Me) and a carboxylic acid.

3.2 Experimental

3.2.1 Synthesis

All chemicals were purchased from Aldrich and Fischer and used without further purification. Melting points were determined on a Fisher-Johns melting point apparatus and are uncorrected. Synthesis of the [(pyrazol-1-yl)methyl]benzamide SR's is reported in Chapter 2.

A wide range of carboxylic acids were allowed to co-crystallise with **2**, **4** and **8**, however, only reactions that produced crystals suitable for single crystal X-ray diffraction will be discussed.

3.2.1.1 Synthesis of 4-[(pyrazol-1-yl)methyl]benzamide : 4-nitrobenzoic acid (1:1), *2a*

2 (0.0250g, 0.124mmol) and 4-nitrobenzoic acid (0.0210g, 0.124mmol) were added to a test tube along with acetonitrile. The mixture was heated gently until components were in solution. Colourless plates suitable for X-ray diffraction were obtained after a few days via slow evaporation of acetonitrile. Mp: 160-163^{o}C. IR (KBr pellet): υ 3333, 3171, 1709, 1526, 1421, 1274, 762 cm^{-1}.

3.2.1.2 Synthesis of 4-[(pyrazol-1-yl)methyl]benzamide : 3,5-dinitrobenzoic acid (1:1), *2b*

2 (0.0250g, 0.124mmol) and 3,5-dinitrobenzoic acid (0.0260g, 0.124mmol) were added to a test tube along with acetonitrile. The mixture was heated gently until components were in solution. Colourless prisms suitable for X-ray diffraction were obtained after a few days via slow evaporation of acetonitrile. Mp: 111-113^{o}C. IR (KBr pellet): υ 3357, 3165, 3085, 1719, 1534, 1275, 738 cm^{-1}.

3.2.1.3 Synthesis of 4-[(pyrazol-1-yl)methyl]benzamide : 2-fluorobenzoic acid (1:1), *2c*

2 (0.0250g, 0.124mmol) and 2-fluorobenzoic acid (0.0140g, 0.124mmol) were added to a test tube along with acetonitrile. The mixture was heated gently until components were in solution. Colourless prisms suitable for X-ray diffraction were obtained after a few days via slow evaporation of acetonitrile. Mp: 108-110^{o}C. IR (KBr pellet): υ 3350, 3185, 1693, 1308, 758 cm^{-1}.

3.2.1.4 Synthesis of 4-[(pyrazol-1-yl)methyl]benzamide : 3-fluorobenzoic acid (1:1), *2d*

2 (0.0250g, 0.124mmol) and 3-fluorobenzoic acid (0.0140g, 0.124mmol) were added to a test tube along with acetonitrile. The mixture was heated gently until components were in solution. Colourless prisms suitable for X-ray diffraction were obtained after a few days via slow evaporation of acetonitrile. Mp: 95-98^{o}C. IR (KBr pellet): υ 3344, 3175, 3085, 1719, 1592, 1298, 756 cm^{-1}.

3.2.1.5 Synthesis of 4-[(pyrazol-1-yl)methyl]benzamide : benzoic acid (1:1), *2e*

2 (0.0250g, 0.124mmol) and benzoic acid (0.0140g, 0.124mol) were added to a test tube along with acetonitrile. The mixture was heated gently until components were in solution. Colourless prisms suitable for X-ray diffraction were obtained after a few days via slow

evaporation of acetonitrile. Mp: 99-101^{o}C. IR (KBr pellet): υ 3383, 3231, 1699, 1388, 1275, 758 cm^{-1}.

3.2.1.6 Synthesis of 4-[(pyrazol-1-yl)methyl]benzamide : oxalic acid (2:1), *2f*

2 (0.0250g, 0.124mmol) and oxalic acid (0.0110g, 0.124mmol) were added to a test tube along with acetonitrile. The mixture was heated gently until components were in solution. Colourless plates suitable for X-ray diffraction were obtained after a few days via slow evaporation of acetonitrile. Mp: 143-145^{o}C. IR (KBr pellet): υ 3377, 3175, 1653, 1408, 1109, 751 cm^{-1}.

3.2.1.7 Synthesis of 4-[(pyrazol-1-yl)methyl]benzamide : succinic acid (2:1), *2g*

2 (0.0250g, 0.124mmol) and succinic acid (0.0150g, 0.124mol) were added to a test tube along with acetonitrile. The mixture was heated gently until components were in solution. Colourless prisms suitable for X-ray diffraction were obtained after a few days via slow evaporation of acetonitrile. Mp: 146-149^{o}C. IR (KBr pellet): υ 3410, 3125, 1719, 1421, 1176, 731 cm^{-1}.

3.2.1.8 Synthesis of 4-[(pyrazol-1-yl)methyl]benzamide : fumaric acid (2:1), *2h*

2 (0.0250g, 0.124mmol) and fumaric acid (0.0150g, 0.124mmol) were added to a test tube along with acetonitrile. The mixture was heated gently until components were in solution. Colourless prisms suitable for X-ray diffraction were obtained after a few days via slow evaporation of acetonitrile. Mp: 162-165^{o}C. IR (KBr pellet): υ 3297, 3138, 1706, 1414, 1169, 758 cm^{-1}.

3.2.1.9 Synthesis of 4-[(3,5-dimethylpyrazol-1-yl)methyl]benzamide : 4-nitrobenzoic acid (1:1), *4a*

4 (0.0250g, 0.109mmol) and 4-nitrobenzoic acid (0.0180g, 0.109mmol) were added to a test tube along with acetonitrile. The mixture was heated gently until components were in solution. Colourless plates suitable for X-ray diffraction were obtained after a few days via slow evaporation of acetonitrile. Mp: 147-150^{o}C. IR (KBr pellet): υ 3390, 3170, 1706, 1516, 1419, 1271, 717 cm^{-1}.

3.2.1.10 Synthesis of 4-[(3,5-dimethylpyrazol-1-yl)methyl]benzamide : 4-hydroxybenzoic acid (1:1), 4b

4 (0.0250g, 0.109mmol) and 4-hydroxybenzoic acid (0.0150g, 0.109mmol) were added to a test tube along with acetonitrile. The mixture was heated gently until components were in solution. Colourless prisms suitable for X-ray diffraction were obtained after a few days via slow evaporation of acetonitrile. Mp: 144-147^{o}C. IR (KBr pellet): υ 3457, 3196, 2525, 1829, 1696, 1429, 1265, 1148, 774 cm^{-1}.

3.2.1.11 Synthesis of 4-[(3,5-dimethylpyrazol-1-yl)methyl]benzamide : fumaric acid (2:1), 4c

4 (0.0250g, 0.109mmol) and fumaric acid (0.0130g, 0.109mmol) were added to a test tube along with acetonitrile. The mixture was heated gently until components were in solution. Colourless blocks suitable for X-ray diffraction were obtained after a few days via slow evaporation of acetonitrile. Mp: 180-183^{o}C. IR (KBr pellet): υ 3397, 3191, 2482, 1912, 1706, 1547, 1407, 1269, 977, 771 cm^{-1}.

3.2.1.12 Synthesis of 3-[(pyrazol-1-yl)methyl]benzamide : DL-malic acid (1:1), 8a

8 (0.0200g, 0.0990mmol) and DL-malic acid (0.0130g, 0.0990mol) were added to a test tube along with ethanol. The mixture was heated gently until components were in solution. Colourless plates suitable for X-ray diffraction were obtained after a few days via slow evaporation of acetonitrile. Mp: 111-114^{o}C. IR (KBr pellet): υ 3457, 3149, 1696, 1400, 1046, 769 cm^{-1}.

3.2.1.13 Synthesis of 3-[(pyrazol-1-yl)methyl]benzamide : 3,5-dinitrobenzoic acid (1:1), 8b

8 (0.0200g, 0.0990mmol) and 3,5-dinitrobenzoic acid (0.0210g, 0.0990mol) were added to a test tube along with ethanol. The mixture was heated gently until components were in solution. Brown blocks suitable for X-ray diffraction were obtained after a few days via slow evaporation of acetonitrile. Mp: 119-122^{o}C. IR (KBr pellet): υ 3413, 3093, 2678, 2541, 1967, 1701, 1546, 1350, 732 cm^{-1}.

3.3 Results

All hydrogen bond geometries are listed in Table 3.1. A summary of the crystallographic information for each compound is displayed in Tables A.7-A.19.

Table 3.1 Hydrogen bond geometries for **2a**-**2h**, **4a**-**4c** and **8a**-**8b**.

Compound	D-H···A	D-H / Å	H···A / Å	D···A / Å	<(DHA) / °
2a[i]	N(27)-H(27B)...N(12)#1	0.93(3)	1.65(4)	2.566(3)	169(3)
	N(27)-H(27B)...N(12)#1	0.90(3)	1.96(3)	2.861(3)	173(3)
	N(27)-H(27B)...N(12)#1	0.90(3)	2.14(3)	3.023(3)	165(3)
2b[ii]	O(31)-H(31)...O(27)	0.95(2)	1.63(2)	2.5661(11)	172.0(19)
	N(27)-H(27A)...O(32)	0.922(18)	2.007(18)	2.9224(13)	172.1(15)
	N(27)-H(27B)...N(12)#1	0.888(17)	2.171(18)	3.0312(13)	163.2(15)
2c[iii]	O(31)-H(31)...O(17)	1.00(2)	1.55(2)	2.5415(17)	173.4(19)
	N(17)-H(17A)...O(32)	0.94(2)	1.95(2)	2.879(2)	171.8(18)
	N(17)-H(17B)...N(22)#1	0.89(2	2.12(2)	2.954(2)	156.3(18)
2d[iv]	N311-H31A1...O721	0.88	2.08	2.945(8)	167.8
	N311-H31B1...N124#1	0.88	2.12	2.96(4)	158.7
	N411-H41A1...O821	0.88	2.01	2.876(10)	166.2
	N411-H41B1...N224#2	0.88	2.14	2.99(5)	161.2
	O711-H711...O311	0.84	1.74	2.562(8)	165.0
	O811-H811...O411	0.84	1.71	2.535(9)	167.7
	N312-H31A2...O722	0.88	1.99	2.849(8)	165.0
	N312-H31B2...N123#1	0.88	2.15	2.96(2)	151.8
	N412-H41A2...O822	0.88	2.01	2.864(8)	164.3
	N412-H41B2...N223#2	0.88	2.16	2.96(3)	151.2
	O712-H712...O312	0.84	1.74	2.573(7)	168.8
	O812-H812...O412	0.84	1.73	2.557(7)	167.4
	N313-H31A3...O723	0.88	2.09	2.946(8)	165.2
	N313-H31B3...N122#1	0.88	2.15	2.99(3)	158.9
	N413-H41A3...O823	0.88	2.09	2.957(8)	166.1
	N413-H41B3...N222#2	0.88	2.15	2.99(3)	159.3
	O713-H713...O313	0.84	1.75	2.572(7)	166.0
	O813-H813...O413	0.84	1.73	2.559(7)	166.7
	N314-H31A4...O724	0.88	2.02	2.881(8)	165.9
	N314-H31B4...N121#1	0.88	2.12	2.94(5)	153.2
	N414-H41A4...O824	0.88	1.96	2.824(9)	166.3
	N414-H41B4...N221#2	0.88	2.16	2.98(4)	155.0
	O714-H714...O314	0.84	1.73	2.550(7)	166.2
	O814-H814...O414	0.84	1.74	2.570(7)	167.5
	N315-H31A5...O725	0.88	1.96	2.822(12)	164.7
	N315-H31B5...N125#3	0.88	2.14	2.97(3)	156.0
	N415-H41A5...O825	0.88	2.06	2.921(9)	166.3
	N415-H41B5...N225#4	0.88	2.13	2.95(3)	155.3

	O715-H715...O315	0.84	1.72	2.549(9)	171.1
	O815-H815...O415	0.84	1.72	2.540(8)	164.0
2e[v]	N(17)-H(17A)...O(32)	0.911(16)	2.066(17)	2.9740(15)	174.2(14)
	N(17)-H(17B)...N(52)#1	0.865(16)	2.147(16)	2.9946(16)	166.4(14)
	O(31)-H(31)...O(17)	0.899(16)	1.683(17)	2.5692(13)	168.0(15)
	N(47)-H(47A)...O(62)	0.917(16)	1.948(17)	2.8599(15)	172.5(14)
	N(47)-H(47B)...N(22)#1	0.839(16)	2.195(16)	2.9840(15)	156.8(14)
	O(61)-H(61)...O(47)	0.896(16)	1.682(17)	2.5702(13)	170.4(15)
2f[vi]	N(27)-H(27A)...O(32)	0.91(3)	2.05(3)	2.932(3)	164(3)
	O(31)-H(31)...O(27)	0.89(3)	1.63(3)	2.515(2)	171(3)
2g[vii]	N(17)-H(17A)...O(32)	0.89(2)	1.99(3)	2.868(2)	166.9(18)
	N(17)-H(17B)...N(22)#2	0.94(2)	2.06(2)	2.978(2)	162.6(18)
	O(31)-H(31)...O(17)	0.88(3)	1.71(3)	2.586(2)	172(2)
2h[viii]	N(17)-H(17A)...O(32)	0.933(18)	1.942(18)	2.8548(16)	165.4(15)
	N(17)-H(17B)...N(22)#2	0.887(17)	2.118(18)	2.9713(17)	161.2(16)
	O(31)-H(31)...O(17)	0.932(18)	1.644(19)	2.5694(14)	171.4(17)
4a[ix]	N(17)-H(17A)...O(32)	0.91(2)	1.98(2)	2.871(2)	168(2)
	N(17)-H(17B)...N(22)#1	0.96(2)	2.12(2)	3.066(2)	169(2)
	O(31)-H(31)...O(17)	1.05(2)	1.54(2)	2.5801(19)	170(2)
4b[x]	N(17)-H(17A)...O(35)	0.879(19)	2.01(2)	2.8829(17)	171.5(17)
	N(17)-H(17B)...O(32)#1	0.87(2)	2.16(2)	2.9978(17)	162.1(17)
	O(31)-H(31)...N(22)#2	0.94(2)	1.67(2)	2.5812(16)	162.0(17)
	O(34)-H(34)...O(17)	0.911(19)	1.685(19)	2.5906(15)	172.5(18)
4c[xi]	N(17)-H(17A)...O(32)	0.831(17)	2.012(18)	2.8387(13)	172.6(16)
	N(17)-H(17B)...O(34)#1	0.871(17)	2.476(18)	3.2960(14)	157.2(14)
	O(31)-H(31)...O(17)	0.915(17)	1.725(17)	2.6358(11)	173.2(16)
	O(34)-H(34)...N(22)#2	0.874(15)	1.830(16)	2.6966(12)	170.9(14)
8a[xii]	O(31)-H(31)...O(17A)	0.88(3)	1.73(4)	2.581(19)	163(3)
	O(31)-H(31)...O(17B)	0.88(3)	1.70(4)	2.56(3)	166(3)
	N(17A)-H(17A)...O(32)	0.88	2.05	2.907(11)	163.8
	N(17B)-H(17C)...O(32)	0.88	2.07	2.915(16)	162.1
	N(17A)-H(17B)...O(33)#1	0.88	2.49	3.342(12)	161.6
	N(17B)-H(17D)...O(33)#1	0.88	2.40	3.276(16)	173.1
	O(33)-H(33)...O(35)#2	0.91(3)	1.87(3)	2.781(2)	174(3)
	O(34)-H(34)...N(22)#3	0.95(3)	1.73(3)	2.646(3)	162(3)
8b[xiii]	O(31)-H(31)...O(11)	1.00(2)	1.54(2)	2.538(2)	173(2)
	O(41)-H(41)...N(22)	0.86(2)	1.71(2)	2.574(2)	176(3)
	N(11)-H(11A)...O(32)	0.84(2)	2.09(3)	2.920(3)	171(2)
	N(11)-H(11B)...O(42)#1	0.90(3)	2.00(3)	2.871(3)	162(2)

i) #1 x+1/2,y+1/2,z ; (ii) #1 x,-y+1/2,z-1/2; (iii) #1 -x,-y,-z+1; (iv) #1 -x,-y+1,-z, #2 -x+1,-y,-z+1, #3 -x,-y+1,-z+1, #4 -x+1,-y,-z+2; (v) #1 -x,-y,-z+1; (vi) #1 -x-1,-y,-z; (vii) #1 -x+2,-y+3,-z, #2 -x+3/2,y+1/2,-z+1/2; (viii) #1 -x+1,-y+2,-z, #2 -x+1/2,y+1/2,-z+1/2; (ix) #1 x+1,y,z; (x) #1 x+1/2,-y+1/2,z+1/2, #2 -x+1,-y+1,-z+1; (xi) #1 -x+2,-y+2,-z+1, #2 x+1/2,-y+3/2,z+1/2; (xii) #1 -x+1/2,-y+1/2,-z, #2 x,y-1,z, #3 x+1/2,y-1/2,z; (xiii) #1 -x+1,y,-z+3/2.

3.3.1 Crystal structure of 4-[(pyrazol-1-yl)methyl]benzamide : 4-nitrobenzoic acid (1:1), 2a

The crystal structure of **2a** shows the formation of a binary 1:1 supermolecule through an acid-amide heteromeric dimer via O-H•••O and N-H•••O hydrogen bonds (2.555(3) Å and 2.852(3) Å respectively), Figure 3.8. All hydrogen-bond donor and acceptors are satisfied since dimers are extended into a 1D chain via an N-H•••N hydrogen bonds (3.023(3) Å) between the *anti* amide hydrogen atom and the pyrazole nitrogen.

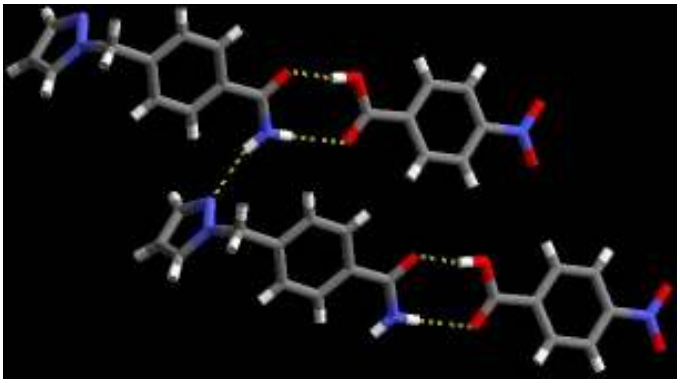

Figure 3.8 Two 1:1 supermolecules observed in the crystal structure of **2a**. Dimers are extended into a 1D chain via secondary N-H•••N hydrogen bonds.

3.3.2 Crystal structure of 4-[(pyrazol-1-ylmethyl)]benzamide : 3,5-dinitrobenzoic acid (1:1), 2b

Isostructural to **2a**, **2b** is a 1:1 supermolecule driven by the acid-amide synthon. The acid interacts with the amide via O-H•••O and N-H•••O hydrogen bonds (2.5661(11) Å and 2.9224(13) Å respectively), Figure 3.9, leaving the pyrazole nitrogen to accept a secondary, N-H•••N hydrogen bond (3.0312(13) Å) from the *anti* amide hydrogen atom resulting in a 1D chain.

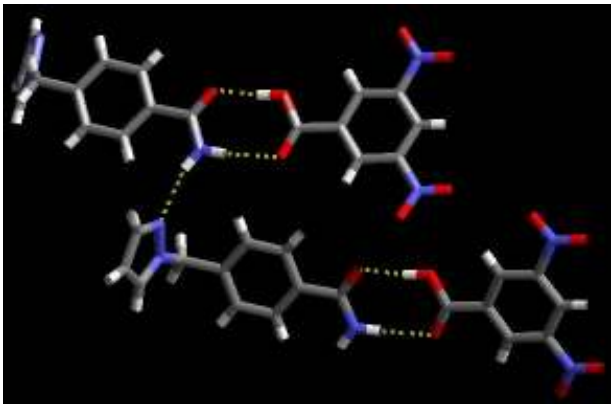

Figure 3.9 Two 1:1 supermolecules observed in the crystal structure of **2b**. Dimers are extended into a 1D chain via secondary N-H•••N hydrogen bonds.

3.3.3 Crystal structure of 4-[(pyrazol-1-yl)methyl]benzamide : 2-fluorobenzoic acid (1:1), 2c

Similar connectivity to **2a** and **2b** is observed in the 1:1 supermolecule **2c**, with the acid-amide heteromeric dimer forming via O-H•••O and N-H•••O hydrogen bonds (2.5145(17) Å and 2.879(2) Å respectively), Figure 3.10. The *anti* amide hydrogen atom interacts with the free pyrazole nitrogen, however in this case, instead of a 1D chain forming, two N-H•••N hydrogen bonds (2.954(2) Å) combine between two amide species producing a tetrameric species.

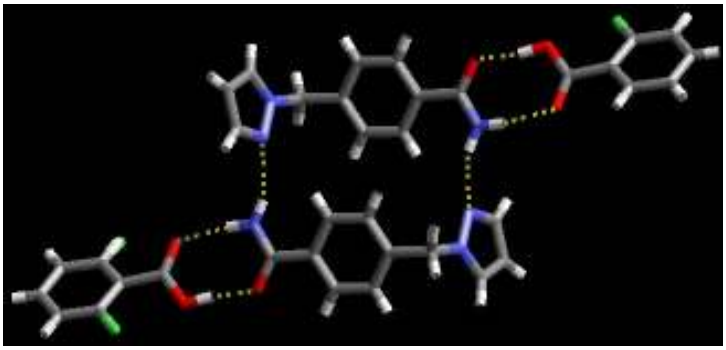

Figure 3.10 Two 1:1 supermolecules observed in the crystal structure of **2c**, which form a tetramer via two N-H•••N hydrogen bonds.

3.3.4 Crystal structure of 4-[(pyrazol-1-yl)methyl]benzamide : 3-fluorobenzoic acid (1:1), 2d

The 1:1 co-crystal, **2d**, contains 10 inequivalent dimeric supermolecules each possessing an acid-amide heteromeric dimer (O-H•••O 2.535(9) Å and N-H•••O 2.876(10) Å; O-H•••O 2.557(7) Å and N-H•••O 2.864(8) Å; O-H•••O 2.559(7) Å and N-H•••O 2.957(8) Å; O-H•••O 2.570(7) Å and N-H•••O 2.824(9) Å; O-H•••O 2.540(8) Å and N-H•••O 2.921(9) Å; O-H•••O 2.562(8) Å and N-H•••O 2.945(8) Å; O-H•••O 2.573(7) Å and N-H•••O 2.849(8) Å; O-H•••O 2.572(7) Å and N-H•••O 2.946(8) Å; O-H•••O 2.550(7) Å and N-H•••O 2.881(8) Å; O-H•••O 2.549(9) Å and N-H•••O 2.822 (12) Å), Figure 3.11. The *anti* amide hydrogen atom in each case interacts with the pyrazole nitrogen of an adjacent dimer via a N-H•••N hydrogen bond (2.99(5) Å; 2.96(3) Å; 2.99(3) Å; 2.98(4) Å; 2.95(3) Å; 2.96(4) Å; 2.96(2) Å; 2.99(3) Å; 2.94(5) Å; 2.97(3) Å) resulting in 10, discrete tetramers.

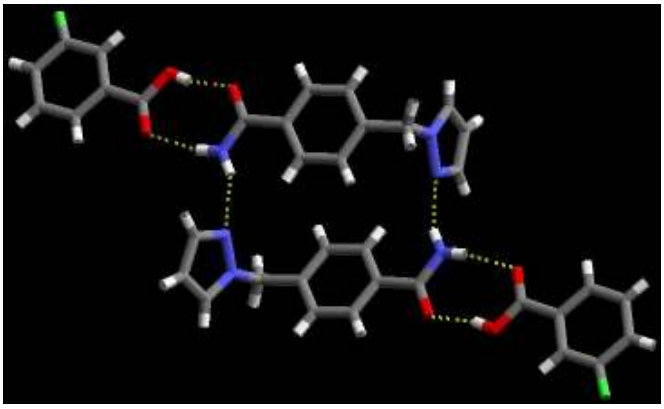

Figure 3.11 Two 1:1 supermolecules observed in the crystal structure of **2d**, which form a tetramer via two N-H•••N hydrogen bonds.

3.3.5 Crystal structure of 4-[(pyrazol-1-yl)methyl]benzamide : benzoic acid (1:1), 2e

2e contains two inequivalent 1:1 binary supermolecules constructed from heteromeric acid-amide dimers (O-H•••O 2.5692(13) Å and N-H•••O 2.9740(15) Å; O-H•••O 2.5702(13) Å and N-H•••O 2.8599(15) Å), Figure 3.12. Each co-crystal is linked to an adjacent symmetry related co-crystal through an N-H•••N interaction between the *anti* hydrogen atom of the amide and the free pyrazole nitrogen atom (N-H•••N 2.9946(16) Å and 2.9840(15) Å) resulting in two, discrete tetramers.

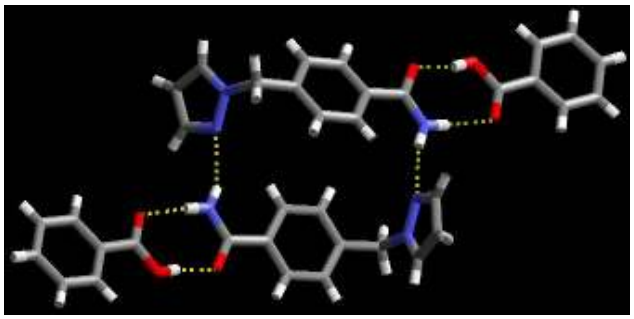

Figure 3.12 Two 1:1 supermolecules observed in the crystal structure of **2e**, which form a tetramer via two N-H•••N hydrogen bonds.

3.3.6 Crystal structure of 4-[(pyrazol-1-yl)methyl]benzamide : oxalic acid (2:1), 2f

The crystal structure of **2f** shows a trimeric supermolecule constructed via two symmetry related acid-amide heteromeric dimers (O-H•••O 2.932(3) Å and N-H•••O 2.515(2) Å), Figure 3.13. Adjacent trimers are organized through long N–H•••O contacts (*ca.* 3.26 Å) between the *anti* proton of the amide and an -OH moiety on a neighboring supermolecule.

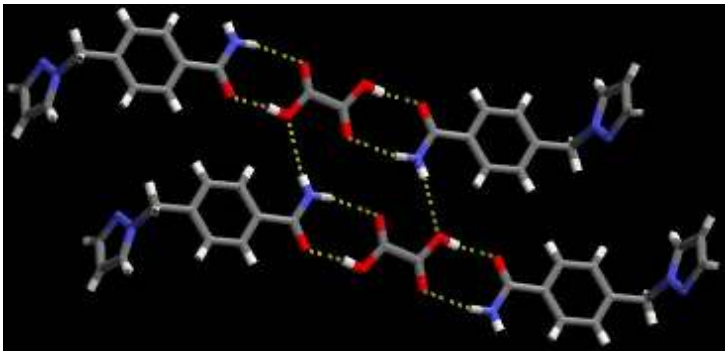

Figure 3.13 Two 2:1 supermolecules observed in the crystal structure of **2f**. Trimers are extended into a 1D chain via long N-H•••O interactions.

3.3.7 Crystal structure of 4-[(pyrazol-1-yl)methyl]benzamide : succinic acid (2:1), 2g

Similar connectivity to **2f** is observed in the 2:1 supermolecule **2g** with the diacid forming two symmetry related acid-amide heteromeric dimers via O-H•••O and N-H•••O hydrogen bonds (2.586(2) Å and 2.868(2) Å, respectively) between two amide species, Figure 3.14. Adjacent supermolecules are interconnected through a secondary N-H•••N interaction between the *anti* proton of the amide and the free pyrazole nitrogen atom (N-H•••N 2.978(2) Å), and oriented perpendicular to each other.

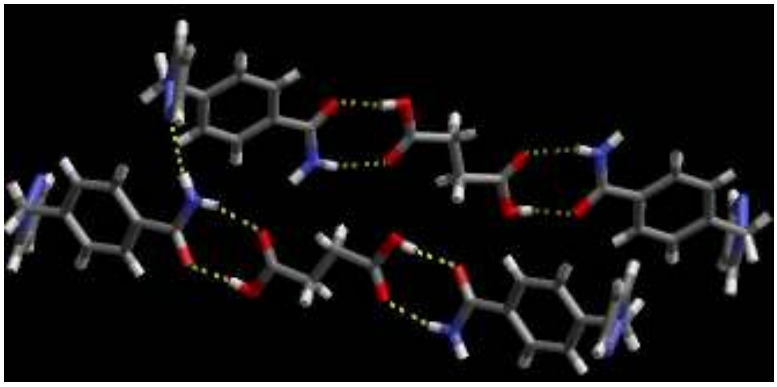

Figure 3.14 The 2:1 supermolecule observed in the crystal structure of **2g**. Trimers are extended into a 1D chain via N-H•••O hydrogen bonds.

3.3.8 Crystal structure of 4-[(pyrazol-1-yl)methyl]benzamide : fumaric acid (2:1), 2h

The crystal structure of **2h** is isostructural with **2g** with the diacid sandwiched between two amide species and interacting via O-H•••O and N-H•••O hydrogen bonds (2.5694(14) Å and 2.8548(16) Å respectively), Figure 3.15. Adjacent supermolecules are interconnected through a

secondary N-H•••N interaction between the *anti* proton of the amide and the free pyrazole nitrogen atom (N-H•••N 2.9713(17) Å), and oriented perpendicular to each other.

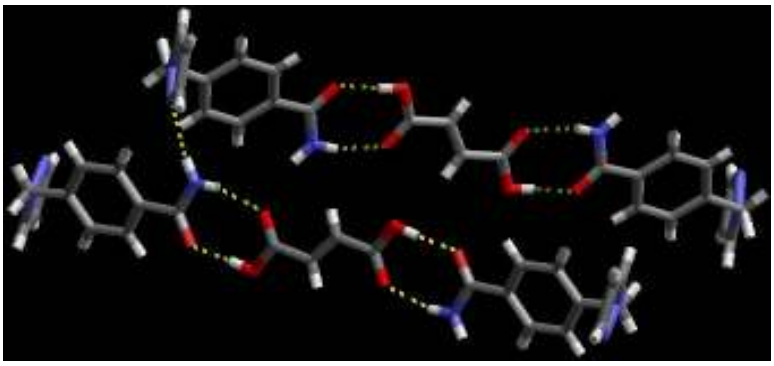

Figure 3.15 The 2:1 supermolecule observed in the crystal structure of **2h**. Trimers are extended into a 1D chain via N-H•••O hydrogen bonds.

3.3.9 Crystal structure of 4-[(3,5-dimethylpyrazol-1-yl)methyl]benzamide : 4-nitrobenzoic acid (1:1), 4a

The crystal structure of **4a** shows the formation of a binary 1:1 supermolecule through an acid-amide heteromeric dimer via O-H•••O and N-H•••O hydrogen bonds (2.5801(19) Å and 2.871(2) Å, respectively), Figure 3.16. The dimer is extended into a 1D chain via an N-H•••N hydrogen bonds (3.066(2) Å) between the *anti* amide hydrogen atom and the pyrazole nitrogen.

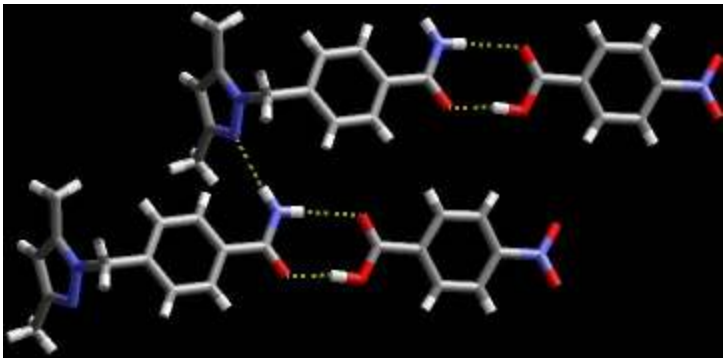

Figure 3.16 Two binary 1:1 supermolecules observed in the crystal structure of **4a**. Dimers are extended into a 1D chain via secondary N-H•••N hydrogen bonds.

3.3.10 Crystal structure of 4-[(3,5-dimethylpyrazol-1-yl)methyl]benzamide : 4-hydroxybenzoic acid (1:1), 4b

A four component ring is observed in the 1:1 supermolecule, **4b**. The acid-amide heteromeric dimer is again the prevalent interaction via O-H•••O and N-H•••O hydrogen bonds

(2.6358(11) Å and 2.8387(13) Å, respectively), Figure 3.17. The hydroxyl group of the acid forms an O-H•••N (2.6966(12) Å) hydrogen bond to the pyrazole nitrogen with the *anti* hydrogen atom of the amide binding to the hydroxyl oxygen, N-H•••O (*ca.* 3.29 Å) which results in the extension of the tetramers into a zigzag chain.

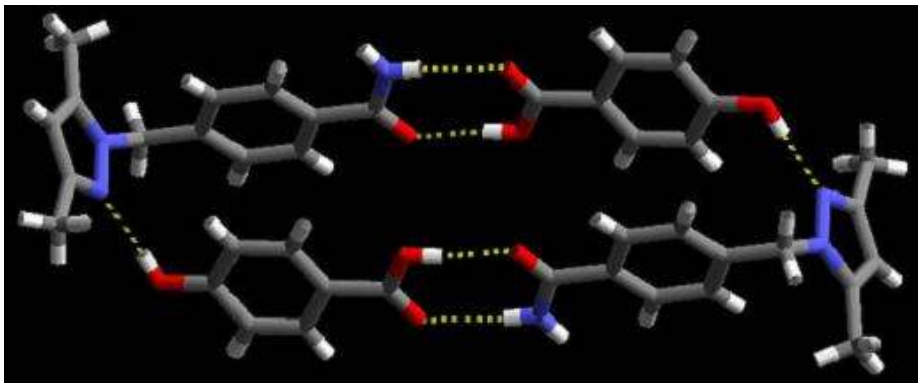

Figure 3.17 Two 1:1 supermolecules observed in the crystal structure of **4b**. Dimers interact via secondary O-H•••N hydrogen bonds to form a tetramer.

3.3.11 Crystal structure of 4-[(3,5-dimehtylpyrazol-1-yl)methyl]benzamide : fumaric acid (2:1), 4c

4c is a 2:1 supermolecule with three hydrogen-bonding interactions present, Figure 3.18. The acid-amide heteromeric dimer is observed via O-H•••O and N-H•••O hydrogen bonds (2.5906(15) Å and 2.8829(17) Å, respectively) however, unlike the case of co-crystal **1h**, the diacid does not form two symmetry related acid-amide dimers; the second acid moiety in fact forms an O-H•••N hydrogen bond (2.5812(16) Å) to the pyrazole nitrogen. Two trimeric co-crystals interact via N-H•••O hydrogen bonds (2.9978(17) Å) between the *anti* amide hydrogen atom and an adjacent acid carbonyl oxygen to produce a hexamer.

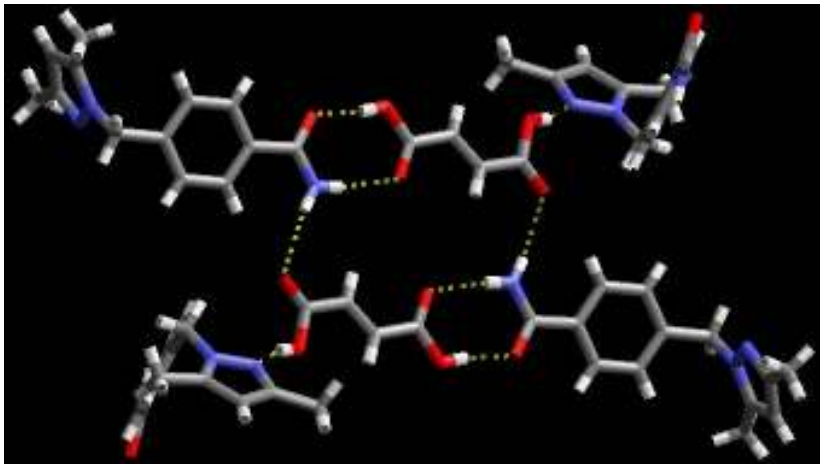

Figure 3.18 Two 2:1 supermolecules observed in the crystal structure of **4c**. Trimers interact via N-H•••O hydrogen bonds to form a hexamer.

3.3.12 Crystal structure of 3-[(pyrazol-1-yl)methyl]benzamide : DL-malic acid (2:1), 8a

The crystal structure of **8a** shows a trimeric supermolecule similar to that observed in **4c**, Figure 3.19. The asymmetric diacid, forms an acid-amide heteromeric dimer via O-H•••O and N-H•••O hydrogen bonds (2.581(19) Å and 2.907(11) Å respectively) with the second acid moiety forming an O-H•••N hydrogen bond (2.646(3) Å) to a pyrazole nitrogen acceptor. The trimers are extended into layers via an O-H•••O hydrogen bond (2.781(2) Å) between the free hydroxyl groups of one acid and the carbonyl oxygen of an adjacent acid.

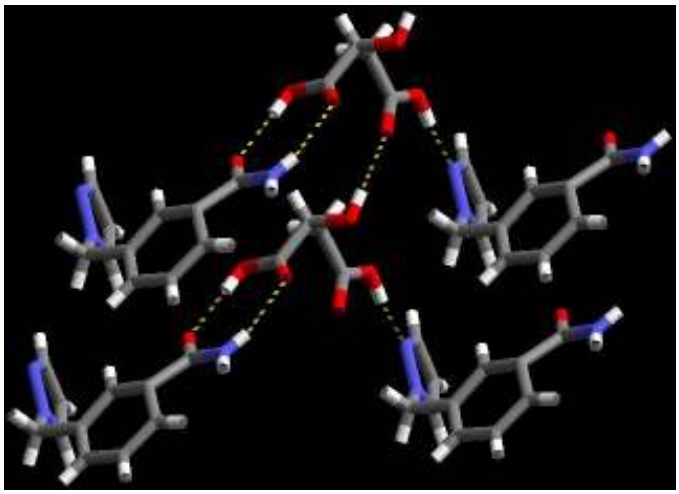

Figure 3.19 Two 2:1 supermolecules observed in the crystal structure of **8a**. Trimers interact via O-H•••O hydrogen bonds forming layers.

3.3.13 Crystal structure of 3-[(pyrazol-1-yl)methyl]benzamide : 3,5-dinitrobenzoic acid (1:2), 8b

The crystal structure of **8b** shows two carboxylic acids and one SR. One of the carboxylic acids forms an acid-amide heteromeric dimer via O-H•••O and N-H•••O hydrogen bonds (2.538(2) Å and 2.920(3) Å, respectively) with the second carboxylic acid interacting with the pyrazole nitrogen acceptor via an O-H•••N hydrogen bond (2.574(2) Å). Two trimeric co-crystals interact via N-H•••O hydrogen bonds (2.871(3) Å) between the *anti* amide hydrogen atom and an adjacent acid carbonyl oxygen to produce a hexamer, Figure 3.20.

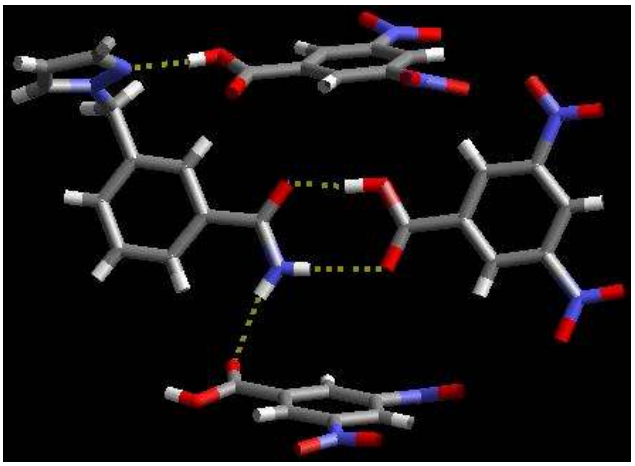

Figure 3.20 The 2:1 supermolecule observed in the crystal structure of **8b**. Trimers interact via N-H•••O hydrogen bonds to form a hexamer.

3.4 Discussion

3.4.1 Controlling the location of the carboxylic acid in binary co-crystals

All three SR's **2**, **4** and **8**, possess a heterocyclic nitrogen atom that is a poorer hydrogen-bond acceptor (based on MEP surfaces) than the heterocyclic nitrogen atom in isonicotinamide. Structural analysis of 13 acid•••pyrazole benzamide co-crystals shows that the acid-amide heteromeric dimer appears in every single case, Figure 3.21. This result demonstrates that it is possible, through simple covalent modifications (i.e. changing the heterocycle in the SR), to make the amide moiety the best hydrogen-bond acceptor, thus completely changing the binding preference between the incoming carboxylic acid and the SR.

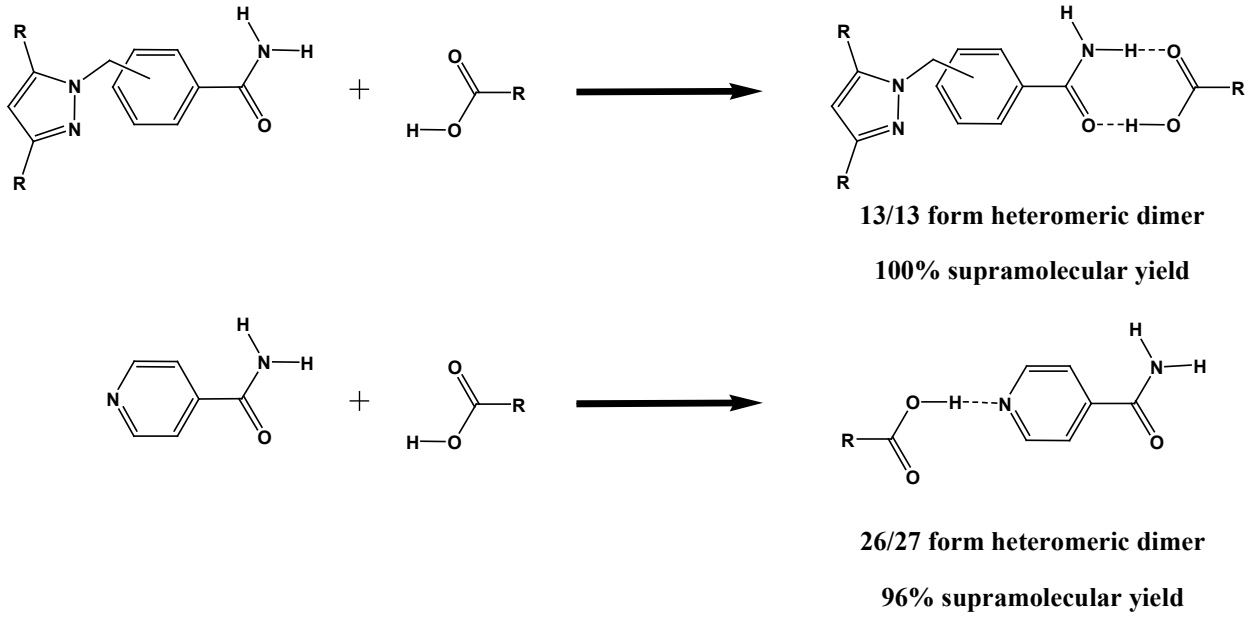

Figure 3.21 Comparison of acid-pyrazole and acid-amide interactions.

3.4.2 Assessing the competitive capability of the pyrazole functionality

Although a supramolecular yield of 100% was obtained, it is pertinent to scrutinize the activity of the pyrazole as a hydrogen-bond acceptor. In order to develop a hierarchy of interactions it is necessary to have more than one potential binding site in the system, and consequently it is essential to establish whether the pyrazole is active enough to partake in hydrogen bonding.

In the case of 4-[(pyrazol-1-ylmethyl)]-benzamide (MEP=-236kJ/mol), the acid forms a heteromeric dimer with the amide moiety leaving the pyrazole nitrogen to interact with the *anti* amide hydrogen atom in 7 of 8 examples, Figure 3.22. This demonstrates the pyrazole is 'active', however it does not compete successfully with the amide for the incoming acid.

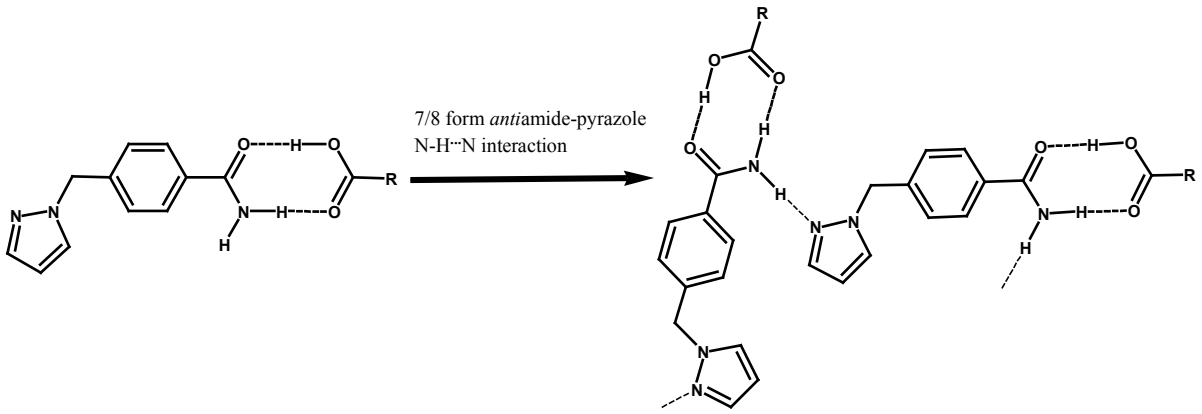

Figure 3.22 Secondary interactions in 4-[(pyrazol-1-ylmethyl)]-benzamide co-crystals.

If the pyrazole is "boosted" with electron-donating substituents (e.g. methyl groups increases the MEP to -246kJ/mol) the N-heterocycle takes on a more important structural role.

In the co-crystal incorporating a mono-carboxylic acid (**4a**), in order to satisfy all hydrogen bond possibilities, the secondary interaction again is an N-H•••N hydrogen bond between the pyrazole nitrogen and the *anti* amide hydrogen atom, Figure 3.23.

However, when the carboxylic acid is more complex (**4b** and **4c**) through the inclusion of a second donor group (i.e. a hydroxyl (**4b**) or second acid (**4c**) functionality), the pyrazole nitrogen forms an O-H•••N hydrogen bond with the much better '-OH' hydrogen-bond donor instead of with the *anti* amide hydrogen atom, Figure 3.23.

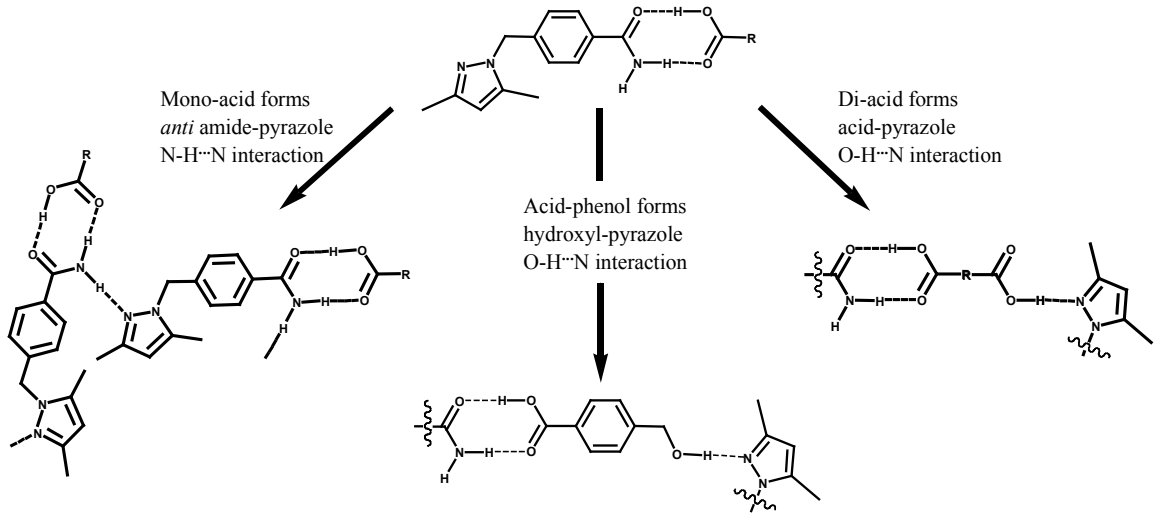

Figure 3.23 Secondary interactions in 4-[(3,5-dimethylpyrazol-1-ylmethyl)]-benzamide co-crystals.

3-[(pyrazol-1-ylmethyl)]-benzamide (MEP=-255kJ/mol), which, through a simple isomer change becomes an even better acceptor than both 4-[(pyrazol-1-ylmethyl)]-benzamide and 4-[(3,5-dimethylpyrazol-1-ylmethyl)]-benzamide) (by -19kJ/mol and -11kJ/mol, respectively) is comparable to 4-[(3,5-dimethylpyrazol-1-ylmethyl)]-benzamide).

In the di-acid co-crystal, **8a**, the ever-present acid-amide heteromeric dimer is observed between the SR and the better of the two acid moieties[8] (the two acid moieties in DL-malic are electronically different due to the hydroxyl group at the C2 position) with the second acid forming an O-H•••N hydrogen bond to the pyrazole nitrogen. Similarly, in the co-crystal, **8b**, the acid-amide heteromeric dimer is observed between the acid and the SR with a second carboxylic acid forming an O-H•••N hydrogen bond to the pyrazole nitrogen, Figure 3.24.

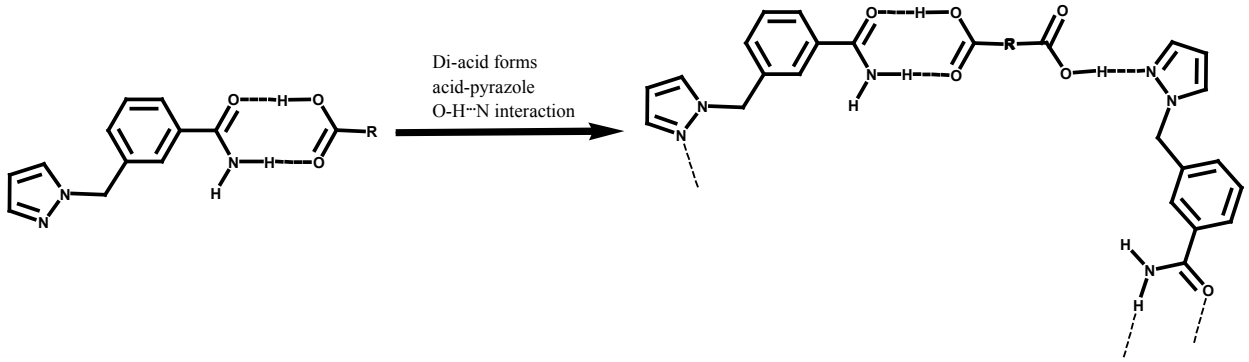

Figure 3.24 Secondary interaction in 3-[(pyrazol-1-ylmethyl)]-benzamide : diacid co-crystals.

The synthesis and structural analysis of 13 co-crystals between pyrazole-benzamide SR's and a carboxylic acid have now provided reliable answers to the questions presented at the beginning of this chapter.

I. Can the hydrogen-bond acceptor ability (based on MEP surfaces) be lowered such that the incoming acid will form a heteromeric acid-amide heteromeric dimer via O-H•••O and N-H•••O hydrogen bonds?

The MEP surface was lowered sufficiently to move the incoming carboxylic acid to the amide site in all 13 cases. These results, in conjunction with those previously reported for isonicotinamide[2] and benzimidazole-benzamides,[6] validate MEP surface calculations as an effective tool in the control and prediction of hydrogen bonds in N-heterocycle/amide systems, Figure 3.25.

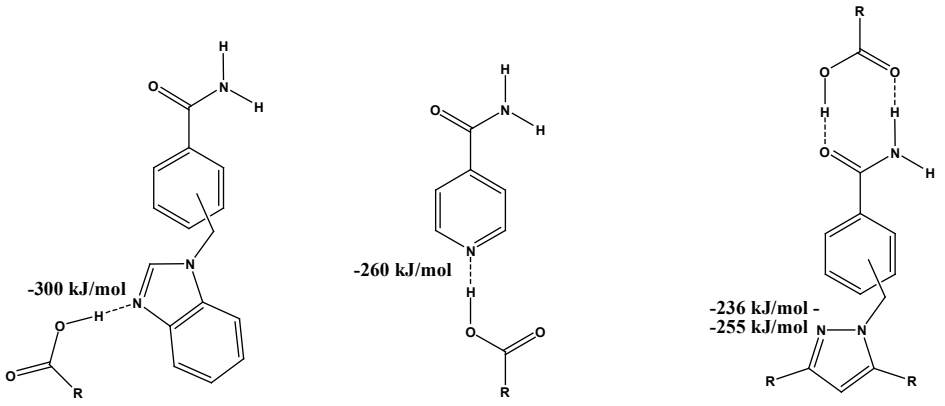

Figure 3.25 Hierarchical approach to controlling hydrogen bond interactions in N-heterocycle/amide systems.

II. Can the hydrogen-bond acceptor ability (based on MEP surfaces) be fine-tuned through minor covalent modifications to "turn up" the acceptor strength of the N-heterocycle?

Subtle covalent changes (adding methyl groups or changing the isomer) to the SR's were enough to change the MEP surface (by -11kJ/mol and -19kJ/mol respectively).

These changes activated the pyrazole nitrogen and were sufficient to compete with the amide for a secondary interaction, Figure 3.26.

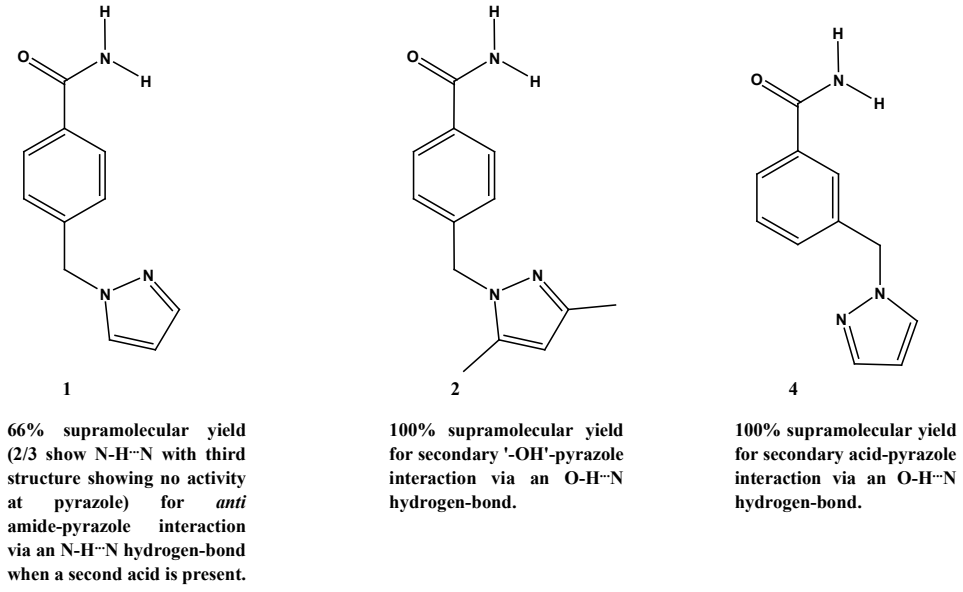

Figure 3.26 Fine-tuning the acceptor strength of the N-heterocycle.

References

1. Some elegant examples of sequential "crystal engineering": (a) S. Ferlay and W. Hosseini, *Chem. Commun.*, 2004, 788; (b) J. C. MacDonald, P. C. Dorrestein, M. M. Pilley, M. M. Foote, J. L. Lundburg, R. W. Henning, A. J. Schultz and J. L. Manson, *J. Am. Chem. Soc.*, 2000, **122**, 11692; (c) P. Dechambenoit, S. Ferlay and M. W. Hosseini, *Cryst. Growth Des*., 2005, **5**, 2310; (d) T. –J. M. Luo, J. C. MacDonald and G. T. R. Palmore, *Chem. Mater.*, 2004, **16**, 4916.
2. (a) C. B. Aakeröy, A. M. Beatty and B. A. Helfrich, *J. Am. Chem. Soc.*, 2002, **124**, 14425; (b) C. B. Aakeröy, A. M. Beatty, B. A. Helfrich and M. Nieuwenhuyzen, *Cryst. Growth Des.*, 2003, **3**, 159; (c) C. B. Aakeröy, J. Desper and B. A. Helfrich, *CrystEngComm.*, 2004, **6**, 19; (d) B. R. Bhogala, S. Basavgu and A. Nangia, *CrystEngComm.*, 2005, **7**, 551; (e) P. Vishweshwar, A. Nangia and V. M. Lynch, *Cryst. Growth Des.*, 2003, **3**, 783.
3. Cambridge Structural Database v. 5.29 (January 2008).
4. (a) M. C. Etter, *Acc. Chem. Res.*, 1990, **23**, 120; (b) M. C. Etter, *J. Phys. Chem.,* 1991, **95**, 4601.
5. C. B. Aakeröy, J. Desper and J. F. Urbina, *Cryst. Growth Des.*, 2005, **5**, 1283.
6. C. A. Hunter, *Angew. Chem. Int. Ed*, 2004, **43**, 5310-5324.
7. Molecular structures for isonicotinamide and benzimidazole-1-yl benzamide were constructed using Spartan '06 (Wavefunction, Inc. Irvine, CA). Both molecules were optimized using AM1, with the maxima and minima in the electrostatic potential surface (0.002 e/au isosurface) determined using a positive point charge in the vacuum as a probe.
8. A CSD[3] search of malic acid revealed a 94% supramolecular yield for salts of malic acid with the carboxylic acid group nearest to the carbon appended with the hydroxyl functionality deprotonated.

CHAPTER 4 - Ditopic Pyridine/Pyrazole and Pyridine/Indazole Supramolecular Reagents for Refining Co-crystal Synthesis

4.1 Introduction

Although reliable co-crystal synthesis has been demonstrated with isonicotinamide[1] and pyrazol-1-yl benzamide SR's,[2] attention now needs to be turned toward SR's that possess two chemically and geometrically similar sites with different hydrogen-bond acceptor abilities. This will allow for a more stringent examination of an MEP-based description of charge, and its connection to hydrogen-bond ability.

A suitable system should contain two heterocycles that offer different hydrogen-bond acceptors (based upon MEP, surfaces[3]) lacking self-complementarity.

In addition, the two heterocycles should be uncoupled (e.g. by a methylene bridge), thus allowing for subtle fine-tuning of each individual heterocycle without affecting the other.

When choosing which heterocycles to use, pyridine is a well-known hydrogen-bond acceptor[1, 4] and therefore provides a good starting point, Figure 4.1.

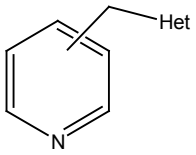

Figure 4.1 Pyridine-based SR's (Het= N-heterocycle).

Previous studies have incorporated pyridine and benzimidazole[5] into the SR, Figure 4.2, giving two binding sites with different hydrogen-bond acceptor strengths.

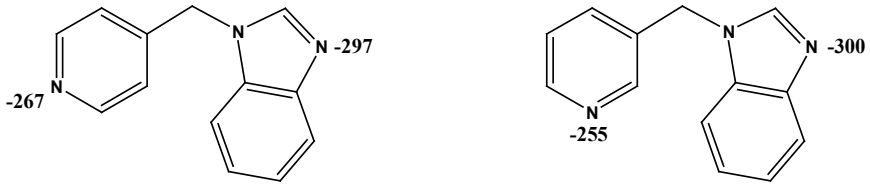

Figure 4.2 [Benzimidazol-1-yl)methyl]pyridine SR's and MEP surface values (kJ/mol).

In 1:1 binary co-crystals, the incoming hydrogen-bond donor interacts with the benzimidazole in all cases.[6] This agrees with MEP surface calculations that show the benzimidazole nitrogen with a more negative charge than pyridine and hence is the better hydrogen-bond acceptor.

If an MEP-based approach is viable, it should be possible to move an acid to the pyridine if a significantly weaker but structurally similar five-membered heterocyclic hydrogen-bond acceptor is used instead of benzimidazole.

In addition to this, benzimidazole also has a tendency to deprotonate a carboxylic acid. 57% of all 1:1 two component crystal structures containing a [benzimidazol-1-yl)methyl]pyridine SR and a carboxylic acid resulted in proton transfer from the carboxylic acid to the benzimidazole nitrogen atom.[6] This severely hinders control of co-crystallisations and thus, replacing benzimidazole with a similar but weaker five-membered hydrogen-bond acceptor will allow for this issue to be addressed.

Consequently, a new family of SR's will be designed to answer two questions:

I. Can the hydrogen-bond acceptor strength of the second N-heterocycle be lowered such that pyridine becomes the best acceptor?

II. Can the hydrogen-bond acceptor strength of the second N-heterocycle be lowered (compared to benzimidazole) to prevent deprotonation of the incoming carboxylic acid?

With this in mind, a family of SR's have been developed in which pyridine is combined with a weaker (based on pKa and charge approximations[7]) but geometrically similar N-heterocycle (pyrazole or indazole), Figure 4.3. Through a series of co-crystallisations, the potential to form co-crystals (determined by infra-red spectroscopy) and a hierarchy of preferential binding (determined by single crystal X-ray diffraction) will be determined.

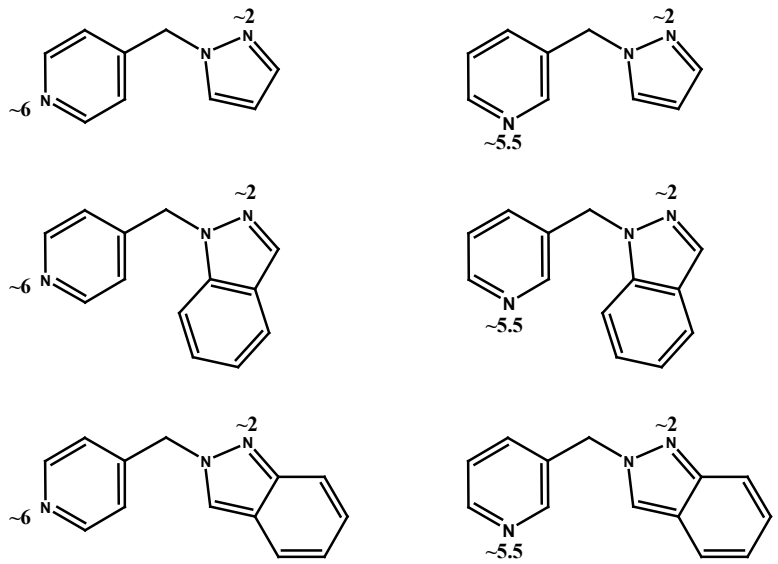

Figure 4.3 Pyridine/pyrazole and pyridine/indazole based SR's with pK_a values of the conjugate acids.

4.2 Experimental

4.2.1 Synthesis

All chemicals were purchased from Aldrich and Fischer and used without further purification. Melting points were determined on a Fisher-Johns melting point apparatus and are uncorrected.

4.2.1.1 Synthesis of 4-[(pyrazol-1-yl)methyl]pyridine, 13

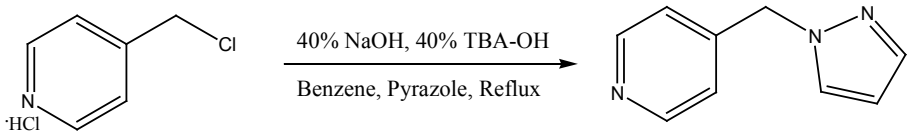

To a round bottom flask, 4-picolylchloride hydrochloride (3.00g, 18.0mmol), pyrazole (1.20g, 18.0mmol), 40% $NaOH_{(aq)}$ (48mL), 40% tetrabutylammonium hydroxide (24 drops) and benzene (240mL) were added. The biphasic solution was stirred at reflux for 8 hours, cooled to room temperature and stirred over night. On completion of the stir, the benzene layer was extracted and the solvent removed under vacuum. The crude product was flushed through a silica plug (ethyl acetate as eluent), to yield a brown oil, **13**, (2.23g, 76.6%). ^1H NMR (δ_H; 400MHz, $CDCl_3$): 5.32 (s 2H), 6.32 (t, J = 4.4Hz, 1H), 6.99 (d, J = 5.6Hz, 2H), 7.43 (d, J =

2.4Hz, 1H), 7.57 (d, J = 1.6Hz, 1H), 8.53 (dd, J^1 = 4.4Hz, J^2 = 1.6Hz, 2H), Figure B.13a; ^{13}C NMR, (δ_C; 50MHz, $CDCl_3$): 54.38, 106.50, 121.82, 129.93, 140.22, 146.14, 149.94, Figure B.13b.

4.2.1.2 Synthesis of 3-[(pyrazol-1-yl)methyl]pyridine, 14

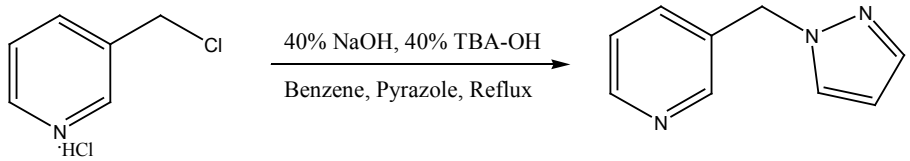

To a round bottom flask, 3-picolylchloride hydrochloride (0.500g, 2.94mmol), pyrazole (0.200g, 2.94mmol), 40% $NaOH_{(aq)}$ (8mL), 40% tetrabutylammonium hydroxide (4 drops) and benzene (40mL) were added. The biphasic solution was stirred at reflux for 8 hours, cooled to room temperature and stirred over night. On completion of the stir, the benzene layer was extracted and the solvent removed under vacuum. The crude product was flushed through a silica plug (ethyl acetate as eluent), to yield a brown oil, **14**, (0.303g, 64.8%). ^{1}H NMR (δ_H; 400MHz, $CDCl_3$): 5.25 (s, 2H), 6.22 (t, J = 4.4Hz, 1H), 7.17 (dd, J^1 = 8Hz, J^2=4Hz, 1H), 7.35 (d, J = 2.4Hz, 1H), 7.41-7.43 (m, 1H), 8.43 (s, 1H), 8.46 (d, J = 4Hz, 1H), Figure B.14a; ^{13}C NMR, (δ_C; 50MHz, $CDCl_3$): 53.16, 106.34, 123.68, 129.40, 132.43, 135.29, 139.97, 148.71, 149.30, Figure B.14b.

4.2.1.3 Synthesis of 4-[(indazol-1-yl)methyl]pyridine, 15 and 4-[(indazole-2-yl)methyl]pyridine, 16

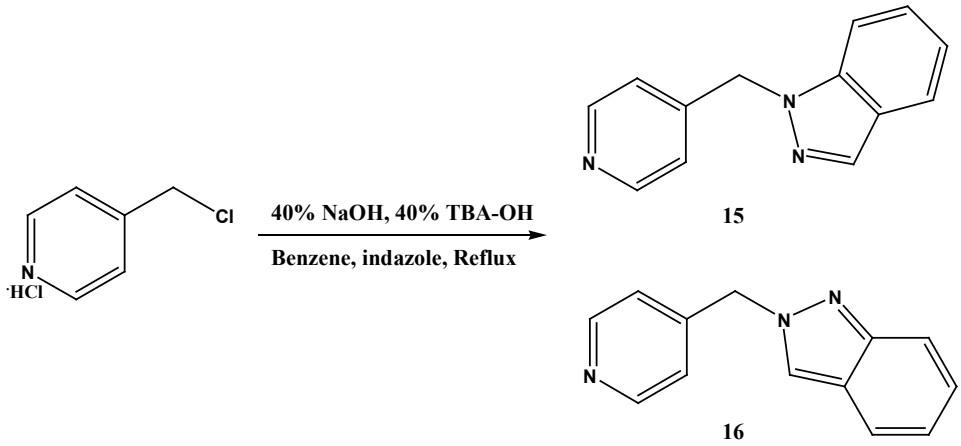

To a round bottom flask, 4-picolylchloride hydrochloride (0.500g, 3.04mmol), indazole (0.390g, 3.04mmol), 40% $NaOH_{(aq)}$ (8mL), 40% tetrabutylammonium hydroxide (4 drops) and

benzene (40mL) were added. The biphasic solution was stirred at reflux for 8 hours, cooled to room temperature and stirred over night. On completion of the stir, the benzene layer was extracted and the solvent removed under vacuum. The two product isomers were separated by column chromatography (hexanes:ethyl acetate; 20:1 → hexanes:ethyl acetate; 1:1), to yield a pale yellow solid **15**, (0.249g, 39.0%). Mp: 83-85°C. ^{1}H NMR (δ_H; 400MHz, $CDCl_3$): 5.48 (s, 2H), 6.90 (d, J = 12Hz, 1H), 7.09 (q, J = 16Hz, 2H) 7.20-7.30 (m, 1H), 7.67 (d, J = 16Hz, 2H), 7.98 (s, 1H), 8.41 (d, J = 8Hz, 1H), Figure B.15a; ^{13}C NMR, (δ_C; 50MHz, $CDCl_3$): 51.54, 108.82, 121.02, 121.34, 121.68, 124.34, 126.80, 134.07, 139.64, 145.79, 150.17, Figure B.15b; and a brown oil, **16**, (0.151g, 23.6%). ^{1}H NMR (δ_H; 400MHz, $CDCl_3$): 5.62 (s, 2H), 7.08 (d, J = 12Hz, 2H), 7.14 (d, J = 16Hz, 1H), 7.32 (t, J = 16Hz, 1H), 7.70 (dd, J^1 = 28Hz, J^2 = 16Hz, 1H), 7.99 (s, 1H), 8.57 (d, J = 12Hz, 2H), Figure B.16a; ^{13}C NMR, (δ_C; 50MHz, $CDCl_3$): 55.47, 117.31, 120.32, 121.76, 121.90, 121.93, 123.77, 126.23, 144.98, 149.04, 149.84, Figure B.16b.

4.2.1.4 Synthesis of 3-[(indazol-1-yl)methyl]pyridine, 17 and 3-[(indazole-2-yl)methyl]pyridine, 18

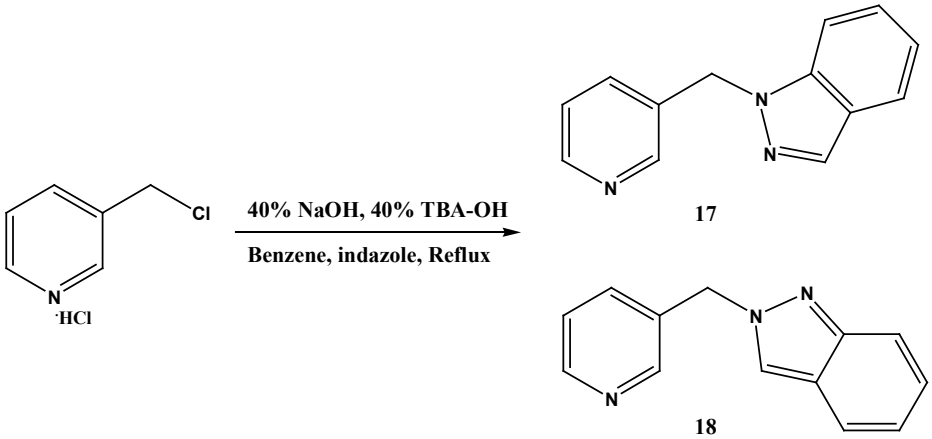

To a round bottom flask, 3-picolylchloride hydrochloride (0.500g, 3.04mmol), indazole (0.390g, 3.04mmol), 40% $NaOH_{(aq)}$ (8mL), 40% tetrabutylammonium hydroxide (4 drops) and benzene (40 mL) were added. The biphasic solution was stirred at reflux for 8 hours, cooled to room temperature and stirred over night. On completion of the stir, the benzene layer was extracted and the solvent removed under vacuum. The two product isomers were separated by column chromatography (hexanes:ethyl acetate; 20:1 → hexanes:ethyl acetate; 1:1), to yield an off white solid **17**, (0.146g, 23.0%). Mp: 73-76°C. ^{1}H NMR (δ_H; 400MHz, $CDCl_3$): 5.38 (s, 2H), 7.11-7.19 (m, 2H), 7.34 (d, J = 4Hz, 2H), 7.44 (d, J = 16Hz, 1H), 7.74 (dt, J^1 = 16Hz, J^2 = 4Hz,

1H), 8.05 (s, 1H), 8.49 (dd, J^1 = 8Hz, J^2 = 4Hz, 1H), 8.56 (d, J = 4Hz, 1H), Figure B.17a; ^{13}C NMR, (δ_C; 50MHz, $CDCl_3$): 50.16, 108.83, 120.83, 121.20, 123.50, 124.31, 126.60, 132.37, 133.77, 134.81, 139.35, 148.60, 149.20, Figure B.17b; and a brown oil, **18**, (0.0989g, 16.0%). ^{1}H NMR (δ_H; 400MHz, $CDCl_3$): 5.55 (s, 2H), 7.03-7.11 (m, 1H), 7.18-7.32 (m, 2H), 7.51-7.55 (m, 1H), 7.60-7.64 (m, 1H), 7.69-7.74 (m, 1H), 7.90 (s, 1H) 8.53 (dd, J^1 = 8Hz, J^2 = 4Hz, 1H), 8.57 (d, J = 4Hz, 1H), Figure B.18a; ^{13}C NMR, (δ_C; 50MHz, $CDCl_3$): 54.33, 117.28, 120.25, 121.77, 121.93, 123.11, 123.51, 126.08, 131.57, 135.25, 148.73, 148.95, 149.33, Figure B.18b.

4.2.1.5 Synthesis of 4-[(indazol-1-yl)methyl]pyridine : 4-nitrobenzoic acid (1:1), 15a

15 (0.015g, 0.72mmol) and 4-nitrobenzoic acid (0.012g, 0.72mmol) were added to a test tube along with acetonitrile. The mixture was heated gently until components were in solution. Colourless prisms suitable for X-ray diffraction were obtained after a few days via slow evaporation of acetonitrile. Mp: 159-162^{o}C. IR (KBr pellet): υ 3443, 2449, 1879, 1700, 1520, 1282, 765, 718 cm^{-1}.

4.2.1.6 Synthesis of 4-[(indazol-1-yl)methyl]pyridine : 3,5-dinitrobenzoic acid (1:1), 15b

15 (0.015g, 0.72mmol) and 3,5-dinitrobenzoic acid (0.015g, 0.72mmol) were added to a test tube along with acetonitrile. The mixture was heated gently until components were in solution. Yellow prisms suitable for X-ray diffraction were obtained after a few days via slow evaporation of acetonitrile. Mp: 132-135^{o}C. IR (KBr pellet): υ 3408, 3098, 2469, 1905, 1700, 1542, 1350, 732 cm^{-1}.

4.2.1.7 Synthesis of 4-[(indazol-1-yl)methyl]pyridine : succinic acid (1:1), 15c

15 (0.015g, 0.72mmol) and succinic acid (0.009g, 0.7mmol) were added to a test tube along with acetonitrile. The mixture was heated gently until components were in solution. Colourless prisms suitable for X-ray diffraction were obtained after a few days via slow evaporation of acetonitrile. Mp: 120-123^{o}C. IR (KBr pellet): υ 3442, 2918, 2546, 1926, 1711, 1609, 1184, 750 cm^{-1}.

4.2.1.8 Synthesis of 3-[(indazol-1-yl)methyl]pyridine : 4-nitrobenzoic acid (1:2), 17a

17 (0.015g, 0.72mmol) and 4-nitrobenzoic acid (0.012g, 0.72mmol) were added to a test tube along with acetonitrile. The mixture was heated gently until components were in solution.

Colourless prisms suitable for X-ray diffraction were obtained after a few days via slow evaporation of acetonitrile. Mp: 164-167^{o}C. IR (KBr pellet): υ 3458, 2429, 1878, 1700, 1510, 1346, 1273, 762 cm^{-1}.

4.2.1.9 Synthesis of 3-[(indazol-1-yl)methyl]pyridine : 3,5-dinitrobenzoic acid (1:1), 17b

17 (0.015g, 0.72mmol) and 3,5-dinitrobenzoic acid (0.015g, 0.72mmol) were added to a test tube along with acetonitrile. The mixture was heated gently until components were in solution. Yellow prisms suitable for X-ray diffraction were obtained after a few days via slow evaporation of acetonitrile. Mp: 130-132^{o}C. IR (KBr pellet): υ 3397, 2502, 1938, 1710, 1534, 1350, 1046, 731 cm^{-1}.

4.3 Results

All hydrogen bond geometries are listed in Table 4.1. A summary of the crystallographic information for each compound is displayed in Tables A.20-A.24.

Table 4.1 Hydrogen bond geometries for **15a-15c** and **17a-17c**.

Compound	D-H···A	D-H / Å	H···A / Å	D···A / Å	<(DHA) / ^{o}
15a	O(31)-H(31)...N(21)	0.980(18)	1.633(17)	2.6107(14)	175.3(16)
15b	O(31)-H(31)...N(21)	1.15(2)	1.39(2)	2.5409(16)	177.5(18)
15c^{i}	O(31)-H(31)...N(12) O(41)-H(41)...N(21)	0.90(3) 1.01(3)	1.81(3) 1.64(3)	2.705(2) 2.611(2)	171(2) 160(2)
17a	O(31)-H(31)...N(13) O(41)-H(41)...N(21)	0.959(14) 1.012(14)	1.688(14) 1.585(14)	2.6378(11) 2.5840(11)	170.1(14) 168.4(13)
17b	O(51)-H(51)...N(21) O(61)-H(61)...N(41)	0.84 0.84	1.74 1.68	2.579(6) 2.518(6)	178.3 177.1

(i) #1 -x+1,y,-z+1/2, #2 -x+1/2,-y-1/2,-z.

4.3.1 MEP surface calculations

In order to rank the hydrogen-bonding capability of the N-heterocyclic compounds included in this study, we calculated molecular electrostatic potential (MEP) surfaces for all compounds,[8] Table 4.2 and Figure 4.4. It has previously been shown[3] that such an approach is feasible even if the calculations are performed at a relatively low level of theory (AM1), which makes this a versatile and readily accessible tool.

Table 4.2 Molecular electrostatic surface potential calculations.

Ligand	$E(N_{Py})$ kJ mol^{-1}	$E(N_{Pz\ or\ Iz})$ kJ mol^{-1}
13	-270	-238
14	-279	-244
15	-282	-222
16	-265	-238
17	-264	-224
18	-258	-238

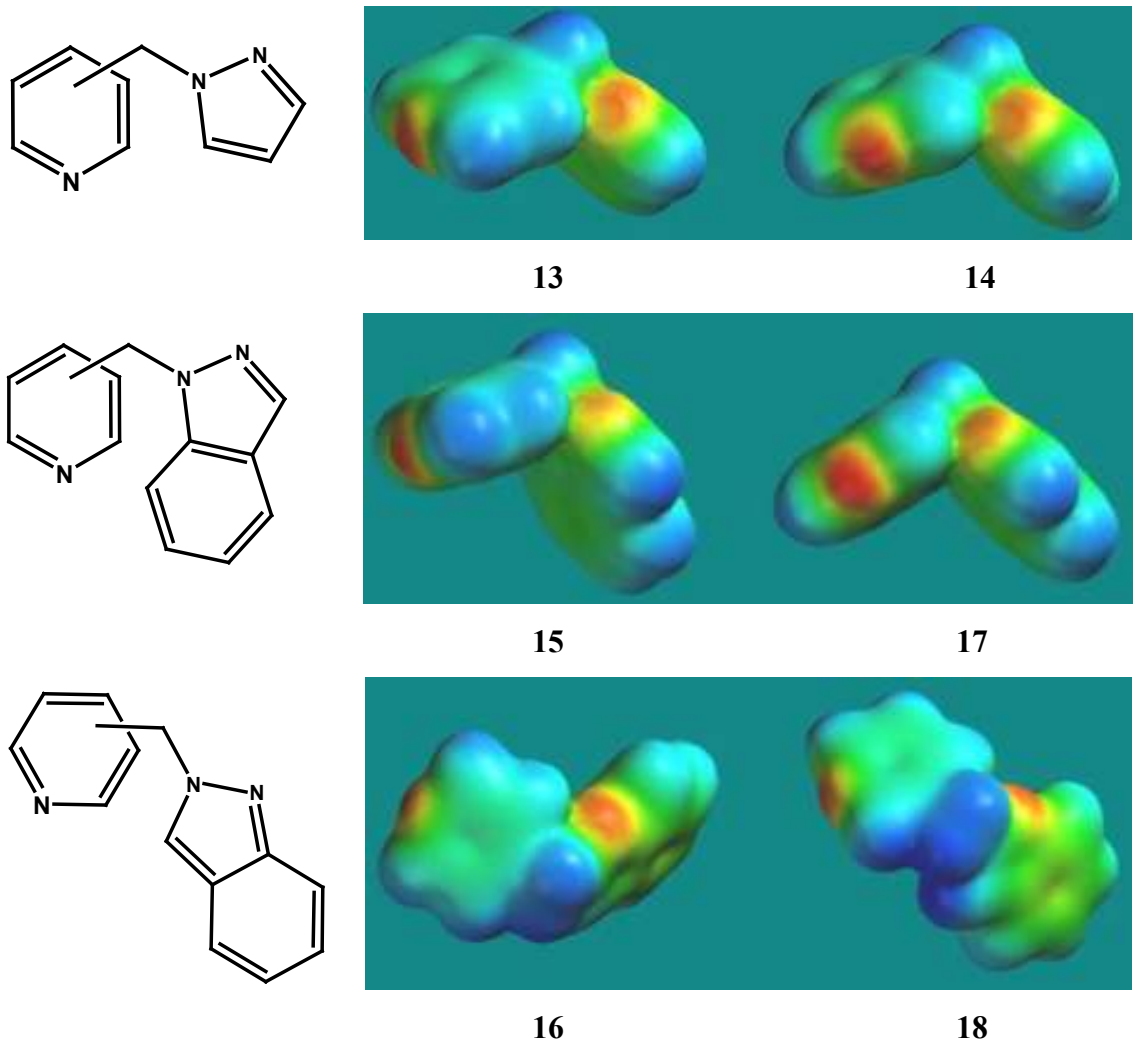

Figure 4.4 Molecular electrostatic potential surfaces for (pyrazol-1-yl)methylpyridine and (indazol-1-yl)methylpyridine SR's.

4.3.2 Crystal structure of 4-(indazol-1-yl)methylpyridine : 4-nitrobenzoic acid (1:1), 15a

The crystal structure of **15a** shows a 1:1 binary co-crystal with the carboxylic acid and the pyridyl moiety interacting via an acid-pyridyl O-H•••N hydrogen bond (2.6107(14) Å), Figure 4.5. There are no other significant hydrogen bonds present, as the indazole nitrogen is not participating in any hydrogen bonding.

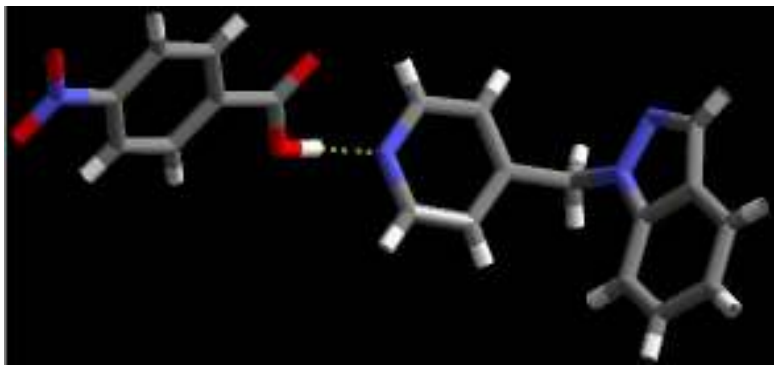

Figure 4.5 The 1:1 binary supermolecule observed in the crystal structure of **15a**.

4.3.3 Crystal structure of 4-(indazol-1-yl)methylpyridine : 3,5-dinitrobenzoic acid (1:1), 15b

Similar to **15a**, **15b** is a 1:1 binary co-crystal with the carboxylic acid and the pyridyl moiety interacting via an O-H•••N hydrogen bond (2.5409(16) Å), Figure 4.6. The indazole nitrogen atom is not participating in any hydrogen bonding.

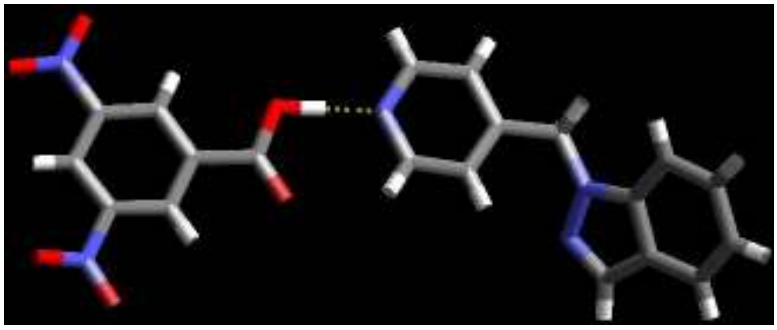

Figure 4.6 The 1:1 binary supermolecule observed in the crystal structure of **15b**.

4.3.4 Crystal structure of 4-(indazol-1-yl)methylpyridine : succinic acid (1:1), 15c

Both the pyridine and the indazole nitrogen atoms participate in hydrogen bonding in co-crystal **15c**. The diacid forms two symmetry related O-H•••N hydrogen bonds (2.611(2) Å) between succinic acid and two pyridyl nitrogen atoms on separate SR's, Figure 4.7. Similarly,

the diacid also forms a sandwich between two indazole moieties via two symmetry related O-H•••N hydrogen bonds (2.705(2) Å) producing a 1-D chain.

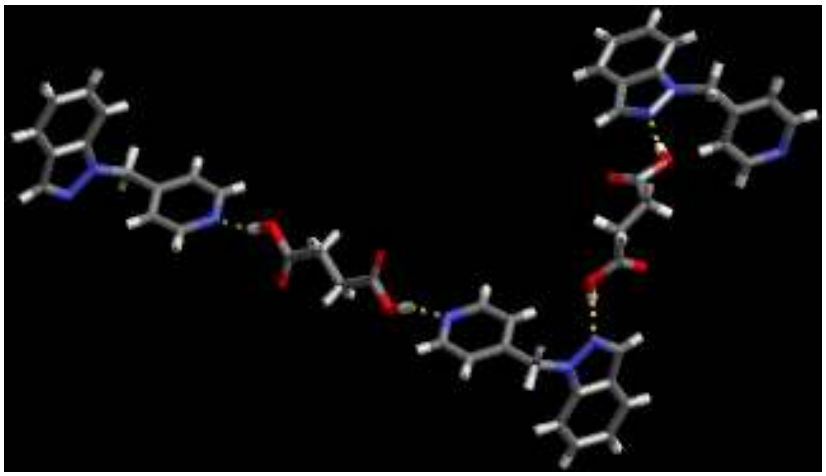

Figure 4.7 A section of the 1-D chain observed in the crystal structure of **15c**.

4.3.5 Crystal structure of 3-(indazol-1-yl)methylpyridine : 4-nitrobenzoic acid (1:2), 17a

17a consists of two carboxylic acids and one SR interacting via two independent O-H•••N hydrogen bonds between one acid and the pyridine nitrogen atom (2.5840(11) Å) and a second acid and the indazole nitrogen atom (2.6378(11) Å), Figure 4.8.

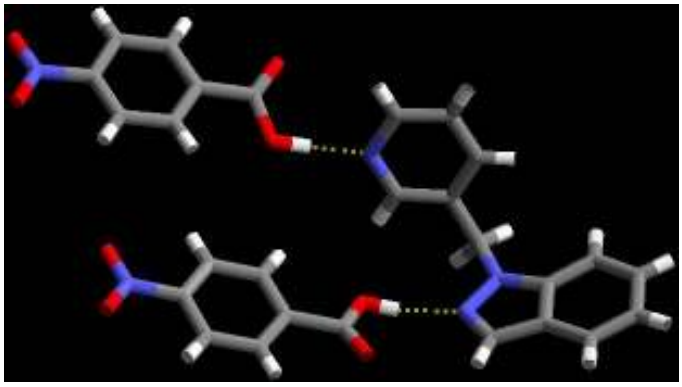

Figure 4.8 The 1:1 binary supermolecule observed in the crystal structure of **17a**.

4.3.6 Crystal structure of 3-(indazol-1-yl)methylpyridine : 3,5-dinitrobenzoic acid (1:1), 17b

The crystal structure of **17b** shows two similar 1:1 binary co-crystals with the two carboxylic acids and two SR's interacting via O-H•••N hydrogen bonds (2.579(6) Å and 2.518(6) Å respectively), Figure 4.9.

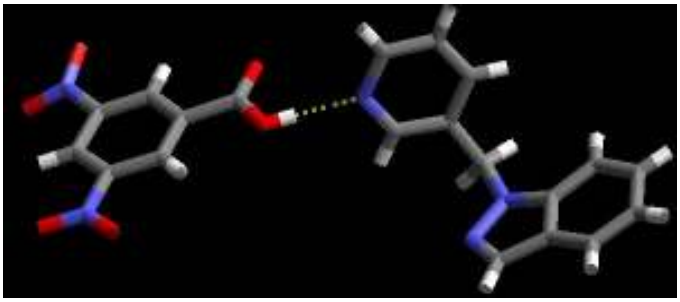

Figure 4.9 The 1:1 binary supermolecule observed in the crystal structure of **17b**.

4.3.7 Determining co-crystal formation by infra-red (IR) spectroscopy

Along with the five crystal structures reported, IR spectroscopy was carried out on a number of co-crystallisation reactions.[9] Although it is not possible to determine specific connectivity and stoichiometry within a co-crystal via this method, IR spectroscopy is still a highly effective tool for the identification of co-crystals. Distinct stretches at ~2500 cm^{-1} and ~1900 cm^{-1} are indicative of O-H•••N hydrogen bonds between the two individual components, Figure 4.10, and allows for a large number of co-crystallisation reactions to be carried out and monitored, Table 4.3.

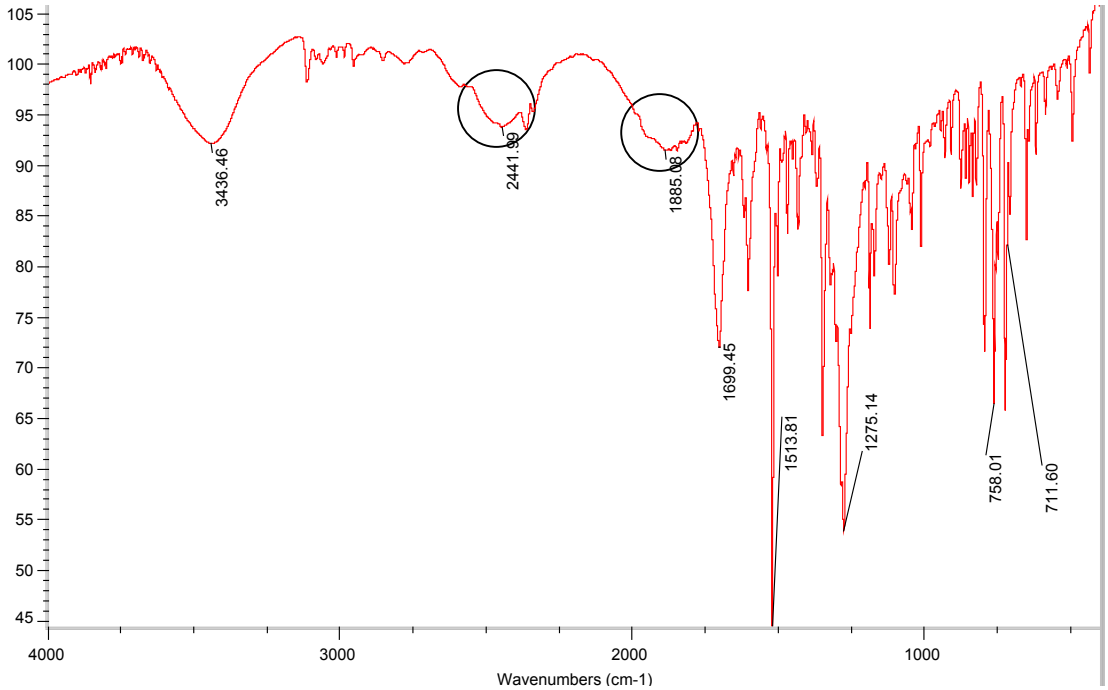

Figure 4.10 IR spectrum of **15a** displaying the O-H•••N stretches (circled).

Table 4.3 IR data.

SR	Carboxylic Acid	O-H···N stretches / cm^{-1}
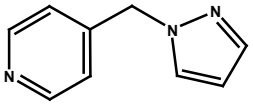 **13**	4-Nitrobenzoic Acid	2528 & 2051
	3,5-Dinitrobenzoic Acid	2500 & 2100
	4-Fluorobenzoic Acid	×
	3-Cyanobenzoic Acid	2502 & 1912
	Succinic Acid	2588 & 1991
	Fumaric Acid	2469 & 1898
	Oxalic Acid	2575 & 1931
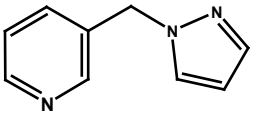 **14**	4-Nitrobenzoic Acid	2502 & 1951
	3,5-Dinitrobenzoic Acid	2482 & 1955
	3-Cyanobenzoic Acid	2422 & 1965
	Succinic Acid	×
	Fumaric Acid	2535 & 1905
	Oxalic Acid	2594 & 2100
	3,5-Difluorobenzoic Acid	2531 & 1918
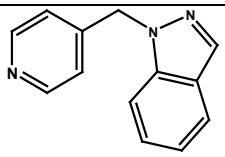 **15**	4-Nitrobenzoic Acid[i]	2449 & 1879
	3,5-Dinitrobenzoic Acid[i]	2469 & 1905
	Succinic Acid[i]	2546 & 1926
	4-Fluorobenzoic Acid	2462 & 1918
	Fumaric Acid	2482 & 1925
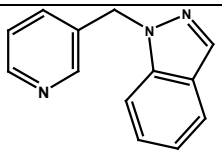 **17**	4-Nitrobenzoic Acid[i]	2429 & 1878
	3,5-Dinitrobenzoic Acid[i]	2502 & 1938
	3-Cyanobenzoic Acid	2515 & 1898
	3,5-Difluorobenzoic Acid	2455 & 1965
	Fumaric Acid	2535 & 1859

(i) Crystal structure determined

4.4 Discussion

4.4.1 Determining the best hydrogen-bond acceptor site in the ditopic SR

O-H···N hydrogen-bond stretches were observed in the IR spectra of 22 of the 24 (92%) co-crystallisations.

Single crystal data confirms that O-H···N hydrogen bonds between the incoming carboxylic acid and the pyridine of the SR was present in all cases, Figure 4.11.

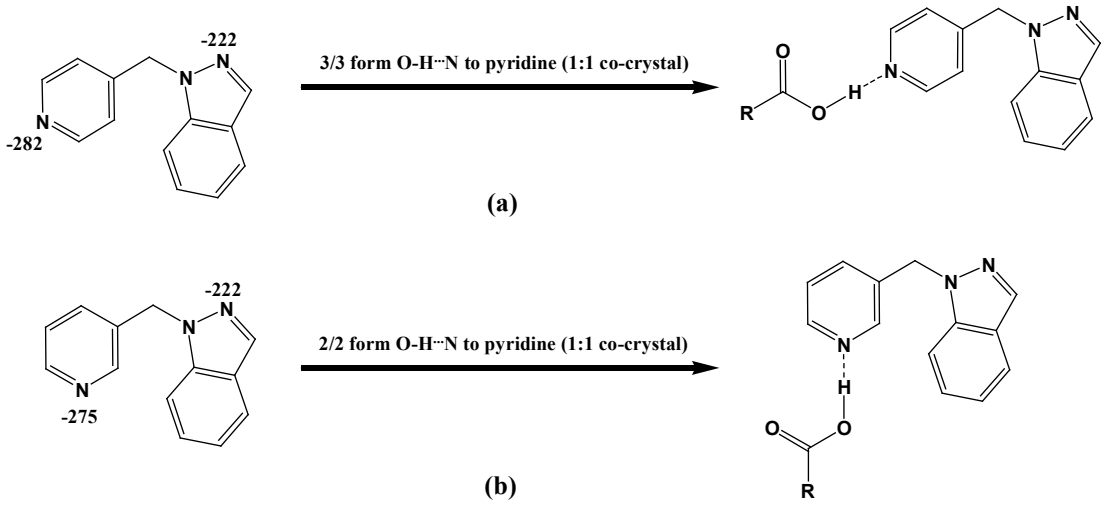

Figure 4.11 Co-crystals of (a) 4-(indazol-1-yl)methylpyridine and (b) 3-(indazol-1-yl)methylpyridine with carboxylic acids.

All co-crystallisations were set up in a 1:1 ratio however, **17a** contains two molecules of 4-nitrobenzoic acid interacting at both pyridine and indazole nitrogen atoms of one SR, Figure 4.12a. Also, 1**5c** shows the indazole nitrogen is able to accept a hydrogen bond, Figure 4.12b.

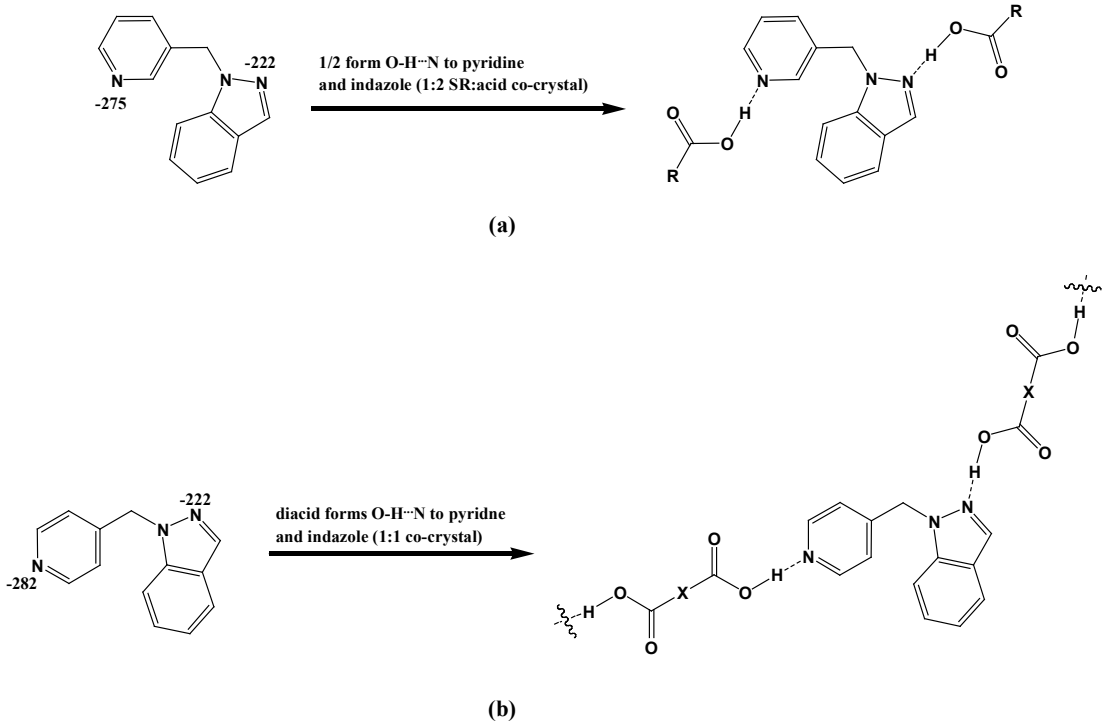

Figure 4.12 Acceptor ability of indazole nitrogen in co-crystals of (a) 4-(indazol-1-yl)methylpyridine and (b) 3-(indazol-1-yl)methylpyridine with carboxylic acids.

Although hydrogen-bond interactions are observed between a carboxylic acid and the indazole nitrogen atom of the SR's, it is clear that indazole is the second-best acceptor. This is evidenced by (a) the lack of 1:1 co-crystals composed solely of O-H•••N hydrogen bonds between the acid and the indazole moiety and (b) the shorter acid-pyridine O-H•••N hydrogen-bond lengths compared to acid-indazole, Table 4.4.

Table 4.4 Acid-pyridine O-H•••N hydrogen-bond lengths compared to acid-indazole O-H•••N hydrogen-bond lengths.

Co-crystal	Acid-pyridine O-H•••N hydrogen-bond lengths / Å	Acid-indazole O-H•••N hydrogen-bond lengths / Å
15c	2.611(2)	2.705(2)
17a	2.5840(11)	2.6378(11)

The structural analysis of five co-crystals between (indazol-1-yl)methylpyridine SR's and a carboxylic acid have provided reliable answers to the questions addressed at the beginning of this chapter.

I. Can the hydrogen-bond acceptor strength of the second N-heterocycle be lowered such that pyridine becomes the best acceptor?

The MEP of the second N-heterocycle was lowered sufficiently to move the incoming carboxylic acid to the pyridine moiety. MEP surface calculations provide practical guidelines for identifying best and second-best acceptor sites in ditopic SR's, Figure 4.13.

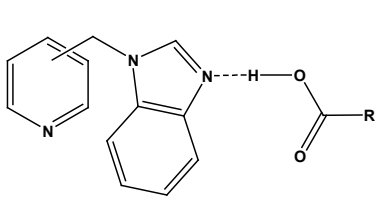

100% supramolecular yield for an acid-benzimidazole interaction via an O-H···N hydrogen-bond.

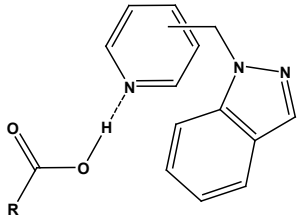

100% supramolecular yield for an acid-pyridine interaction via an O-H···N hydrogen-bond.

Figure 4.13 Hierarchical approach to controlling hydrogen-bond interactions in pyridine/N-heterocycle SR's.

II. Can the hydrogen-bond acceptor strength of the second N-heterocycle be lowered (compared to benzimidazole) to prevent deprotonation of the incoming carboxylic acid?

Replacing benzimidazole with indazole reduced the hydrogen-bond acceptor strength from ~-300 kJ/mol to ~-223kJ/mol. This decrease was significant enough to change the frequency of deprotonation from ~50% in benzimidazole systems to 0% in indazole systems, Figure 4.14.

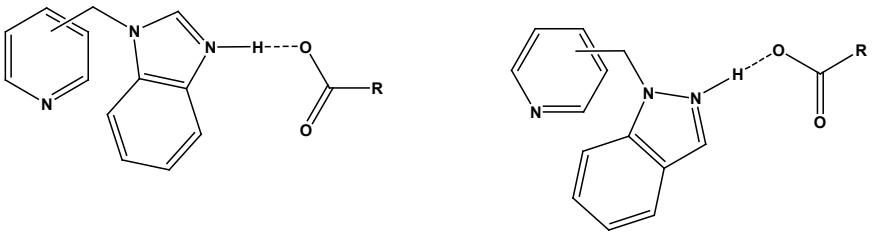

53% supramolecular yield for deprotonation of the carboxylic acid by benzimidazole.

0% supramolecular yield for deprotonation of the carboxylic acid by indazole.

Figure 4.14 Ability to fine-tune the acceptor strength of the N-heterocycle to prevent deprotonation of the incoming carboxylic acid.

This adds substance to the results previously obtained for benzimidazole-pyridine ditopic systems[5] validating MEP surface calculations as a tool for predicting a hierarchy of hydrogen-bond acceptors in ditopic heterocycle SR's.

References

1. (a) C. B. Aakeröy, A. M. Beatty and B. A. Helfrich, *J. Am. Chem. Soc.*, 2002, **124**, 14425; (b) C. B. Aakeröy, A. M. Beatty, B. A. Helfrich and M. Nieuwenhuyzen, *Cryst. Growth Des.*, 2003, **3**, 159; (c) C. B. Aakeröy, J. Desper and B. A. Helfrich, *CrystEngComm.*, 2004, **6**, 19; (d) B. R. Bhogala, S. Basavgu and A. Nangia, *CrystEngComm.*, 2005, **7**, 551; (e) P. Vishweshwar, A. Nangia and V. M. Lynch, *Cryst. Growth Des.*, 2003, **3**, 783.
2. For a discussion on pyrazol-1-yl benzamide co-crystals, see Chapter 3.
3. C. A. Hunter, *Angew. Chem. Int. Ed*, 2004, **43**, 5310-5324.
4. (a) G. S. Papaefstathiou, A. J. Kipp and L. R. MacGillivray, *Chem. Commun.*, 2001, 2462; (b) T. L. Nguyen, F. W. Fowler and J. W. Lauher, *J. Am. Chem. Soc.*, 2001, **123**, 11057; (c) V. R. Pedireddi, A. Ranganathan and S. Chatterjee, *Tetrahedron Lett.*, 1998, **39**, 9831; (d) M. Vinodu and I. Goldberg, *Cryst. Eng. Comm.*, 2005, **7**, 133; (e) R. D. B. Walsh, M. W. Bradner, S. Fleischman, L. A. Morales, B. Moulton, N. Rodriguez-Hornedo and M. J. Zaworotko, *Chem. Commun.*, 2003, 186; (f) N. Shan and W. Jones, *Tetrahedron Lett.*, 2003, **44**, 3687.
5. C. B. Aakeröy, J. Desper and J. F. Urbina, *Chem. Commun.*, 2005, 2820.
6. C. B. Aakeröy, J. Desper and J. F. Urbina, *unpublished results*.
7. pKa values for the conjugate acids were estimated from *Dissociation constants of organic bases in aqueous solution*, Butterworth and Co., London, 1965.
8. Molecular structures for **13**-**18** were constructed using Spartan ’06 (Wavefunction, Inc. Irvine, CA). All six molecules were optimized using AM1, with the maxima and minima in the electrostatic potential surface (0.002 e/au isosurface) determined using a positive point charge in the vacuum as a probe.
9. Co-crystallisation reactions frequently yielded homogeneous powders, which were analysed by IR.

CHAPTER 5 - Employing Ditopic Pyrimidine/Bis-Pyrazole Supramolecular Reagents to Construct Co-crystals and Inorganic-Organic Hybrid Materials

5.1 Introduction

Pyrazole is a good hydrogen-bond acceptor,[1] however, in SR's when pyrazole is coupled to a hydrogen-bond acceptor such as an amide moiety[2] or a pyridyl functionality,[3] the ability to act as a hydrogen-bond acceptor is relatively poor.

In order to assess the hydrogen-bond acceptor ability of pyrazole in a ditopic SR, a system needs to be designed in which pyrazole is the best hydrogen-bond acceptor. This can be achieved by pairing pyrazole with a considerably poorer hydrogen-bond acceptor (based on approximated pK_a values of the conjugate acids). Furthermore, the acceptor strength of the pyrazole nitrogen atom can be fine-tuned through simple covalent modifications to the ring (e.g. by adding electron donating methyl groups) allowing for a range of acceptor strengths to be obtained.

When choosing the second weaker hydrogen-bond acceptor, pyrimidine, Figure 5.1, is a good candidate.

pK_a = ~1.1 **pK_a = ~2.5**

Figure 5.1 Pyrimidine and pyrazole with pK_a values of the conjugate acids.

The conjugate acid of pyrimidine has a significantly lower pK_a than pyrazole (1.1 cf: 2.5)[4] and coupled with the limited number of co-crystals in the CSD[5] (there are only three 1:1 co-crystals between a carboxylic acid and pyrimidine[6]), makes it a suitable target for such a study.

Additionally, pyrimidine-pyrazole[4, 7] systems have been exploited in coordination chemistry as chelating ligands, Figure 5.2. It makes sense then to have a structurally similar backbone that can be implemented to examine a MEP-based approach to co-crystal predictability as well as to provide control over metal coordination.

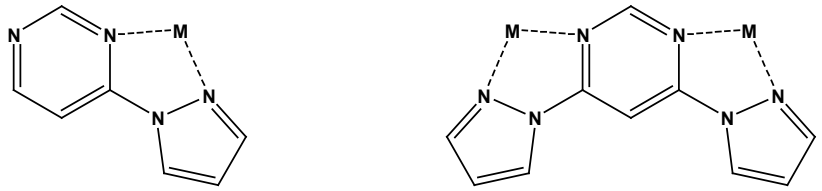

Figure 5.2 Pyrimidine-pyrazole as a chelating ligand.

This chapter will address two questions:

I. Is pyrazole a better hydrogen-bond acceptor than pyrimidine?

II. Can pyrimidine/pyrazole ligands be used successfully as chelating ligands to construct reliable coordination complexes?

With this in mind, a family of SR's has been targeted in which pyrimidine is appended with two pyrazole arms, Figure 5.3. This makes pyrazole the better hydrogen-bond acceptor (based on pKa and charge approximations[4]) compared to pyrimidine.

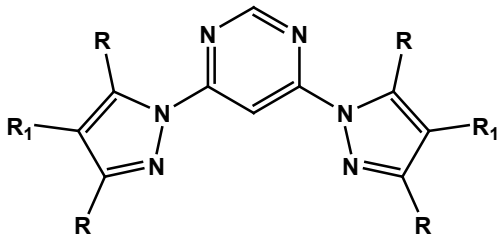

1) R=H, R_1=H
2) R=Me, R_1=H
3) R=Me, R_1=Br
4) R=H, R_1=Br
5) R=H, R_1=I

Figure 5.3 Target pyrimidine/bis-pyrazole SR's.

Through a series of co-crystallisations, the potential to form co-crystals (determined by infra-red spectroscopy) and a hierarchy of preferential binding, Figure 5.4, (determined by single crystal X-ray diffraction) will be established.

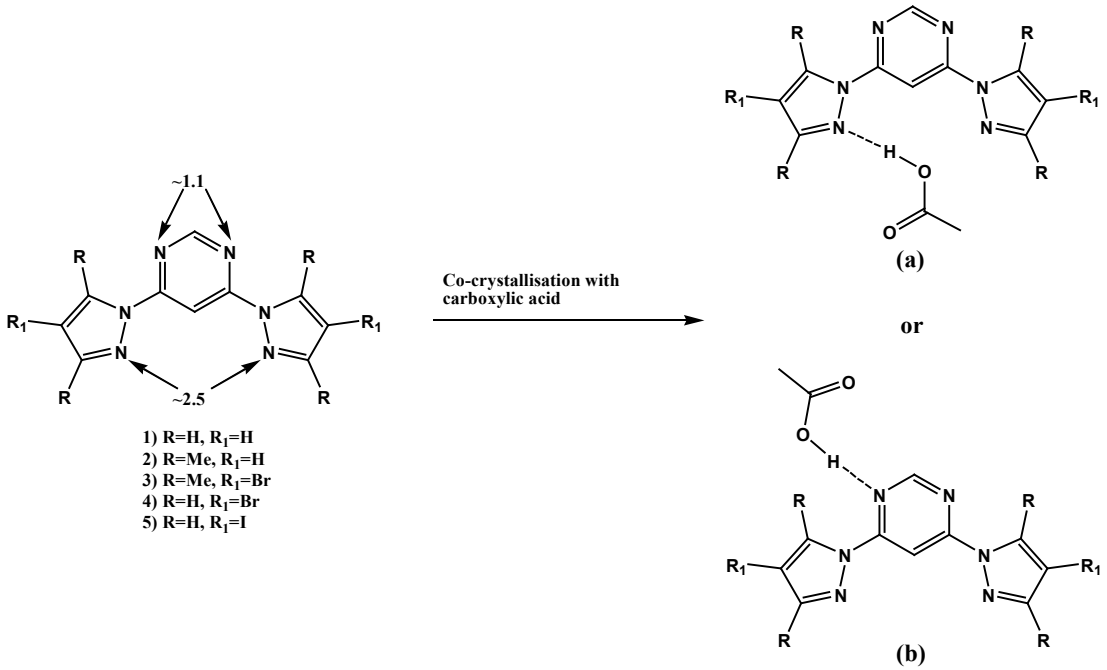

Figure 5.4 Target pyrimidine/bis-pyrazole SR's with pKa numbers and the potential co-crystallisation products. The pKa values for the conjugate acids indicate the pyrazole nitrogen atom is the better acceptor and consequently co-crystallisation product (a) is expected.

Additionally, the direct N-C coupling between pyrazole and pyrimidine creates a suitable bidentate chelate ligand, Figure 5.5, for the construction of extended metal-containing architectures.

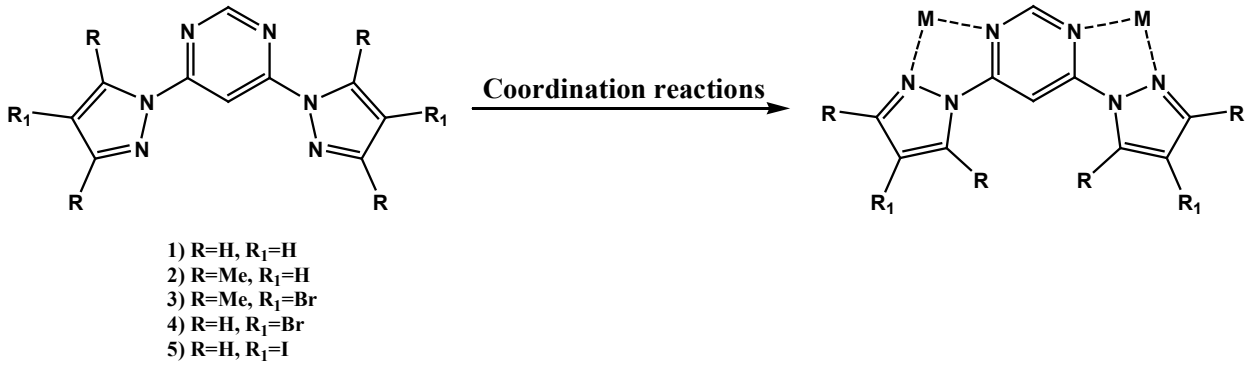

Figure 5.5 Target pyrimidine/bis-pyrazole ligands and the potential inorganic-organic hydrid materials.

5.2 Experimental

5.2.1 Synthesis

All chemicals were purchased from Aldrich and Fischer and used without further purification. 4-Bromo-3,5-dimethylpyrazole and 4-iodopyrazole were synthesised via previously published procedures.[8,9] Melting points were determined on a Fisher-Johns melting point apparatus and are uncorrected.

5.2.1.1 Synthesis of 4,6-bis(pyrazol-1-yl)pyrimidine, 19

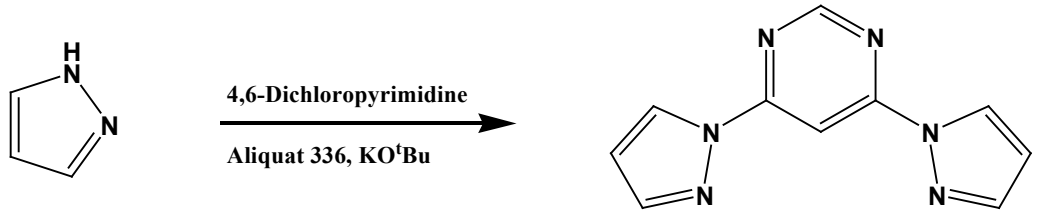

To a round bottom flask, pyrazole (0.500g, 7.35mmol), Aliquat® 336 (trioctylmethylammonium chloride) (0.196g, 0.490mmol) and potassium *tert*-butoxide (1.47g, 13.1mmol) were added and stirred for 30min at 120°C. 4,6-Dichloropyrimidine (1.64g, 11mmol) was added to the reaction and stirred overnight. The reaction was cooled and methylene chloride (25mL) was added. The organics were washed with water (3x25mL), dried over $MgSO_4$ and reduced to a white solid. The solid was purified by column chromatography (hexanes → 30:1 hexanes:ethyl acetate) to yield **19** as a white solid, (0.200g, 25%). Mp: 120-123°C. ^{1}H NMR (δ_H; 200MHz, $CDCl_3$): 6.53 (t, J = 2Hz, 2H), 7.82 (d, J = 1.4Hz, 2H), 7.98 (d, J = 0.6Hz, 1H), 8.57 (d, J = 4Hz, 2H), 8.80 (s, 1H), Figure B.19a; ^{13}C NMR, (δ_C; 50MHz, $CDCl_3$): 95.68, 109.01, 127.79, 143.93, 158.00, 158.79, Figure B.19b.

5.2.1.2 Synthesis of 4,6-bis(3,5-dimethylpyrazol-1-yl)pyrimidine, 20

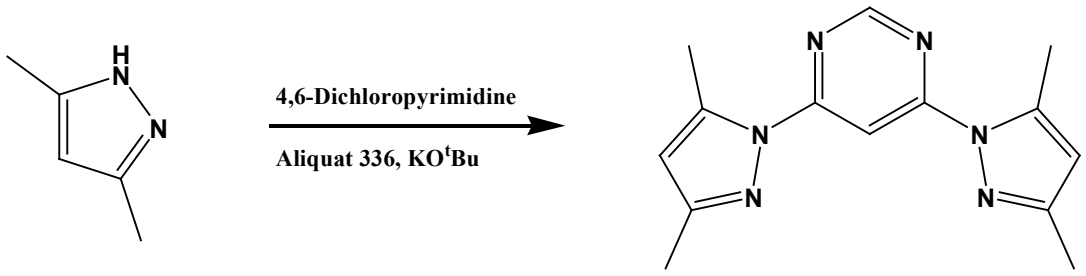

To a round bottom flask, 3,5-dimethylpyrazole (0.500g, 5.2mmol), Aliquat® 336 (0.139g, 0.343mmol) and potassium *tert*-butoxide (1.04g, 9.27mmol) were added and stirred for 30min at 120°C. 4,6-Dichloropyrimidine (1.63g, 10.9mmol) was added to the reaction and stirred overnight. The reaction was cooled and methylene chloride (25mL) was added. The organics were washed with water (3x25mL), dried over $MgSO_4$ and reduced to a white solid. The solid was purified by column chromatography (hexanes → 30:1 hexanes:ethyl acetate) to yield **20** as a white solid, (0.260g, 37.3%). Mp: 127-130°C. ^{1}H NMR (δ_H; 200MHz, $CDCl_3$): 2.31 (s, 3H), 2.72 (s, 3H), 6.02 (s, 2H), 8.38 (d, *J* = 1.2Hz, 1H), 8.75 (d, *J* = 1.2Hz, 1H), Figure B.20a; ^{13}C NMR, (δ_C; 50MHz, $CDCl_3$): 13.75, 15.36, 99.43, 110.65, 142.79, 151.59, 156.80, 160.57, Figure B.20b.

5.2.1.3 Synthesis of 4,6-bis(4-bromo-3,5-dimethylpyrazol-1-yl)pyrimidine, 21

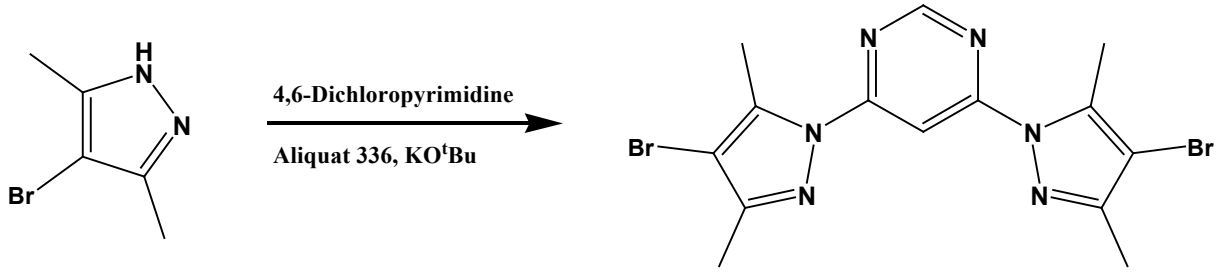

To a round bottom flask, 4-bromo-3,5-dimethylpyrazole (0.500g, 2.86mmol), Aliquat® 336 (0.0760g, 0.189mmol) and potassium *tert*-butoxide (0.570g, 5.09mmol) were added and stirred for 30min at 120°C. 4,6-Dichloropyrimidine (0.200g, 1.36mmol) was added to the reaction and stirred overnight. The reaction was cooled and methylene chloride (25mL) was added. The organics were washed with water (3x25mL), dried over $MgSO_4$ and reduced to a white solid. The solid was purified by column chromatography (hexanes → 30:1 hexanes:ethyl acetate) to yield **21** as a white solid, (0.157g, 27.1%). Mp: 247-250°C. ^{1}H NMR (δ_H; 200MHz, $CDCl_3$): 2.31 (s, 3H), 2.74 (s, 3H), 7.97 (s, 1H), 8.78 (s, 1H), Figure B.21a; ^{13}C NMR, (δ_C; 50MHz, $CDCl_3$): 12.74, 14.46, 98.94, 100.94, 140.32, 150.49, 156.91, 160.49, Figure B.21b.

5.2.1.4 Synthesis of 4,6-bis(4-bromopyrazol-1-yl)pyrimidine, 22

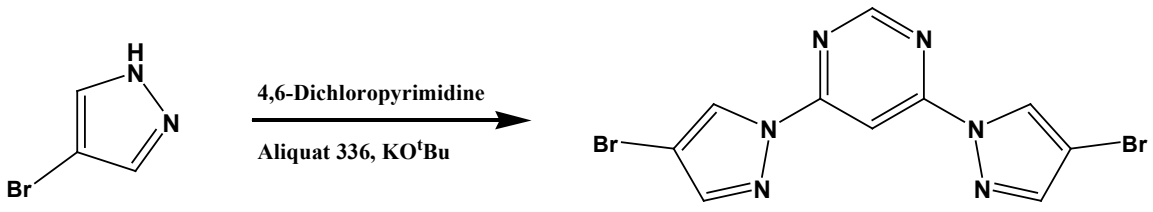

To a round bottom flask, 4-bromopyrazole (0.500g, 3.40mmol), Aliquat® 336 (0.0910g, 0.225mmol) and potassium *tert*-butoxide (0.680g, 6.05mmol) were added and stirred for 30min at 120°C. 4,6-Dichloropyrimidine (0.241g, 1.62mmol) was added to the reaction and stirred overnight. The reaction was cooled and methylene chloride (25mL) was added. The organics were washed with water (3x25mL), dried over $MgSO_4$ and reduced to a white solid. The solid was purified by column chromatography (hexanes → 30:1 hexanes:ethyl acetate) to yield **22** as a white solid, (0.222g, 35.2%). Mp: 212-215°C. ^{1}H NMR (δ_H; 200MHz, $CDCl_3$): 7.76 (d, J = 0.8Hz, 2H), 8.40 (d, J = 1Hz, 1H), 8.61 (d, J = 0.8Hz, 2H), 8.79 (d, J = 1Hz, 1H), Figure B.22a; ^{13}C NMR, (δ_C; 100MHz, $CDCl_3$): 94.94, 98.17, 127.93, 144.55, 158.14, 158.24, Figure B.22b.

5.2.1.5 Synthesis of 4,6-bis(4-iodoopyrazol-1-yl)pyrimidine, 23

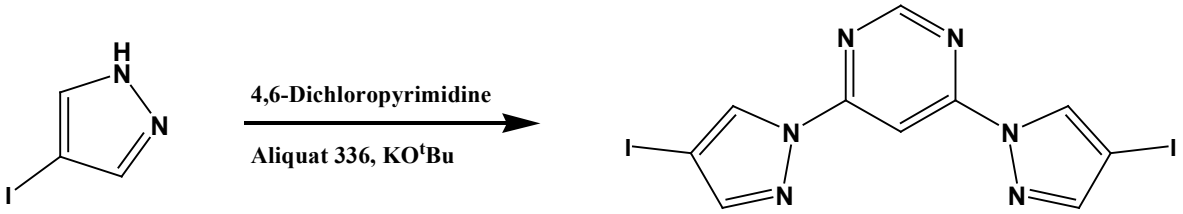

To a round bottom flask, 4-iodopyrazole (1.00g, 5.16mmol), Aliquat® 336 (0.138g, 0.341mmol) and potassium *tert*-butoxide (1.03g, 9.18mmol) were added and stirred for 30min at 120°C. 4,6-Dichloropyrimidine (0.370g, 2.46mmol) was added to the reaction and stirred overnight. The reaction was cooled and methylene chloride (50mL) was added. The organics were washed with water (3x50mL), dried over $MgSO_4$ and reduced to a white solid. The solid was purified by column chromatography (hexanes → 30:1 hexanes:ethyl acetate) to yield **23** as a white solid, (0.430g, 37.4%). Mp: 220-222°C. ^{1}H NMR (δ_H; 200MHz, $CDCl_3$): 7.80 (s, 2H), 8.40 (d, J = 1Hz, 1H), 8.66 (d, J = 0.6Hz, 2H), 8.78 (d, J = 1Hz, 1H), Figure B.23a; ^{13}C NMR, (δ_C; 50MHz, $CDCl_3$): 94.98, 108.47, 132.41, 148.66, 158.09, 158.41, Figure B.23b.

5.2.1.6 Synthesis of 4,6-bis(pyrazol-1-yl)pyrimidine : 3,5-dinitrobenzoic acid (1:1), 19a

19 (0.0250g, 0.118mmol) and 3,5-dinitrobenzoic acid (0.0250g, 0.118mmol) were added to a test tube along with acetonitrile. The mixture was heated gently until components were in solution. Colourless prisms suitable for X-ray diffraction were obtained after a few days via slow evaporation of acetonitrile. Mp: 123-126°C. IR (KBr pellet): υ 3432, 3135, 3094, 2500, 1865, 1696, 1055, 1350, 733 cm^{-1}.

5.2.1.7 Synthesis of 4,6-bis(pyrazol-1-yl)pyrimidine : 4-nitrobenzoic acid (1:1), 19b

19 (0.0250g, 0.118mmol) and 4-nitrobenzoic acid (0.0200g, 0.118mmol) were added to a test tube along with acetonitrile. The mixture was heated gently until components were in solution. Colourless plates suitable for X-ray diffraction were obtained after a few days via slow evaporation of acetonitrile. Mp: 164-167^{o}C. IR (KBr pellet): υ 3450, 3138, 2475, 1905, 1719, 1593, 1527, 1388, 712 cm^{-1}.

5.2.1.8 Synthesis of 4,6-[bis(3,5-dimethylpyrazol-1-yl)pyrimidine]copper(II) dichloride, 20a

20 (0.0150g, 0.0560mmol) was dissolved in acetonitrile and combined with an acetonitrile solution of $CuCl_2$ (0.00300g, 0.00187mmol). Blue needles suitable for X-ray diffraction were obtained after a few days via slow evaporation of acetonitrile. Mp: 270-273^{o}C (dec). IR (KBr pellet): υ 2925, 1603, 1475, 1317, 1035, 723 cm^{-1}.

5.3 Results

All hydrogen bond geometries for **19a** and **19b** are listed in Table 5.1. A summary of the crystallographic information for each compound is displayed in Tables A.25-A.28.

Table 5.1 Hydrogen bond geometries for **19a-19b**

Compound	D-H···A	D-H / Å	H···A / Å	D···A / Å	<(DHA) / º
19a	O411-H411...N221	0.93(3)	1.70(3)	2.625(3)	174(3)
	O412-H412...N222	0.92(3)	1.73(3)	2.656(3)	175(2)
	O413-H413...N223	0.93(3)	1.73(3)	2.656(3)	178(2)
19b	O(41)-H(41)...N(22)	0.90(2)	1.79(2)	2.6917(18)	172.8(17)

5.3.1 MEP calculations

In order to rank the hydrogen-bonding capability of the N-heterocyclic compounds included in this study, we calculated molecular electrostatic potential (MEP) surfaces for all compounds,[10] Table 5.2 and Figure 5.6. It has previously been shown[11] that such an approach is feasible even if the calculations are performed at a relatively low level of theory (AM1), which makes this a versatile and readily accessible tool.

Table 5.2 Molecular electrostatic potential surface calculations.

Ligand	$E(N_{Pym})$ kJ mol^{-1}	$E(N_{Pz})$ kJ mol^{-1}
19	-208	-219
20	-163	-230
21	-146	-211
22	-185	-186
23	-175	-191

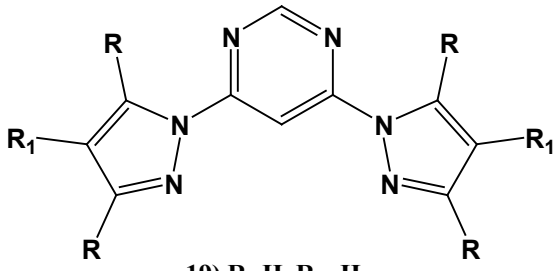

19) R=H, R_1=H
20) R=Me, R_1=H
21) R=Me, R_1=Br
22) R=H, R_1=Br
23) R=H, R_1=I

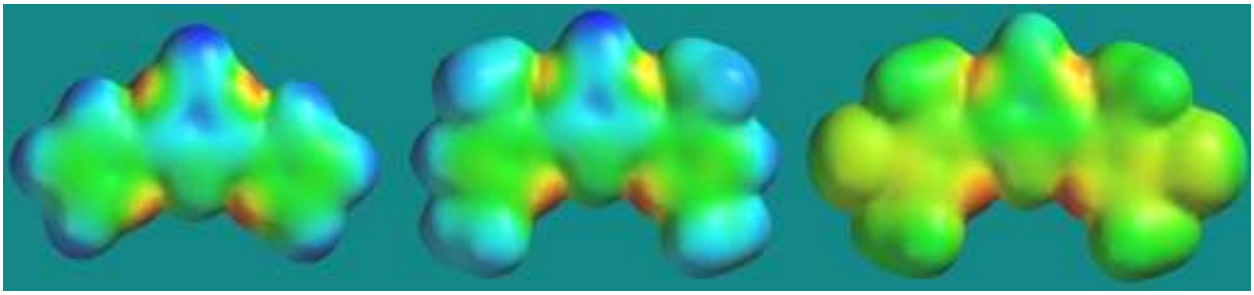

19 **20** **21**

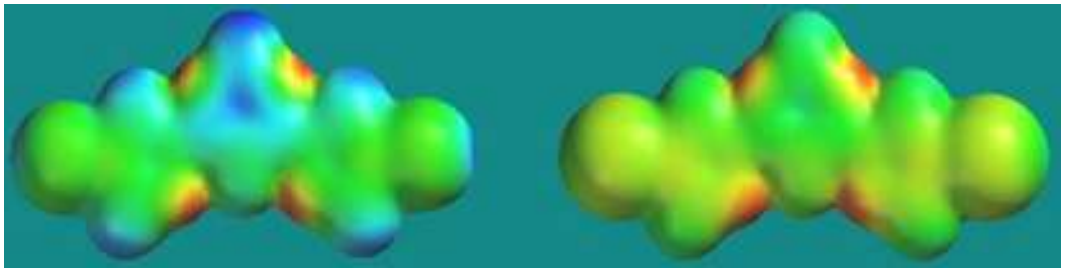

22 **23**

Figure 5.6 Molecular electrostatic potential surfaces for 4,6-bis(pyrazol-1-yl)pyrimidine SR's.

5.3.2 Crystal structure of 4,6-bis(3,5-dimethylpyrazol-1-yl)pyrimidine, 20

The crystal structure of **20** shows both pyrazole arms located in the *trans* orientation with respect to pyrimidine and pyrazole nitrogen atoms, Figure 5.7.

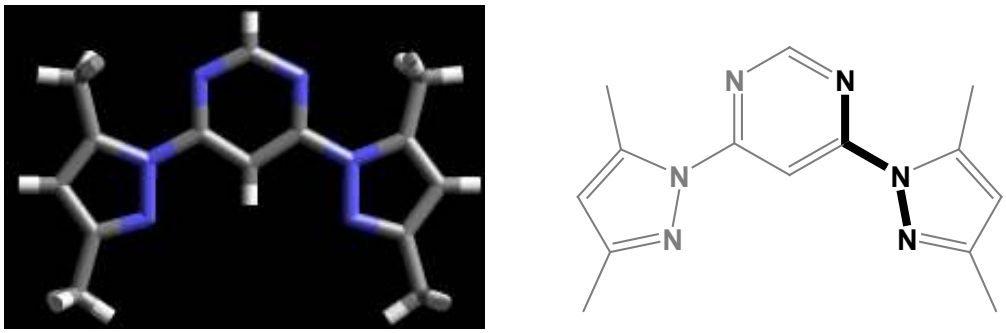

Figure 5.7 One molecule of **20** observed in the crystal structure showing *trans* orientation.

5.3.3 Crystal structure of 4,6-bis(pyrazol-1-yl)pyrimidine : 3,5-dinitrobenzoic acid (1:1), 19a

The crystal structure of **19a** shows three structurally similar dimeric supermolecules with the incoming carboxylic acid and one of the *trans* pyrazole moieties interacting via an O-H•••N hydrogen bond (2.625(3) Å, 2.656(3) Å, 2.656(3) Å respectively), Figure 5.8. Neither pyrimidine nitrogen atom is participating in any hydrogen bonding.

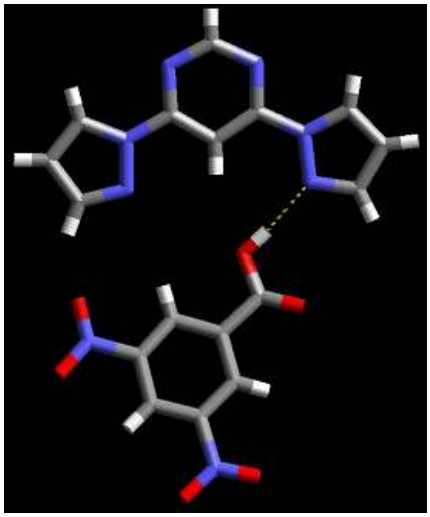

Figure 5.8 One of the three 1:1 binary supermolecule observed in the crystal structure of **19a**.

5.3.4 Crystal structure of 4,6-bis(pyrazol-1-yl)pyrimidine : 4-nitrobenzoic acid (1:1), 19b

Similar to **19a**, **19b** is a 1:1 binary co-crystal with the carboxylic acid and one of the *trans* pyrazole moieties interacting via an O-H•••N hydrogen bond (2.6917(18) Å), Figure 5.9. Neither pyrimidine nitrogen atom is participating in any hydrogen bonding.

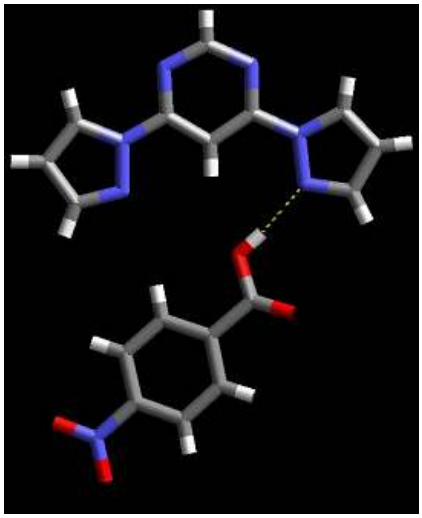

Figure 5.9 The 1:1 binary supermolecule observed in the crystal structure of **19b**.

5.3.5 Crystal structure of 4,6-[bis(3,5-dimethylpyrazol-1-yl)pyrimidine]copper(II) dichloride, 20a

The coordination complex **20a** shows **20** chelating to a five-coordinate copper centre (Cu-N 2.031(2) Å and 2.047(2) Å, respectively). A dinuclear ion is produced via two Cu-Cl-Cu bridges (Cu-Cl 2.3156(7) Å, 2.6656(8) Å, 2.3156(7) Å and 2.6657(8) Å respectively) to a symmetry related copper centre giving a Cu-Cu distance of ~3.640 Å, Figure 5.10a. The fifth coordination site of each copper ion is occupied by a terminal chloride ion (Cu-Cl 2.2434(8) Å).

A second copper ion is also observed with **20** chelating to a tetrahedral copper centre (Cu-N 2.015(2) Å and 2.043(2) Å, respectively), Figure 5.10b. The two remaining sites on the copper ion are occupied by terminal chloride ions (Cu-Cl 2.2131(8) Å and 2.2427(8) Å respectively).

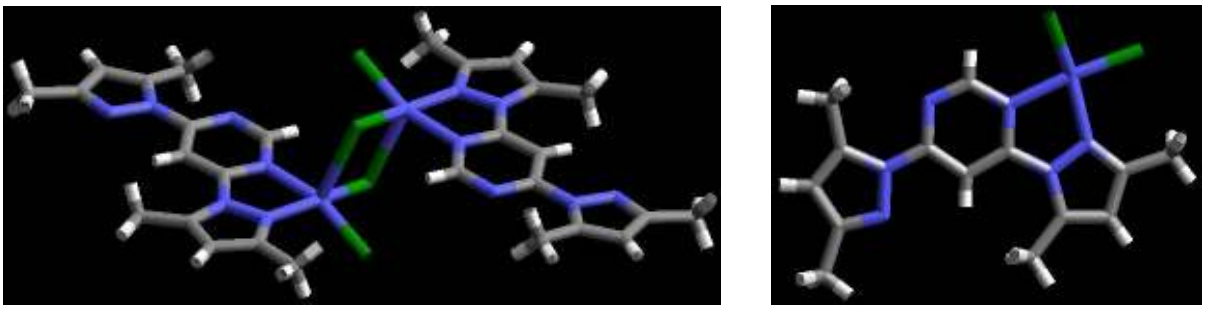

(a) (b)

Figure 5.10 Two different complex ions observed in the crystal structure **20a** showing: (a) two symmetry related five-coordinate copper(II) ions interconnected by two Cu-Cl-Cu bridges and (b) tetrahedral copper(II) ion with two terminal chloride ions.

5.3.6 Determining co-crystal formation by infra-red (IR) spectroscopy

Along with the two crystal structures reported, IR spectroscopy was carried out on a number of co-crystallisation reactions.[12] Although it is not possible to determine specific connectivity and stoichiometry within a co-crystal via this method, IR spectroscopy is still a highly effective tool for the identification of co-crystals. Distinct stretches at ~2500 cm^{-1} and ~1900 cm^{-1} are indicative of O-H•••N hydrogen bonds between the two individual components, Figure 5.11, and allows for a large number of co-crystallisation reactions to be analysed, Table 5.3.

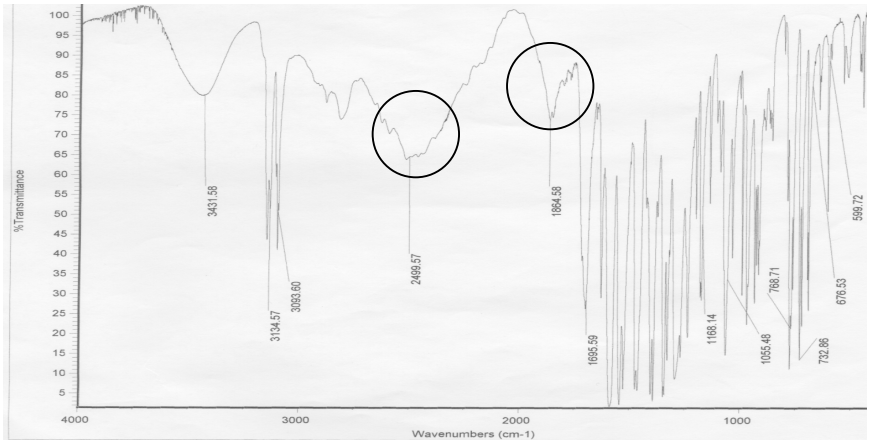

Figure 5.11 IR spectrum of **19a** displaying the O-H•••N stretches (circled).

Table 5.3 IR data.

SR	Carboxylic Acid	O-H•••N stretches / cm^{-1}
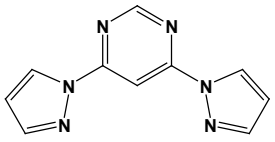 **19**	3,5-Dinitrobenzoic Acid[1]	2500 & 1865
	4-Nitrobenzoic Acid[i]	2475 & 1905
	2-Fluorobenzoic Acid	×
	Benzoic Acid	×
	Fumaric Acid	2523 & 1898
	Succinic Acid	2546 & 1993
	Oxalic Acid	2541 & 1977
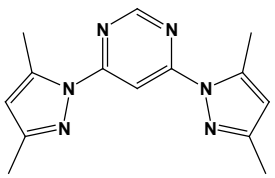 **20**	3,5-Dinitrobenzoic Acid	2522 & 1938
	4-Nitrobenzoic Acid	2555 & 1958
	2-Fluorobenzoic Acid	×
	3-Cyanobenzoic Acid	2555 & 1925
	Benzoic Acid	2455 & 1918
	Fumaric Acid	2535 & 1916
	Succinic Acid	2548 & 1945
	Oxalic Acid	2508 & 1938

(i) Crystal structure determined

5.4 Discussion

5.4.1 Assessing potential orientations of 4,6-bis(pyrazol-1-yl)pyrimidine SR's

Based on single crystal data the *trans* orientation is favoured in the SR (**20**) and in co-crystals (**19a** and **19b**), Figure 5.9. The *cis* orientation however, is observed in the presence of metal ions due to the preference for a metal-chelate, Figure 5.12.

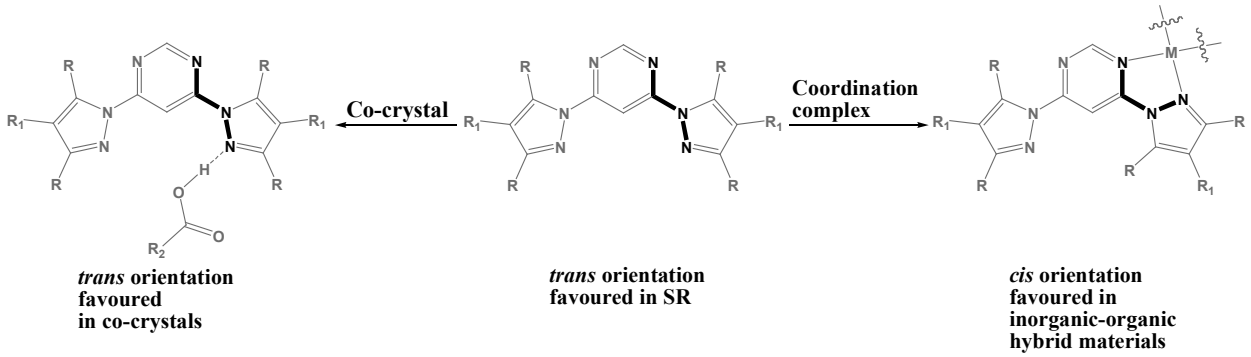

Figure 5.12 Favoured orientations of 4,6-bis(pyrazol-1-yl)pyrimidine SR's.

5.4.2 Determining the best hydrogen-bond acceptor site in the ditopic SR

O-H•••N hydrogen-bond stretches were observed in the IR spectra of 12 of the 15 (80%) co-crystallisations.

Based on single crystal data for **19a** and **19b**, it was established that the co-crystal was formed via an O-H•••N hydrogen bond between the carboxylic acid and the pyrazole nitrogen, Figure 5.13.

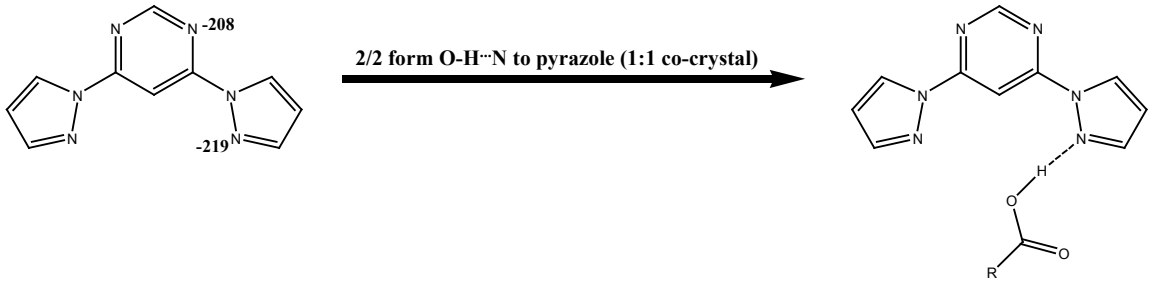

Figure 5.13 Co-crystals of 4,6-bis(pyrazol-1-yl)pyrimidine and carboxylic acids.

5.4.3 Addressing reliability of 4,6-bis(pyrazol-1-yl)pyrimidine as a chelating ligand

The crystal structure of **20a** shows the pyrimidine-pyrazole chelating to two different copper ions, Figure 5.14.

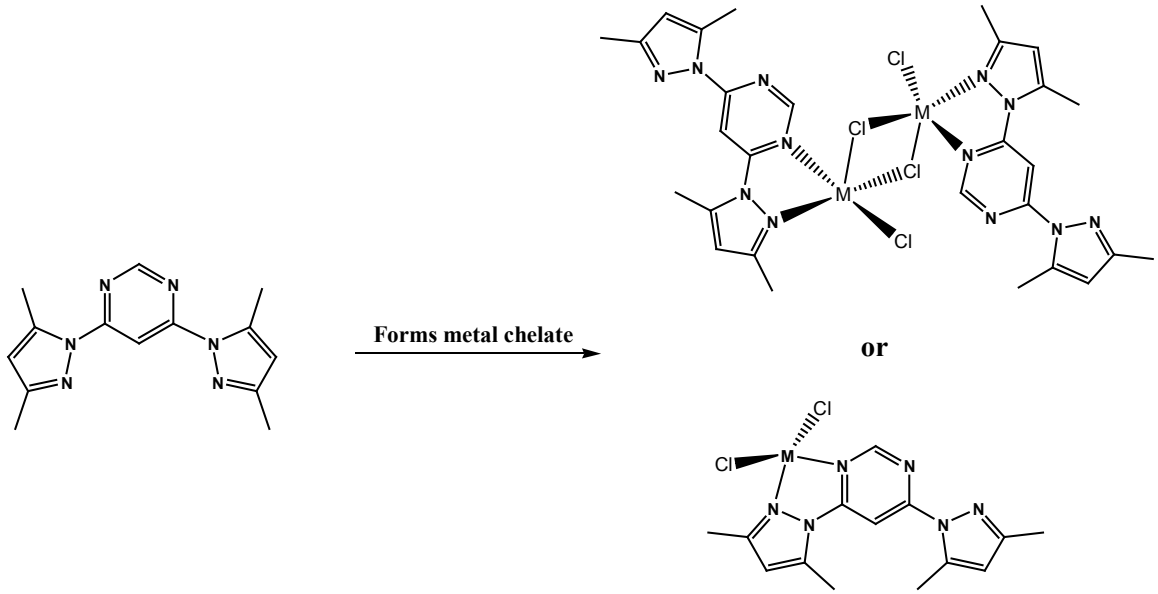

Figure 5.14 Metal coordination complexes of 4,6-bis(3,5-methylpyrazol-1-yl)pyrimidine.

This crystal structure when paired with ~40 pyrimidine-pyrazole coordination complexes previously synthesised,[4, 7] Figure 5.15, supports the idea that pyrimidine-pyrazole can be used as a reliable chelating ligand.

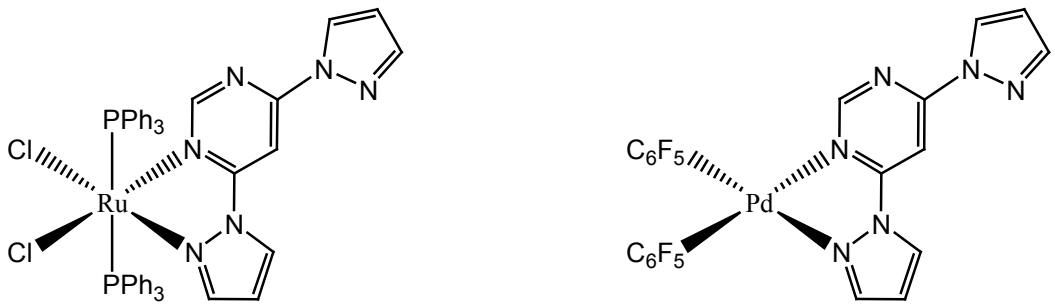

Figure 5.15 Two examples of previously synthesised pyrimidine-pyrazole coordination complexes.[7b, 7c]

The structural analysis of the two co-crystals **19a** and **19b** between 4,6-bis(pyrazol-1-yl)pyrimidine and a carboxylic acid and the inorganic-organic hybrid, **20a**, have provided answers to the questions addressed at the beginning of this chapter.

I. Is pyrazole a better hydrogen-bond acceptor than pyrimidine?

The MEP surface calculations confirm that pyrazole is more electrostatic than pyrimidine. This directly translates into hydrogen-bond acceptor strength with the two co-crystals showing hydrogen-bond interactions at the pyrazole nitrogen atom and no interactions at both pyrimidine nitrogen atoms, Figure 5.16. This adds weight to MEP surface calculations as a tool for predicting a hierarchy of hydrogen-bond acceptors in ditopic heterocycle SR's.

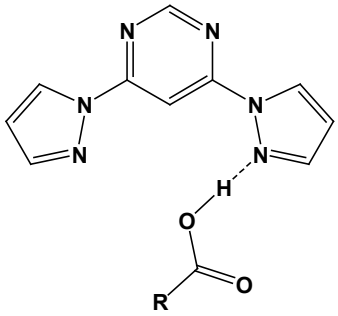

100% supramolecular yield for an acid-pyrazole interaction via an O-H···N hydrogen-bond.

Figure 5.16 Hydrogen-bond preference in co-crystals between pyrazole/pyrimidine SR's and carboxylic acids.

II. Can pyrimidine/pyrazole ligands be used successfully as chelating ligands to construct reliable coordination complexes?

The family of pyrimidine/pyrazole ligands can be employed to construct hybrid materials with the ability of pyrimidine/pyrazole to act as a chelating ligand shown in **20a**, Figure 5.17. Backed up by structurally similar pyrimidine/pyrazole complexes previously synthesised,[4, 7] these chelating ligands offer a reliable approach to constructing predictable coordination complexes.

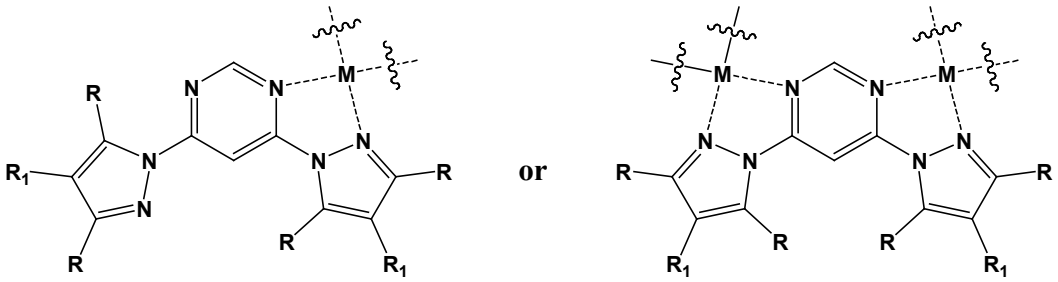

Figure 5.17 Pyrazole/pyrimidine chelating ligands.

References

1. C. B. Aakeröy, J. Desper and M. E. Fasulo, *CrystEngComm.*, 2006, **8**, 586.
2. For a discussion on pyrazol-1-yl benzamide co-crystals, see Chapter 3.
3. For a discussion on (pyrazol-1-yl)methylpyridine and (indazol-1-yl)methylpyridine co-crystals, see Chapter 4.
4. J. Elguero, A. Fruchier, A. de la Hoz, F. A. Jalón, B. R. Manzano, A. Otero and F. Gómez-de la Torre, *Chem. Ber.*, 1996, **129**, 589.
5. Cambridge Structural Database v. 5.29 (January 2008).
6. (a) S. Valiyaveettil, V. Enkelmann, K. Mullen, *Chem. Commun*., 1994, 2097; (b) G. Tennant, V. Mecillo, S. Parsons, D. Messenger, *Private Communication*, 2005; (c) Z. J. Li, Y. Abramov, J. Bordner, J. Leonard, A. Medek, A. V. Trask, *J. Am. Chem. Soc*., 2006, **128**, 8199; (d) Z. Travnicek, J. Marek, K. Dolezal, M. Strnad, *Z. Kristallogr.*, 1997, **212**, 538.
7. (a) P. J. Steel and E. C. Constable, *J. Chem. Res. Synopses*, 1989, 189; (b) J. Elguero, A. Guerrero, F. Gómez-de la Torre, A. de la Hoz, F. A. Jalón, B. R. Manzano and A. Rodríguez, *New J. Chem.*, 2001, **25**, 1050; (c) F. Gómez-de la Torre, A. de la Hoz, F. A. Jalón, B. R. Manzano and A. Rodríguez, *Inorg. Chem.*, 2000, **39**, 1152; (d) B. R. Manzano, F. A. Jalón, I. M. Ortiz, M. L. Soriano, F. Gómez-de la Torre, J. Elguero, M. A. Maestro, K. Mereiter and T. D. W. Claridge, *Inorg. Chem.*, 2008, **47**, 413; (e) E. V. Peresypkina, M. B. Bushuev, A. V. Virovets, V. P. Krivopalov, L. G. Lavrenova and S. V. Larionov, *Acta Crystallogr. Sect. B,*, 2005, **B61**, 164; (f) E. Escrivá, J. Garcia-Lozano, J. Martínez-Lillo, H. Nuñez, J. Server-Carrió, L. Soto, R. Carrasco and J. Cano, *Inorg. Chem.*, 2003, **42**, 8328; (g) L. S. Tuero, J. García-Lozano, E. E. Monto, M. B. Borja, F. Dahan, J. –P. Tuchagues and J. –P. Legros, *J. Chem. Soc. Dalton Trans.*, 1991, 2619; (h) M. Benetó, L. Soto, J. García-Lozano, E. Escrivá, J. –P. Legros and F. Dahan, *J. Chem. Soc. Dalton Trans.*, 1991, 1057; (i) L. Soto, J. García, E. Escrivá, J. –P. Legros, J. –P. Tuchagues, F. Dahan, and A. Fuertes, *Inorg. Chem.*, 1989, **28**, 3378; (j) J. García-Lozano, J. Server-Carrió, E. Escrivá, J. V. Foldago and M. C. Molla, *Polyhedron*, 1997, **16**, 939.
8. A. Osawa, T. Kaiho, T. Ito, M. Okada, C. Kawabata, K. Yamaguchi and H. Igeta, *Chem. Pharm. Bull*., 1988, **36**, 3638.

9. S. F. Vasilevsky, S. V. Klyatskaya, E. V. Tretyakov and J. Elguero, *Heterocycles*, 2003, **60**, 879.
10. Molecular structures for **19-23** were constructed using Spartan '06 (Wavefunction, Inc. Irvine, CA). All five molecules were optimized using AM1, with the maxima and minima in the electrostatic potential surface (0.002 e/au isosurface) determined using a positive point charge in the vacuum as a probe.
11. C. A. Hunter, *Angew. Chem. Int. Ed*, 2004, **43**, 5310-5324.
12. Co-crystallisation reactions frequently yielded homogeneous powders, which were analysed by IR.

CHAPTER 6 - Using [(pyrazol-1-yl)methyl]benzamide SR's to construct 1-D inorganic-organic hybrid materials

6.1 Introduction

The construction of inorganic-organic hybrid materials with the overall goal of developing systems with specific properties e.g. magnetic,[1] catalytic,[2] and storage[3] via supramolecular synthesis is a rapidly growing field within crystal engineering focused on (i) ligand-metal interactions to yield coordination polymers[4] and (ii) ligand-metal interactions paired with non-covalent interactions.[5]

A significant level of control is required for a specific design to be applied reliably and the introduction of non-covalent interactions (e.g. hydrogen bonding) may allow for easier, flexible dimensionality control and improved solubility of coordination networks. However, the reliability of such architectures is likely to be affected by the introduction of competitive forces, which can cause structural interference from the numerous undesired hydrogen bonds that can potentially form between the ligand and solvent molecules or counter ions. Consequently a robust supramolecular motif is necessary in order to prevent a high level of unpredictability.

The amide-amide self-complementary homomeric dimer lends itself well to such a study as it was demonstrated to be a fairly robust synthon (69% supramolecular yield) in the presence of competitive forces such as a N-heterocycle.[6]

In order to be able to assess the ability of such ligands to achieve the desired metal-containing extended structural motif in the absence of potentially disruptive counter-ions, a set of neutral coordination complexes were targeted, Figure 6.1. In addition, by using chelating ligands, the number of possible geometries that each metal ion could adopt will be restricted, thereby simplifying the assembly process further.

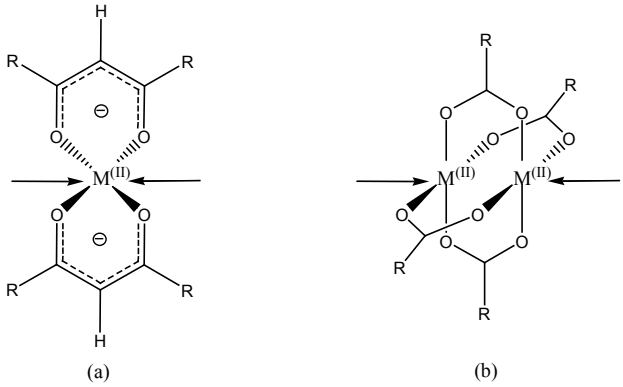

(a) (b)

Figure 6.1 (a) Bidentate acetylacetonate (*acac*) and (b) acetate "paddle-wheel" complexes.

The supramolecular target in each case presented in this study is first of all an infinite 1-D chain, Figure 6.2. Therefore, each metal complex is required to have exactly two available binding sites that could be occupied by N-heterocycle/amide ligands.

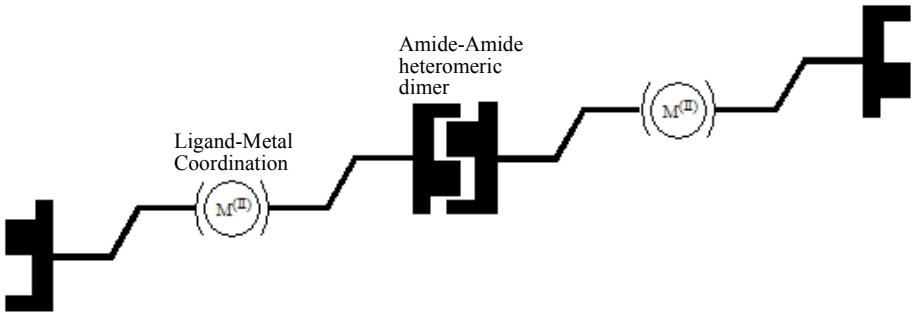

Figure 6.2 Representation of supramolecular 1-D chain via both metal coordination and amide-amide hydrogen bonding.

Bidentate acetylacetonate (*acac*) and acetate "paddle-wheel" complexes are particularly useful in this context as they both produce neutral complexes (with $M^{(II)}$ metal ions) that present two open binding sites suitable for heterocycle coordination, Figure 6.1.

Isonicotinamide,[7] and (benzimidazol-1-yl)benzamides,[8] Figure 6.3, have both previously been used to construct 1-D chains through coordination to Ag(I), Figure 6.4a and isonicotinamide has also been used effectively with *acac* and "paddle-wheel" complexes[5d, 9] to construct 1-D chains, Figure 6.4b. However, an extensive survey of the effectiveness of a series of N-heterocycle/amide ligands to direct the assembly of neutral coordination complexes into infinite 1-D chains has never been addressed.

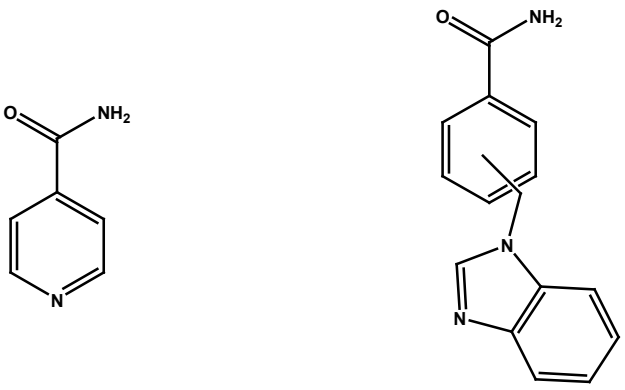

(a) (b)

Figure 6.3 (a) Isonicotinamide; (b) (benzimidazol-1-yl)benzamides

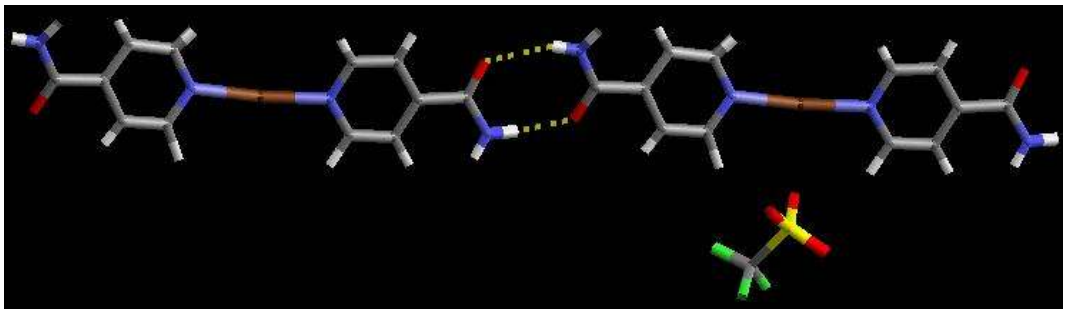

(a)

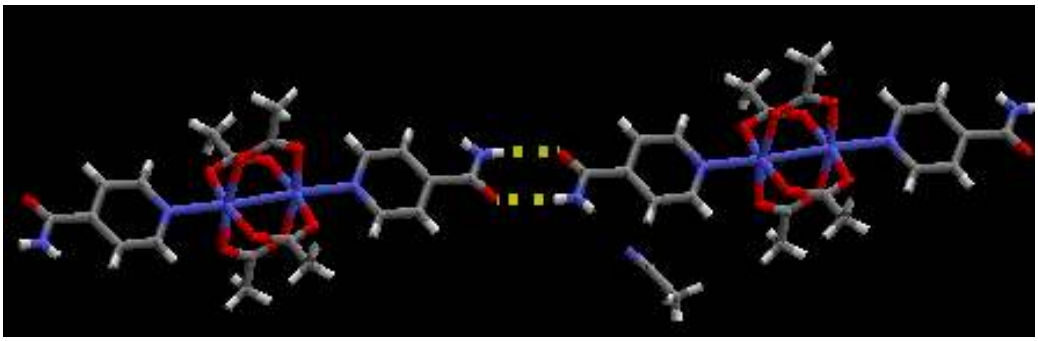

(b)

Figure 6.4 **1**-D chains constructed from (a) isonicotinamide and Ag(OTf);[7a] and (b) isonicotinamide and $Cu(OAc)_2$.[9a]

Consequently, the goal of this study is to establish the robustness of a supramolecular synthetic strategy based upon a ligand comprising an N-heterocycle (for binding to the metal ion), and an amide (for providing intermolecular amide•••amide synthons).

A series of hybrid materials will be constructed between [(pyrazol-1-yl)methyl]benzamide ligands, Figure 6.5 and *acac* or "paddle-wheel" type coordination complexes. Subsequent analysis of single crystal X-ray structures will allow for the robustness of such systems to be addressed.

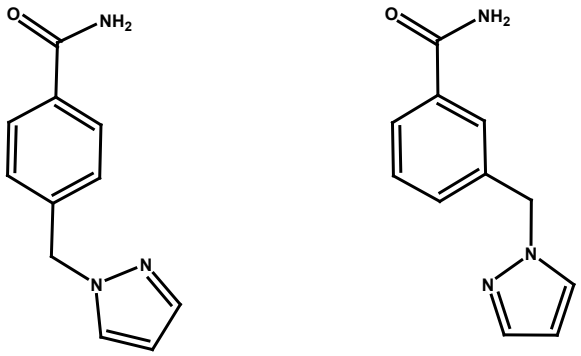

2 **8**

Figure 6.5 [(Pyrazol-1-yl)methyl]benzamide ligands.

6.2 Experimental

6.2.1 Synthesis

All chemicals were purchased from Aldrich and Fischer and used without further purification. Synthesis of the [(pyrazol-1-yl)methyl]benzamide ligands is reported in chapter 2. Melting points were determined on a Fisher-Johns melting point apparatus and are uncorrected.

6.2.1.1 Synthesis of [4-(pyrazol-1-yl)methyl]benzamide : bis-(hexafluoroacetylacetonato) copper(II), 2i

2 (0.0250g, 0.124mmol) and *bis*-(hexafluoroacetylacetonato)copper(II) (0.0300g, 0.0545mmol) were added to a vial along with chloroform. The solution was heated gently to dissolve the components and allowed to stand under ambient conditions. Green prisms, **2i**, suitable for X-ray diffraction were formed after a few days. Mp 132-135˚C. IR (KBr pellet): υ 3477, 3368, 1679, 1647, 1469, 1256, 1211, 1131 cm^{-1}.

6.2.1.2 Synthesis of [4-(pyrazol-1-yl)methyl]benzamide : bis-(dibenzoylmethanato)nickel(II), 2j

2 (0.0200g, 0.099mmol) and *bis*-(dibenzoylmethanato)nickel(II) (0.0240g, 0.0498mmol) were added to a vial along with ethanol. The solution was heated gently to dissolve the components and allowed to stand under ambient conditions. Yellow blocks, **2j**, suitable for X-

ray diffraction were formed after a few days. Mp 152-155˚C. IR (KBr pellet): υ 3443, 1665, 1597, 1553, 1473, 1415, 720 cm^{-1}.

6.2.1.3 Synthesis of [3-(pyrazol-1-yl)methyl]benzamide : bis-(hexafluoroacetylacetonato) copper(II), *8c*

8 (0.0250g, 0.124mmol) and *bis*-(hexafluoroacetylacetonato)copper(II) (0.0300g, 0.0545mmol) were added to a vial along with chloroform. The solution was heated gently to dissolve the components and allowed to stand under ambient conditions. Green prisms, **8b**, suitable for X-ray diffraction were formed after a few days. Mp 137-140˚C. IR (KBr pellet): υ 3498, 3391, 1666, 1643, 1558, 1256, 1202 cm^{-1}.

6.2.1.4 Synthesis of tetrakis(μ-2-fluorobenzoato-O,O')-bis(4-(pyrazol-1-yl)methylbenzamide)-dicopper(II), *2k*

2 (0.0150g, 0.0750mmol) and copper 2-fluorobenzoate (0.0147g, 0.0430mmol) were added to a beaker and dissolved in acetonitrile. A few drops of acetic acid were added to make the solution transparent and the solution was allowed to stand under ambient conditions. Aqua prisms, **2k**, suitable for X-ray diffraction were formed after a few days. Mp 208-211˚C. IR (KBr pellet): υ 3428, 1682, 1632, 1402, 760 cm^{-1}.

6.2.1.5 Synthesis of tetrakis(μ-acetato-O,O')-bis(4-(pyrazol-1-yl)methylbenzamide)-dicopper(II), *2l*

2 (0.015g, 0.075mmol) and copper acetate (0.0082g, 0.045mmol) were added to a beaker and dissolved in acetonitrile. A few drops of acetic acid were added to make the solution transparent and the solution was allowed to stand under ambient conditions. Green prisms, **2l**, suitable for X-ray diffraction were formed after a few days. Mp 149-151˚C. IR (KBr pellet): υ 3416, 3278, 1614, 1440, 692 cm^{-1}.

6.2.1.6 Synthesis of tetrakis(μ-acetato-O,O')-bis(3-(pyrazol-1-yl)methylbenzamide)-dicopper(II), *8d*

8 (0.015g, 0.082mmol) and copper acetate (0.0082g, 0.045mmol) were added to a beaker and dissolved in acetonitrile. A few drops of acetic acid were added to make the solution transparent and the solution was allowed to stand under ambient conditions. Green blocks, **8c**,

suitable for X-ray diffraction were formed after a few days. Mp 188-190˚C. IR (KBr pellet): υ 3453, 1677, 1447, 1427, 1403, 1366 cm^{-1}.

6.3 Results

All hydrogen bond geometries are listed in Table 6.1. A summary of the crystallographic information for each compound is displayed in Tables A.29-A.34.

Table 6.1 Hydrogen bond geometries for **2i-2l** and **8c-8d**

Compound	D-H•••A	D-H / Å	H•••A / Å	D•••A / Å	<(DHA) / ^{o}
2i[i]	N(47)-H(47A)...O(24)#1 N(47)-H(47B)...O(12)#2	0.87(2) 0.82(2)	2.21(2) 2.27(2)	2.9963(19) 3.0105(18)	150.5(18) 150(2)
2j[ii]	N(87)-H(87A)...O(41)#3	0.88	2.27	2.943(2)	133.4
8c[iii]	N(47)-H(47A)...O(14) N(47)-H(47B)...O(12)#2	0.82(2) 0.85(2)	2.61(2) 2.38(2)	3.2986(19) 3.1466(18)	143.2(19) 150.0(19)
2k[iv]	N(27)-H(27A)...O(27)#2 N(27)-H(27B)...O(48)#3	0.88 0.88	1.99 2.43	2.859(3) 3.098(3)	168.8 132.9
2l[v]	N(17)-H(17A)...O(31)#2 N(17)-H(17B)...N(1S)	0.87(4) 0.80(4)	2.24(4) 2.26(4)	3.086(3) 3.045(4)	164(3) 167(4)
8d[vi]	N(27)-H(27A)...O(27)#2 N(27)-H(27B)...O(31)#3	0.78(2) 0.81(2)	2.16(2) 2.47(2)	2.9359(18) 3.1634(18)	172(2) 144(2)

(i) #1 -x+1,-y+1,-z+1, #2 x-1,y,z; (ii) #1 -x+1,-y+1,-z+1, #2 -x+2,-y,-z, #3 x,y+1,z; (iii) #1 -x+1,-y+1,-z+1, #2 x,-y+3/2,z-1/2; (iv) #1 -x+1,-y+1,-z+1, #2 -x+1,-y,-z+1, #3 -x+1/2,y-1/2,-z+1/2; (v) #1 -x+1,-y+2,-z, #2 -x+1,-y+1,-z+1; (vi) #1 -x+1,-y,-z, #2 -x,-y+2,-z+1, #3 -x+1,-y+1,-z+1.

6.3.1 Crystal structure of [4-(pyrazol-1-yl)methylbenzamide]bis-(hexafluoroacetyl acetonato)copper(II), *2i*

The complex ion in the crystal structure of **2i** has a combination of both pyrazole N coordination to two copper ions (Cu-N, 2.0320(13) Å) as well as carbonyl O coordintion (Cu-O, 2.2297(12) Å) from two 4-[(pyrazol-1-yl)methyl]benzamide ligands, **2**. This results in a metallocycle with a Cu•••Cu distance of approximately 10.3 Å, Figure 6.6. Similarly, both *syn* and *anti* amide hydrogen atoms form hydrogen bonds to oxygen atoms of two *hfacac* ligands (N-H•••O, 2.9963(19) and 3.0105(18) Å respectively).

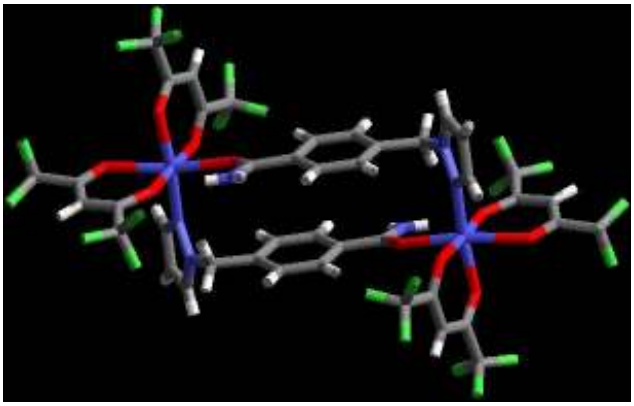

Figure 6.6 Metallacycle observed in the crystal structure of **2i**.

6.3.2 Crystal structure of [4-(pyrazol-1-yl)methylbenzamide]bis-(dibenzoylmethanato) nickel(II), 2j

The coordination complex, **2j**, contains two different nickel(II) centres. Two 4-[(pyrazol-1-yl)methyl]benzamide ligands, **2**, occupy the available axial positions via coordination through the pyrazole nitrogen (Ni-N 2.006(12) Å). However, the amide does not form a self-complementary homomeric hydrogen-bond dimer but instead an O-H•••O hydrogen bond (ca. 2.733 Å) forms between the amide carbonyl and the ethanol hydroxyl group. The *syn*-hydrogen atom of the amide forms a N-H•••O hydrogen bond (2.943(2) Å) to an *acac* oxygen atom, Figure 6.7. Ni•••Ni distances are approximately 10.5 Å.

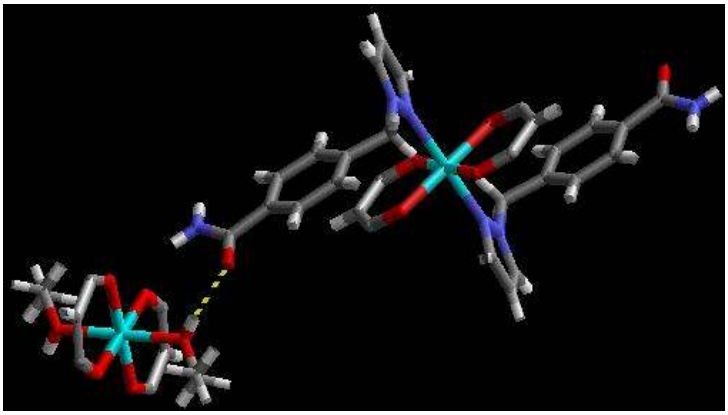

Figure 6.7 Part of the 1-D chain in the crystal structure of **2j**.

6.3.3 Crystal structure of [3-(pyrazol-1-yl)methylbenzamide]bis-(hexafluoroacetylacetonato) copper(II), 8c

The inorganic-organic hybrid species, **8c**, is isostructural to **2i** and comprises two hf*acac* ligands and two 3-[(pyrazol-1-yl)methyl]benzamide ligands, **8**. The hf*acac* ligands occupy three equatorial sites and one axial site of the octahedral copper(II) ion with two 3-[(pyrazol-1-yl)methyl]benzamide ligands occupying the two remaining coordination sites via pyrazole nitrogen coordination (Cu-N, 2.0040(13) Å) and amide carbonyl coordination (Cu-O, 1.9725(12) Å). The amide carbonyl oxygen present on the pyrazole coordinating ligand and the pyrazole N on the amide coordinating ligand occupy the two free sites on a second copper(II) centre resulting in the formation of a metallocycle, Figure 6.8. Additionally, both the *syn* and *anti*-amide hydrogen atoms form hydrogen bonds to oxygen atom of the *hfacac* ligand (N-H•••O, 3.2986(19) and 3.1466(18) Å repectively). The two copper(II) ions present in the metallocycle are approximately 9.1 Å apart.

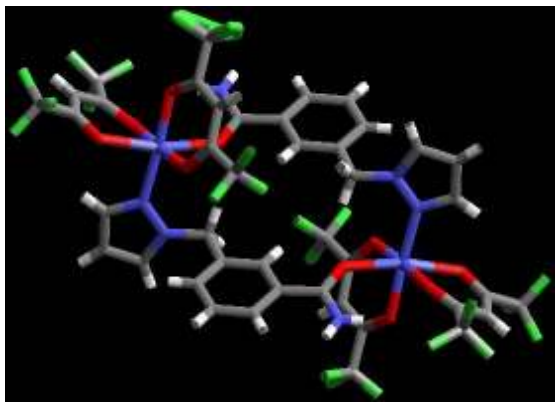

Figure 6.8 Metallacycle observed in the crystal structure of **8c**.

6.3.4 Crystal structure of tetrakis(μ-2-fluorobenzoato-O,O')-bis(4-(pyrazol-1-yl)methyl benzamide)-dicopper(II), 2k

The inorganic-organic hybrid species, **2k**, is comprised of two 4-[(pyrazol-1-yl)methyl]benzamide ligands, **2**, coordinating to the free axial sites of a copper(II) 2-fluorobenzoate "paddle wheel" unit (Cu-N, 2.165(2) Å). 1-dimensional chains are produced through self-complementary homomeric amide-amide dimers via N-H•••O hydrogen bonds (2.859(3) Å) between the *syn*-hydrogen atom and the carbonyl oxygen of another amide, Figure 6.9. Additionally, the *anti*-hydrogen atom of the amide moiety interacts with a 2-fluoro benzoate

oxygen atom via a N-H•••O hydrogen bond (3.098(3) Å) and the Cu•••Cu distance within the "paddle wheel" unit is 2.6480(5) Å.

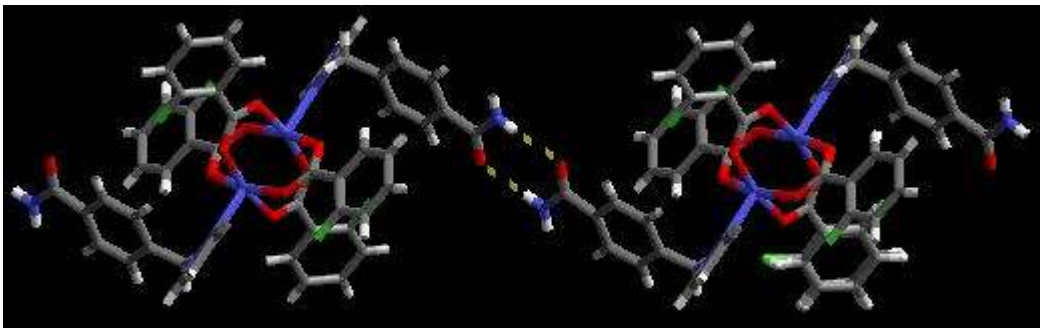

Figure 6.9 Part of the 1-D chain observed in the crystal structure of **2k**.

6.3.5 Crystal structure of tetrakis(μ-acetato-O,O')-bis(4-(pyrazol-1-yl)methylbenzamide)-dicopper(II), 2l

The complex ion in the crystal structure **2l** contains two 4-[(pyrazol-1-yl)methyl]benzamide ligands, **2**, coordinating to the free axial sites of a copper(II) acetate "paddle wheel" unit (Cu-N, 2.191(2) Å). The 1-dimensional chain is disrupted in this case, by the *syn*-hydrogen atom interacting with an acetate oxygen atom via a N-H•••N hydrogen bond (3.086(3) Å), Figure 6.10. Acetonitrile is also present in the crystal structure, interacting with the *anti*-hydrogen atom of the amide moiety via a N-H•••N hydrogen bond (3.045(4) Å). Cu•••Cu distance within the "paddle wheel" unit is 2.6282(5) Å.

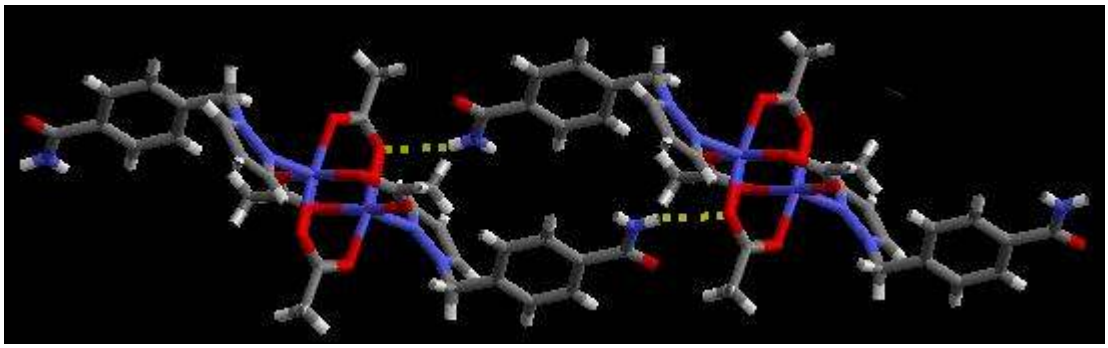

Figure 6.10 Primary non-covalent interactions observed in the crystal structure of **2l**.

6.3.6 Crystal structure of tetrakis(μ-acetato-O,O')-bis(3-(pyrazol-1-yl)methylbenzamide)-dicopper(II), 8d

The coordination complex, **8d**, consists of two 3-[(pyrazol-1-yl)methyl]benzamide ligands, **8**, coordinating to the available axial positions of a copper(II) acetate "paddle wheel"

unit via the pyrazole nitrogen, (Cu-N, 2.1908(12) Å). The complex is extended into 1-dimensional chains through self complementary homomeric amide-amide dimers via N-H•••O hydrogen bonds (2.9359(18) Å) between the *syn*-hydrogen atom and the carbonyl oxygen of another amide, Figure 6.11. Additionally, the *anti*-hydrogen atom of the amide moiety interacts with an acetate oxygen atom via a N-H•••O hydrogen bond (3.1634(18) Å) and the Cu•••Cu distance within the "paddle wheel" unit is 2.6596(3) Å.

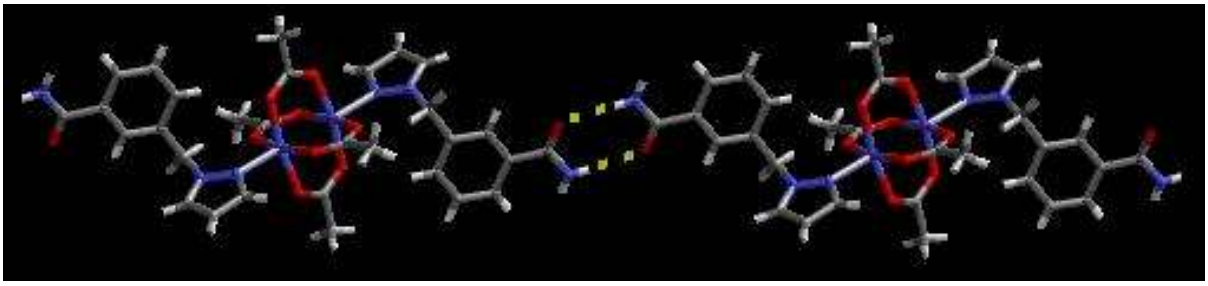

Figure 6.11 Part of the 1-D chain observed in the crystal structure of **8d**.

6.4 Discussion

The connectivity observed in the six structures presented herein, indicate that a degree of control can be established, for the construction of 1-D chains. However, complementing our results with existing crystallographic information will allow for a more thorough structural study to be carried out.

These structures are accompanied by two *acac* coordination complexes obtained utilising 4-[(2-methylbenzimidazol-1-yl)methyl]benzamide,[10] Figure 6.12. In addition, a CSD[11] search of isonicotinamide and nicotinamide (a search of imidazole and pyrazole amide ligands yielded no hits) in the presence of an *acac* or "paddle wheel" metal complex, Table 6.3, gives a total of 25 structures.

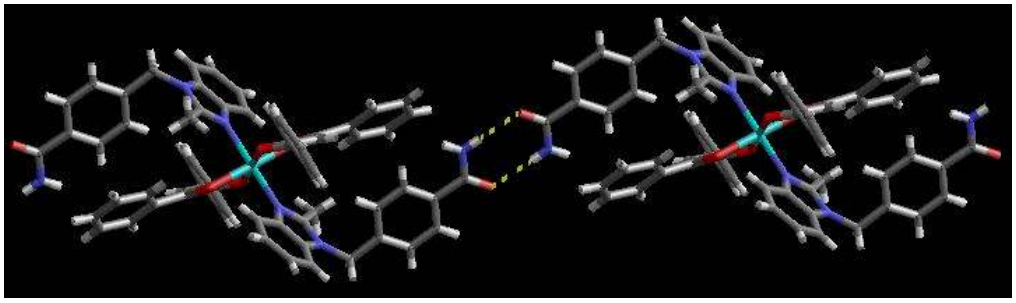

(a)

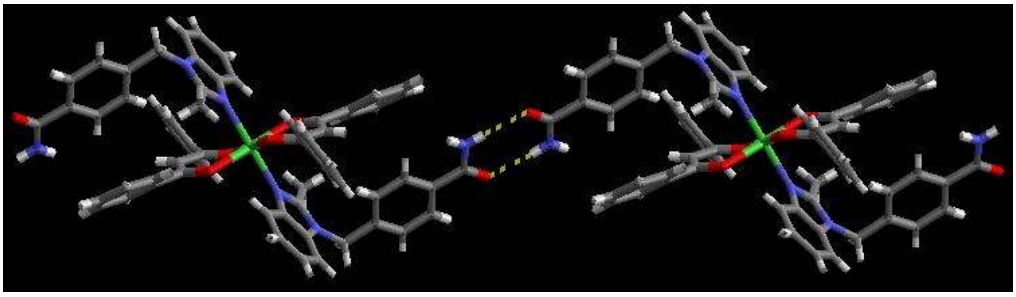

(b)

Figure 6.12 Coordination complexes between 4-[(2-methylbenzimidazol-1-yl)methyl]benzamide and (a) $Co(DBM)_2$; (b) $Ni(DBM)_2$.[10]

Table 6.2 *Acac*- and "paddle-wheel" coordination complexes of isonicotinamide and nicotinamide (CSD codes in bold in parentheses).

Metal complex	Desired metal coordination	Amide-amide dimer yielding 1-D chain
Isonicotinamide+$Co(DBM)_2$+$CHCl_3$ **(HAJPOY)** [5d]	✓	✓
Isonicotinamide+$Ni(DBM)_2$+PhBr **(HAJPUE)** [5d]	✓	✓
Isonicotinamide+$Co(DBM)_2$+DMF **(HAJQAL)** [5d]	✓	✓
Isonicotinamide+$Ni(DBM)_2$+$CHCl_3$+THF **(HAJQEP)** [5d]	✓	✓
Isonicotinamide+$Rh(OAc)_2$+$(CH_3)_2O$ **(BEDHEY)** [9a]	✓	✓
Isonicotinamide+$Cu(OAc)_2$+MeCN **(EMAWAQ)** [9b]	✓	✓
Isonicotinamide+$Cu(OAc)_2$ **(TALKEX)** [9c]	✓	×
Nicotinamide+$Rh(OAc)_2$+$(CH_3)_2O$ **(BEDHIC)** [9c]	✓	✓
Nicotinamide+$Cu(OAc)_2$ **(BENQEQ)** [9d]	✓	✓
Nicotinamide+$Cu(OAc)_2$ **(BENQAM)** [9d]	×	×
Nicotinamide+$Cu(OAc)_2$+H_2O **(BEXNOH01)** [9e]	✓	×
Nicotinamide+$Zn(OAc)_2$+H_2O **(TAYFIJ)** [9f]	✓	×
Nicotinamide+$Cu(OPr)_2$ **(VORWUV)** [9g]	✓	✓

Nicotinamide+Cu(OVal)$_2$ **(GETQEC)** [9h]	✓	✓
Nicotinamide+Cu(OHep)$_2$ **(CAYHIT01)** [9i]	✓	✓
Nicotinamide+Cu(OHep)$_2$ **(CAYHIT)** [9i]	✓	×
Nicotinamide+Cu(ONon)$_2$ **(CAYHUF)** [9i]	✓	×
4-[(2-methylbenzimidazol-1-yl) methyl]benzamide + Co(DBM)$_2$+THF[10]	✓	✓
4-[(2-methylbenzimidazol-1-yl) methyl]benzamide + Ni(DBM)$_2$+THF[10]	✓	✓
2i	×	×
2j	✓	×
8c	×	×
2k	✓	✓
2l	✓	×
8d	✓	✓

Analysis of the 25 data points gives a supramolecular yield of 88% for the desired coordination chemistry and geometry and a 68% supramolecular yield for the formation of an infinite 1-D chain, Figure 6.13.

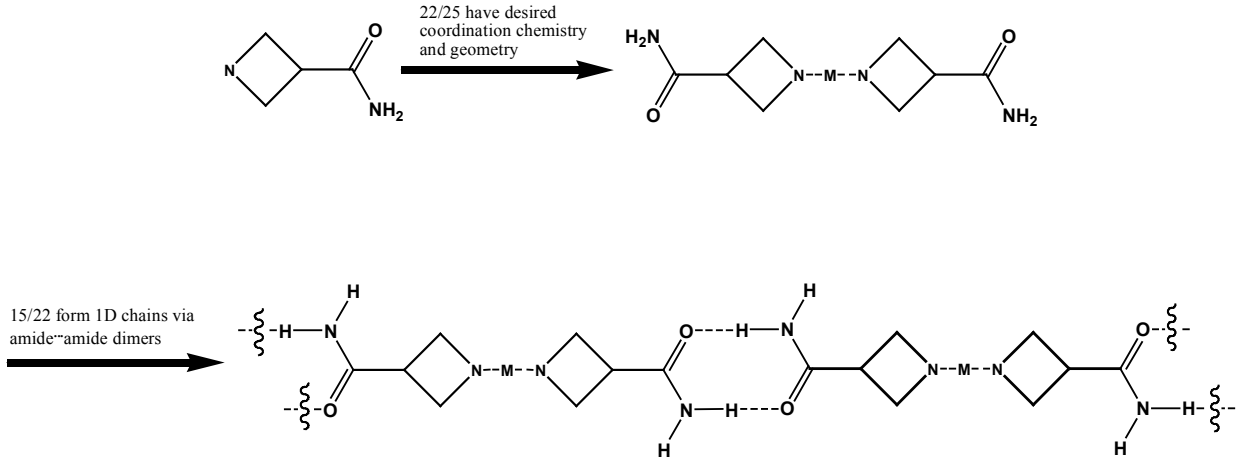

Figure 6.13 Formation of desired 1-D architectures.

The nine structures that do not form the desirable architectures can be rationalised using three disruptive factors:

I. The ability of the amide to coordinate to the metal

Three structures in which the desired coordination chemistry was not attained (**2i**, **8c** and **BENQAM**), demonstrate the issue associated with the amide binding directly to the metal ion via its C=O moiety, Figure 6.14. Even though this is a potential interaction, the fact it only occurs in 12% of cases demonstrates the effectiveness of the supramolecular design.

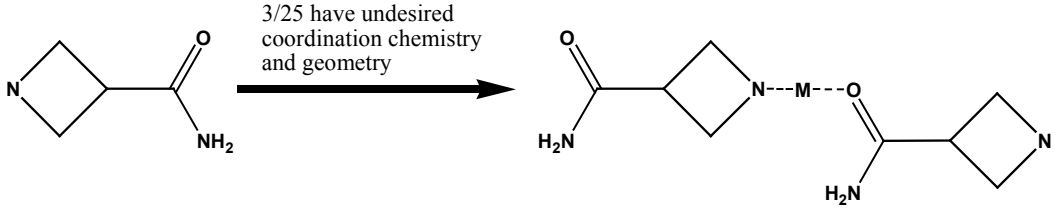

Figure 6.14 Amide coordination to metal centre.

II. The ability of the amide to hydrogen bond to the chelating ligands

The amide•••amide interaction is disrupted in three cases (**2l**, **TALKEX**, and **CAYHIT**) due to an oxygen atom from an acetate ligand (as part of the 'paddle-wheel' complex) successfully competing for the attention of the *syn*-amide hydrogen atom, which prevents the formation of a 1-D chain, Figure 6.15.

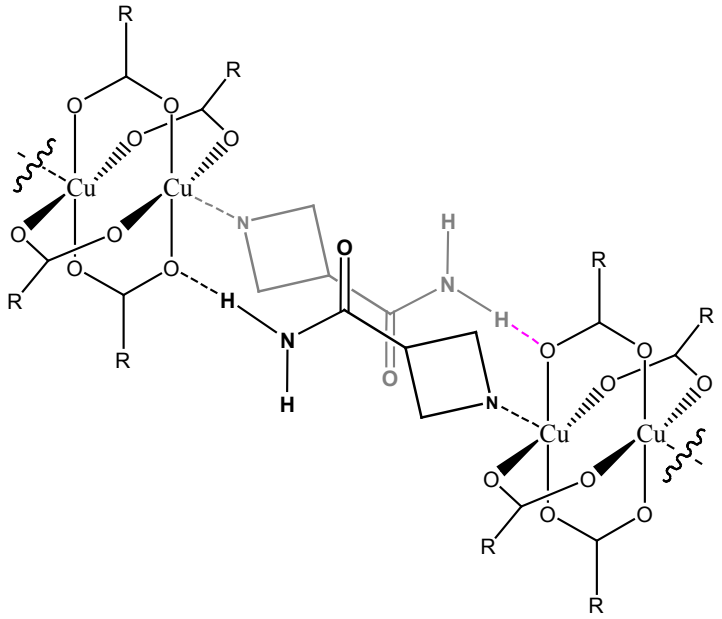

Figure 6.15 Amide-acetate N-H•••O hydrogen bonding.

III. The ability of the amide to hydrogen bond to solvent molecules

The presence of potentially disruptive solvent molecules is another factor shown to disrupt the desired architecture. Many such compounds are capable of acting as hydrogen-bond donors/acceptors as well as coordinating to the metal. Three cases discussed, **2j**, (ethanol as a ligand), **BEXNOH1**, and **TAYFIJ** (both with non-coordinating H_2O), all possess potential hydrogen bonding solvent molecules and in all three cases the amide•••amide synthon is disrupted, Figure 6.16. This being said, the use of solvents that cannot partake in hydrogen bonding is feasible with nine of the structures presented in this study possessing the desired 1-D motif in the presence of solvents such as chloroform, acetonitrile, DMF, bromobenzene, acetone and THF.

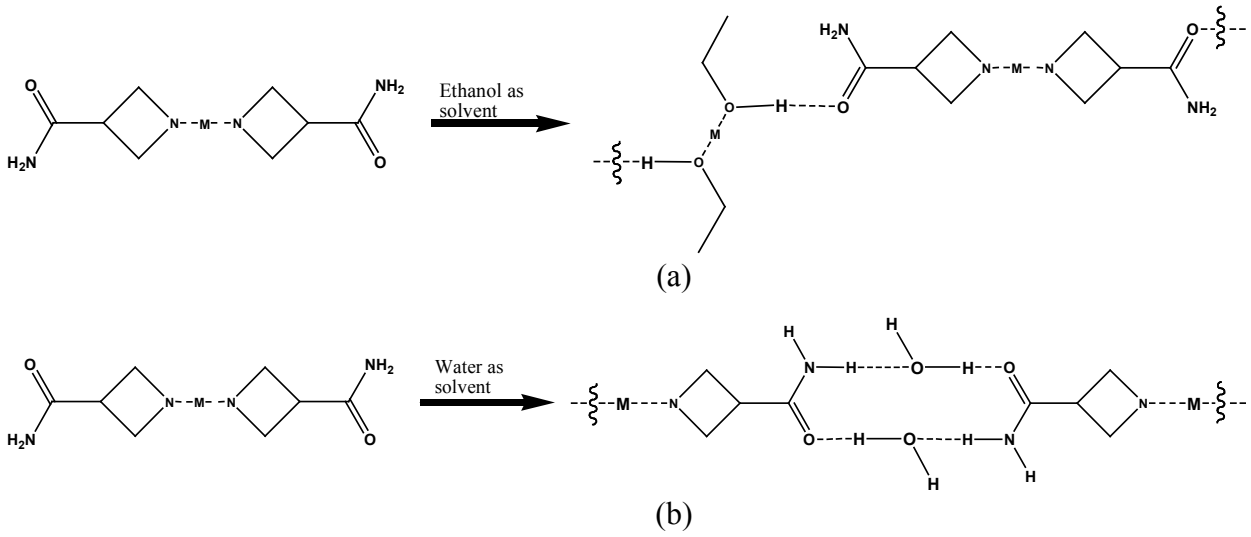

Figure 6.16 Disruptive effect of (a) ethanol as a solvent and (b) water as a solvent.

References

1. (a) D. –Z. Gao, D. –L. Liao, Z. –H. Jiang and S. –P. Yan, *Transition Met. Chem.*, 2008, **33**, 107; (b) X. –Y. Wang, Z. –M. Wang and S. Gao, *Chem. Commun*., 2008, **3**, 281; (c) Z. –F. Ju, Q. –X. Yao, W. Wu and J. Zhang, *Dalton Trans.*, 2008, **3**, 355; (d) R. K. Selvan, V. Krishnan, C. O. Augustin, H. Bertagnolli, C. S. Kim and A. Gedanken, *Chem. Mater*., 2008, **20**, 429; (e) E. Pardo, R. Carrasco, R. Ruiz-Garcia, M. Julve, F. Lloret, M. C. Munoz, Y. Journaux, E. Ruiz and J. Cano, *J. Am. Chem. Soc.,* 2008, **130**, 576 (f) M. Tuncel, A. Oezbuelbuel and S. Serin, *Reactive & Functional Polymers*, 2008, **68**, 292; (g) A. R. Parent, S. Vedachalam, C. P. Landee and M. M. Turnbull, *J. Coord. Chem.*, 2008, **61**, 93; (h) N. Roques, D. Maspoch, F. Luis, A. Camon, K. Wurst, A. Datcu, C. Rovira, D. Ruiz-Molina and J. Veciana, *J. Mater. Chem.*, 2007, **18**, 98; (i) J. –P. Costes, R. Gheorghe, M. Andruh, S. Shova and J-M Clemente Juan, *New J. Chem.*, 2006, **30**, 572; (j) O. Atakol, R. Boca, I. Ercan, F. Ercan, H. Fuess, W. Haase and R. Herchel, *Chem. Phys. Lett.*, 2006, **423**, 192.
2. (a) A. Greatti, M. Scarpellini, R. A. Peralta, A. Casellato, A. J. Bortoluzzi, F. R. Xavier, R. Jovito, M. Aires de Brito, B. Szpoganicz, Z. Tomkowicz, M. Rams, W. Haase and A. Neves, *Inorg. Chem.*, 2008, **47**, 1107; (b) W. T. Jenkins and J. S. Patrick, *J. Inorg. Biochem.*, 1986, **27**, 163; (c) J. G. Zalatan, I. Catrina, R. Mitchell, P. K. Grzyska, P. J. O'Brien, D. Herschlag, A. Hengge, and C. Alvan, *J. Am. Chem. Soc.*, 2007, **129**, 9789; (d) S. L. Gantt, S. G. Gattis and C. A. Fierke, *Biochem.*, 2006, **45**, 6170; (e) Y. –M. Hou, S. –Q. Gu, H. Zhou and L. Ingerman, *Biochem*., 2005, **44**, 12849.
3. (a) M. Du, X. –J. Jiang and X. –J. Zhao, *Inorg. Chem*., 2007, **46**, 3984; (b) O. M. Yaghi, H. Li, C. Davis, D. Richardson and T. L. Groy, *Acc*. *Chem. Res*., 1998, **31**, 474; (c) M. Kawano, T. Kawamichi, T. Haneda, T. Kojima and M. Fujita, *J. Am. Chem. Soc.*, 2007, **129**, 15418; (d) K. Takaoka, M. Kawano, T. Hozumi, S. –I. Ohkoshi, and M. Fujita, *Inorg. Chem.*, 2006, **45**, 3976; (e) M. Fujita, J. Yazaki, and Ogura, K., *J. Am. Chem. Soc.,* 1990, **112**, 5645; (f) M. Fujita, D. Oguro, M. Miyazawa, H. Oka, K. Yamaguchi, and K. Ogura, *Nature*, 1995, **378**, 469; (g) S. M. Hawxwell, G. M. Espallargas, D. Bradshaw, M. J. Rosseinsky, J. Timothy A. J. Florence, J. van de Streek and L. Brammer, *Chem. Commun.*, 2007, **15**, 1532; (h) H. Li, M. Eddaoudi, T. L. Groy, and O. M. Yaghi, *J. Am. Chem. Soc.*, 1998, **120**, 8571. (i) A. C. Sudik,

A. R. Millward, N. W. Ockwig, A. P. Côté, J. Kim, and O. M. Yaghi, *J. Am. Chem. Soc.,* 2005, **127**, 7110.

4. (a) M. B. Duriska, S. R. Batten and D. J. Price, *Aus. J. Chem.*, 2006, **59**, 26; (b) M. Du, X. –J. Zhao, S. R. Batten and J. Ribas, *Cryst. Growth. Des.*, 2005, **5**, 901; (c) R. Matsuda, R. Kitaura, S. Kitigawa, Y. Kubota, T. C. Kobayashi, S. Horike and M. Takata, *J. Am. Chem. Soc.*, 2004, **126**, 14063; (d) X. –H. Bu, M. –L. Tong, H. –C. Chang, S. Kitigawa and S. Batten, *Angew. Chem. Int. Ed.*, 2003, **43**, 192; (e) B. F. Abrahams, S. R. Batten, B. F. Hoskins and R. Robson, *Inorg. Chem.*, 2003, **42**, 2654; (f) T. K. Maji, S. Kitigawa, *Pure and Appl. Chem.*, 2007, **79**, 2150; (g) D. B. Cordes, C. V. K. Sharma and R. Rogers, *Cryst. Growth Des.*, 2007, **7**, 1943; (h) R. Robson, *J. Chem. Soc.*, *Dalton Trans.*, 2000, 3735.
5. (a) C. B. Aakeröy, N. Schultheiss and J. Desper, *Dalton. Trans.*, 2006, 1627; (b) C. B. Aakeröy, N. Schultheiss and J. Desper, *CrystEngComm*, 2006, **9**, 421; (c) C. B. Aakeröy, N. Schultheiss and J. Desper, *Inorg. Chem.*, 2005, **44**, 4983; (d) C. B. Aakeröy, J. Desper and J. Valdés-Martínez, *CrystEngComm*, 2004, **6**, 413; (e) C. B. Aakeröy, A. M. Beatty and K. R. Lorimer, *J. Chem. Soc., Dalton Trans.*, 2000, **21**, 3869, (f) C. B. Aakeröy, A. M. Beatty, D. S. Leinen and K. R. Lorimer, *Chem. Commun.*, 2000, **11**, 935; (g) T. J. Burchell, D. J. Eisler and R. J. Puddephatt, *Inorg. Chem.*, 2004, **43**, 5550; (h) M. D. Stephenson, T. J. Prior and M. J. Hardie, *Cryst. Growth Des.*, 2008, **8**, 643; (i) L. Brammer, *Chem. Soc. Rev.*, 2004, **33**, 476 and references therein, (j) H. Hofmeier, A. El-ghayoury, A. P. H. J. Schenning and U. S. Schubert, *Chem. Commun.*, 2004, 318, (k) D. G. Kruth, K. M. Fromm and J.–M. Lehn, *Eur. J. Inorg. Chem.*, 2001, 1523; (l) E. Breuning, U. Ziener, J. –M. Lehn, E. Wegelius and K. Rissanen, *Eur. J. Inorg. Chem.*, 2001, 1515; (m) C. L. Schauer, E. Matwey, F. W. Fowler and J. W. Lauher, *J. Am. Chem. Soc.*, 1997, **119**, 10245; (n) E. Deiters, V. Bulach and M. W. Hosseini, *New J. Chem.*, 2008, **32**, 99; (o) T. J. Burchell, D. J. Eisler and R. J. Puddephatt, *Chem. Commun.*, 944; (p) N. L. S. Yue, D. J. Eisler, M. C. Jennings and R. Puddephatt, *Inorg. Chem*., 2004, **43**, 7671; (q) J. Pansanel, A. Jouaiti, S. Ferlay, M. W. Hosseini, J. –M. Planeix and N. Kyritsakas, *New. J. Chem.*, 2006, **30**, 71, (r) D. Natale and C. Mareque-Rivas, *Chem. Commun.*, 2008, 425; (s) S. Martínez-Vargas, S. Hernández-Ortega, R. A. Toscano, D. Salazar-Mendoza and J. Valdés-Martínez, *CrystEngComm.*, 2008, **10**, 86.
6. For a discussion on the robustness of the amide dimer, see Chapter 2.

7. (a) C. B. Aakeröy and A. Beatty, *Cryst. Eng*., 1998, **1**, 39; (b) C. B. Aakeröy and A. Beatty, *Chem. Commun*., 1998, 1067.
8. C. B. Aakeröy, J. Desper, M. M. Smith and J. F. Urbina, *Dalton Trans.*, 2005, **14**, 2462.
9. (a) J. K. Bera, T. –T. Vo, R. A. Walton and K. R. Dunbar, *Polyhedra*, 2003, **22**, 3009; (b) C. B. Aakeröy, A. Beatty, J. Desper, M. O'Shea and J. Valdés-Martínez, *Dalton Trans.*, 2003, 3956; (c) J. –P. Zhang, Y. –Y. Lin, X. –C. Huang and X. –M. Chen, *J. Am. Chem. Soc.*, 2005, **127**, 5495; (d) B.Kozlevcar, I.Leban, I.Turel, P.Segedin, M.Petric, F.Pohleven, A.J.P.White, D.J.Williams and J.Sieler, *Polyhedra*, 1999, **18**, 755; (e) G.V.Tsintsadze, R.A.Kiguradze, A.N.Shnulin and Kh.S.Mamedov, *Zh. Strukt. Khim*, 1984, **25**, 82; (f) K.Smolander, M.Macko, M.Valko and M.Melnik, *Anal. Sci. X-Ray struct. Anal. Online,* 2005, **21**, x167; (g) D.Chakrabarty, H.Nagase, M.Kamijo, T.Endo and H.Ueda, *Anal. Chem. Scand.*, 1992, **46**, 29; (h) A.S.Antsyshkina, T.V.Koksharova, G.G.Sadikov, I.S.Gritsenko, V.S.Sergienko and O.A.Egorova, *Zu. Neorg. Khim.*, 2006, **51**, 972; (i) B.Kozlevcar, N.Lah, I.Leban, I.Turel, P.Segedin, M.Petric, F.Pohleven, A.J.P.White, D.J.Williams and G.Giester, *Croat. Chem. Acta.*, 1999, **72**, 42.
10. C. B. Aakeröy; J. Desper and J. F. Urbina, *unpublished results*.
11. Cambridge Structural Database version 5.29 (January 2008).

CHAPTER 7 - Functionalised Bis-pyrazole Ligands: A Tool for Construction of Inorganic-organic Hybrid Materials

7.1 Introduction

Chelating ligands provide an avenue towards reliable assembly coordination networks. The use of ligands that can bind to a metal ion via two or more coordination sites has been exploited[1] and offers an advantage for controlling and predicting coordination complexes. Figure 7.1 shows three examples within a diverse range of chelating ligands available.

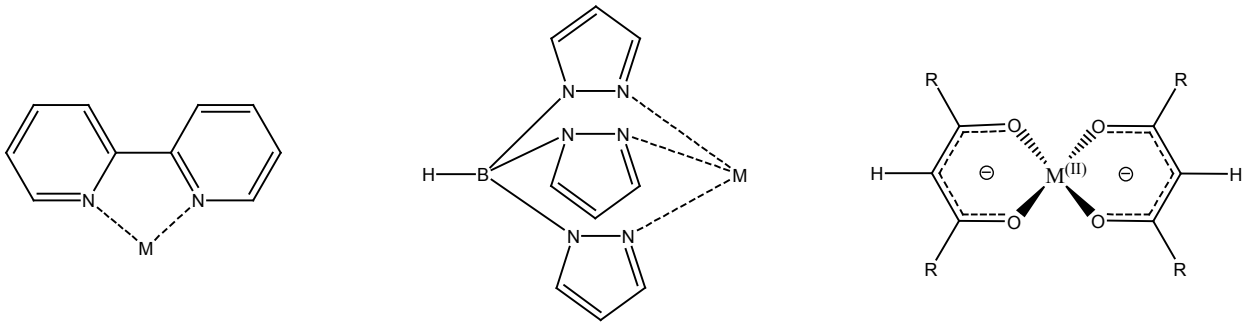

(a) (b) (c)

Figure 7.1 Examples of chelating ligands; (a) 2,2'-bipyridine;[2] (b) trispyrazolylborate;[3] (c) acetylacetonate.[4]

2,2'-Bipyridine,[2] trispyrazolylborate[3] and acetylacetonate (*acac*)[4] ligands have been utilised to 'block off' coordination sites of transition metals allowing for control over metal coordination, geometry and network dimensionality.

It is clear then in order to gain an additional level of predictability, chelating ligands should be employed.

1,3-Bis-benzylpyrazole, Figure 7.2a, is a potential chelating ligand as the flexible benzylpyrazole arms could allow a metal ion to "sit" between the two pyrazole rings. 1,3-Bis-benzylpyrazole has been used to construct coordination polymers,[5] however its use as a chelating ligand has been limited to organometallic compounds[6] in which the C-H bond is replaced with a direct C-M bond, 'locking' the bis-pyrazole arms into position, Figure 7.2b.

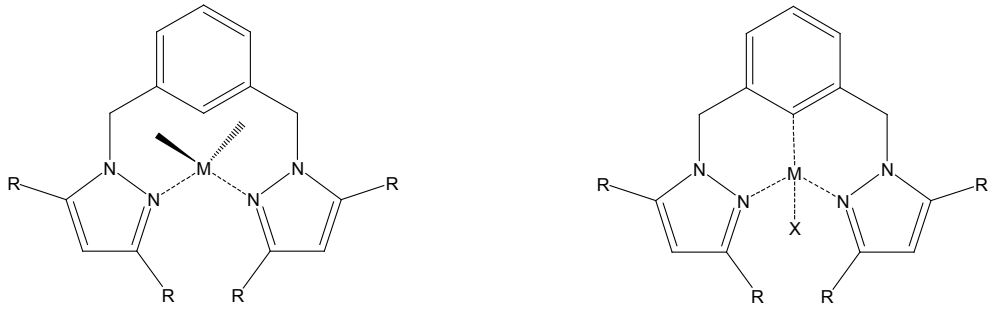

(a) (b)

Figure 7.2 1,3-Bis-benzylpyrazole as a chelating ligand in (a) coordination complexes and (b) organometallic compounds.

2,6-Bis[(pyrazol-1-yl)methyl]pyridine,[7] Figure 7.3, is an effective tridentate chelating ligand so it is feasible that 1,3-bisbenzylpyrazole can act as a bidentate chelating ligand.

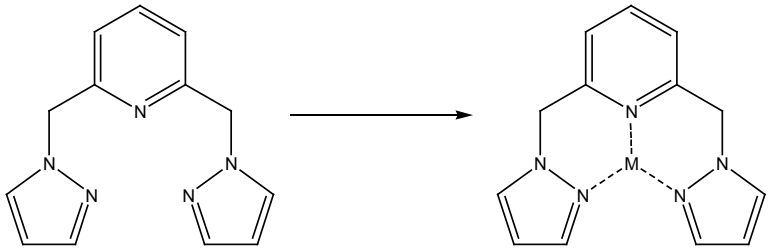

Figure 7.3 2,6-Bis[(pyrazol-1-yl)methyl]pyridine as a chelating ligand.

If 1,3-bis-benzylpyrazole can be reliably used to coordinate a metal ion, appending a second functionality capable of either (i) coordination to a second metal or (ii) forming self-complementary hydrogen bonds, Figure 7.4, would make construction of bimetallic systems and extended supramolecular coordination complexes possible.

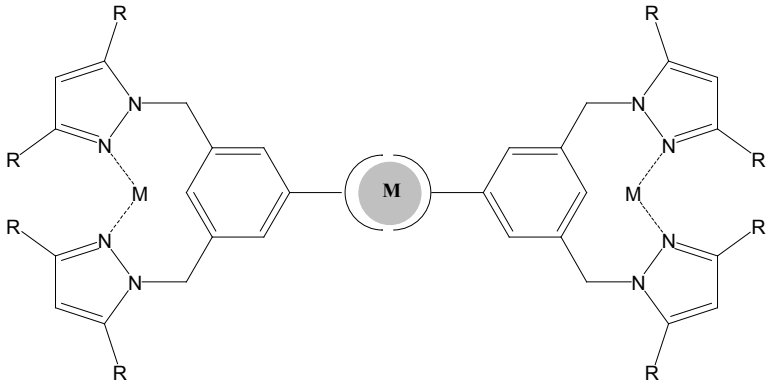

(a)

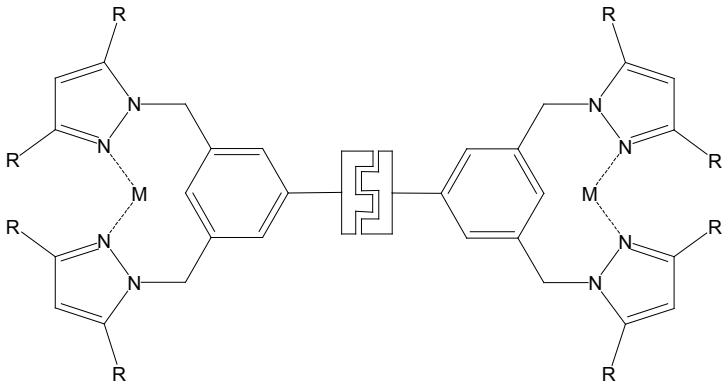

(b)

Figure 7.4 Functionalised 1,3-bis-benzylpyrazole systems.

With this in mind, a new family of SR's will be designed to answer the following questions:

I. Can functionalised 1,3-bis-benzylpyrazole ligands be employed as chelating ligands?

Consequently, a family of ligands has been targeted in which 1,3-bis-benzylpyrazole is paired with a pyridyl or pyrazole functionality, Figure 7.5. Through a series of metal-coordination and organometallic reactions, the potential of 1,3-bis-benzylpyrazole as a chelating ligand (determined by single crystal X-ray diffraction and NMR) will be addressed.

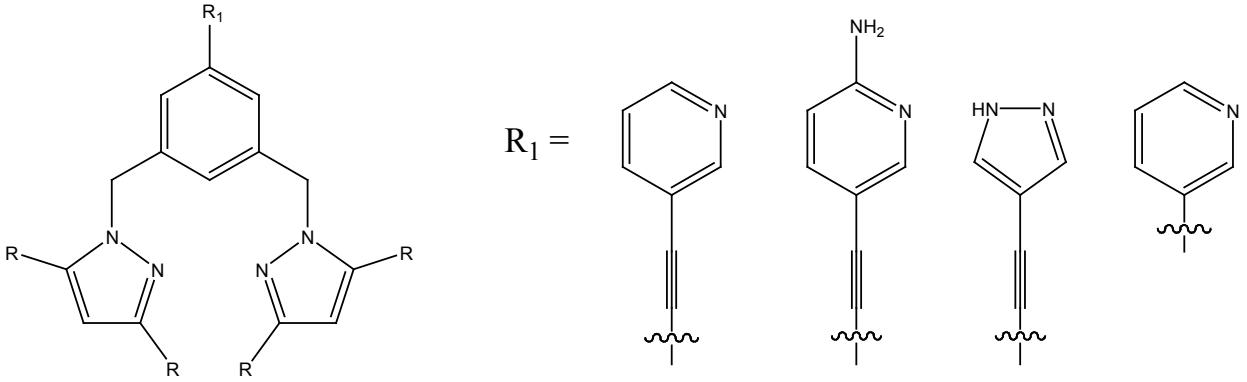

R = H or Me

Figure 7.5 Target 1,3-bis-pyrazole SR's.

7.2 Experimental

7.2.1 Synthesis

All chemicals were purchased from Aldrich and Fischer and used without further purification. 4-Iodopyrazole was synthesised via a previously published procedure.[8] Melting points were determined on a Fisher-Johns melting point apparatus and are uncorrected.

7.2.1.1 Synthesis of 1-bromo-3,5-bis(bromomethyl)benzene, 24

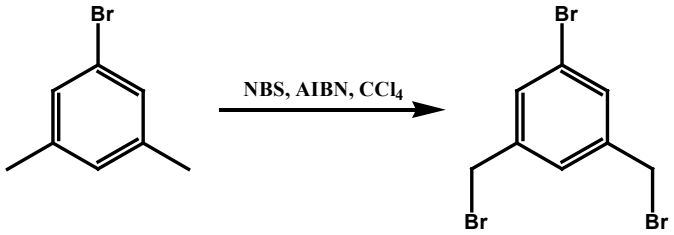

To a round bottom flask, 1-bromo-*3,5*-dimethylbenzene (10.0g, 54.0mmol), N-bromosuccinimide (NBS) (20.6g, 114mmol), azobisisobutyronitrile (AIBN) (0.460g, 2.80mmol) and CCl_4 (150mL) were added and stirred at reflux for 3 hours. The reaction was cooled to room temperature and the solution filtered to remove the succinimide. The CCl_4 filtrate was concentrated in vacuum and the resulting orange solid recrystallised from ethanol to give a white solid, **24**, (5.38g, 30.0%). Mp: 84-86^{o}C. ^{1}H NMR (δ_H; 400MHz, $CDCl_3$): 4.42 (s, 4H), 7.35 (s, 1H), 7.48 (d, J = 2.8Hz, 2H), Figure B.24.

7.2.1.2 Synthesis of 1-bromo-3,5-bis[(pyrazol-1-yl)methyl]benzene, 25

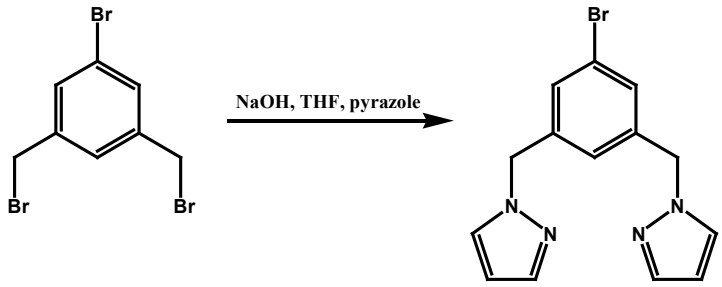

To a round bottom flask, pyrazole (5.40g, 79.0mmol) and THF (150mL) were added. To this solution, NaOH pellets (32.0g, 790mmol) were added and the reaction was stirred at room temperature for 2 hours. On completion, **24** (10.9g, 32.0mmol) in THF (150mL) was added and the reaction mixture stirred at room temperature for 2 days. On completion, water was added to dissolve any excess NaOH, the organic layer was separated, dried over $MgSO_4$ and the solvent

removed under vacuum to yield **25** as a white solid (8.73g, 86.6%). Mp: 67-70°C. ^{1}H NMR (δ_H; 200MHz, $CDCl_3$): 5.21 (s, 4H), 6.27 (t, *J* = 2.2Hz, 2H), 6.91 (s, 1H), 7.19 (s, 2H), 7.38 (d, *J* = 2.2Hz, 2H), 7.54 (d, *J* = 1.8Hz, 2H), Figure B.25.

7.2.1.3 Synthesis of 1-bromo-3,5-bis[(3,5-dimethylpyrazol-1-yl)methyl]benzene, 26

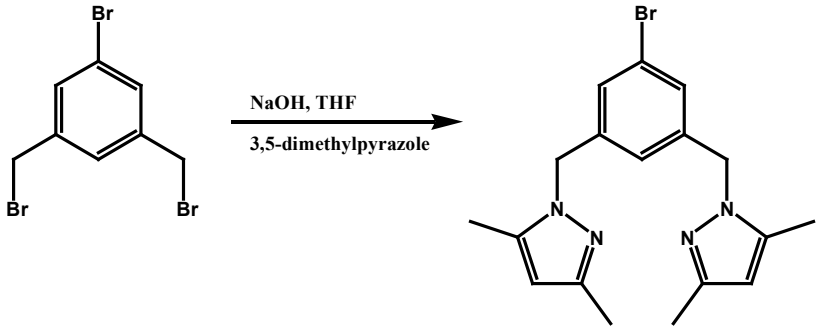

To a round bottom flask, 3,5-dimethylpyrazole (3.60g, 10.9mmol) and THF (75mL) were added. To this solution, NaOH pellets (8.32g, 208mmol) were added and the reaction was stirred at room temperature for 2 hours. On completion, **24** (1.20g, 20.8mmol) in THF (75mL) was added and the reaction mixture stirred at room temperature for 2 days. On completion, water was added to dissolve any excess NaOH, the organic layer was separated, dried over $MgSO_4$ and the solvent removed under vacuum to yield **26** as a white solid (3.86g, 95.0%). Mp: 68-70°C. ^{1}H NMR (δ_H; 200MHz, $CDCl_3$): 2.10 (s, 6H), 2.23 (s, 6H), 5.11 (s, 4H), 5.84 (s, 2H), 6.61 (s, 1H), 7.06 (s, 2H), Figure B.26.

7.2.1.4 Synthesis of 1-trimethylsilanylethynyl-3,5-bis[(pyrazol-1-yl)methyl]benzene, 27

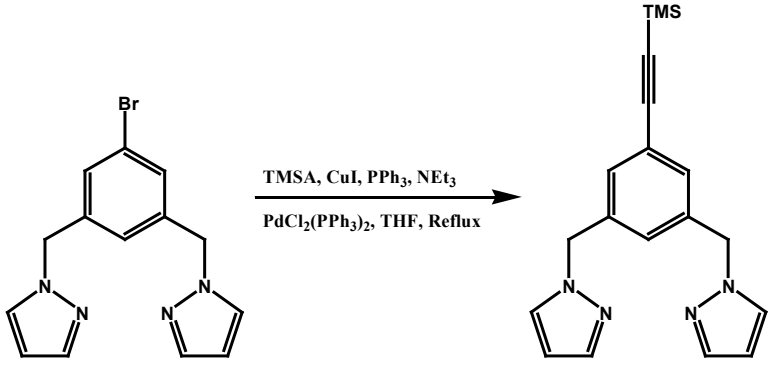

THF (30mL) and NEt_3 (30mL) were added to a round bottom flask and nitrogen bubbled through the solution for 10 minutes. To this, **25** (2.0g, 6.3mmol), trimethylsilylacetylene (TMSA) (0.88g, 9.0mmol), CuI (0.036g, 0.19mmol), PPh_3 (0.13g, 0.50mmol) and $PdCl_2(PPh_3)_2$ (0.13g, 0.19mmol) were added and the solution stirred at 75°C for 24 hours at which point more

trimethylsilylacetylene (0.88g, 9.0mmol), CuI (0.036g, 0.19mmol), PPh_3(0.13g, 0.50mmol) and $PdCl_2(PPh_3)_2$ (0.13g, 0.19mmol) were added and stirred for a further 24 hours. Upon completion, the solution was diluted with ethyl acetate and washed with water (3x25mL) and $NaCl_{(aq)}$ (25mL). The ethyl acetate layer was separated, dried over $MgSO_4$ and reduced to a brown oil. The residue was purified by column chromatography (hexanes → hexanes:ethyl acetate; 1:1), to yield **27** as a brown oil, (2.00g, 92%). ^{1}H NMR (δ_H; 200MHz, $CDCl_3$): 0.21 (s, 9H), 5.16 (s, 4H), 6.23 (t, *J* = 2Hz, 2H), 6.94 (s, 1H), 7.21 (s, 2H), 7.33 (d, *J* = 2.2Hz, 2H), 7.50 (d, *J* = 1.4Hz, 2H), Figure B.27.

7.2.1.5 Synthesis of 1-trimethylsilanylethynyl-3,5-bis[(3,5-dimethylpyrazol-1-yl)methyl]benzene, 28

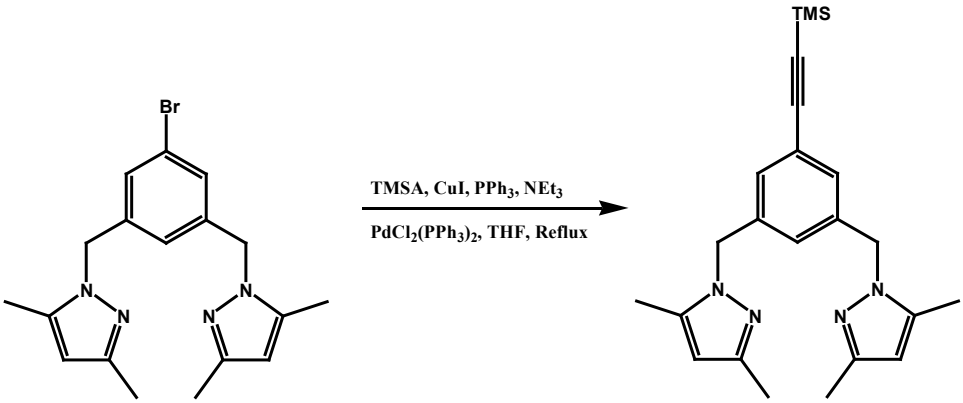

THF (30mL) and NEt_3(30mL) were added to a round bottom flask and nitrogen bubbled through the solution for 10 minutes. To this, **26** (2.00g, 5.35mmol), trimethylsilylacetylene (0.680g, 6.89mmol), CuI (0.0390g, 0.203mmol), PPh_3 (0.110g, 0.422mmol) and $PdCl_2(PPh_3)_2$ (0.110g, 0.158mmol) were added and the solution stirred at 75^{o}C for 24 hours at which point more trimethylsilylacetylene (0.680g, 6.89mmol) was added and stirred for a further 24 hours. Upon completion, the solution was diluted with ethyl acetate and washed with water (3x25mL) and $NaCl_{(aq)}$ (25mL). The ethyl acetate layer was separated, dried over $MgSO_4$ and reduced to a brown oil. The residue was purified by column chromatography (hexanes → hexanes:ethyl acetate; 1:1), to yield **28** as a brown oil, (1.67g, 79.6%). ^{1}H NMR (δ_H; 200MHz, $CDCl_3$): 0.22 (s, 9H), 2.08 (s, 6H), 2.23 (s, 6H), 5.11 (s, 4H), 5.83 (s, 2H), 6.61 (s, 1H), 7.09 (d, *J* = 0.6Hz, 2H), Figure B.28.

7.2.1.6 Synthesis of 1-ethynyl-3,5-bis[(pyrazol-1-yl)methyl]benzene, 29

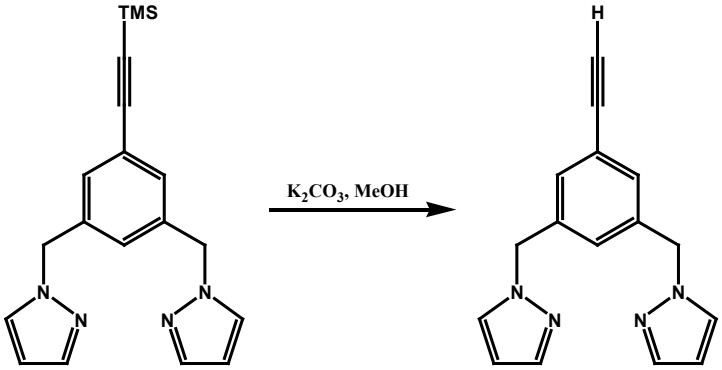

To a round bottom flask, **27** (1.74g, 5.18mmol), K_2CO_3 (0.716g, 5.18mmol) and methanol (40mL) were added and stirred at room temperature over night. The solution was diluted with diethyl ether and washed with water (4x25mL). The diethyl ether was separated, dried over $MgSO_4$ and reduced to a white solid. The solid was purified by column chromatography (hexanes → hexanes:ethyl acetate; 1:1), to yield **29** as a white solid, (1.02g, 76.0%). Mp: 92-95^oC. ^1H NMR (δ_H; 200MHz, $CDCl_3$): 3.05 (s, 1H), 5.24 (s, 4H), 6.29 (t, J = 2.2Hz, 2H), 6.99 (s, 1H), 7.21 (s, 2H), 7.37 (d, J = 1.8Hz, 2H), 7.54 (d, J = 1.8Hz, 2H), Figure B.29.

7.2.1.7 Synthesis of 1-ethynyl-3,5-bis[(3,5-dimethylpyrazol-1-yl)methyl]benzene, 30

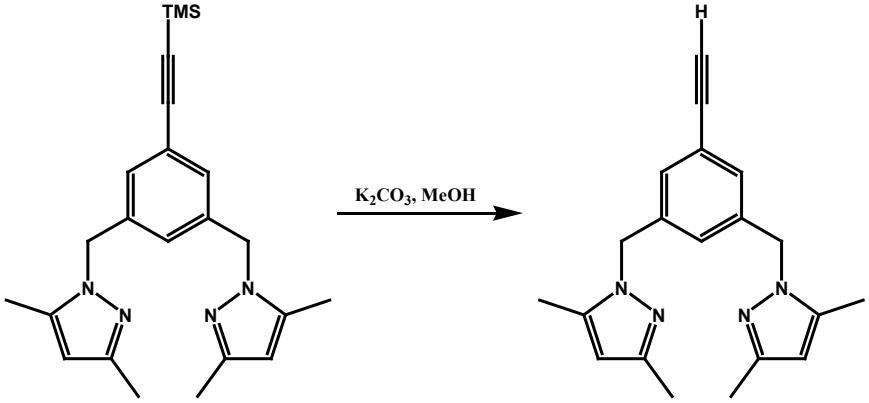

To a round bottom flask, **28** (1.67g, 4.23mmol), K_2CO_3 (0.584g, 4.23mmol) and methanol (40mL) were added and stirred at room temperature over night. The solution was diluted with diethyl ether and washed with water (4x25mL). The diethyl ether was separated, dried over $MgSO_4$ and reduced to a white solid. The solid was purified by column chromatography (hexanes → hexanes:ethyl acetate; 1:1), to yield **30** as a white solid, (1.16g,

85.0%). Mp: 67-70°C. ^{1}H NMR (δ_H; 200MHz, $CDCl_3$): 2.08 (s, 6H), 2.22 (s, 6H), 3.05 (s, 1H), 5.11 (s, 4H), 5.82 (s, 2H), 6.69 (s, 1H), 7.06 (s, 2H), Figure B.30.

7.2.1.8 Synthesis of 1-[3,5-bis(pyrazol-1-ylmethyl)phenyl]-2-[pyridin-3-yl]ethyne, 31

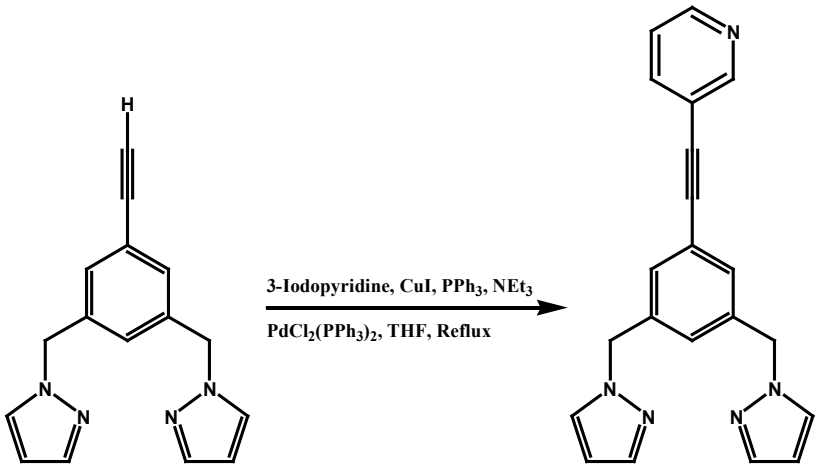

THF (10mL) and NEt_3(10mL) were added to a round bottom flask and nitrogen bubbled through the solution for 10 minutes. To this, **29** (0.25g, 0.95mmol), 3-iodopyridine (0.16g, 0.79mmol), CuI (0.0060g, 0.030mmol), PPh_3 (0.016g, 0.063mmol) and $PdCl_2(PPh_3)_2$ (0.016g, 0.023mmol) were added and the solution stirred at 75°C for 24 hours. Upon completion, the solution was diluted with ethyl acetate and washed with water (3x25mL) and $NaCl_{(aq)}$ (25mL). The ethyl acetate layer was separated, dried over $MgSO_4$ and reduced to a brown oil. The residue was purified by column chromatography (hexanes → hexanes:ethyl acetate; 1:1), to yield a yellow solid. Recrystallisation from ethanol yielded **31** as a white solid (0.23g, 85%). Mp: 54-56°C. ^{1}H NMR (δ_H; 200MHz, $CDCl_3$): 5.30 (s, 4H), 6.31 (t, J = 2.2Hz, 2H), 7.03 (s, 1H), 7.21-7.31 (m, 3H), 7.42 (d, J = 1.4Hz, 2H), 7.57 (d, J = 1.4Hz, 2H), 7.76 (dt, J^1 = 8Hz, J^2 = 1.8Hz, 1H), 8.54 (dd, J^1 = 5.0Hz, J^2 = 1.6Hz, 1H), 8.72 (d, J = 2.2Hz, 1H), Figure B.31a; ^{13}C NMR, (δ_C; 50MHz, $CDCl_3$): 55.22, 86.80, 91.67, 106.29, 123.06, 123.75, 126.93, 129.47, 130.18, 130.80, 137.89, 138.49, 139.97, 148.76,152.22, Figure B.31b.

7.2.1.9 Synthesis of 1-[3,5-bis(3,5-dimethylpyrazol-1-ylmethyl)phenyl]-2-[pyridin-3-yl]ethyne, 32

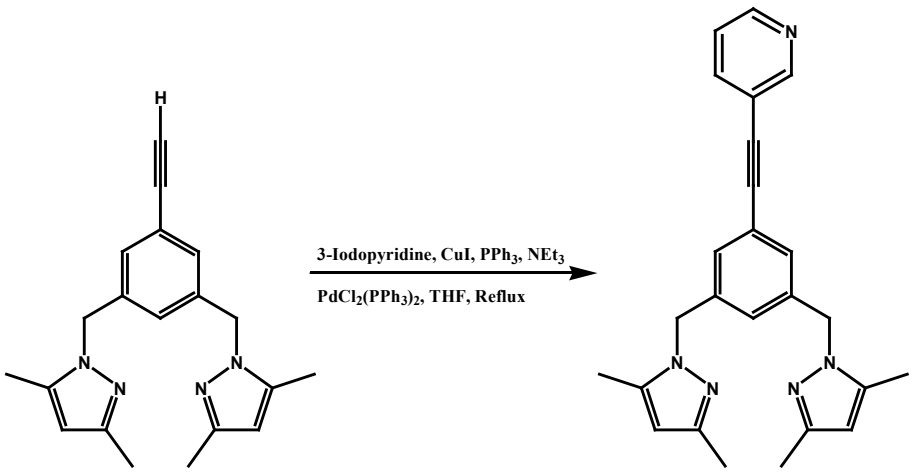

THF (10mL) and NEt_3(10mL) were added to a round bottom flask and nitrogen bubbled through the solution for 10 minutes. To this, **30** (0.25g, 0.79mmol), 3-iodopyridine (0.13g, 0.66mmol), CuI (0.0050g, 0.0025mmol), PPh_3 (0.014g, 0.052mmol) and $PdCl_2(PPh_3)_2$ (0.014g, 0.019mmol) were added and the solution stirred at 75°C for 24 hours. Upon completion, the solution was diluted with ethyl acetate and washed with water (3x25mL) and $NaCl_{(aq)}$ (25mL). The ethyl acetate layer was separated, dried over $MgSO_4$ and reduced to a brown oil. The residue was purified by column chromatography (hexanes → hexanes:ethyl acetate; 1:1), to yield **32** as a yellow solid, (0.19g, 57 %). Mp: 75-78°C. ^{1}H NMR (δ_H; 200MHz, $CDCl_3$): 2.13 (s, 6H), 2.25 (s, 6H), 5.16 (s, 4H), 5.86 (s, 2H), 6.73 (s, 1H), 7.13 (d, J = 1.6Hz, 2H), 7.26 (dd, J^1 = 7.6Hz, J^2 = 2.6Hz, 1H), 7.78 (dt, J^1 = 7.6Hz, J^2 = 2.0Hz, 1H), 8.53 (d, J = 3.6Hz, 1H), 8.73 (d, J = 1.4Hz, 2H), Figure B.32a; ^{13}C NMR, (δ_C; 100MHz, $CDCl_3$): 11.10, 13.53, 51.89, 86.43, 92.09, 105.75, 120.16, 123.05, 123.41, 125.28, 128.79, 138.46, 138.50, 139.26, 147.88, 148.62, 152.15, Figure B.32b.

7.2.1.10 Synthesis of 1-[3,5-bis(pyrazol-1-ylmethyl)phenyl]-2-[2-aminopyridin-5-yl]ethyne, 33

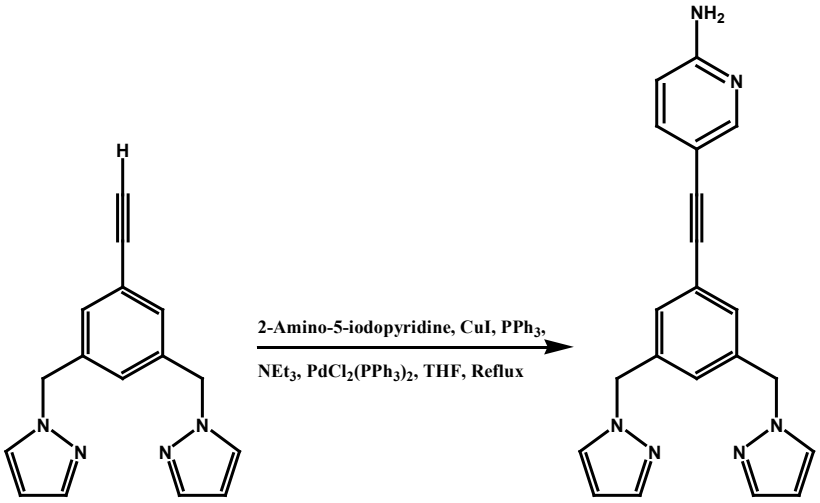

THF (25mL) and NEt_3(25mL) were added to a round bottom flask and nitrogen bubbled through the solution for 10 minutes. To this, **29** (0.50g, 1.90mmol), 2-amino-5-iodopyridine (0.35g, 1.6mmol), CuI (0.012g, 0.060mmol), PPh_3 (0.033g, 0.13mmol) and $PdCl_2(PPh_3)_2$ (0.033g, 0.047mmol) were added and the solution stirred at 75°C for 24 hours. Upon completion, the solution was diluted with ethyl acetate and washed with water (3x50mL) and $NaCl_{(aq)}$ (50mL). The ethyl acetate layer was separated, dried over $MgSO_4$ and reduced to a brown oil. The residue was purified by column chromatography (hexanes → hexanes:ethyl acetate; 1:1), to yield **33** as a yellow solid, (0.30g, 53%). Mp: 148-151°C. ^{1}H NMR (δ_H; 200MHz, $CDCl_3$): 4.72 (s, 2H), 5.28 (s, 4H), 6.30 (t, *J* = 2.0Hz, 2H), 6.45 (d, *J* = 8.6Hz, 1H), 6.98 (s, 1H), 7.25 (d, *J* = 1.2Hz, 2H), 7.40 (d, *J* = 2.2Hz, 2H), 7.48 (d, *J* = 2.6Hz, 1H), 7.53 (d, *J* = 2.6Hz, 1H), 7.56 (d, *J* = 2.0Hz, 1H), 8.22 (d, *J* = 2.2Hz, 1H), Figure B.33a; ^{13}C NMR, (δ_C; 50MHz, $CDCl_3$): 55.28, 89.00, 106.21, 107.99, 109.28, 124.59, 126.20, 129.41, 129.88, 130.76, 137.65, 139.84, 140.37, 151.34, 157.57, Figure B.33b.

7.2.1.11 Synthesis of 1-[3,5-bis(3,5-dimethylpyrazol-1-ylmethyl)phenyl]-2-[2-aminopyridin-5-yl]ethyne, 34

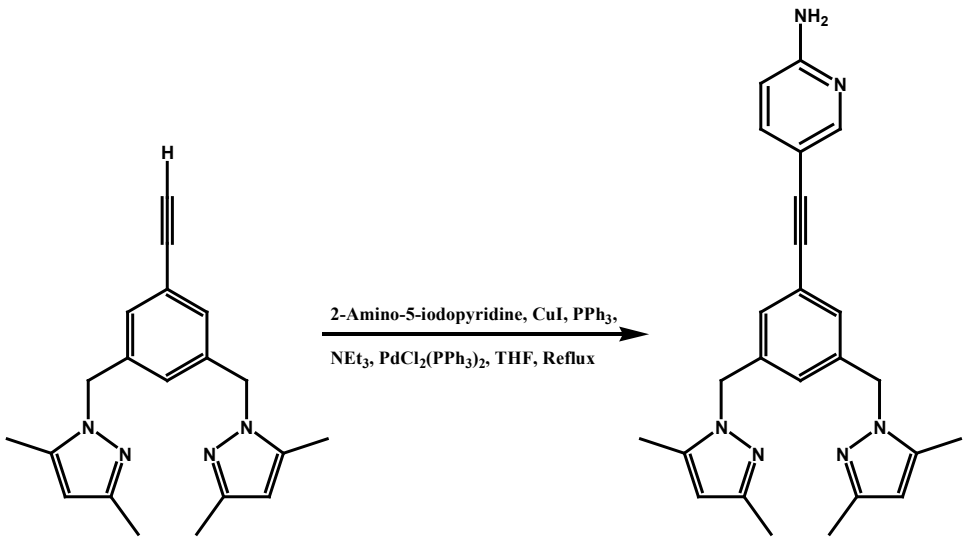

THF (10mL) and NEt_3(10mL) were added to a round bottom flask and nitrogen bubbled through the solution for 10 minutes. To this, **30** (0.25g, 7.9mmol), 2-amino-5-iodopyridine (0.14g, 0.66mmol), CuI (0.0050g, 0.025mmol), PPh_3 (0.014g, 0.052mmol) and $PdCl_2(PPh_3)_2$ (0.014g, 0.019mmol) were added and the solution stirred at 75°C for 24 hours. Upon completion, the solution was diluted with ethyl acetate and washed with water (3x50mL) and $NaCl_{(aq)}$ (50mL). The ethyl acetate layer was separated, dried over $MgSO_4$ and reduced to a brown oil. The residue was purified by column chromatography (hexanes → hexanes:ethyl acetate; 1:1), to yield **34** as a yellow solid, (0.18g, 67%). Mp: 122-125°C. ^{1}H NMR (δ_H; 200MHz, $CDCl_3$): 2.12 (s, 6H), 2.24 (s, 6H), 5.15 (s, 4H), 5.85 (s, 2H), 6.44 (dd, J^1 = 8.6Hz, J^2 = 0.8Hz, 1H), 6.66 (s, 1H), 7.07 (s, 2H), 7.51 (dd, J^1 = 8.6Hz, J^2 = 2.2Hz, 1H), 8.15 (d, J = 2.8Hz, 1H), Figure B.34a; ^{13}C NMR, (δ_C; 100MHz, DMSO-d^6): 10.38, 13.11, 50.76, 104.90, 107.48, 123.88, 124.95, 127.89, 128.48, 131.22, 133.98, 138.66, 139.19, 146.04, 150.34, 151.06, 159.10, Figure B.34b.

7.2.1.12 Synthesis of 1-(1-butoxyethyl)-4-iodopyrazole, 35

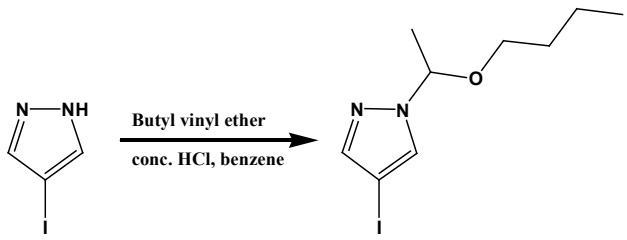

To a round bottom flask, 4-iodopyrazole (0.250g, 1.29mmol), butyl vinyl ether (0.34g, 3.38mmol), conc. HCl (1 drop) and benzene (10mL) were added and the reaction stirred at 35°C for 2 hours. $NaHCO_3$ and K_2CO_3 added to the reaction and the benzene extracted, dried over $MgSO_4$ and reduced to yield **35** as a colourless oil, (0.349g, 92.1%). ^1H NMR (δ_H; 200MHz, $CDCl_3$): 0.86 (t, *J* = 7.4Hz, 3H), 1.25-1.56 (m, 4H), 1.62 (d, *J* = 6.2Hz, 3H), 3.20-3.46 (m, 2H), 5.48 (q, *J* = 6.2Hz, 1H), 7.50 (s, 1H), 7.63 (s, 1H), Figure B.35.

7.2.1.13 Synthesis of 1-[3,5-bis(pyrazol-1-ylmethyl)phenyl]-2-[1-(1-butoxyethyl)-pyrazol-4-yl]ethyne, 36

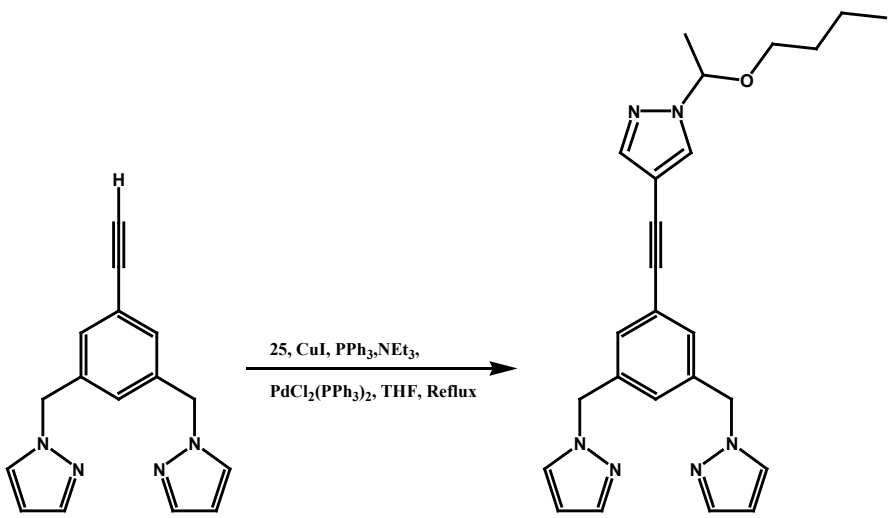

THF (25mL) and NEt_3(25mL) were added to a round bottom flask and nitrogen bubbled through the solution for 10 minutes. To this, **29** (0.50g, 1.9mmol), **35** (0.48g, 1.6mmol), CuI (0.012g, 0.060mmol), PPh_3 (0.033g, 0.13mmol) and $PdCl_2(PPh_3)_2$ (0.033g, 0.047mmol) were added and the solution stirred at 75°C for 24 hours. Upon completion, the solution was diluted with ethyl acetate and washed with water (3x50mL) and $NaCl_{(aq)}$ (50mL). The ethyl acetate layer was separated, dried over $MgSO_4$ and reduced to a brown oil. The residue was purified by column chromatography (hexanes → hexanes:ethyl acetate; 1:1), to yield **36** as a yellow oil, (0.36g, 51%). ^1H NMR (δ_H; 200MHz, $CDCl_3$): 0.87 (t, *J* = 7.2Hz, 3H), 1.22-1.54 (m, 4H), 1.64 (d, *J* = 6.2Hz, 3H), 3.21-3.46 (m, 2H), 5.27 (s, 4H), 5.48 (q, *J* = 6.2Hz, 1H), 6.29 (t, *J* = 2.0Hz, 2H), 6.98 (s, 1H), 7.22 (s, 2H), 7.39 (s, 2H), 7.55 (d, *J* = 1.8Hz, 2H), 7.63 (s, 1H), 7.75 (s, 1H), Figure B.36.

7.2.1.14 Synthesis of 1-[3,5-bis(3,5-dimethylpyrazol-1-ylmethyl)phenyl]-2-[1-(1-butoxyethyl)-pyrazol-4-yl]ethyne, 37

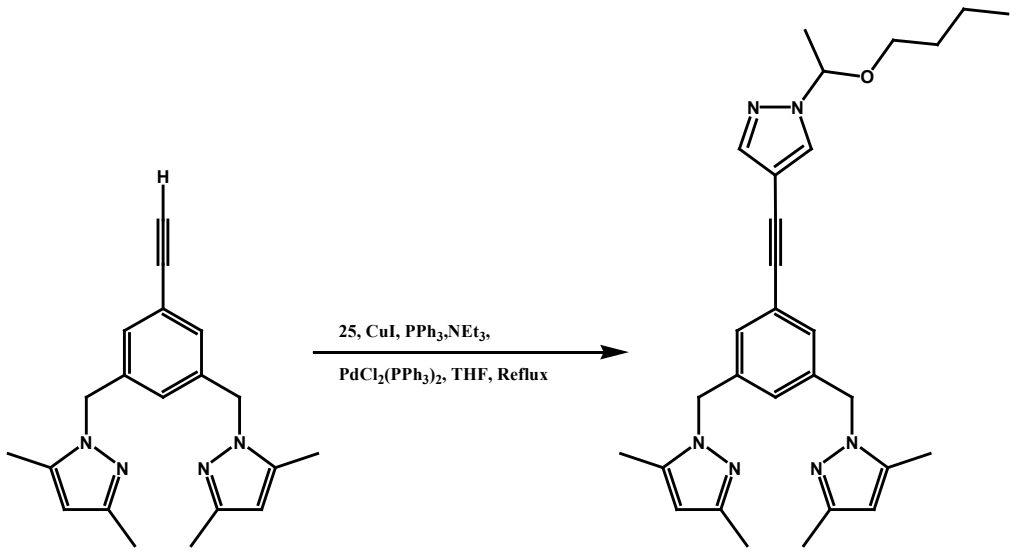

THF (25mL) and NEt_3(25mL) were added to a round bottom flask and nitrogen bubbled through the solution for 10 minutes. To this, **30** (0.53g, 1.7mmol), **35** (0.41g, 1.4mmol), CuI (0.010g, 0.053mmol), PPh_3 (0.029g, 0.11mmol) and $PdCl_2(PPh_3)_2$ (0.029g, 0.041mmol) were added and the solution stirred at 75^oC for 24 hours. Upon completion, the solution was diluted with ethyl acetate and washed with water (3x50mL) and $NaCl_{(aq)}$ (50mL). The ethyl acetate layer was separated, dried over $MgSO_4$ and reduced to a brown oil. The residue was purified by column chromatography (hexanes → hexanes:ethyl acetate; 1:1), to yield **37** as a yellow oil, (0.21g, 30%). ^1H NMR (δ_H; 200MHz, $CDCl_3$): 0.87 (t, J = 7.4Hz, 3H), 1.25-1.58 (m, 4H), 1.64 (d, J = 5.8Hz, 3H), 2.12 (s, 3H), 2.24 (s, 3H), 3.21-3.46 (m, 2H), 5.14 (s, 4H), 5.48 (q, J = 6.2Hz, 1H), 5.84 (s, 2H), 6.68 (s, 1H), 7.07 (d, J = 2.4Hz, 2H), 7.51 (s, 1H), 7.63 (s, 1H), Figure B.37.

7.2.1.15 Synthesis of 1-[3,5-bis(pyrazol-1-ylmethyl)phenyl]-2-[pyrazol-4-yl]ethyne, 38

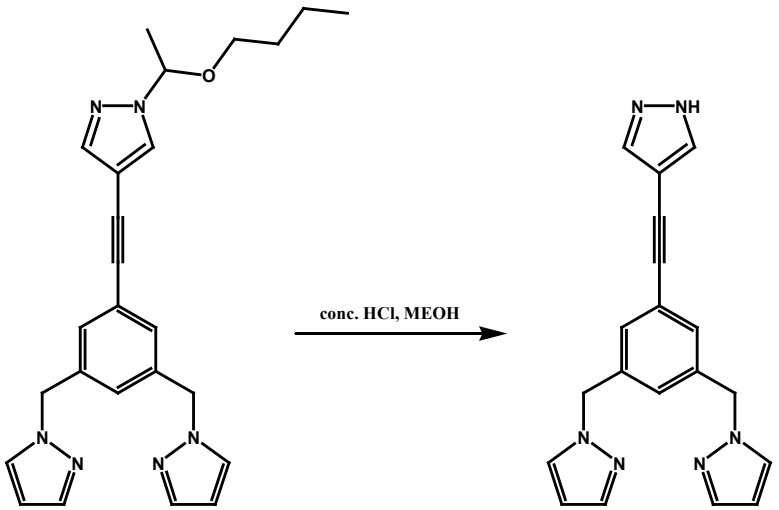

To a round bottom flask, **36** (0.36, 0.84mmol), chloroform (50mL), water (12.5mL) and conc. HCl (2.5mL) were added and stirred at room temperature overnight. The solution was neutralized with $NaHCO_3$ and the organic layer separated. The aqueous layer was washed with chloroform, the organic extracts combined, dried over $MgSO_4$ and reduced to yield **38** as a yellow solid, (0.25g, 90%). Mp: 76-79^{o}C. ^{1}H NMR (δ_H; 200MHz, $CDCl_3$): 5.27 (s, 4H), 6.30 (t, J = 2.2Hz, 2H), 6.96 (s, 1H), 7.22 (d, J = 1.4Hz, 2H), 7.41 (d, J = 2.6Hz, 2H), 7.57 (d, J = 1.4Hz, 2H), 7.70 (s, 2H), Figure B.38a; ^{13}C NMR, (δ_C; 100MHz, $CDCl_3$): 55.30, 106.25, 124.65, 126.23, 128.47, 128.58, 129.92, 131.97, 132.06, 132.16, 137.67, 139.91, Figure B.38b.

7.2.1.16 Synthesis of 1-[3,5-bis(3,5-dimethylpyrazol-1-ylmethyl)phenyl]-2-[pyrazol-4-yl]ethyne, 39

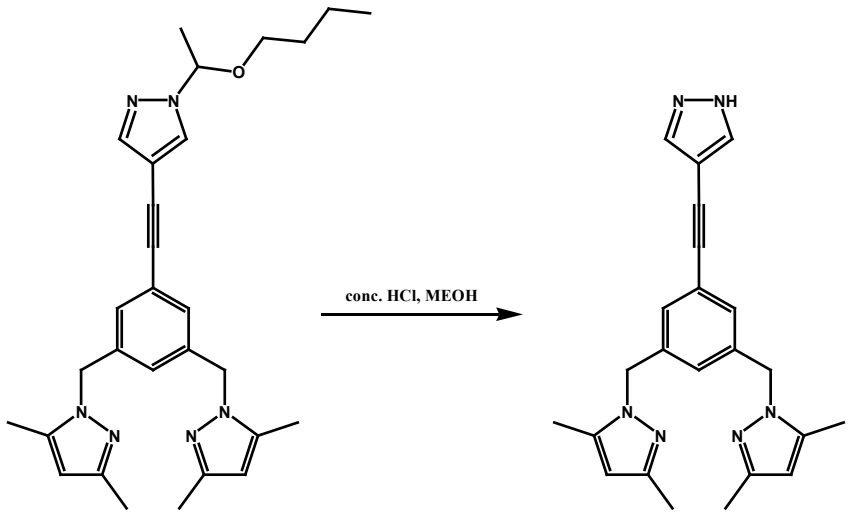

To a round bottom flask, **37** (0.21, 0.55mmol), chloroform (33mL), water (8.2mL) and conc. HCl (1.65mL) were added and stirred at room temperature for 2 days. The solution was neutralized with $NaHCO_3$ and the organic layer separated. The aqueous layer was washed with chloroform, the organic extracts combined, dried over $MgSO_4$ and reduced to yield **39** as a white solid, (0.12g, 69%). Mp: 195-198^oC. ^1H NMR (δ_H; 200MHz, $CDCl_3$): 2.11 (s, 3H), 2.24 (s, 3H), 5.13 (s, 4H), 5.85 (s, 2H), 6.65 (s, 1H), 7.05 (s, 2H), 7.68 (s, 2H), Figure B.39a; ^{13}C NMR, (δ_C; 50MHz, $CDCl_3$): 11.07, 13.49, 51.93, 89.27, 105.70, 124.29, 124.57, 128.42, 128.66, 131.92, 132.11, 138.14, 139.33, 147.78, Figure B.39b.

7.2.1.17 Synthesis of 1-iodo-3,5-bis(bromomethyl)benzene, 40

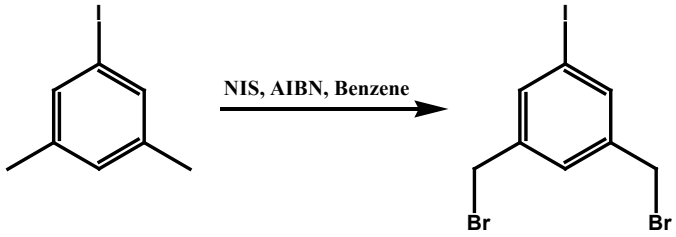

To a round bottom flask, 1-iodo-3,5-dimethylbenzene (1.068g, 6.93mmol), N-iodosuccinimide (NIS) (2.70g, 15.2mmol), AIBN (0.230g, 1.39mmol) and benzene (50mL) were added and stirred at reflux for 3 hours. The reaction was cooled to room temperature and the solution filtered to remove the succinimide. The benzene filtrate was removed in vacuum and the resulting red solid was recrystallised from ethanol. The resulting white solid was collected by filtration to yield **40**, (0.962g, 35.5%). Mp: 93-96^oC. ^1H NMR (δ_H; 400MHz, $CDCl_3$): 4.38 (s, 4H), 7.38 (s, 1H), 7.67 (s, 2H), Figure B.40.

7.2.1.18 Synthesis of 1-iodo-3,5-bis[(pyrazol-1-yl)methyl]benzene, 41

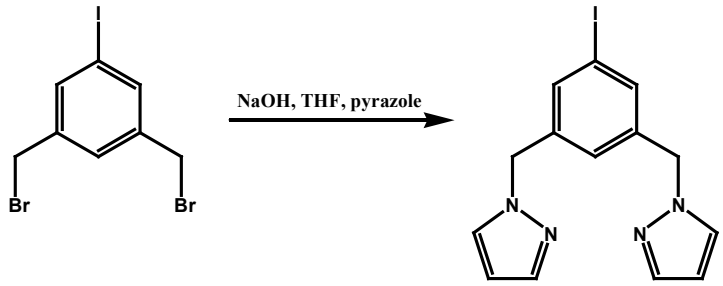

To a round bottom flask, pyrazole (0.183g, 2.69mmol) and THF (25mL) were added. To this solution, NaOH pellets (1.08g, 26.9mmol) were added and the reaction was stirred at room temperature for 2 hours. On completion, **40** (0.486g, 1.25mmol) in THF (25mL) was added and

the reaction mixture stirred at room temperature for 2 days. On completion, water was added to dissolve any excess NaOH, the organic layer was separated, dried over $MgSO_4$ and the solvent removed under vacuum to yield **41** as a white solid (0.390g, 85.7%). Mp: 58-61°C. ^{1}H NMR (δ_H; 200MHz, $CDCl_3$): 5.19 (s, 4H), 6.27 (t, *J* = 2.2Hz, 2H), 6.94 (s, 1H), 7.36 (d, *J* = 2.2Hz, 2H), 7.41 (d, *J* = 1.4Hz, 2H), 7.53 (d, *J* = 1.0Hz, 2H), Figure B.41.

7.2.1.19 Synthesis of [1-(pyridin-3-yl)-3,5-bis(pyrazol-1-ylmethyl)phenyl], 42

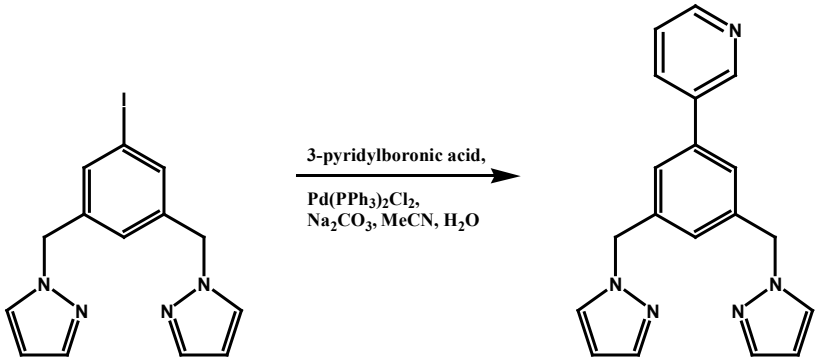

MeCN (15mL) and water (15mL) were added to a round bottom flask and nitrogen bubbled through the solution for 10 minutes. To this, **41** (0.390g, 1.07mmol), 3-pyridylboronic acid (0.189g, 1.54mmol), Na_2CO_3 (0.246g, 2.32mmol) and $PdCl_2(PPh_3)_2$ (0.0186g, 0.0265mmol) were added and the solution stirred at 75°C for 48 hours. Upon completion, the solution was diluted with ethyl acetate and washed with water (3x50mL) and $NaCl_{(aq)}$ (50mL). The ethyl acetate layer was separated, dried over $MgSO_4$ and reduced to a brown oil. The residue was purified by column chromatography (hexanes → hexanes:ethyl acetate; 1:1), to yield **42** as a yellow solid, (0.217g, 64.4%). Mp: 40-43°C. ^{1}H NMR (δ_H; 200MHz, $CDCl_3$): 5.36 (s, 4H), 6.29 (t, *J* = 2.2Hz, 2H), 7.07 (s, 1H), 7.29 (s, 2H), 7.35 (dd, J^1 = 4.4Hz, J^2 = 2.4Hz, 1H), 7.44 (d, *J* = 2.2Hz, 2H), 7.56 (d, *J* = 2.2Hz, 2H), 7.79 (dt, J^1 = 8.2Hz, J^2 = 2.0Hz, 1H), 8.56 (d, *J* = 4.8Hz, 1H), 8.74 (d, *J* = 1.8Hz, 1H), Figure B.42a; ^{13}C NMR, (δ_C; 50MHz, $CDCl_3$): 55.33, 106.22, 123.73, 125.79, 126.26, 129.57, 134.84, 135.85, 138.45, 138.76, 139.82, 147.61, 148.23, Figure B.42b.

7.2.1.20 Synthesis of chloro[4-(pyridin-3-yl)-2,6-bis[(pyrazol-1-yl-αN2methyl)phenyl-αC]-palladium(II)], 43

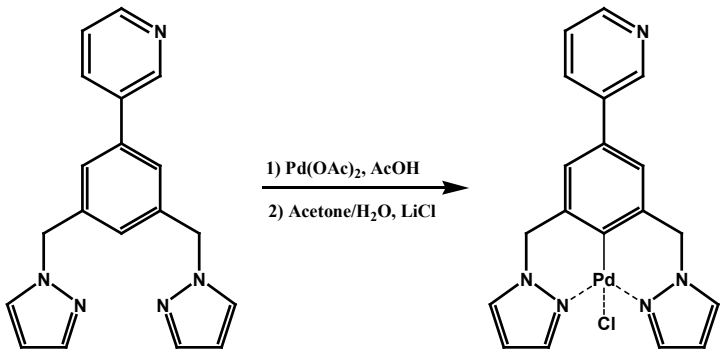

To a round bottom flask, **42** (0.031g, 0.099mmol), $Pd(OAc)_2$ (0.027g, 0.12mmol) and acetic acid (5mL) were added and stirred at reflux for 2 days. Upon completion, the solution was reduced under vacuum to give a brown solid. The solid was redissolved in acetone/water (3mL/2mL) and stirred in the presence of LiCl (0.025g, 0.59mmol) at room temperature for 2 days. Upon completion, the solution was filtered to yield **43** as a brown solid (0.045g, 100%). Mp: >300°C. ^{1}H NMR (δ_H; 200MHz, $CDCl_3$): 5.55 (s, 4H), 6.47 (s, 2H), 7.50 (s, 3H), 7.94 (s, 2H), 8.06 (d, 8Hz, 1H), 8.20 (s, 2H), 8.58 (s, 1H), 8.88 (s, 1H), Figure B.43.

7.2.1.21 Synthesis of 1-[3,5-bis(pyrazol-1-ylmethyl)phenyl]-2-[pyridin-3-yl]ethyne cobalt(II) dichloride, 31a

20 (0.025mg, 0.074mmol) and $CoCl_2$ (0.0060mg, 0.025mmol) were added to a beaker and dissolved in acetonitrile. Blue plates suitable for X-ray diffraction were obtained after a few days. Mp: >300°C. IR (KBr pellet): υ 3112, 2919, 2217, 1627, 1414, 1275, 1070, 765.

7.2.1.22 Synthesis of 1-[3,5-bis(pyrazol-1-ylmethyl)phenyl]-2-[2-aminopyridin-5-yl]ethyne silver(I) hexafluorophosphate, 33a

22 (0.010g, 0.028mmol) and $AgPF_6$ (0.0071mg, 0.028mmol) were added to a beaker and dissolved in acetonitrile. Colourless rods suitable for X-ray diffraction were obtained after a few days. Mp: 245-248°C (dec). IR (KBr pellet): υ 3426, 3192, 2914, 2213, 1634, 1511, 1296, 1137, 840.

7.3 Results

All hydrogen-bond geometries for **33** are listed in Table 7.1. A summary of the crystallographic information for each compound is displayed in Tables A35-A37.

Table 7.1 Hydrogen-bond geometries for **33**.

Compound	D-H···A	D-H / Å	H···A / Å	D···A / Å	<(DHA) / °
33[i]	N(36)-H(36A)...N(31)#1	0.945(18)	2.047(18)	2.9875(16)	173.1(14)
	N(36)-H(36B)...N(52)#2	0.901(18)	2.335(17)	3.0192(16)	132.8(14)

(i) #1 -x,-y,-z+2, #2 -x+1,-y,-z+1.

7.3.1 Crystal structure of 1-[3,5-bis(pyrazol-1-ylmethyl)phenyl]-2-[2-aminopyridin-5-yl]ethyne, 33

The crystal structure of **33** shows two symmetry related N-H···N hydrogen bonds (3.0192(16) Å) between the *anti* hydrogen atom of the amino group and the pyrazole nitrogen atom resulting in a $R_2^2(28)$ motif, Figure 7.6. The homomeric aminopyridine $R_2^2(8)$ dimer also forms via two symmetry related N-H···N hydrogen bonds (2.9875(16) Å) which extends the network.

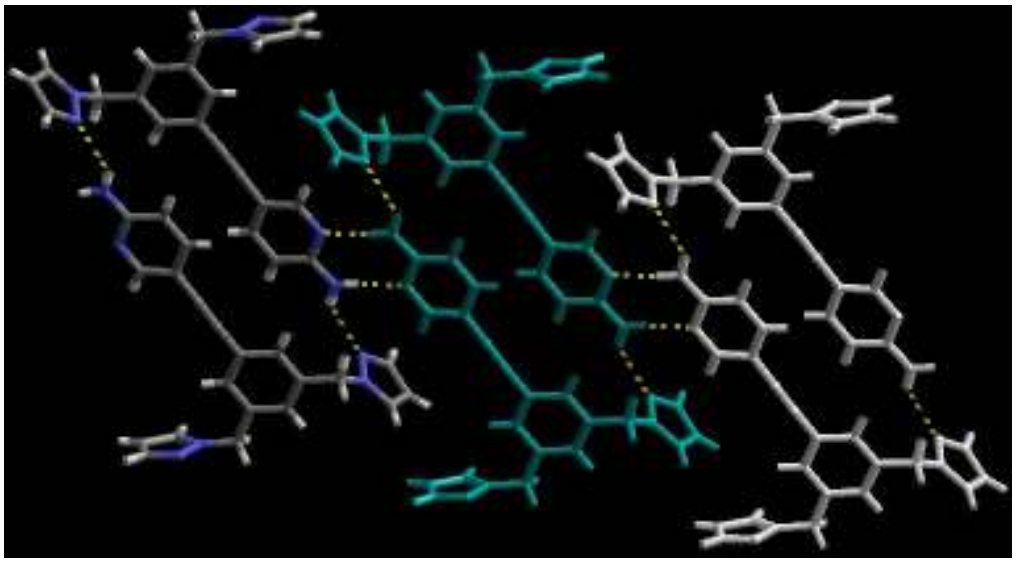

Figure 7.6 Section of the extended network observed in the crystal structure of **33** via N-H···N hydrogen bonds ($R_2^2(28)$ motifs are highlighted).

7.3.2 Crystal structure of [1-[3,5-bis(pyrazol-1-ylmethyl)phenyl]-2-[pyridin-3-yl]ethyne]cobalt(II) dichloride, 31a

The complex ion in the crystal structure of **31a** has a combination of both pyrazole N and pyridine N coordination to two symmetry related tetrahedral cobalt(II) ions (Co-N, 2.033(3) Å and 2.022(3) Å respectively). Coordination from two 1-[3,5-bis(pyrazol-1-ylmethyl)phenyl]-2-[pyridin-3-yl]ethyne ligands, **31**, results in a metallacycle with a Co•••Co distance of approximately 11.5 Å, Figure 7.7. The two remaining sites on the cobalt ion are occupied by chloride ions (Co-Cl, 2.2253(14) Å and 2.2468(12) Å, respectively).

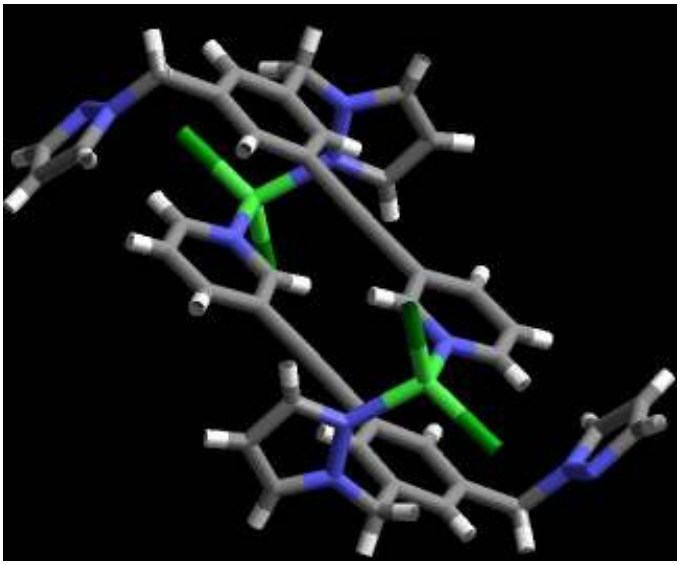

Figure 7.7 Metallacycle observed in the crystal structure of **31a**.

7.3.3 Crystal structure of [1-[3,5-bis(pyrazol-1-ylmethyl)phenyl]-2-[2-aminopyridin-5-yl]ethyne]silver(I) hexafluorophosphate, 33a

The complex ion in the crystal structure of **33a** has a combination of both pyrazole N and pyridine N coordination to two symmetry related tetrahedral silver(I) ions (Ag-N, 2.331(8) Å and 2.273(7) Å respectively). Coordination from two 1-[3,5-bis(pyrazol-1-ylmethyl)phenyl]-2-[2-aminopyridin-5-yl]ethyne ligands, **33**, results in a metallacycle with an Ag•••Ag distance of approximately 11.5 Å, Figure. 7.8. The two remaining sites on the silver ion are occupied by an acetonitrile solvent molecule (Ag-N, 2.474(11) Å) and a pyrazole N from a third 1-[3,5-bis(pyrazol-1-ylmethyl)phenyl]-2-[2-aminopyridin-5-yl]ethyne, **33**, ligand (Ag-N, 2.306(7) Å) which results in a 1D chain of metallacycles.

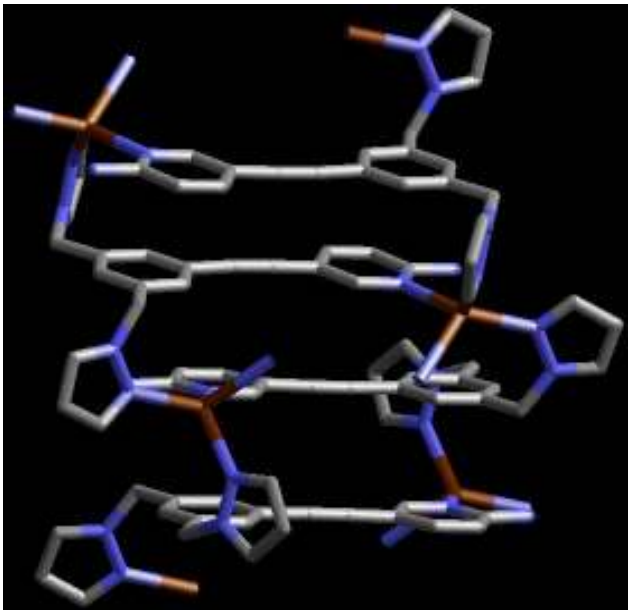

Figure 7.8 Extended metallacycle observed in the crystal structure of **33a** (hydrogen atoms and acetonitrile molecules have been removed for clarity).

7.4 Discussion

7.4.1 Assessing 1,3-bis-benzylpyrazole as a potential chelating ligand

In the two coordination complexes presented, a metallacycle is formed between two tetrahedral metal ions and two bis-pyrazole ligands, Figure 7.9a. The observed cyclic arrangement is consistent with the structure observed for ligand **33**, Figure 7.9b.

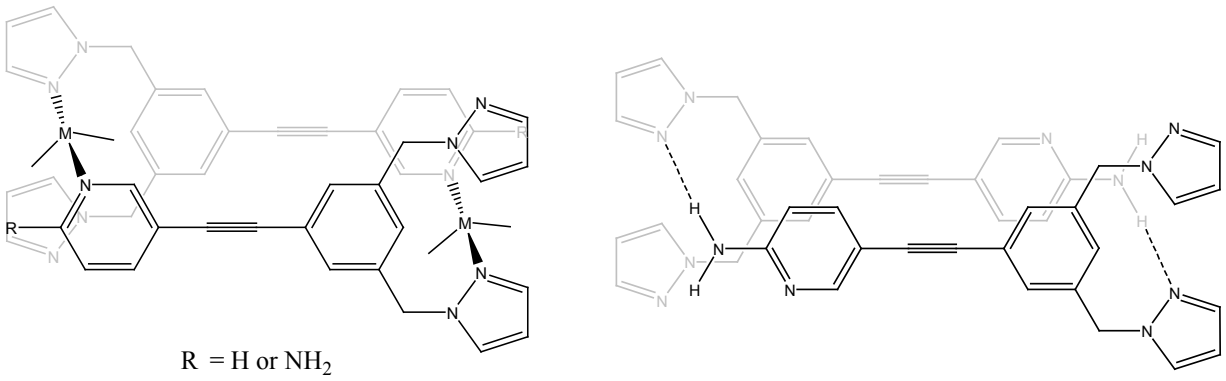

Figure 7.9 (a) Metallacycle observed in the crystal structures of **31a** and **33a**; (b) $R_2^2(28)$ motif observed in the crystal structure of **33**.

The coordination complexes **31a** and **33a** show that 1,3-bis-benzylpyrazole based species cannot act as chelating ligands in coordination complexes, which is supported by the coordination polymers previously constructed.[5] The metallacycle products observed are attributed to (i) the competitive coordination of the pyridyl moiety and (ii) the steric bulk of the aromatic C(4)-H group located between the methylene bridges, which forces the pyrazole arms into an anti-parallel fashion, Figure 7.10.

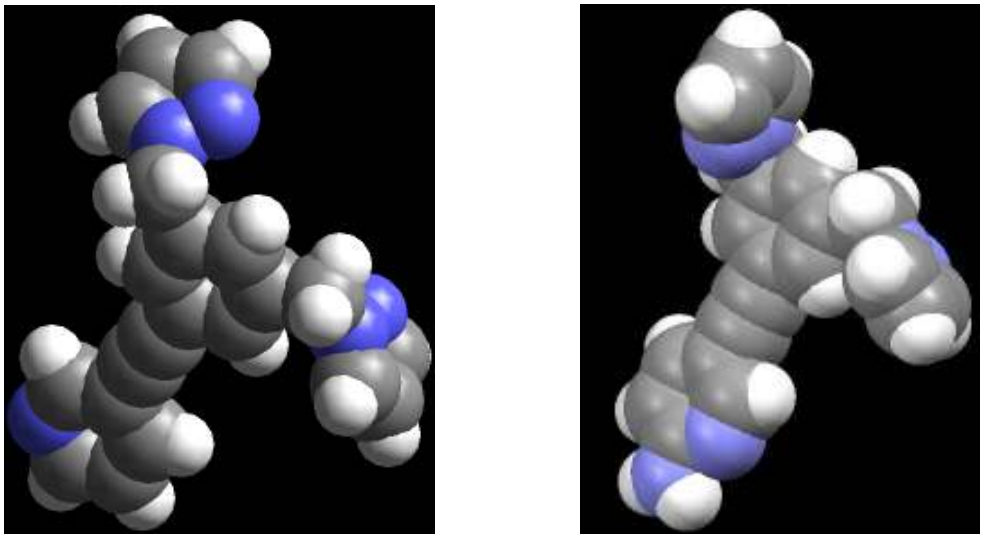

(a) (b)

Figure 7.10 Steric bulk of aromatic C-H group; (a) ligand 31 from crystal structure of **31a** and (b) ligand **33** observed in crystal structure.

When compared to the structurally similar 2,6-bis[(pyrazol-1-yl)methyl]pyridine,[7] it is clear the C(4)-H group plays a major role in controlling coordination complexes with 2,6-bis[(pyrazol-1-yl)methyl]pyridine able to act as a chelating ligand and 1,3-bis-benzylpyrazole not, Figure 7.11.

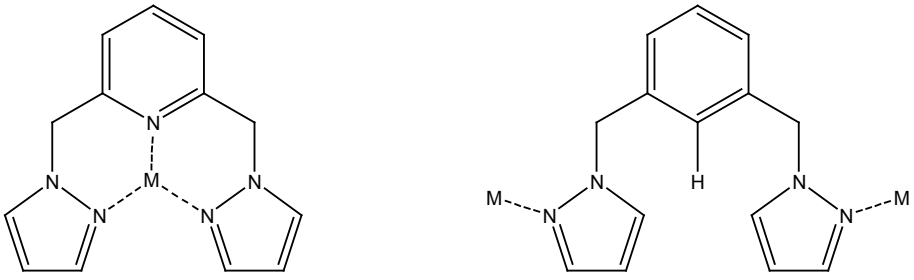

(a) (b)

Figure 7.11 2,6-bis[(pyrazol-1-yl)methyl]pyridine (a) compared to 1,3-bis-benzylpyrazole (b).

7.4.2 'Locking' the 1,3-bis-benzylpyrazole arms

In order to utilise 1,3-bis-benzylpyrazole as a chelating ligand, the pyrazole arms were locked into place by formation of the organometallic product.

However, in ligands containing an ethynyl spacer, the desired organometallic product was not formed, due to coordination of the ethynyl group, Figure 7.12.

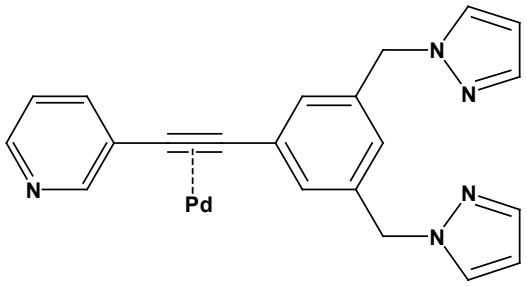

Figure 7.12 Undesirable side product of organometallic reaction.

Consequently, ligand **42** was designed and synthesised, which removed the competition of the ethynyl group allowing for successful M-C bond formation while retaining the pyridyl coordination site, Figure 7.13.

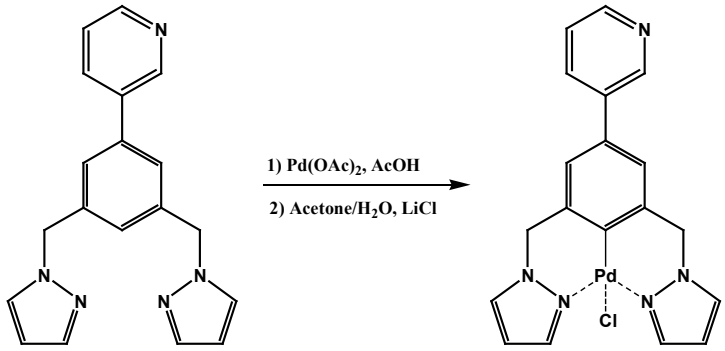

42 **43**

Figure 7.13 Formation of the 'locked' chelate organometallic system.

Analysis of the ^{1}H NMR spectra of **42** and **43** confirms the formation of the organometallic species due to the disappearance of the C(4)-H peak at 7.07ppm, Figure 7.14. Also, minimal shifts in the pyridyl protons at 8.56 and 8.74ppm confirm that the pyridine is not coordinating to the palladium.

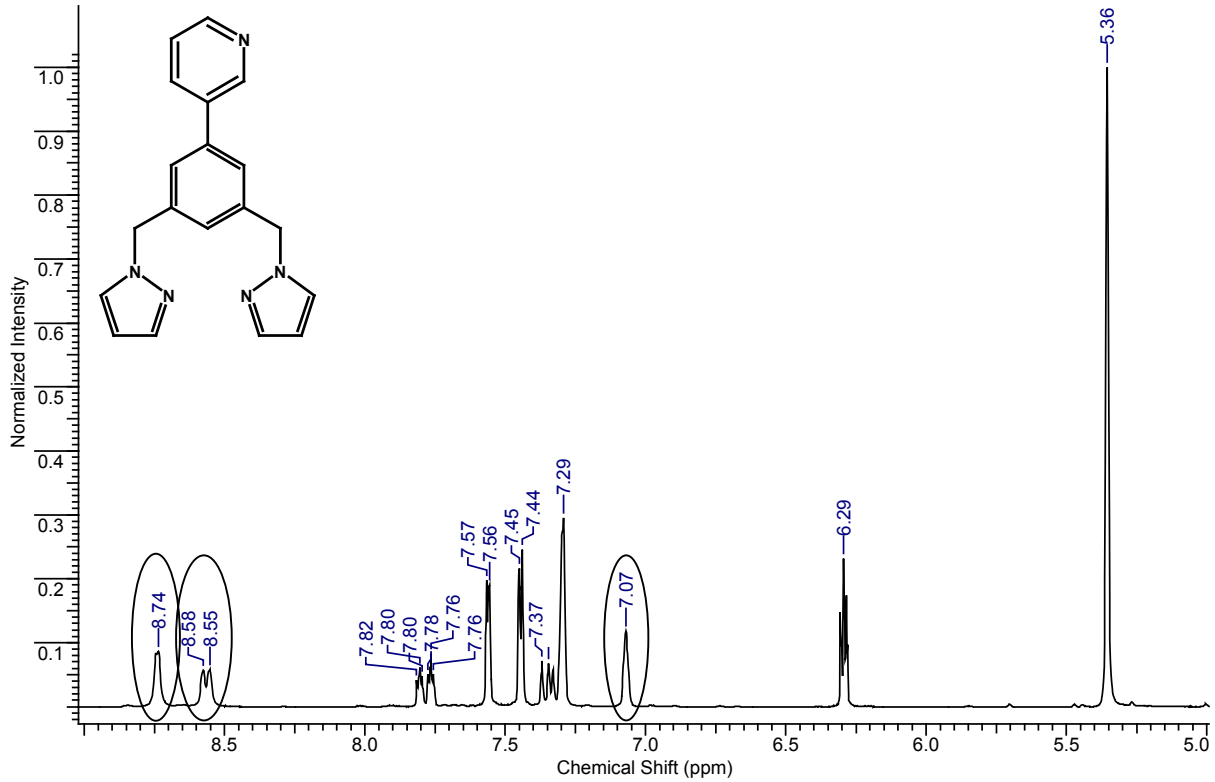

(a)

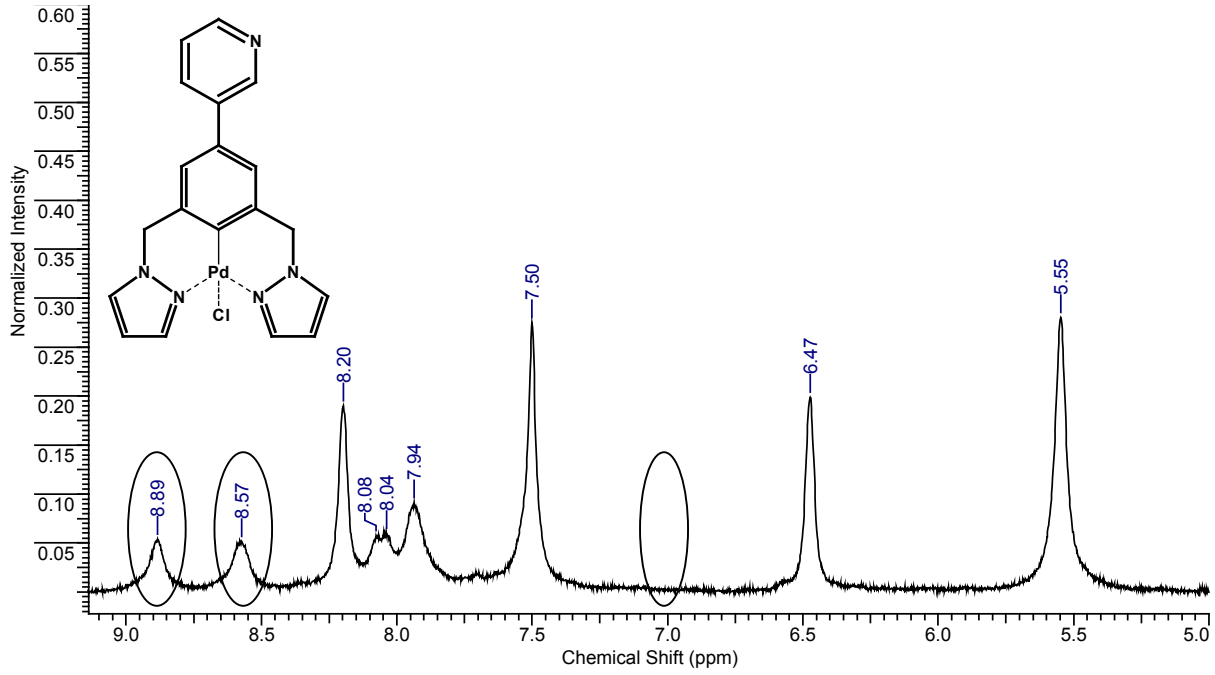

(b)

Figure 7.14 ^{1}H NMR spectra of (a) **42** and (b) **43**.

Structural analysis of two coordination complexes **31a** and **33a** and NMR analysis of **43** paired with previous studies of bis-benzylpyrazole ligands have provided an answer to the question addressed at the beginning of this chapter.

I. Can functionalised 1,3-bis-benzylpyrazole ligands be employed as chelating ligands?

1,3-Bis-benzylpyrazole does not act as chelating ligand in coordination complexes due to steric hindrance from C(4)-H. In cases when no second metal coordination site is present[5] the product of the reaction with a metal ion is a coordination polymer, Figure 7.14a, however it seems when a second coordination site is available (i.e. a pyridyl functionality) the most favorable arrangement is a metallacycle, Figure 7.14b.

1,3-Bis-benzylpyrazole is successfully employed as a chelating ligand by forming the neutral organometallic species,[6] Figure 7.14c. By forming a Pd-C, the steric interference of the C(4)-H group is removed and the pyrazole arms are locked into position, leaving the second coordination site free.

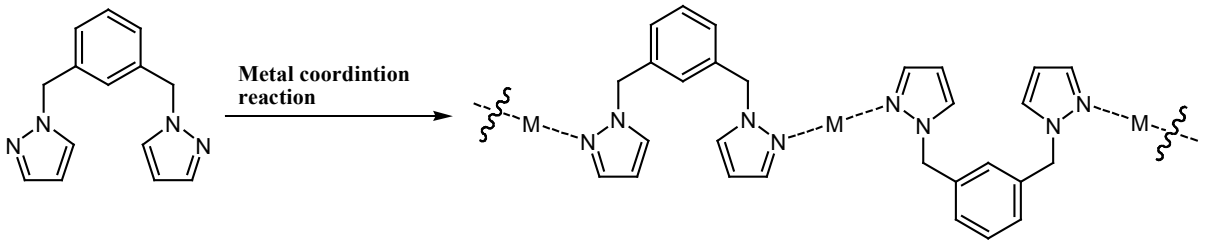

(a)

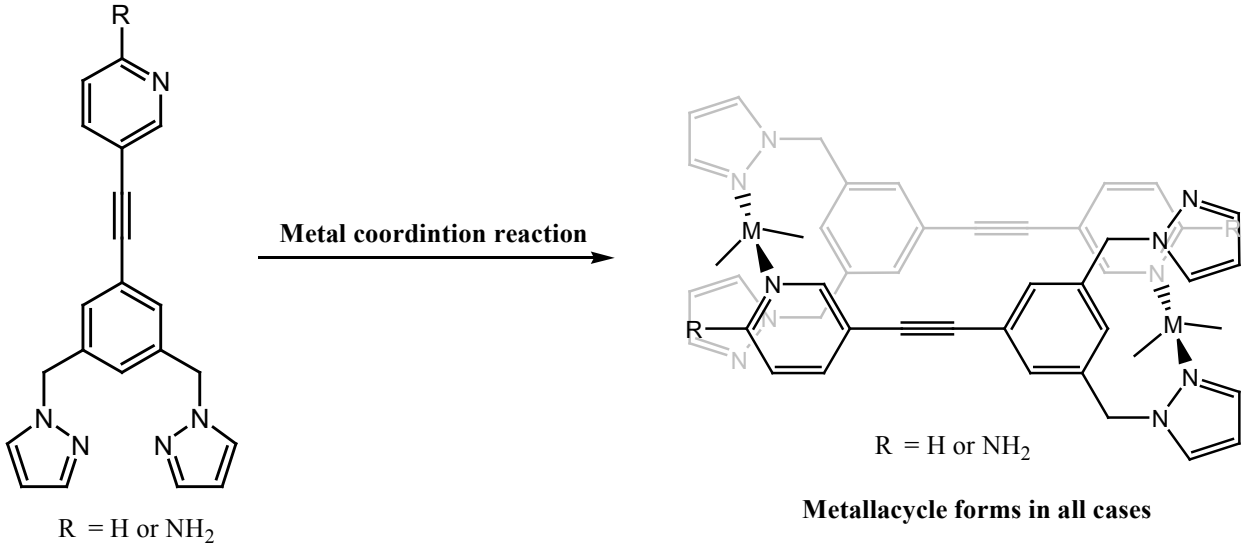

(b)

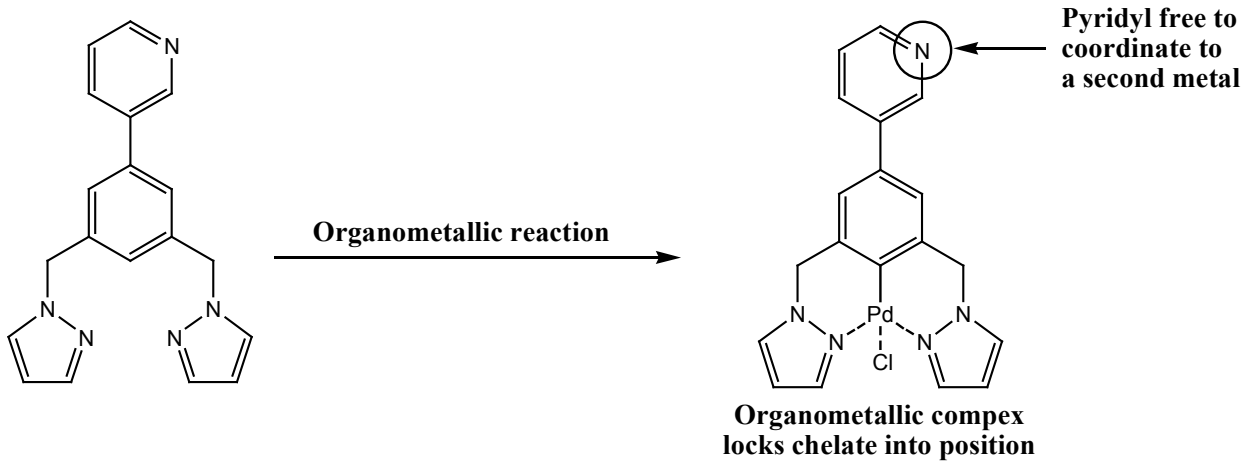

(c)

Figure 7.15 1,3-Bis-benzylpyrazole based ligands in (a) coordination polymers, (b) coordination complexes and (c) organometallic species.

References

1. A search in Sci-Finder of the term "chelate" gave 51995 hits. Some elegant examples of chelating ligands: (a) M. Fujita, J. Yazaki and K. Ogura, *J. Am. Chem. Soc.*, 1990, **112**, 5645; (b) M. Fujita, D. Oguro, M. Miyazawa, H. Oka, K. Yamaguchi, and K. Ogura, *Nature*, 1995, **378**, 469; (c) J. A. Casares, P. Espinet, K. Soulantica, I. Pascual and G. A. Orpen, *Inorg. Chem.*, 1997, **36**, 5251; (d) M. Chas, D. Abella, V. Blanco, E. Pia, G. Blanco, A. Fernandez, C. Plata-Iglesias, C. Peinador and J. M. Carlos, *Chem.-Eur. J.*, 2007, **13**, 8572; (e) V. Carlos, M. Chas, D. Abella, C. Peinador, J. M. Quintela, *J. Am. Chem. Soc*., 2007, **129**, 13978; (f) M. Yoshizawa, M. Tamura and M. Fujita, *Angew. Chem. Int. Ed.*, 2007, **46**, 3874; (g) Y. Nishioka, T. Yamaguchi, M. Yoshizawa and M. Fujita, *J. Am. Chem. Soc.*, 2007, **129**, 7000; (h) T. M. Fyles and C. C. Tong, *New J. Chem.*, 2007, **31**, 655; (i) D. K. Chand, K. Birhada, M. Kawano, S. Sakamoto, Y. Shigeru, K. Yamaguchi and M. Fujita, *Chem. Asian J.*, 2006, 1, 82; (j) R. Mukherjee, *Coord. Chem. Rev.*, 2000, **203**, 151 and references therein; (k) M. Heller and U. S. Schubert, *Eur. J. Org. Chem.*, 2003, 947 and references therein; (l) J. I. van der Vlugt, S. Demeshko, S. Dechert and F. Meyer, *Inorg. Chem.*, 2008, **47**, 1576; (m) S. Vargas-Matinez, S. Ortega-Hernandez, R. A. Toscano, D. Salazar-Mendoza and J. Valdés-Martínez, *CrystEngComm.*, 2008, 10, 86; (n) J. P. Sauvage and C. O. Dietrick-Buchecker, *Chem. Rev.*, 1987, **87**, 795; (o) J. P. Sauvage, *Acc. Chem. Res.*, 1998, **31**, 611; (p) M. Fujita, M. Aoyagi, F. Ibukuro, K. Ogura and K. Yamaguchi, *J. Am. Chem. Soc.*, 1998, **120**, 611.
2. (a) R. E. Marsh, M. Kapon, S. Hu, F. H. Herbstein, *Acta Crystallogr., Sect.B*, 2002, **58**, 62; (b) J. A. Smith, J. –R. Galan-Mascaros, R. Clerac, J. –S. Sun, X. Ouyang, K. R. Dunbar, *Polyhedron*, 2001, **20**, 1727; (c) Y. Rodriguez-Martin, J. Gonzalez-Platas, C. Ruiz-Perez, *Acta Crystallogr., Sect.C*, 1999, **55**, 1087; (d) D. J. Chesnut, R. C. Haushalter, J. Zubieta, *Inorg. Chim. Acta*, 1999, **292**, 41; (e) Z. Qin, M. C. Jennings, R. J. Puddephatt, *Inorg. Chem.*, 2001, **40**, 6220; (f) M. Yoshizawa, T. Kusukawa, M. Kawano, T. Ohhara, I. Tanaka, K. Kurihara, N. Niimura, M. Fujita, *J. Am. Chem. Soc.*, 2005, **127**, 2798; (g) J. A. R. Navarro, M. A. Romero and J. M. Salas, *J. Chem. Soc., Dalton Trans.*, 1997, 1001; (h) J. A. R. Navarro, M. A. Romero, J. M. Salas and M. Quiros, *Inorg. Chem.*, 1997, **36**, 3277.

3. (a) K. Uehara, S. Hikichi, A. Inagaki, M. Akita, *Chem.-Eur. J.*, 2005, **11**, 2788; (b) J. Campora, P. Palma, D. del Rio, J. A. Lopez, P. Valerga, *Chem.Commun.*, 2004, 1490; (c) A. J. Canty, H. Jin, A. S. Roberts, B. W. Skelton, P. R. Traill, A. H. White, *Organometallics*, 1995, **14**, 199; (d) M. A. Halcrow, L. M. L. Chia, X. Liu, E. J. L. McInnes, L. J. Yellowlees, F. E. Mabbs, I. J. Scowen, M. McPartlin, J. E. Davies, *J. Chem. Soc., Dalton Trans.*, 1999, 1753; (e) C. A. Kilner, E. J. L.McInnes, M. A. Leech, G. S. Beddard, J. A. K. Howard, F. E. Mabbs, D. Collison, A. J. Bridgeman, M. A. Halcrow, *Dalton Trans.*, 2004, 236; (f) K. Uehara, S. Hikichi, M. Akita, *J. Chem. Soc., Dalton Trans.*, 2002, 3529.
4. For a discussion on *acac* chelating ligands, see Chapter 6 and (a) C. B. Aakeröy; J. Desper and J. Valdés-Martínez, *CrystEngComm.*, 2004, **6**, 413; (b) J. K. Bera, T. –T. Vo, R. A. Walton and K. R. Dunbar, *Polyhedra*, 2003, **22**, 3009; (c) C. B. Aakeröy, N. Schultheiss and J. Desper, *Inorg. Chem.*, 2005, **44**, 4983;
5. (a) R. Gupta and R. Mukherjee, *Polyhedron*, 2000, **19**, 719; (b) V. Balamurugan and R. Mukherjee, *Inorg. Chimica Acta*, 2006, **359**, 1376.
6. (a) H. P. Dijkstra, M. D. Meijer, J. Patel, R. Kreiter, G. P. M. van Klink, M. Lutz, A. L. Spek, A. J. Canty and G. van Koten, *Organometallics*, 2001, **20**, 3159; (b) A. J. Canty, J. Patel, B. W. Skelton and A. H. White, *J. Organomet. Chem*, 2000, **607**, 194; (c) A. J. Canty, J. Patel, B. W. Skelton and A. H. White, *J. Organomet. Chem*, 2000, **599**, 194; (d) C. M. Hartshorn and P. J. Steel, *Organometallics*, 1998, **17**, 3487; (e) A. J. Canty, R. T. Honeyman, B. W. Skelton and A. H. White, *J. Organomet. Chem*, 1990, **389**, 277.
7. (a) D. L. Reger, R. F. Semeniuc and M. D. Smith, *Cryst. Growth Des.*, 2005, **5**, 1181; (b) P. Manikandan, M. Subramoni, B. Varghese and P. T. Manoharan, *J. Chem. Soc. Dalton Trans.*, 1998, 3219; (c) Z. Shirin, R. Mukherjee, J. F. Richardson and R. M. Buchanan, *J. Chem. Soc. Dalton Trans.*, 1994, 465; (d) S. Mahapatra and R. Mukherjee, *J. Chem. Soc. Dalton Trans.*, 1992, 2337.
8. S. F. Vasilevsky, S. V. Klyatskaya, E. V. Tretyakov and J. Elguero, *Heterocycles*, 2003, **60**, 879.

CHAPTER 8 - Using Supramolecular Synthons to Construct Bimetallic Nanoparticle Assemblies

8.1 Introduction

We have previously shown that supramolecular synthons[1] can be used to construct discrete two or three component co-crystals[2] and 1-D inorganic-organic chains,[3] even in the presence of potentially disruptive forces. It is pertinent however to test the influence of supramolecular synthons further, by studying the effect of incorporating hydrogen-bond functionalities onto larger architectures.

Nanoparticles, which are substantially larger, Figure 8.1, provide a suitable system for such a study.

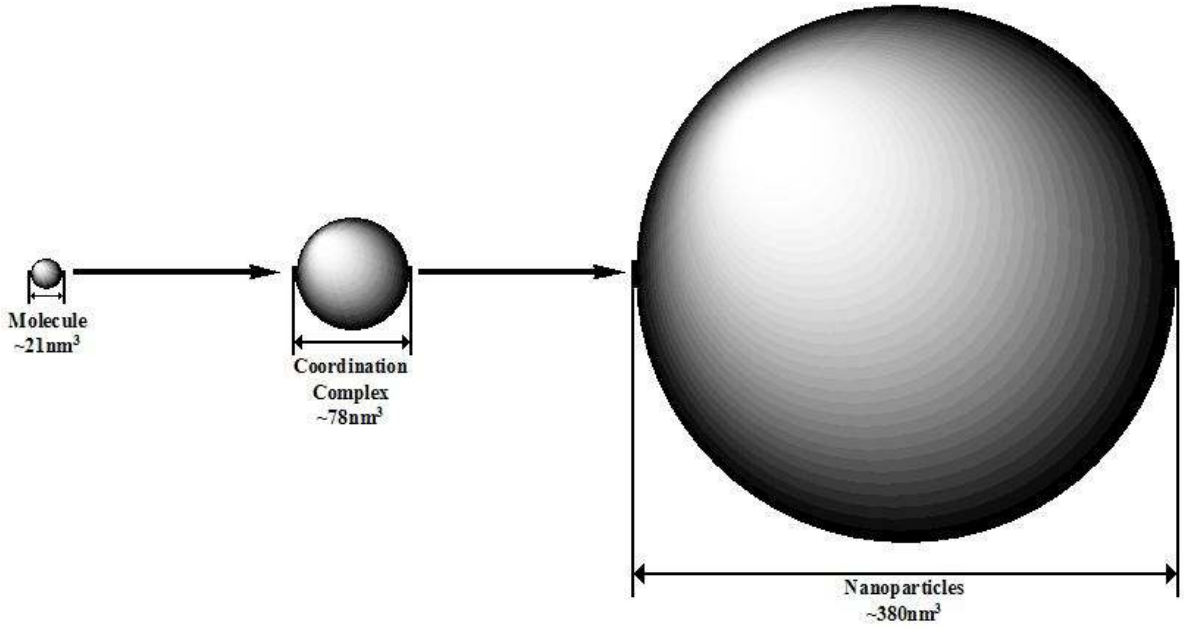

Figure 8.1 Relative volumes of nanoparticles compared to molecules and coordination complexes (the volume for coordination complexes is taken as one repeat unit in the 1-D chain).

One of the first known examples of nanoparticles is in the Lycurgus cup. Made in ~4th century AD[4] from dichroic glass, containing colloidal gold, the cup appears red in transmitted light and green in reflected light. Colloidal gold was first reported in 1618 by Antoli,[5] however

it was over 200 years later in 1857 when Faraday[6] first described the reduction of ionic gold to give particles *"very minute in their dimensions"*,[6] which, when diffused *"produced a beautiful ruby fluid"*.[6]

Since Faraday's report,[6] nanoparticles (particularly gold nanoparticles) have been studied extensively within materials science[7] due to their inherent physical properties (e.g. catalytic,[8] therapeutic,[9] and optical[10]).

Nanoparticles are stabilised with long chain ligands (~10 carbon atoms) possessing functional groups capable of binding to the metal (e.g. amines and thiols) at one end and (generally) an 'inert' functionality (e.g. methyl group) at the other.[7d, 11] In assemblies of this nature, the nanoparticles can come within close proximity, dictated by interdigitation of the ligands and the van der Waals radii, Figure 8.2a, of the atoms to form an ordered superlattice, Figure 8.2b.[11]

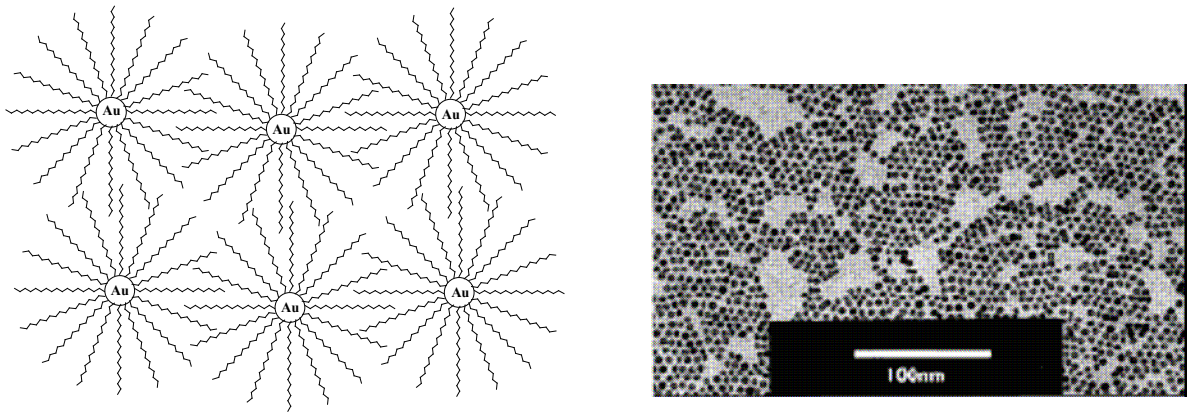

(a) (b)

Figure 8.2 (a) Arrangement of nanoparticles observed in dodecanethiol functionalised gold nanoparticles. Interdigitation of aliphatic chains results in (b) an ordered monodisperse superlattice.[11e]

If however, suitable thio- or amino-based ligands, terminated with functionalities capable of forming reliable and predictable hydrogen bonds, were utilised to "decorate" nanoparticles, the interparticle distance and hence the arrangement of the nanoparticles could be manipulated, Figure 8.3 and consequently, the properties could be tailored. Furthermore, if the complementary ligands are appended to different types of nanoparticles, the construction of bimetallic nanoparticle assemblies is possible.

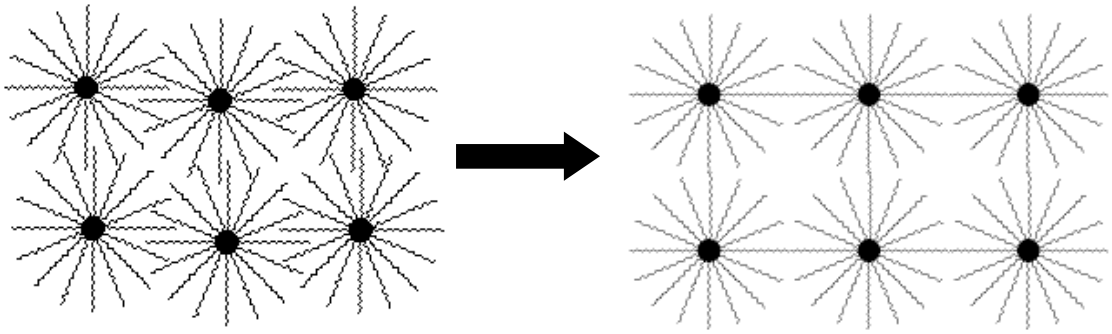

Figure 8.3 From interdigitation to tip-to-tip interactions, the effect of hydrogen bonding on nanoparticle assembly.

Ligands terminated with hydrogen-bonding moieties have been used to functionalise nanoparticles.[12] A good example is 1-(8-11-mercaptooctyl)thymine and 8-(4,6-diamino[1,3,5]triazin-2-yl)octane-1-thiol, Figure 8.4a.[12a] Hydrogen bonding between nanoparticles in this case however is limited due to (i) the potential to form only one type of heteromeric hydrogen-bond motif and (ii) the difficulties surrounding identification of the heteromeric motif versus the homomeric motif, Figure 8.4b.

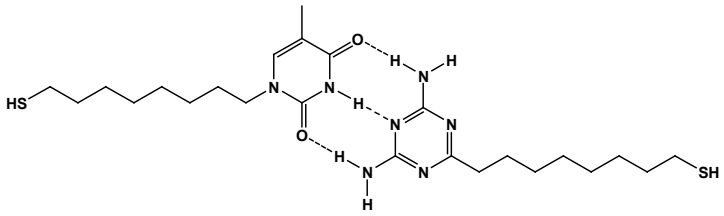

(a)

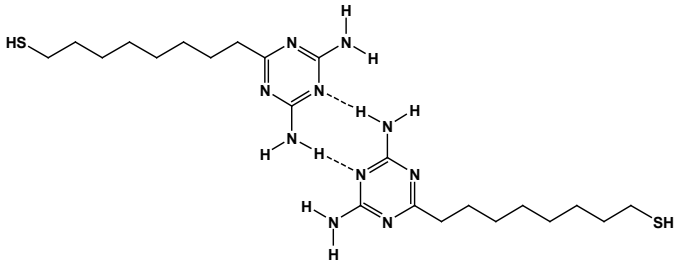

(b)

Figure 8.4 (a) Heteromeric interaction between 1-(8-11-mercaptooctyl)thymine and 8-(4,6-diamino[1,3,5]triazin-2-yl)octane-1-thiol and (b) homomeric interaction between two 4,6-diamino[1,3,5]triazin-2-yl)octane-1-thiol ligands.

With this in mind, a versatile heteromeric synthon needs to be chosen which can be (i) subject to covalent modifications in order to fine-tune hydrogen-bond strength and (ii) identified by a straightforward procedure.

O-H•••N hydrogen bonds are reliable interactions[2, 13] that can be fine-tuned by altering either the strength of the hydrogen-bond acceptor (by changing or modifying the N-heterocycle) or the hydrogen-bond donor (by using different carboxylic acids, alcohols etc.). Also, O-H•••N hydrogen bonds can be identified by infrared (IR) spectroscopy and therefore are an ideal target.

Consequently, suitable ligands should contain:

I. A long (~10 carbon atoms) aliphatic chain anchored with a sulfur functionality (thiol or disulfide)

II. A hydrogen-bond acceptor or donor moiety

Although pyridine is a good hydrogen-bond acceptor, [2a, 2b, 13] imidazole is even better (based on MEP surface calculations[14]), Figure 8.5.

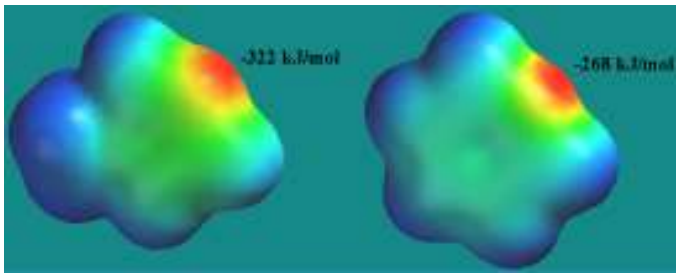

(a) (b)

Figure 8.5 MEP surface calculations of (a) N-methylimidazole and (b) pyridine.

Data in the CSD[15] has shown O-H•••N hydrogen bonds between imidazole and (i) alcohols (11 structures),[16] Figure 8.6a, (ii) carboxylic acids (10 structures),[16c, 17] Figure 8.6b as well as N^{+}-H•••O^{-} interactions between an imidazolium cation and a carboxylate anion (44 structures),[17e, 18] Figure 8.6c.

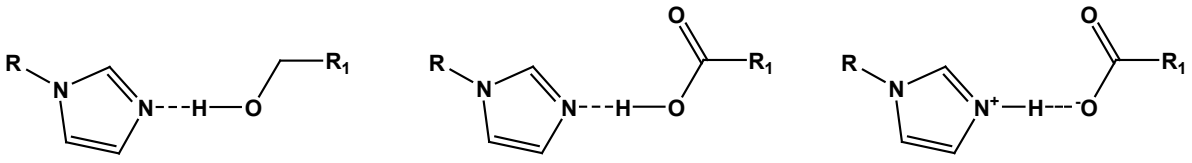

(a) (b) (c)

Figure 8.6 Imidazole as a hydrogen-bond acceptor.

Consequently, an imidazole based disulfide ligand (which is more synthetically viable than an imidazole based thiol), Figure 8.7a, will be synthesised to provide a hydrogen-bond acceptor for 11-mercaptoundecanoic acid, Figure 8.7b and 11-mercaptoundecan-1-ol, Figure 8.7c.

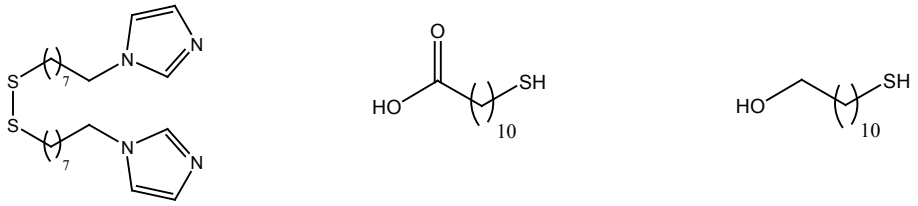

(a) (b) (c)

Figure 8.7 Target ligands; (a) bis(8-imidazol-1-yloctyl)disulfide; (b) 11-mercaptoundecanoic acid and (c) 11-mercaptoundecan-1-ol.

Gold nanoparticles (AuNP's) and silver nanoparticles (AgNP's) will be synthesised via the inverse micelle method.[11a-e] The metal salt is dissolved in a solution of didodecyldimethylammonium bromide (DDAB), reduced with $NaBH_4$ and functionalised with dodecylamine (gold) and dodecanethiol (silver).[19] Ligand exchange will then be performed in order to append the desired, hydrogen-bond functionalised ligands to the nanoparticles, Figure 8.8.

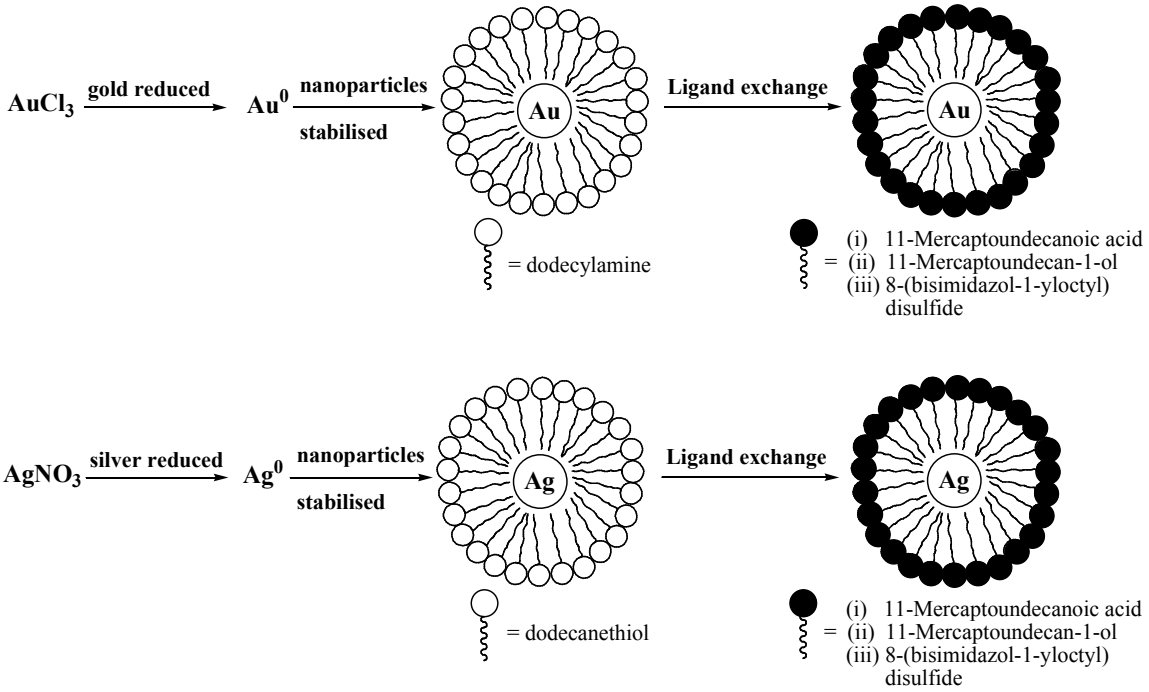

Figure 8.8 Target nanoparticles.

Transmission electron microscopy (TEM) and IR analysis of homomeric and heteromeric nanoparticle assemblies will allow for the following three questions to be answered:

I. Can nanoparticles be synthesised with hydrogen-bond functionalised ligands?

II. Do hydrogen bonds form between nanoparticles?

III. Can supramolecular synthons be used to manipulate nanoparticle assemblies?

8.2 Experimental

8.2.1 Synthesis

All chemicals were purchased from Aldrich and Fischer and used without further purification. Glassware for nanoparticle synthesis was cleaned with (i) soap and water, (ii) aqua regia (3:1 HCl:HNO_3), (iii) conc. H_2SO_4, (iv) KOH base bath and (v) a water rinse followed by oven drying. Melting points were determined on a Fisher-Johns melting point apparatus and are uncorrected. TEM were performed on a Siemens CM100 transmission electron microscope. TEM samples were prepared by placing a drop of the colloidal solution onto a carbon-coated Formvar copper grid. The grids were allowed to dry under ambient conditions (for toluene solutions) and dried using a heat gun for DMSO solutions.

8.2.1.1 Synthesis of 1-bromooctan-8-ol, 44

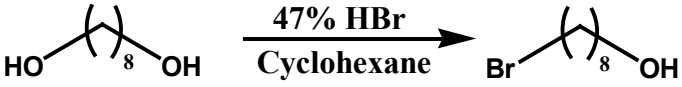

To a round bottom flask, 1,8-octanediol, (5.87g, 40.2mmol) and cyclohexane (106mL) were added. Once in solution, 47% HBr (27mL) was added and the solution stirred at reflux for 6 hours. Upon completion, the reaction mixture was diluted with hexanes and the aqueous layer separated. The organic layer was then washed with $NaHCO_{3(aq)}$ (4 x 50mL) and $NaCl_{(aq)}$ (1 x 50mL), dried over $MgSO_4$ and reduced to a colourless oil, **44**, (5.55g, 66.1%). ^{1}H NMR (δ_H; 200MHz, $CDCl_3$): 1.33-1.47 (m, 8H), 1.55 (quin, J = 6.6Hz, 2H), 1.86 (quin, J = 7.2Hz, 2H), 2.83 (s, 1H), 3.41 (t, J = 6.8Hz, 2H), 3.56 (t, J = 6.6Hz, 2H), Figure B.44.

8.2.1.2 Synthesis of 1-mercaptooctan-8-ol, 45

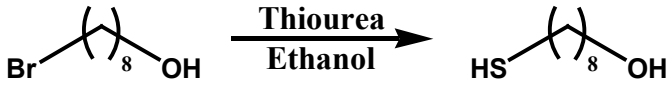

To a round bottom flask, **44** (5.55g, 26.6mmol) and ethanol (150mL) were added. Once in solution, thiourea (4.19g, 55.1mmol) was added and the reaction refluxed for 3 hours, at which point, 10% NaOH (75mL) was added and the reaction refluxed for a further 2 hours. The reaction was then cooled to room temperature and the pH adjusted to 2-3 with 2N HCl. The acidic solution was then washed with dichloromethane (3 x 100mL) and the organic layer separated, dried over $MgSO_4$ and reduced to a white solid/colourless oil, **45**, (4.20g, 97.3%). ^{1}H NMR (δ_H; 200MHz, $CDCl_3$): 1.32-1.40 (m, 8H), 1.52-1.64 (m, 4H), 1.90 (s, 1H), 2.52 (q, J = 3.6Hz, 2H), 3.61 (t, J = 3.2Hz, 2H), Figure B.45.

8.2.1.3 Synthesis of bis(8-hydroxyoctyl)disulfide, 46

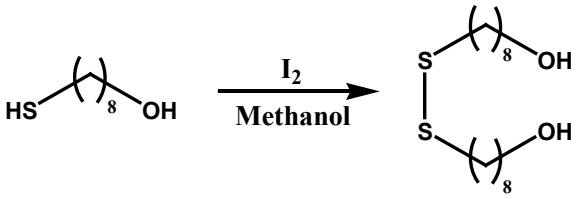

To a round bottom flask, **45**, (2.01g, 12.4mmol) and methanol (10mL) were added. Once in solution, a 0.5M methanolic solution of iodine (~20mL) was added dropwise until the solution remained yellow. The reaction was then quenched with 10% $NaHSO_3$ (50mL) and dichloromethane (50mL). The organic layer was extracted and the aqueous layer was washed with dichloromethane (2 x 50mL). All organic extracts were combined, dried over $MgSO_4$ and reduced to a white solid, **46**, (1.94g, 94.4%). Mp: 32-35^{o}C. ^{1}H NMR (δ_H; 200MHz, $CDCl_3$): 1.34 (s, 16H), 1.54-1.71 (m, 8H), 2.68 (t, J = 7.2Hz, 4H), 3.64 (t, J = 6.6Hz, 4H), Figure B.46.

8.2.1.4 Synthesis of bis(8-bromooctyl)disulfide, 47

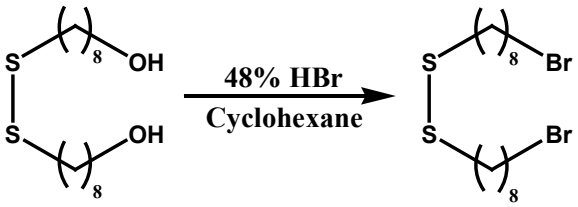

To a round bottom flask, **45** (3.08g, 9.55mmol) and cyclohexane (80mL) were added. Once in solution, 47% HBr (80mL) was added and the reaction refluxed for 24 hours, at which

point a second portion of 47% HBr (80mL) was added and the reaction refluxed for an additional 24 hours. Upon completion, the reaction was diluted with hexanes (100mL) and the aqueous layer extracted. The organic layer was then washed with $NaHCO_{3(aq)}$ (4 x 100mL) and $NaCl_{(aq)}$ (1 x 100mL), separated, dried over $MgSO_4$ and reduced to a yellow liquid, **47**, (3.63g, 84.8%). ^{1}H NMR, (δ_C; 200MHz, $CDCl_3$): 1.32-1.42 (m, 16H), 1.67 (quin, J = 3.6Hz, 4H), 1.85 (quin, J = 3.8Hz, 4H), 2.67 (t, J = 3.6Hz, 4H), 3.39 (t, J = 3.6Hz, 4H), Figure B.47.

8.2.1.5 Synthesis of bis(8-imidazol-1-yloctyl)disulfide, *48*

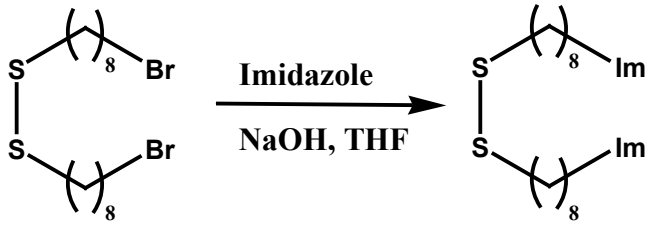

To a round bottom flask, imidazole (1.10g, 16.2mmol) and dry THF (50mL) were added. Once in solution, NaOH pellets (1.62g, 40.5mmol) were added and the reaction stirred for 2 hours. Upon completion, **47** (1.815g, 4.05mmol) in dry THF (50mL) was added and the reaction stirred for 4 days. H_2O was added to dissolve NaBr and excess NaOH pellets and the aqueous layer was saturated with NaCl. The THF layer was extracted, dried over $MgSO_4$ and reduced to a yellow oil. The oil was then dissolved in ethyl acetate (50mL) and washed with 1M NaOH until excess imidazole was removed. The organic layer was extracted, dried over $MgSO_4$ and reduced to a yellow oil, **48**, (0.972g, 56.9%). ^{1}H NMR (δ_H; 200MHz, $CDCl_3$): 1.30-1.43 (m, 16H), 1.58-1.82 (m, 8H), 2.66 (t, J = 7.2Hz, 4H), 3.91 (t, J = 7Hz, 4H), 6.91 (d, J = 1.2Hz, 2H), 7.03 (d, J = 1.2Hz, 2H), 7.45 (s, 2H), Figure B.48a; ^{13}C NMR, (δ_C; 50MHz, $CDCl_3$): 26.32, 28.20, 28.82, 28.90, 28.97, 30.93, 38.80, 46.87, 118.73, 129.06, 136.90, Figure B.48b.

8.2.1.6 Synthesis of dodecylamine functionalised gold nanoparticles, *49*

Didodecyldimethylammonium bromide (DDAB) (1.62g, 3.50mmol) was dissolved in dry toluene (10mL) in a clean, dry, 50ml Erlenmeyer flask. $AuCl_3$ (0.0340g, 0.112mmol) was added to the mixture and the resulting yellow solution was sonicated until $AuCl_3$ was dissolved. The gold ions were then reduced with $NaBH_4$ (0.04ml of a 9.4$M_{(aq)}$ soln.) resulting in a colour change from yellow to deep purple. The purple solution was stirred for a further 15min to ensure complete reduction before being transferred into a clean, dry, 40ml vial. Dodecylamine (0.81g,

4.37mmol) was then added to the vial and shaken vigorously. The purple solution was diluted with absolute ethanol (28mL) and shaken to initiate precipitation. The particles were allowed to settle overnight, the ethanol/toluene mix was carefully removed from the vial using a Pasteur pipette and the particles were dried at room temperature under vacuum for ~1 hour.

8.2.1.7 Ligand exchange of gold nanoparticles, 50-52

The dried particles, **49**, were redissolved in dry toluene (15mL) to give a purple solution. The exchange ligand (11-mercaptoundecanoic acid 0.195g, 0.893mmol; 11-mercaptoundecan-1-ol 0.183g, 0.893mmol; bis(8-imidazol-1-yloctyl)disulfide 0.377g, 0.893mmol) was added to the solution and shaken resulting in immediate precipitation. The particles were allowed to settle and the toluene carefully removed using a Pasteur pipette. The particles were then washed with toluene (2x15mL) followed by dissolution in DMSO via sonication and heating.

8.2.1.8 Synthesis of dodecanethiol functionalised silver nanoparticles, 53

DDAB (1.62g, 3.50mmol) was dissolved in dry toluene (10mL) in a clean, dry, 50ml Erlenmeyer flask. $AgNO_3$ (0.0250g, 0.145mmol) was added and the colourless solution was sonicated to dissolve the $AgNO_3$. The silver ions were then reduced with $NaBH_4$ (0.04ml of 9.4M soln.) resulting in a colour change from colourless to brown. The brown solution was stirred for a further 15min to ensure complete reduction before being transferred into a clean, dry, 40ml vial. Dodecanethiol (0.85g, 4.20mmol) was then added to the vial and shaken vigorously. The brown solution was diluted with absolute ethanol (28mL) and shaken, resulting in precipitation. The particles were centrifuged, the ethanol/toluene mix was decanted and the particles were dried at room temperature under vacuum for ~1 hour.

8.2.1.9 Ligand exchange of silver nanoparticles, 54-55

The dried particles, **53**, were redissolved in dry toluene (15mL) to give a straw coloured solution. The exchange ligand (11-mercaptoundecanoic acid 0.195g, 0.893mmol; 11-mercaptoundecan-1-ol 0.189g, 0.893mmol) was added to the solution and shaken. Precipitation occurred overnight, the particles were allowed to settle and the toluene was carefully removed using a Pasteur pipette. The particles were then washed with toluene (3x15mL) followed by dissolution in DMSO.

8.3 Results

8.3.1 TEM image of dodecylamine functionalised AuNP's

The TEM image of dodecylamine functionalised AuNP's shows a monodisperse superlattice of AuNPs, Figure 8.9. The size of the particles ~8-9nm and the interparticle distance is ~1.5nm.

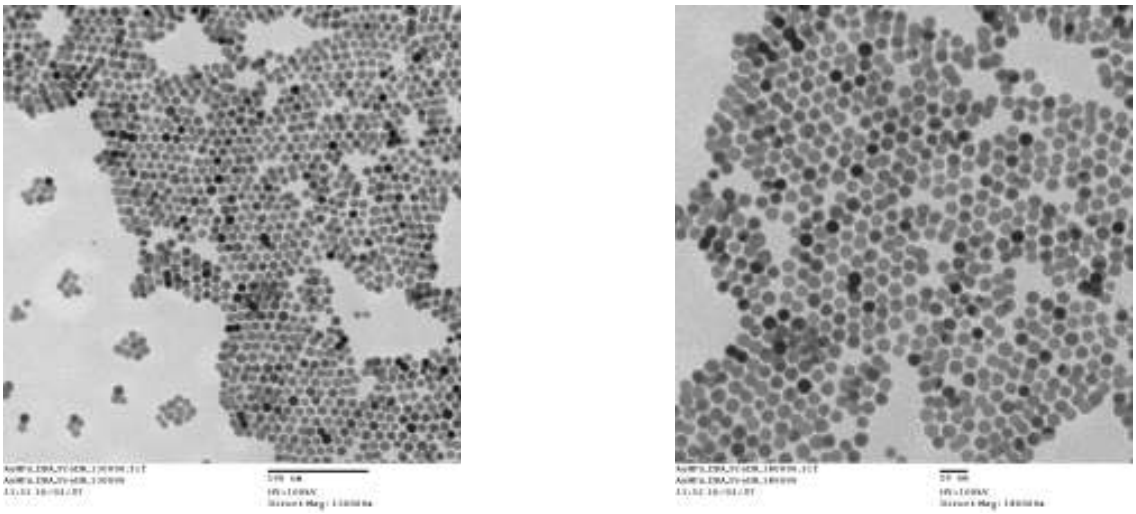

(a) (b)

Figure 8.9 TEM image showing monodisperse dodecylamine functionalised AuNP's; (a) magnification = 130000x; scale = 100nm (b) magnification = 180000x; scale = 20nm.

8.3.2 TEM image of 11-mercaptoundecanoic acid functionalised AuNP's

The TEM image of 11-mercaptoundecanoic acid functionalised gold nanoparticles shows a fractal network of monodisperse nanoparticles ~8-9nm in size, with an interparticle distance of ~3nm, Figure 8.10.

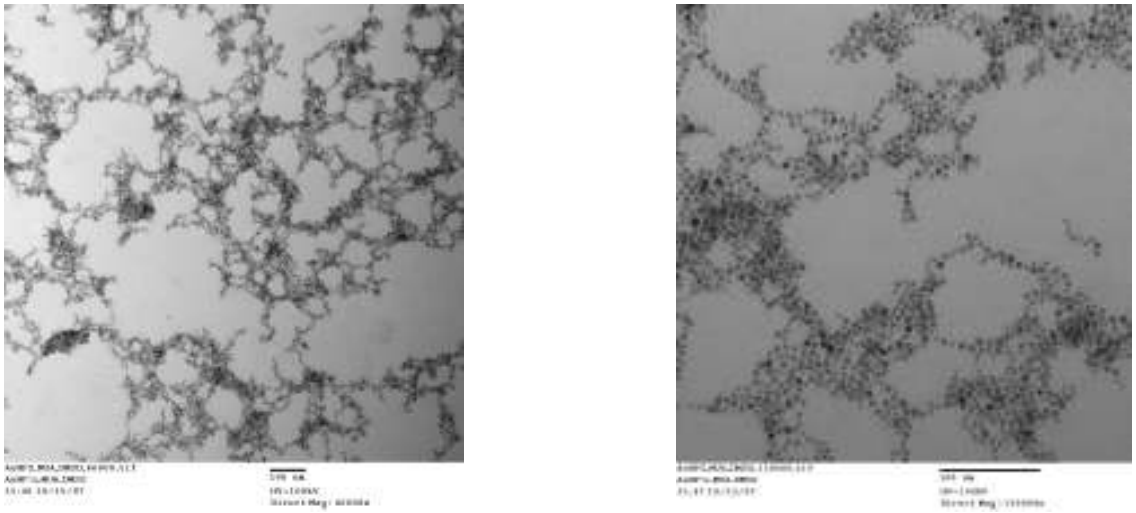

(a) (b)

Figure 8.10 TEM image showing network of monodisperse 11-mercaptoundecanoic acid functionalised AuNP's; (a) magnification = 46000x; scale = 100nm; (b) magnification = 130000x; scale = 100nm.

8.3.3 TEM image of 11-mercaptoundecan-1-ol functionalised AuNP's

The TEM image of 11-mercaptoundecan-1-ol functionalised gold nanoparticles shows monodisperse nanoparticles ~8-9nm in size, with an interparticle distance is ~2.3nm, Figure 8.11.

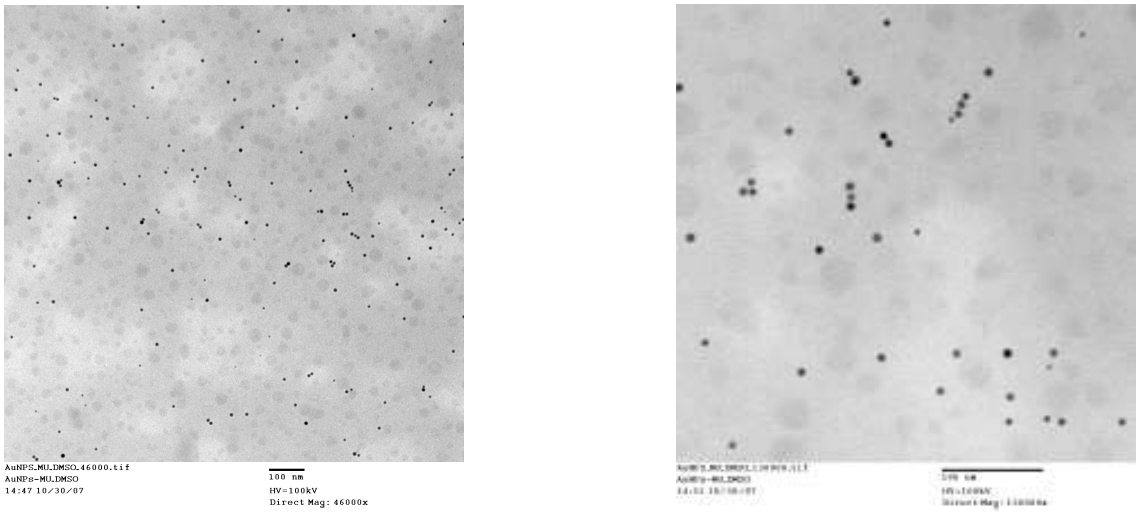

(a) (b)

Figure 8.11 TEM image showing monodisperse 11-mercaptoundecan-1-ol functionalised AuNP's; (a) magnification = 46000x; scale = 100nm; (b) magnification = 130000x; scale = 100nm.

8.3.4 TEM image of bis(8-imidazol-1-yloctyl)disulfide functionalised AuNP's

The TEM image of bis(8-imidazol-1-yloctyl)disulfide functionalised gold nanoparticles shows a monodisperse cluster of nanoparticles ~8-9nm in size with an interparticle distance of ~1.5nm, Figure 8.12.

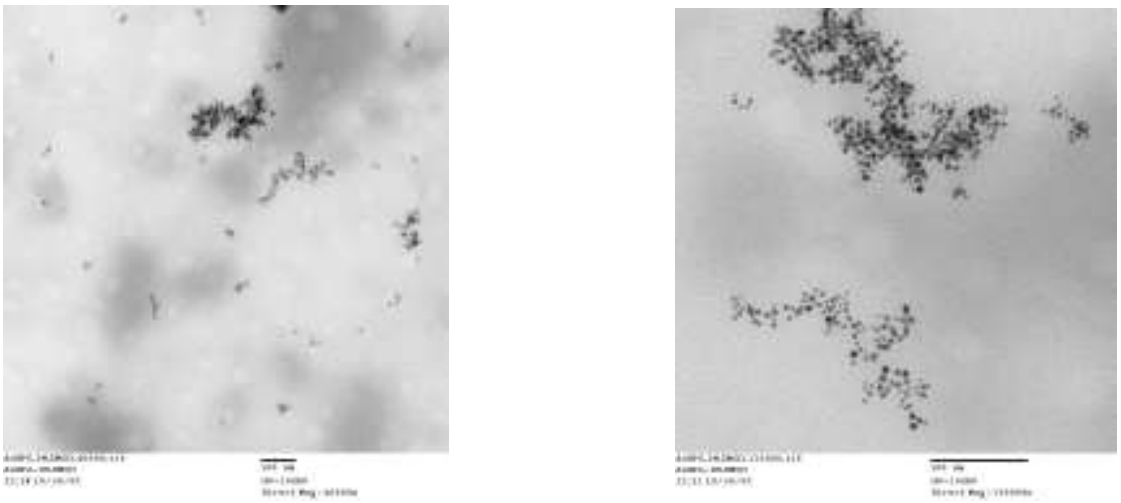

(a) (b)

Figure 8.12 TEM image showing bis(8-imidazol-1-yloctyl)disulfide functionalised AuNP's; (a) magnification = 46000x; scale = 100nm; (b) magnification = 130000x; scale = 100nm.

8.3.5 TEM image of dodecaethiol functionalised AgNP's

The TEM image of dodecanethiol functionalised AgNP's shows monodisperse AgNPs, Figure 8.13. The size of the particles is ~6-7nm and the interparticle distance is ~1.8nm.

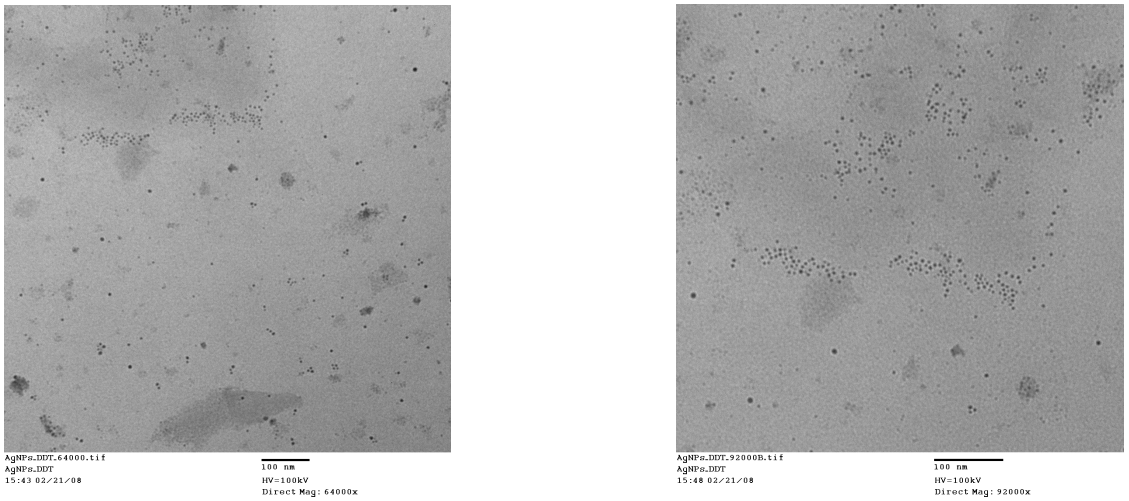

(a) (b)

Figure 8.13 TEM image showing monodisperse dodecanethiol functionalised AgNP's; (a) magnification = 64000x; scale = 100nm; (b) magnification = 92000x; scale = 100nm.

8.3.6 TEM image of 11-mercaptoundecanoic acid functionalised AgNP's

Similar to the TEM image of 11-mercaptoundecanoic acid functionalised gold nanoparticles, silver 11-mercaptoundecanoic acid nanoparticles show a fractal network of monodisperse nanoparticles ~6-7nm in size with an interparticle distance of ~2.4nm, Figure 8.14.

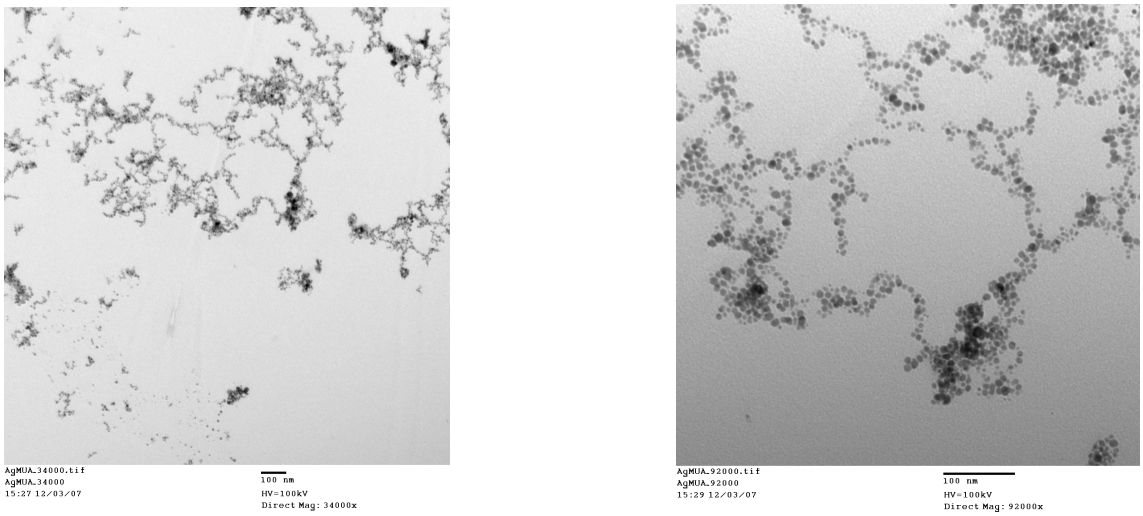

(a) (b)

Figure 8.14 TEM image showing network of monodisperse 11-mercaptoundecanoic acid functionalised AgNP's; (a) magnification = 34000x; scale = 100nm; (b) magnification = 92000x; scale = 100nm.

8.3.7 TEM image of 11-mercaptoundecan-1-ol functionalised AgNP's

Similar to the TEM image of 11-mercaptoundecan-1-ol functionalised gold nanoparticles, the TEM image of silver 11-mercaptoundecan-1-ol nanoparticles shows monodisperse nanoparticles ~6-7nm in size with an interparticle distance of ~2.4nm, Figure 8.15.

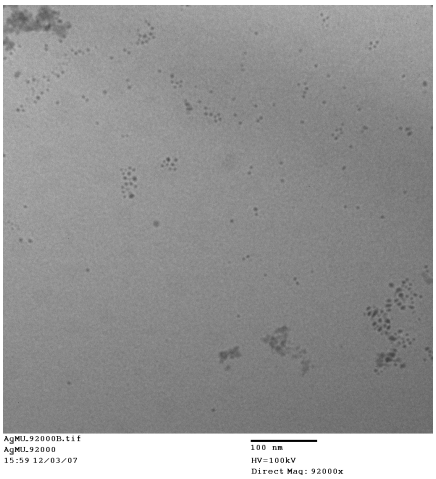

(a)

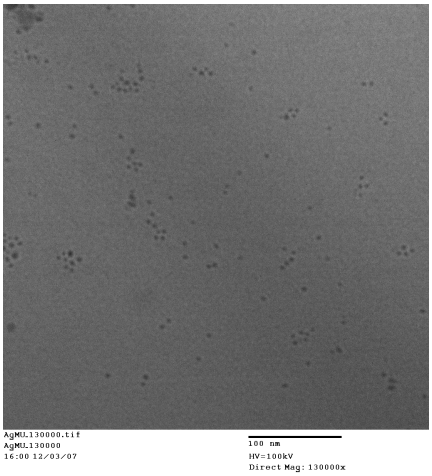

(b)

Figure 8.15 TEM image showing monodisperse 11-mercaptoundecan-1-ol functionalised AgNP's; (a) magnification = 92000x; scale = 100nm; (b) magnification = 130000x; scale = 100nm.

8.3.8 TEM image of 11-mercaptoundecanoic acid functionalised AuNP's + bis(8-imidazol-1-yloctyl)disulfide functionalised AuNP's

Dramatically different from the homomeric nanoparticle assemblies, the TEM image of 11-mercaptoundecanoic acid functionalised gold nanoparticles + bis(8-imidazol-1-yloctyl)disulfide functionalised gold nanoparticles shows a network of monodisperse particles ~8-9nm in size, Figure 8.16.

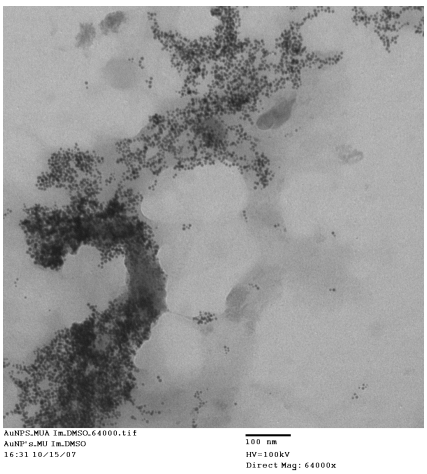

(a)

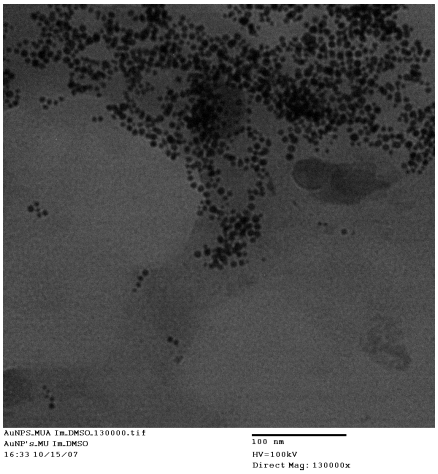

(b)

Figure 8.16 Network of 11-mercaptoundecanoic acid functionalised AuNP's + bis(8-imidazol-1-yloctyl)disulfide functionalised AuNP's observed in the TEM image; (a) magnification = 64000x; scale = 100nm; (b) magnification = 130000x; scale = 100nm.

8.3.9 TEM image of 11-mercaptoundecan-1-ol functionalised AuNP's + bis(8-imidazol-1-yloctyl)disulfide functionalised AuNP's

Significantly different from the homomeric nanoparticle assemblies, the TEM image of 11-mercaptoundecan-1-ol functionalised gold nanoparticles + bis(8-imidazol-1-yloctyl)disulfide functionalised gold nanoparticles shows monodisperse particles ~8-9nm in size forming a dense network, Figure 8.17.

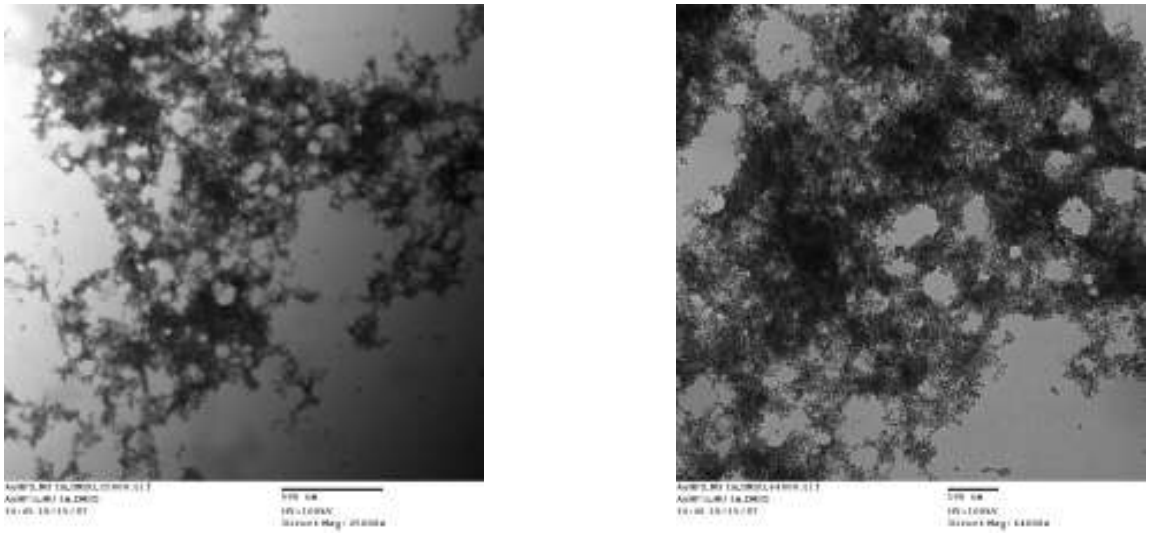

(a) (b)

Figure 8.17 Network of 11-mercaptoundecan-1-ol functionalised AuNP's + bis(8-imidazol-1-yloctyl)disulfide functionalised AuNP's observed in the TEM image; (a) magnification = 25000x; scale = 500nm; (b) magnification = 64000x; scale = 100nm.

8.3.10 TEM image of 11-mercaptoundecanoic acid functionalised AgNP's + bis(8-imidazol-1-yloctyl)disulfide functionalised AuNP's

Dramatically different from the homomeric nanoparticle assemblies, the TEM image of 11-mercaptoundecanoic acid functionalised silver nanoparticles + bis(8-imidazol-1-yloctyl)disulfide functionalised gold nanoparticles shows a cluster of monodisperse particles ~8-9nm in size, Figure 8.18.

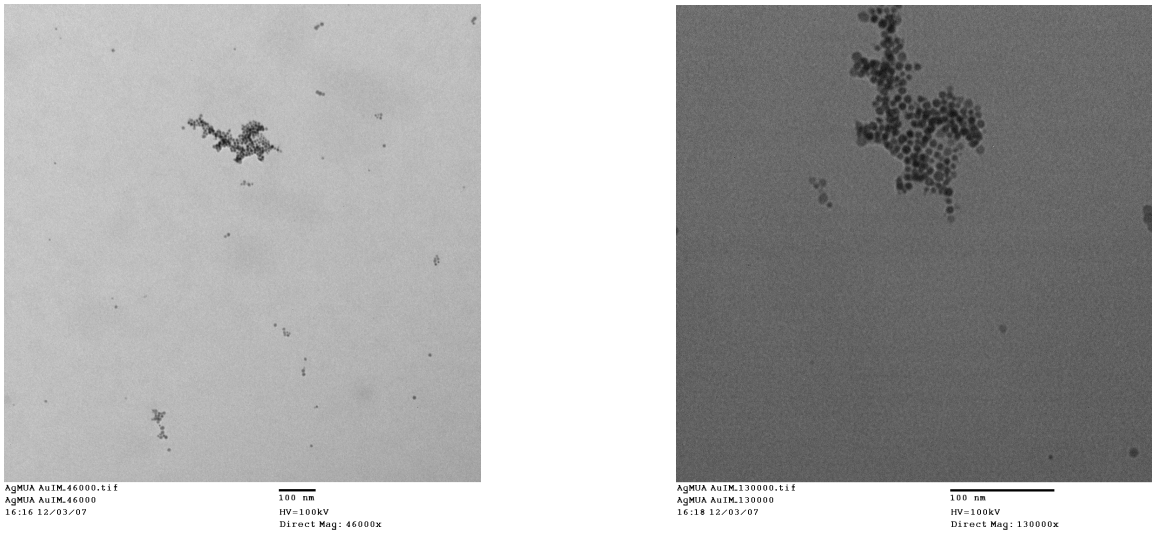

(a) (b)

Figure 8.18 Cluster of 11-mercaptoundecanoic acid functionalised AgNP's + bis(8-imidazol-1-yloctyl)disulfide functionalised AuNP's observed in the TEM image; (a) magnification = 46000x; scale = 100nm; (b) magnification = 130000x; scale = 100nm.

8.3.11 TEM image of 11-mercaptoundecan-1-ol functionalised AgNP's + bis(8-imidazol-1-yloctyl)disulfide functionalised AuNP's

Similar to the TEM image observed for 11-mercaptoundecanoic acid functionalised silver nanoparticles + bis(8-imidazol-1-yloctyl)disulfide functionalised gold nanoparticles and different from the homomeric nanoparticle assemblies, the TEM image of 11-mercaptoundecan-1-ol functionalised silver nanoparticles + bis(8-imidazol-1-yloctyl)disulfide functionalised gold nanoparticles shows a cluster of ~8-9nm nanoparticles, Figure 8.19.

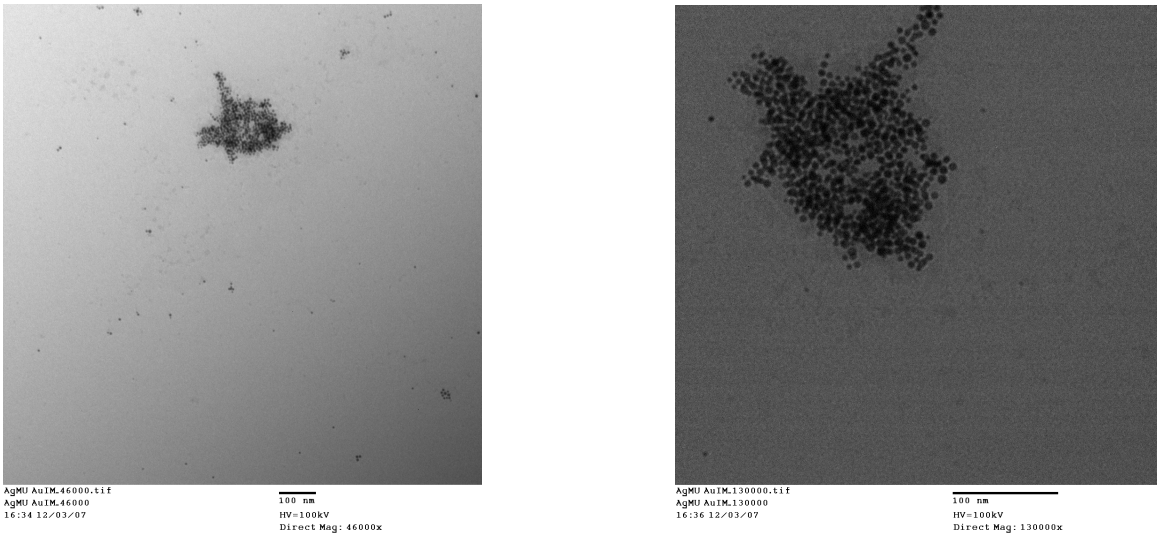

(a) (b)

Figure 8.19 Network of 11-mercaptoundecan-1-ol functionalised AgNP's + bis(8-imidazol-1-yloctyl)disulfide functionalised AuNP's observed in the TEM image; (a) magnification = 46000x; scale = 100nm; (b) magnification = 130000x; scale = 100nm.

8.3.12 Determining nanoparticle "communication" by infra-red (IR) spectroscopy

IR spectroscopy was carried out on heteromeric nanoparticle assemblies.[20] Although it is not possible to determine the exact number of hydrogen-bond interactions between particles via this method, IR spectroscopy is still effective for identifying O-H•••N hydrogen bonds. Broad bands at ~2500 cm^{-1} and ~1900 cm^{-1} are indicative of O-H•••N hydrogen bonds and although only the stretch at ~1900 cm^{-1} is visible, Figure 8.20, it still allows for identification of hydrogen bonding in nanoparticles, Table 8.1.

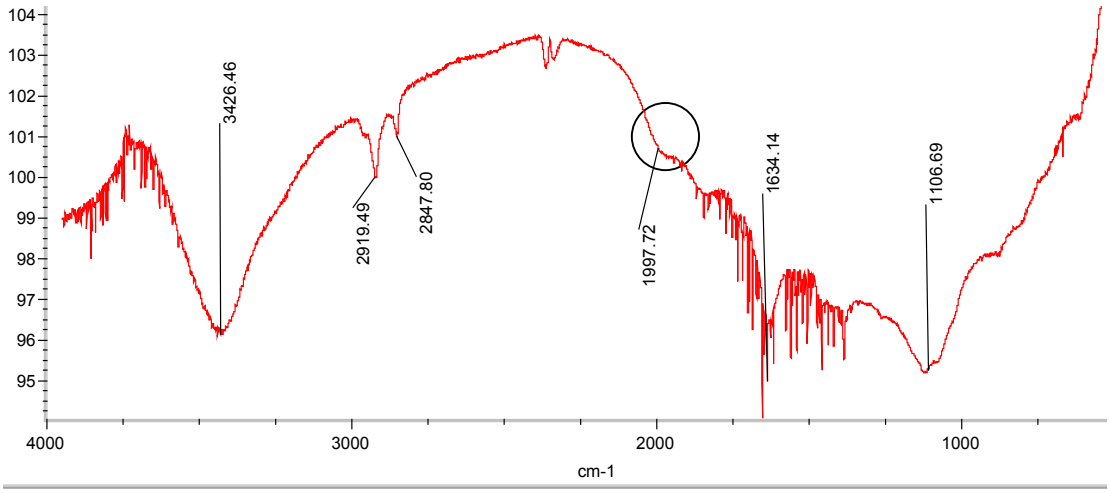

Figure 8.20 IR spectrum of 11-mercaptoundecanoic acid functionalised AuNP's + bis(8-imidazol-1-yloctyl)disulfide functionalised AuNP's showing the 1900 cm^{-1} O-H•••N stretch (circled).

Table 8.1 IR data of heteromeric nanoparticle assemblies.

Ligand 1 (metal)	Ligand 2 (metal)	O-H•••N stretches / cm^{-1}
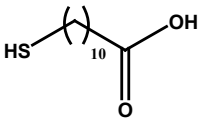 **(Gold)**	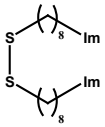 **(Gold)**	1998
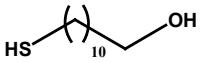 **(Gold)**	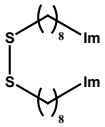 **(Gold)**	1998
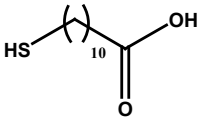 **(Silver)**	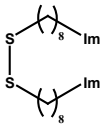 **(Gold)**	1998
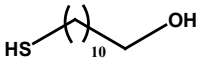 **(Silver)**	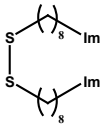 **(Gold)**	1998

8.3.13 Estimating extent of ligand exchange by elemental analysis

Elemental analysis was carried out to estimate the extent of ligand exchange. The ratio of sulfur : nitrogen was calculated for 11-mercaptoundecanoic acid and 11-mercaptoundecan-1-ol AuNP's which was translated into percent ligand exchange (only exchanged ligands contained sulfur), Table 8.2.

Table 8.2 Elemental analysis and estimated % ligand exchange of AuNP's.

AuNP's	**11-Mercaptoundecanoic acid**	**11-Mercaptoundecan-1-ol**
Elemental composition	C=5.62%; H=0.75%; N=0.05%; S=1.20%	C=5.04%; H=0.66%; N=<0.05%; S=1.36%
Sulfur : Nitrogen	10 : 1	12 : 1
Estimated % Ligand exchanged	~90%	~90%

8.4 Discussion

8.4.1 Assessing ligand exchange reactions

The TEM images obtained for the seven, homomeric nanoparticle assemblies clearly show that ligand exchange occurs. Replacing the methyl terminated ligands with ligands terminated with a hydrogen-bond functionality plays a significant role in the ordering of nanoparticles. Dodecylamine gold nanoparticles form an ordered superlattice, whereas particles appended with ligands terminated with hydrogen-bond moieties, produce a different arrangement, Figure 8.21. In the case of 11-mercaptoundecanoic acid particles, fractal type aggregation of particles was observed. This is consistent with particles coated with hydrogen-bond terminated ligands,[12a] with relatively strong interactions (compared to no hydrogen bonding in dodecylamine nanoparticles) between particles causing a chain type arrangement.

In comparison, only a few interactions are observed between 11-mercaptoundecan-1-ol nanoparticles however still significantly different to dodecylamine gold nanoparticles.

Bis(8-imidazol-1-yloctyl) disulfide nanoparticles, which do not form self-complementary hydrogen bonds show a similar assembly to the superlattice obtained with dodecylamine nanoparticles, although less ordered.

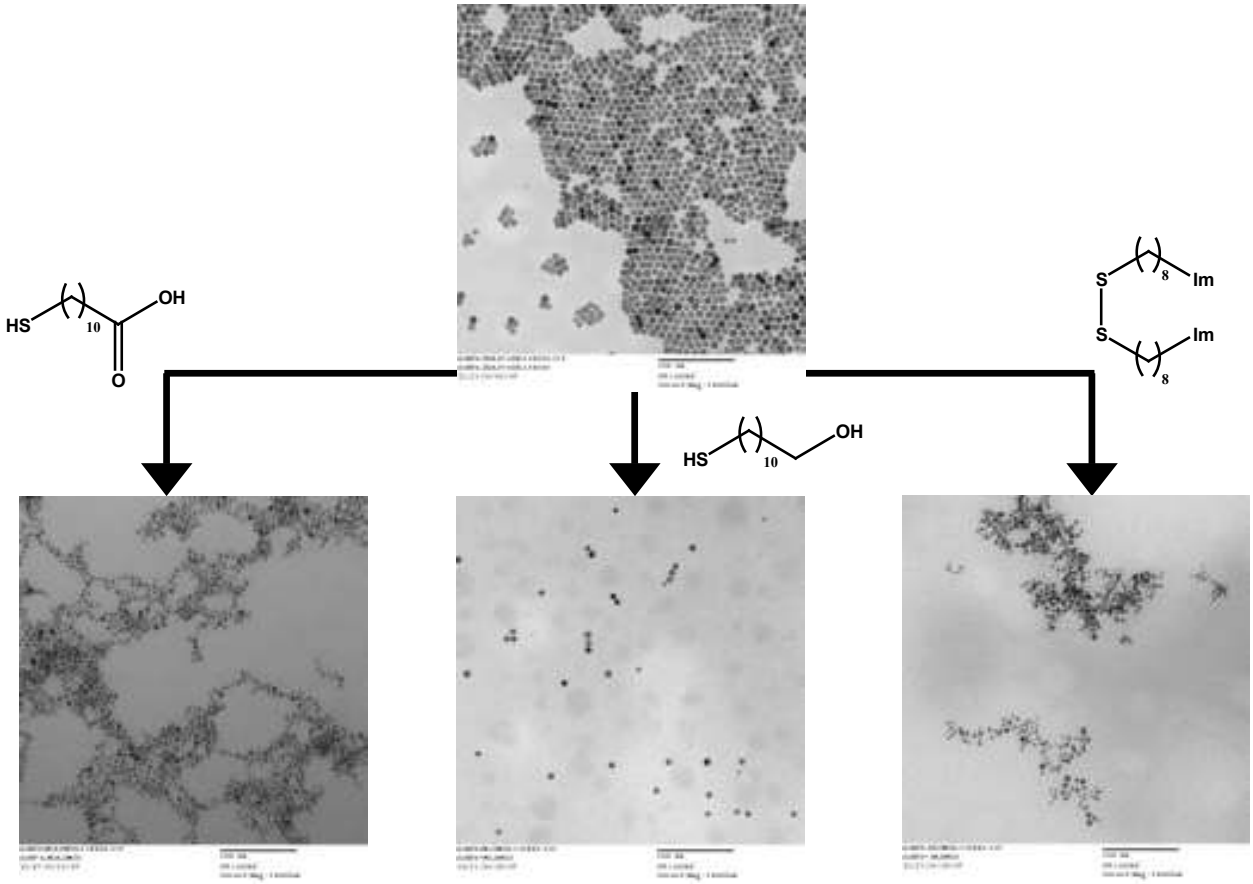

Figure 8.21 Effect of ligand exchange on arrangement of gold nanoparticles; magnification = 130000x; scale = 100nm in all images.

Silver nanoparticles also demonstrate a dramatic change in nanoparticle aggregation upon exchange with hydrogen-bond terminated ligands, Figure 8.22. The fractal aggregation in 11-mercaptoundecanoic acid nanoparticles is observed and confirms ligand exchange. Similarly, 11-mercaptoundecan-1-ol particles show a significant change from the initial dodecanethiol silver nanoparticles.

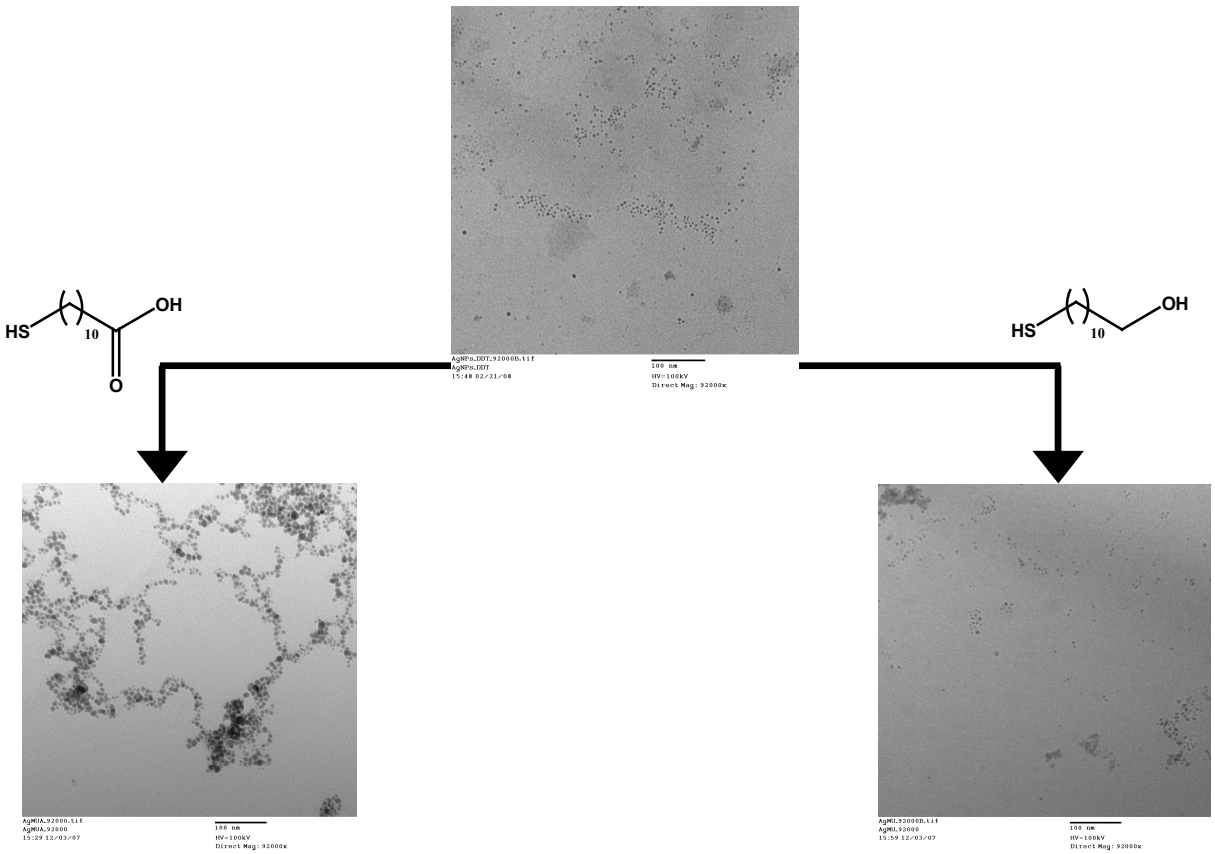

Figure 8.22 Effect of ligand exchange on arrangement of silver nanoparticles; magnification = 92000x; scale = 100nm in all images.

8.4.2 Predicting extent of ligand exchange

Gold nanoparticles were initially functionalised with dodecylamine in order to achieve a high level of exchange. The preference of the gold-sulfur interaction over gold-nitrogen favours ligand exchange and elemental analysis of gold nanoparticles after ligand exchange infer ~90% of dodecylamine ligands were replaced, Figure 8.23.

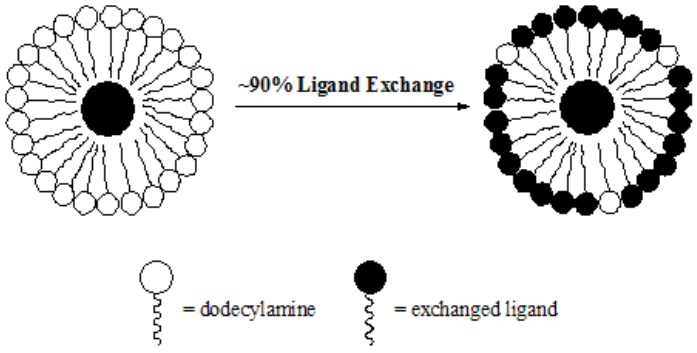

Figure 8.23 Estimated extent of exchange in gold nanoparticles.

8.4.3 Assessing interparticle distances

Interparticle distances were measured from the TEM images of all nanoparticle assemblies, Table 8.3. The noticeable increase in spacing from 'inert' methyl and imidazole groups to hydrogen-bonding functionalities (carboxylic acid and hydroxyl moieties) confirms that hydrogen bonding is taking place between adjacent nanoparticles and is significant enough to adjust interparticle spacing between particles and consequently overall nanoparticle assembly.

Table 8.3 Interparticle distances between nanoparticles.

	Dodecylamine	**Dodecanethiol**	**11-Mercapto-undecanoic acid**	**11-Mercapto-undecan-1-ol**	**Bis(8-imidazol-1-yloctyl)disulfide**
AuNP's	~1.5nm	N/A	~3nm	~2.3nm	~1.5nm
AgNP's	N/A	~1.8nm	~2.4nm	~2.4nm	N/A

8.4.4 Addressing communication between complementary gold nanoparticles

The 1900 cm^{-1} O-H•••N hydrogen-bond stretch was observed in the IR spectra when complementary gold nanoparticles were combined, Figure 8.24. This confirms that heteromeric hydrogen bonding is taking place between the -OH of the acid or alcohol and the nitrogen atom of the imidazole. Similarly, the TEM images of heteromeric nanoparticle assemblies show a different arrangement compared to the homomeric nanoparticle assemblies.

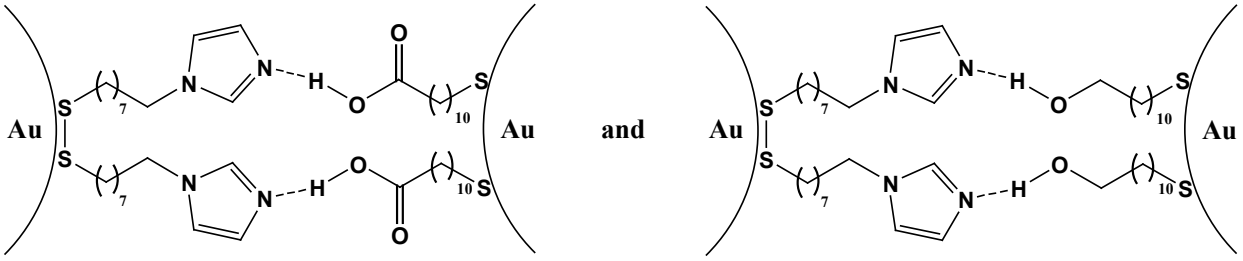

Figure 8.24 Complementary hydrogen bonding between gold nanoparticles.

8.4.5 Addressing communication between complementary gold and silver nanoparticles

Similarly, when complementary gold and silver nanoparticles were combined, the 1900 cm^{-1} O-H•••N hydrogen-bond stretch was observed in both cases confirming heteromeric hydrogen bonding is taking place between gold and silver nanoparticles, Figure 8.25.

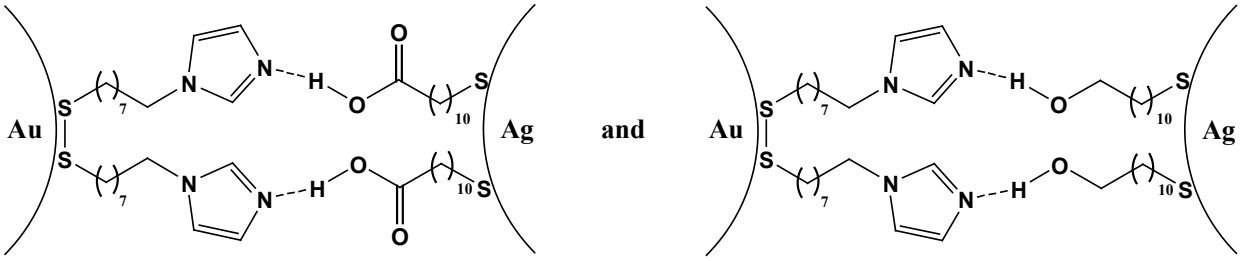

Figure 8.25 Complementary hydrogen bonding between gold and silver nanoparticles.

IR and TEM analysis of homomeric and heteromeric nanoparticle assemblies have provided answers to the questions addressed at the beginning of this chapter.

I. Can nanoparticles be synthesised with hydrogen-bond functionalised ligands?

Elemental analysis confirmed that ligand exchange was successful on nanoparticles with ~90% of ligands replaced for AuNP's, Figure 8.26, allowing for hydrogen-bond functionalised ligands to be appended to the surface of the nanoparticles.

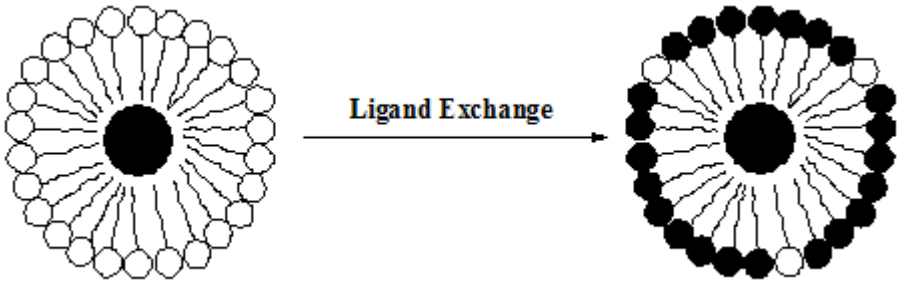

Figure 8.26 Estimated ligand exchange.

TEM images also confirmed ligand exchange, with significant changes observed in the nanoparticle assemblies before and after exchange.

II. Do hydrogen bonds form between nanoparticles?

TEM images of nanoparticle assemblies infer that hydrogen bonding is taking place between nanoparticles. Assemblies in which hydrogen bonding can occur (i.e homomeric acid-acid and alcohol-alcohol as well as heteromeric acid-imidazole and alcohol-imidazole) show major differences (i.e. arrangement of nanoparticles and interparticle distances) in nanoparticle

assemblies, compared to those that cannot form hydrogen bonding (i.e homomeric dodecylamine, dodecanethiol and 8-(imidazol-1-yloctyl)disulfide functionalised nanoparticles).

IR data of heteromeric nanoparticle assemblies confirmed hydrogen bonding between (i) complementary gold nanoparticles and (ii) complementary gold and silver nanoparticles, with the 1900 cm^{-1} O-H•••N hydrogen-bond stretch observed, Figure 8.27.

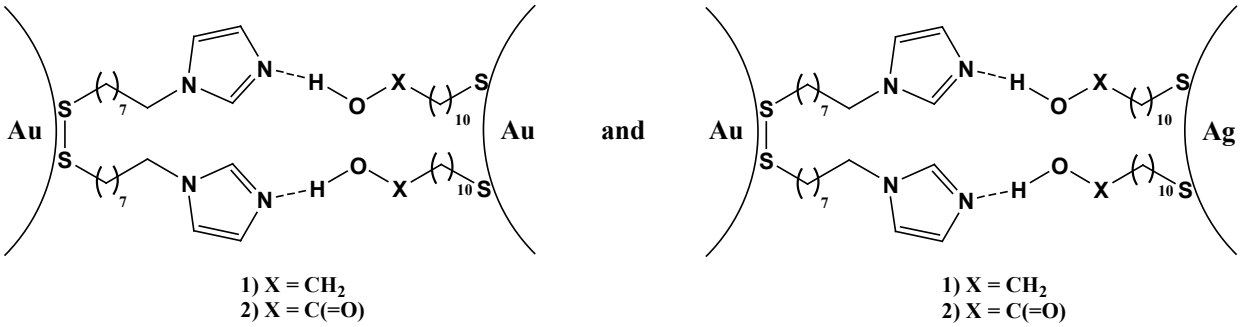

Figure 8.27 Heteromeric hydrogen bonding between complementary nanoparticles.

III. Can supramolecular synthons be used to manipulate nanoparticle assemblies?

It is clear from the TEM images of homomeric and heteromeric nanoparticle assemblies that hydrogen bonding plays a major role in nanoparticle aggregation.

By simply replacing dodecylamine with 11-mercaptoundecanoic acid, the aggregation changes from ordered superlattice to fractal aggregates, Figure 8.28, with an increase in interparticle spacing from ~1.5nm to ~3nm.

Figure 8.28 Extent of hydrogen bonding on the aggregation of nanoparticles; magnification = 130000x; scale = 100nm.

Additionally, when complementary nanoparticles are combined, the formation of heteromeric O-H•••N hydrogen bonds causes dramatic changes in nanoparticle aggregation, Figure 8.29.

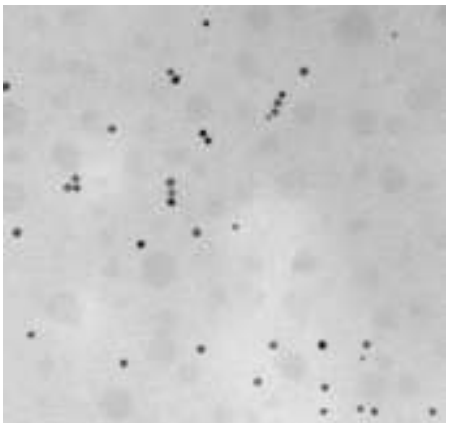

11-mercaptoundecan-1-ol
functionalised AuNP's
magnification = 130000x
scale = 100nm

Nanoparticles
combined

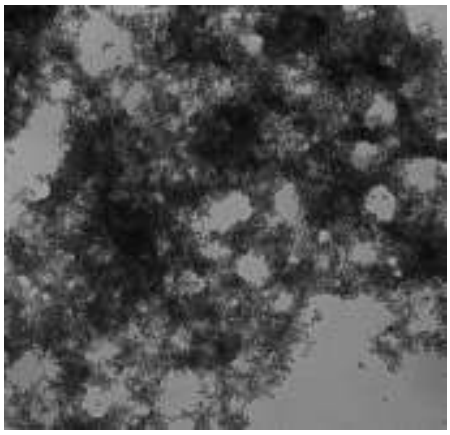

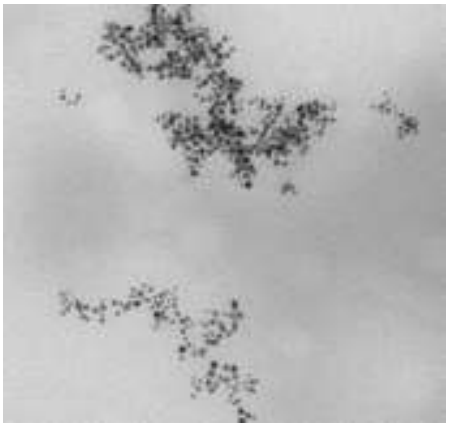

8-(imidazol-1-yloctyl)disulfide
functionalised AuNP's
magnification = 130000x
scale = 100nm

11-mercaptoundecan-1-ol
functionalised AuNP's
+
8-(imidazol-1-yloctyl)disulfide
functionalised AuNP's
magnification = 64000x
scale = 100nm

Figure 8.29 Effect of O-H•••N hydrogen bonds on nanoparticle aggregation.

Although the extent of hydrogen bonding is not quantifiable, the formation of heteromeric imidazole•••acid/alcohol interactions demonstrates the robustness of synthons, even with building blocks significantly larger and more complex than coordination complexes.

References

1. G. R. Desiraju, *Angew. Chem. Int. Ed.,* 1995, **34**, 2311.
2. For a discussion on two component co-crystals see Chapters 3, 4, and 5. Some elegant discussions of co-crystals have also been reported: (a) C. B. Aakeröy, J. Desper and B. A. Helfrich, *CrystEngComm*, 2004, **6**, 19; (b) C. B. Aakeröy, A. M. Beatty, B. A. Helfrich and M. Nieuwenhuyzen, *Cryst. Growth. Des.*, 2003, **3**, 159; (c) J. R. Bowers, G. W. Hopkins, G. P. A. Yap and K. A. Wheeler, *Cryst. Growth. Des.*, 2005, **5**, 727; (d) C. B. Aakeröy, A. M. Beatty and B. A. Helfrich, *Angew. Chem. Int. Ed.*, 2001, **40**, 3240.
3. For a discussion on 1-D inorganic-organic chains via supramolecular synthons see Chapter 6. Also, some elegant discussions have been reported: (a) C. B. Aakeröy and A. Beatty, *Cryst. Eng*., 1998, **1**, 39; (b) C. B. Aakeröy and A. Beatty, *Chem. Commun*., 1998, 1067; (c) C. B. Aakeröy; J. Desper; M. M. Smith and J. F. Urbina, *Dalton Trans.*, 2005, 2462; (d) C. B. Aakeröy; J. Desper and J. Valdés-Martínez, *CrystEngComm.*, 2004, **6**, 413; (e) J. K. Bera, T. –T. Vo, R. A. Walton and K. R. Dunbar, *Polyhedra*, 2003, **22**, 3009; (f) C. B. Aakeröy, A. Beatty, J. Desper, M. O'Shea and J. Valdés-Martínez, *Dalton Trans.*, 2003, 3956.
4. http://www.britishmuseum.org/explore/highlights/highlight_objects/pe_mla/t/the_lycurgus_cup.aspx
5. F. Antonii, *Panacea Aurea-Auro Potabile,* Bibliopolio Frobeniano, Hamburg, 1618.
6. M. Faraday, *Philos, Trans, R. Soc. London,* 1857, **147**, 145
7. (a) J. Turkevich, P.C. Stevenson and J. Hiller, *Discuss. Faraday Soc.*, 1951, **11**, 55; (b) M. A. Hayat, *Colloidal Gold: Principles, Methods and Applications*; Academic Press, New York, 1989 **1-2**; (c) G. Schmid, *Clusters and Colloids*; VCH, Weinheim, 1994; (d) M. Brust, M. Walker, D. Bethell, D. J. Schriffin and R. Whynam, *J. Chem. Soc. Chem. Commun.*, 1994, 801; (e) A. C. Templeton, W. P. Wuelfing and R. W. Murray, *Acc. Chem. Res.*, 2000, **33**, 27; (f) U. Drechsler, B. Erdogan and V. M. Rotello, *Chem. Eur. –J.*, 2004, **10**, 5570.
8. (a) H. Tsunoyama, H. Sakurai, Y. Negishi and T. Tsukuda, *J. Am. Chem. Soc*., 2005, **127**, 9374-9375; (b) D. I. Enache, J. K. Edwards, P. Landon, B. Solsona-Espriu, A. F. Carley, A. A. Herzing, M. Watanabe, C. J. Kiely, D. W. Knight and G. J. Hutchings, *Science*, 2006, **311**, 362-365; (c) C. H. Christensen, B. Jorgsensen, J. Rass-Hansen, K. Egeblad, R. Madsen,

S. K. Klitgaard, S. M .Hansen, M. R. Hansen and H. C. Anderson, *Angew. Chem. Int. Ed.*, 2006, **45**, 4648.

9. (a) D. Pissuwan, S. M. Valenzuela and M. B Cortie, *Trends Biotechnol*. 2006, **24,** 62-67; (b) P. K. Jain, K. S.Lee, I. H. El-Sayed and M. A. El-Sayed, *J. Phys. Chem. B*, 2006, **110**, 7238-7248.
10. (a) U. Freibig and M. Vollmer, *Optical Properties of Metal Clusters*, Springer-Verlag, New York, 1995; (b) A. Taleb, C. Petit and M. P. J. Pileni, *Phys. Chem. B*, 1998, **102**, 2214; (c) Y. Yang, J. Shi, W. Huang, S. Dai and L. Wang, *J. Mater. Sci.*, 2003, **38**, 1243; (d) G. C. Papavassiliou, *Prog. Solid State Chem.*, 1979, **12**, 185; (e) R. Elghanian, J. J. Storhoff, R. C. Mucic, R. L. Letsinger and C. A. Mirkin, *Science*, 1997, **277**, 1078.
11. (a) B. L. V. Prasad, S. I. Stoeva, C. M. Sorensen and K. J. Klabunde, *Chem. Mater.*, 2003, **15**, 935; (b) B. L. V. Prasad, S. I. Stoeva, C. M. Sorensen and K. J. Klabunde, *Langmuir*, 2002, **18**, 7515; (c) X. M. Lin, C. M. Sorensen and K. J. Klabunde, *Chem. Mater.*, 1999, **11**, 198; (d) X. M. Lin, G. M. Wang, C. M. Sorensen and K. J. Klabunde, *J. Phys. Chem. B*, 1999, **103**, 5488; (e) X. M. Lin, H. M. Jaeger, C. M. Sorensen and K. J. Klabunde, *J. Phys. Chem. B*, 2001, **105**, 3353; (f) S. I. Stoeva, B. L. V. Prasad, S. Uma, P. K. Stominov, V. Zaikovski, C. M. Sorensen and K. J. Klabunde, *J. Phys. Chem. B*, 2003, **107**, 7441; (g) S. Stoeva, K. J. Klabunde, C. M. Sorensen and I. Dragieva, *J. Am. Chem. Soc.*, 2002, **124**, 2305.
12. (a) C. R. van den Brom, P. Rudolph, T. T. M. Palstra and B. Hessen, *Chem. Commun.* 2007, 4922; (b) C. R. van den Brom, I. Arfaoui, T. Cren, B. Hessen, T. T. M. Palstra, J. T. M. De Hosson and P. Rudolf, *Adv. Funct. Mater.*, 2007, **17**, 2045; (c) L. Han, M. M. Maye and C.–J. Zhong, *Mat. Res. Soc. Symp. Proc.*, 2001, **635**, C4.5.1; (d) R. Zirbs, F. Kienberger, P. Hinterdorfer and W. H. Binder, *Langmuir*, 2005, **21**, 8414; (e) H. Yao, H. Kojima, S. Sato and K. Kimura, *Langmuir*, 2004, **20**, 10317; (f) A. K. Boal and V. M. Rotello, *Langmuir*, 2000, **16**, 9527; (g) F. X. Zhang, W. Zheng, M. M. Maye, Y. Lou, L. Han and C.–J. Zhong, *Langmuir*, 2000, **16**, 9639; (h) E. Hao and T. Lian, *Chem. Mater.*, 2000, **12**, 3392; (i) J. B. Carroll, B. L. Frankamp and V. M. Rotello, *Chem. Commun.*, 2002, 1892; (j) L. Han, J. Luo, N. N. Kariuki, M. M. Maye, V. W. Jones and C.–J. Zhong, *Chem. Mater.*, 2003, **15**, 29;
13. (a) C. B. Aakeröy, A. M. Beatty and B. A. Helfrich, *J. Am. Chem. Soc.*, 2002, **124**, 14425; (b) B. R. Bhogala, S. Basavgu and A. Nangia, *Cryst. Eng. Comm.*, 2005, **7**, 551; (c) P.

Vishweshwar, A. Nangia and V. M. Lynch, *Cryst. Growth Des.*, 2003, **3**, 783; (d) G. S. Papaefstathiou, A. J. Kipp and L. R. MacGillivray, *Chem. Commun.*, 2001, 2462; (e) T. L. Nguyen, F. W. Fowler and J. W. Lauher, *J. Am. Chem. Soc.*, 2001, **123**, 11057; (f) V. R. Pedireddi, A. Ranganathan and S. Chatterjee, *Tetrahedron Lett.*, 1998, **39**, 9831; (g) M. Vinodu and I. Goldberg, *Cryst. Eng. Comm.*, 2005, **7**, 133; (h) R. D. B. Walsh, M. W. Bradner, S. Fleischman, L. A. Morales, B. Moulton, N. Rodriguez-Hornedo and M. J. Zaworotko, *Chem. Commun.*, 2003, 186; (i) N. Shan and W. Jones, *Tetrahedron Lett.*, 2003, **44**, 3687.

14. Molecular structures for imidazole and pyridine were constructed using Spartan '06 (Wavefunction, Inc. Irvine, CA). Both molecules were optimized using AM1, with the maxima and minima in the electrostatic potential surface (0.002 e/au isosurface) determined using a positive point charge in the vacuum as a probe.
15. Cambridge Structural Database v. 5.29 (January 2008).
16. (a) J. C. Garrison, C. A. Tessier and W. J. Youngs, *J. Organomet. Chem.*, 2005, **690**, 6008; (b) M. N. G. James and M. Matsushima, *Acta Crystallogr. Sect. B*, 1973, **29**, 838; (c) W. –H. Wang, X. –Y. Su, J. –B. Lan, Z. –H. Mao, J. –S. You and R. –G. Xie, *Cryst. Growth Des.*, 2007, **7**, 741; (d) D. F. Rane, R. E. Pike, M. S. Puar, J. J. Wright, A. T. McPhail, *Tetrahedron*, 1988, **44**, 2397; (e) M. Zhong, I. Nowak, J. F. Cannon, M. J. Robins, *J. Org. Chem*., 2006, **71**, 4216; (f) P. L. Arnold, C. Wilson, *Inorg. Chim. Acta*, 2007, **360**, 190.
17. (a) T. Nakamura, T. Ishii, N. Miyata, K. Taniguchi, Y. Tomishima, T. Ueki and M.Sato, *Bioorg. Med. Chem. Lett.*, 2004, **14**, 5305; (b) C. B. Aakeröy, J. Desper, B. Leonard and J. F. Urbina, *Cryst. Growth Des.*, 2005, **5**, 865; (c) P. van Roey, K. A. Bullion, Y. Osawa, L. J. Browne, R. M. Bowman and D. G. Braun, *J. Enzyme Inhib.*, 1991, **5**, 119; (d) P. Van Roey, K. A. Bullion, Y. Osawa, R. M. Bowman and D. G. Braun, *Acta Crystallogr. Sect. C*, 1991, **47**, 1015; (e) M. Czugler, J. G. Angyan, G. Naray-Szabo, E. Weber, *J. Am. Chem. Soc.*, 1986, **108**, 1275; (f) Z. Fei, W. H. Ang, T. J. Geldbach, R. Scopelliti, P. J. Dyson, *Chem. –Eur. J.*, 2006, **12**, 4014.
18. (a) A. Ballabh, D. R. Trivedi, P. Dastidar, *Chem. Mater.*, 2003, **15**, 2136; (b) J. Garbarczyk, K. Pogorzelec-Glaser, *Z. Kristallogr. -New Cryst. Struct.*, 2003, **218**, 567; (c) C. B. Aakeröy, P. B. Hitchcock, *J. Mater. Chem,* 1993, **3**, 1129; (d) D. –D. Lin, J. –G. Liu, D. –J. Xu, *Acta*

Crystallogr., Sect. E, 2006, **62**, o451; (e) K. Deka, M. Laskar, J. B. Baruah, *Polyhedron*, 2006, **25**, 2525; (f) Y. –Q. Sun, J. Zhang, G. –Y. Yang, *Acta Crystallogr., Sect. E*, 2002, **58**, o1100 (g) J. C. MacDonald, M. V. Yigit, K. Mychajlonka, *Cryst. Growth Des.*, 2005, **5**, 2248 (h) J. C. MacDonald, P. C. Dorrestein, M. M. Pilley, *Cryst. Growth Des.*, 2001, **1**, 29; (i) C. B. Aakeröy, D. P. Hughes, M. Nieuwenhuyzen, *J. Am. Chem. Soc*., 1996, **118**, 10134; (j) J. Overgaard, B. Schiott, F. K. Larsen, A. J. Schultz, J. C. MacDonald, B. B. Iversen, *Angew. Chem., Int. Ed.*, 1999, **38**, 1239; (k) J. Fuller, R. T. Carlin, L. J. Simpson, T. E. Furtak, *Chem. Mater*., 1995, **7**, 909.

19. Attempted synthesis of dodecylamine functionalised silver nanoparticles resulted in an insoluble grey precipitate.
20. DMSO solutions of nanoparticles were combined, dried and the residue analysed by IR.

CHAPTER 9 - Summary

The concept of using molecular electrostatic potential (MEP) surfaces to control the outcome of co-crystallisation reactions has been shown to be a highly effective tool.

By utilising such an approach, a hierarchy of hydrogen-bond interactions has been developed for systems containing (i) a N-heterocycle and an amide moiety and (ii) two different N-heterocycles.

We designed and synthesised a family of pyrazole benzamide supramolecular reagents (SR's), which contained a poor hydrogen-bond acceptor (pyrazole) and an amide moiety, Figure 9.1.

Co-crystals between these SR's and hydrogen-bond donors (carboxylic acids) show a change in preference for the incoming carboxylic acid compared to better (based on MEP surfaces) hydrogen-bond acceptors (e.g. pyridine and benzimidazole). The incoming carboxylic acid opts to form a heteromeric acid-amide dimer via an O-H•••O and a N-H•••O hydrogen bond oppose to forming an O-H•••N hydrogen bond to the pyrazole nitrogen atom.

Furthermore, the acceptor strength (based on MEP surfaces) of the pyrazole nitrogen atom was successfully turned up through simple covalent modifications (i.e. isomer change or addition of methyl groups to the pyrazole ring), Figure 9.1.

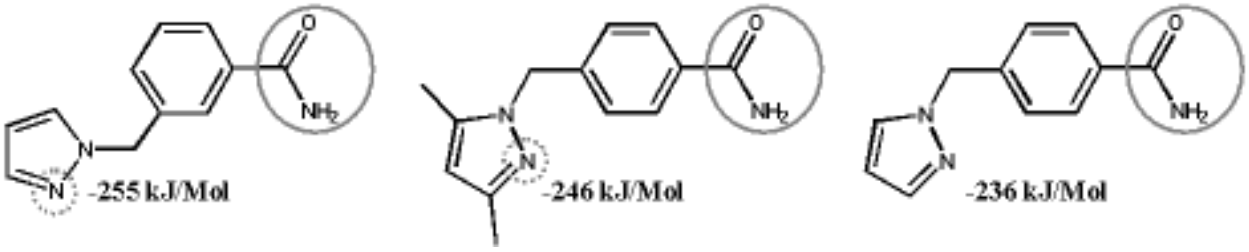

Figure 9.1 Fine-tunability of pyrazole as a hydrogen-bond acceptor based on MEP surface calculations.

This demonstrates the ability to fine-tune the hydrogen-bond acceptor strength and suggests MEP surfaces can be effective as a tool to control the product of co-crystallisation reactions, Figure 9.2.

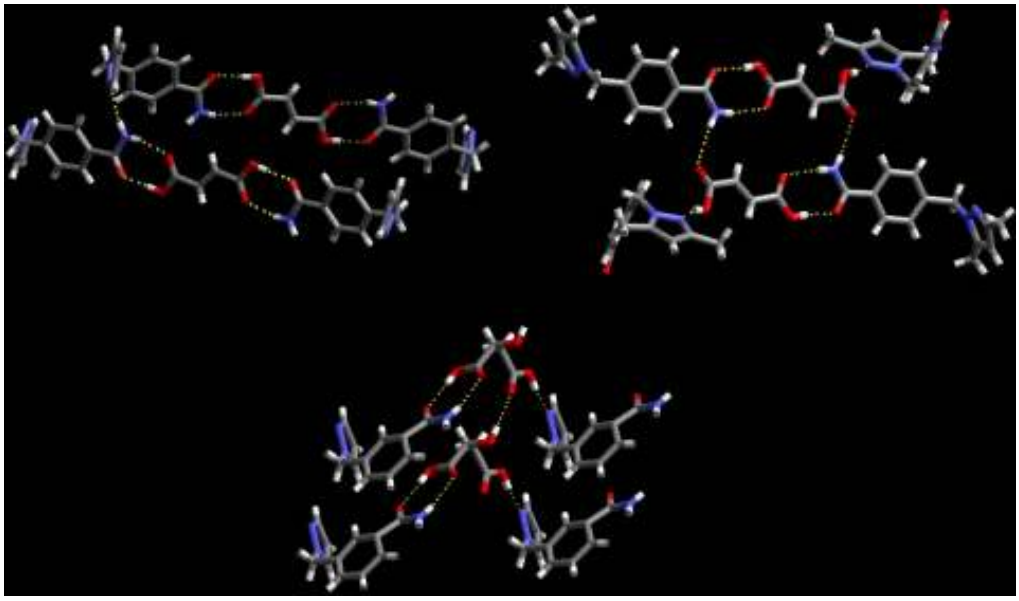

Figure 9.2 Co-crystals between pyrazole benzamide SR's and di-carboxylic acids showing improved hydrogen-bond acceptor ability of pyrazole nitrogen.

The use of MEP surface calculations as a tool for proposing best acceptor/second best acceptor sites was further validated through a more stringent examination of SR's containing two different N-heterocycles. Ditopic pyridine-indazole and pyrimidine-pyrazole SR's were designed and synthesised and subsequent co-crystallisations with carboxylic acids confirm that MEP surface calculations can be an effective tool, even when the calculated charges on the acceptor sites are somewhat similar. In all cases, the incoming carboxylic acid forms an O-H•••N hydrogen bond with the better, more negative hydrogen-bond acceptor (pyridine and pyrazole respectively), Figure 9.3.

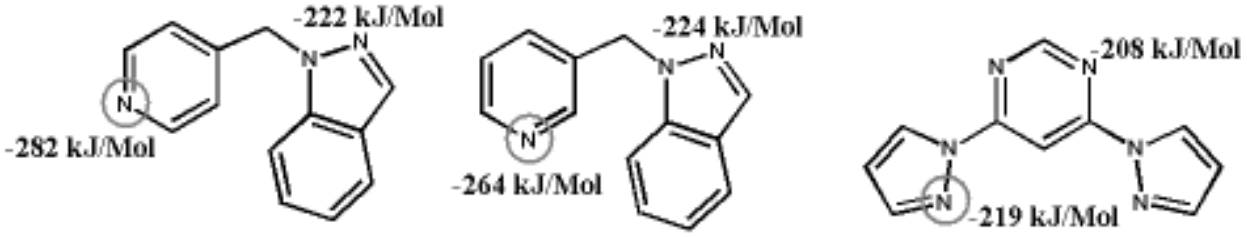

Figure 9.3 Validity of MEP surface calculations in ditopic heterocycle SR's.

The reliability of the amide-amide dimer was exploited to construct inorganic-organic hybrid materials. Combination of pyrazole benzamide ligands with copper(II)carboxylate "paddle-wheel" complexes resulted in the self-assembly of 1-D chains via pyrazole coordination to the neutral metal complex coupled with the formation of the amide-amide dimer, Figure 9.4.

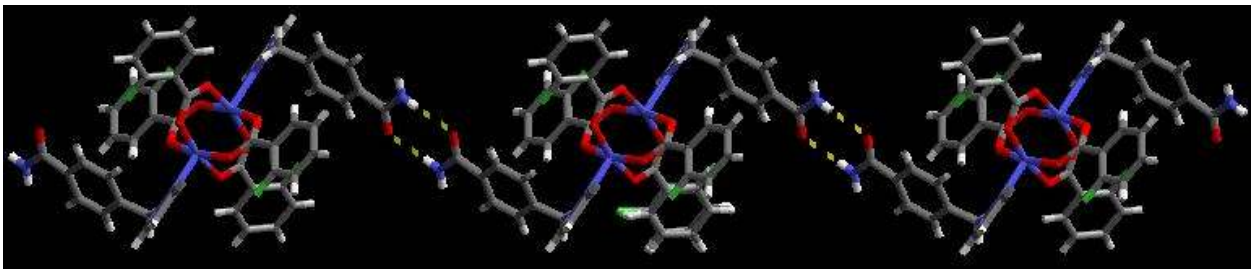

Figure 9.4 Self-assembly of 1-D inorganic-organic chains via combination of pyrazole benzamide ligands and copper "paddle-wheel" complexes.

The influence of supramolecular synthons on much larger architectures was demonstrated by "decorating" the surface of gold and silver nanoparticles with ligands capable of forming reliable hydrogen bonds. Replacing ligands possessing an 'inert' non hydrogen-bonding terminus (i.e. a methyl functionality) with those capable of forming homo- and/or heteromeric hydrogen bonds (i.e. a carboxylic acid, alcohol or imidazole), it is possible to control the interparticle distance between nanoparticles and consequently overall nanoparticle assembly, Figure 9.5.

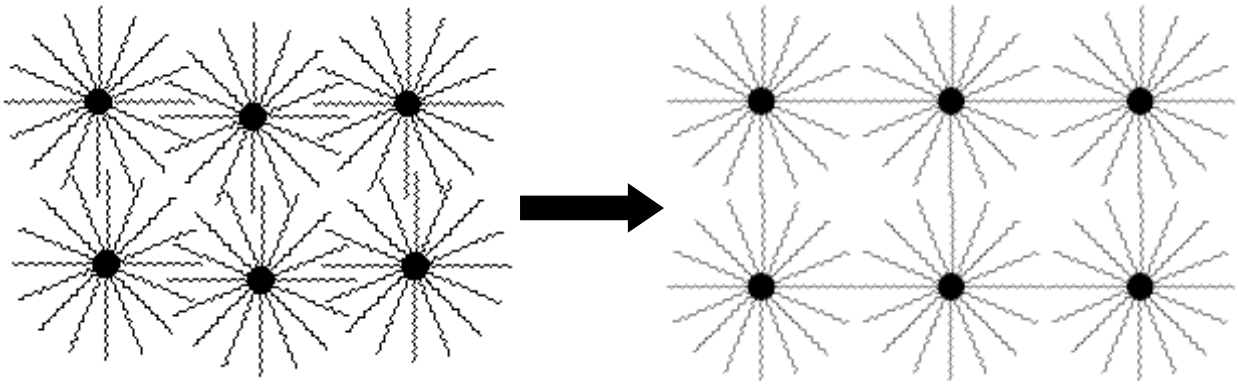

Figure 9.5 From interdigitation to tip-to-tip interactions, the effect of hydrogen bonding on nanoparticle assembly.

The overall ordering of the nanoparticles is dramatically effected by these 'small', yet significant interactions. By changing the terminus on the stabilising ligand from a methyl group to a carboxylic acid, the aggregation of nanoparticles changed from an ordered superlattice to a more 'fractal' assembly, Figure 9.6. Furthermore, the interparticle distance increased from ~1.5nm (the estimated length of one ligand) to ~3nm.

Figure 9.6 Extent of hydrogen bonding on the aggregation of nanoparticles.

Finally, the ability to form O-H•••N hydrogen bonds between carboxylic acid or alcohol functionalised silver nanoparticles and the nitrogen atom of an imidazole moiety, appended to gold nanoparticles, Figure 9.7, shows that, construction of bimetallic nanoparticle assemblies is possible.

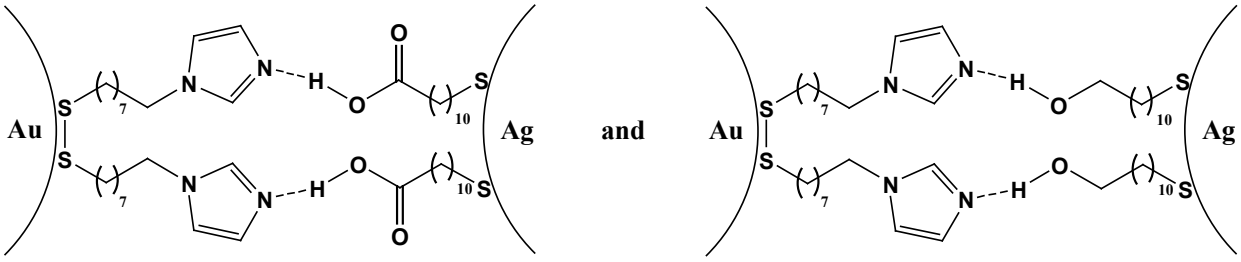

Figure 9.7 Complementary hydrogen bonding between gold and silver nanoparticles.

The results reported herein provide an insight into the versatility and influence of supramolecular synthons. From small molecules to nano-scale architectures, these reliable hydrogen-bond motifs play a major role in assembly, Figure 9.8, and therefore, having a degree of control over supramolecular synthons is of the utmost importance for reliable supramolecular synthesis.

MEP surfaces, shown to be highly effective within the systems discussed herein, could provide the supramolecular chemist with this degree of control.

Consequently, it is necessary to assess the effectiveness of MEP surface calculations as a tool for determining a hierarchy of acceptor or donor sites. Investigating a range of multiple hydrogen-bond donors (i.e. carboxylic acids, alcohols or oximes), more complex hydrogen-bond acceptors (i.e. 3 or more acceptor sites) and halogen-bond donors/acceptors, it will be possible to paint an overall picture of the reliability of MEP surface calculations, which would be invaluable for supramolecular synthesis.

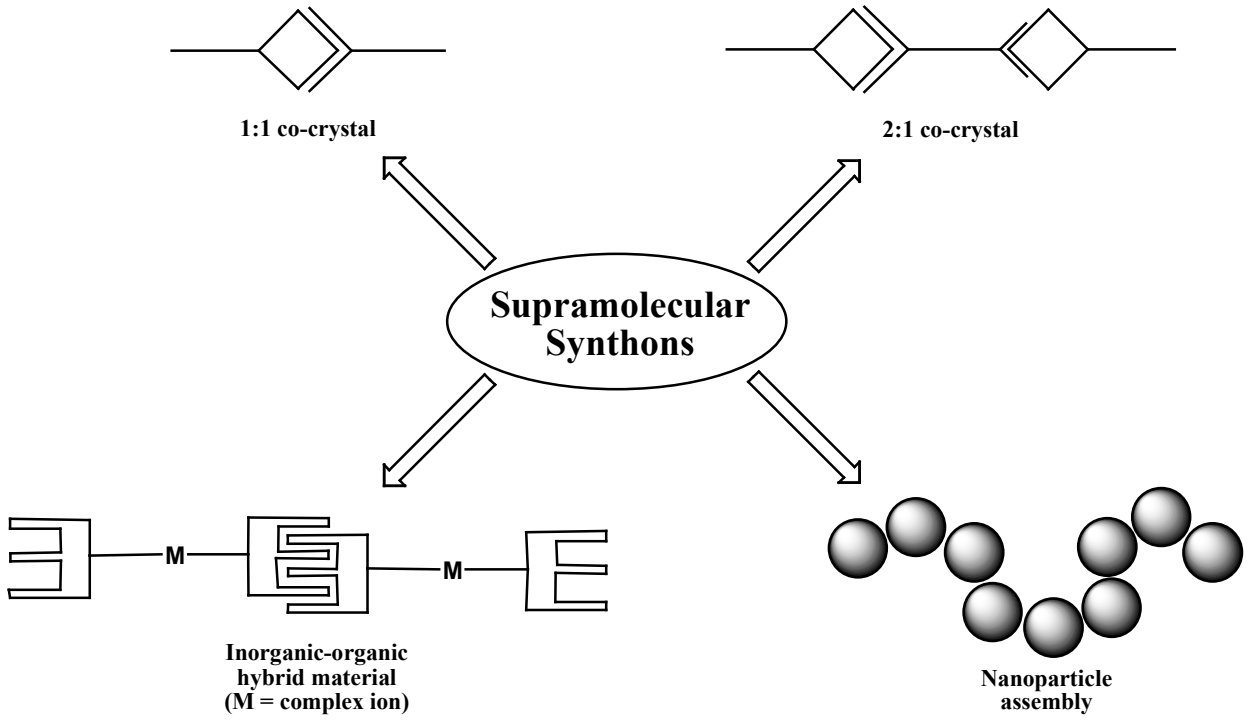

Figure 9.8 The versatility of supramolecular synthons, from small molecules to nano-scale architectures.

Appendix A - Crystal Structure Data

Table A.1 Crystal data and structure refinement for **2**.

Empirical formula	C11 H11 N3 O	
Formula weight	201.23	
Temperature	100(2) K	
Wavelength	0.71073 Å	
Crystal system	Monoclinic	
Space group	P2(1)/c	
Unit cell dimensions	a = 21.660(4) Å	α = 90°.
	b = 4.7544(9) Å	β = 93.912(3)°.
	c = 9.9321(19) Å	γ = 90°.
Volume	1020.4(3) $Å^3$	
Z	4	
Density (calculated)	1.310 Mg/m^3	
Absorption coefficient	0.088 mm^{-1}	
F(000)	424	
Crystal size	0.42 x 0.28 x 0.08 mm^3	
Theta range for data collection	1.88 to 28.40°.	
Index ranges	-28<=h<=27, -6<=k<=6, -13<=l<=9	
Reflections collected	7149	
Independent reflections	2429 [R(int) = 0.0494]	
Completeness to theta = 28.40°	94.3 %	
Absorption correction	None	
Refinement method	Full-matrix least-squares on F^2	
Data / restraints / parameters	2429 / 0 / 142	
Goodness-of-fit on F^2	0.974	
Final R indices [I>2sigma(I)]	R1 = 0.0522, wR2 = 0.1146	
R indices (all data)	R1 = 0.1042, wR2 = 0.1342	
Largest diff. peak and hole	0.302 and -0.229 $e.Å^{-3}$	

Table A.2 Crystal data and structure refinement for **4**.

Empirical formula	C13 H15 N3 O	
Formula weight	229.28	
Temperature	173(2) K	
Wavelength	0.71073 Å	
Crystal system	Monoclinic	
Space group	P2(1)/n	
Unit cell dimensions	a = 8.4005(7) Å	α = 90°.
	b = 8.0671(7) Å	β = 102.621(6)°.
	c = 18.0477(18) Å	γ = 90°.
Volume	1193.50(19) $Å^3$	
Z	4	
Density (calculated)	1.276 g/cm^3	
Absorption coefficient	0.084 mm^{-1}	
F(000)	488	
Crystal size	0.30 x 0.25 x 0.10 mm^3	
Theta range for data collection	2.31 to 28.26°.	
Index ranges	-10<=h<=10, -10<=k<=10, -22<=l<=23	
Reflections collected	8390	
Independent reflections	2789 [R(int) = 0.0919]	
Completeness to theta = 28.26°	94.1 %	
Absorption correction	None	
Refinement method	Full-matrix least-squares on F^2	
Data / restraints / parameters	2789 / 0 / 162	
Goodness-of-fit on F^2	0.934	
Final R indices [I>2sigma(I)]	R1 = 0.0491, wR2 = 0.1184	
R indices (all data)	R1 = 0.0892, wR2 = 0.1309	
Largest diff. peak and hole	0.168 and -0.197 $e.Å^{-3}$	

Table A.3 Crystal data and structure refinement for **6**.

Empirical formula	C13 H14 Br N3 O	
Formula weight	308.18	
Temperature	100(2) K	
Wavelength	0.71073 Å	
Crystal system	Monoclinic	
Space group	P2(1)/n	
Unit cell dimensions	a = 12.437(3) Å	α = 90°.
	b = 8.8195(17) Å	β = 114.488(6)°.
	c = 12.468(2) Å	γ = 90°.
Volume	1244.7(4) $Å^3$	
Z	4	
Density (calculated)	1.645 g/cm^3	
Absorption coefficient	3.294 mm^{-1}	
F(000)	624	
Crystal size	0.15 x 0.15 x 0.15 mm^3	
Theta range for data collection	2.93 to 33.14°.	
Index ranges	-18<=h<=19, -12<=k<=13, -19<=l<=19	
Reflections collected	58663	
Independent reflections	4624 [R(int) = 0.0353]	
Completeness to theta = 33.14°	97.4 %	
Absorption correction	None	
Max. and min. transmission	0.6378 and 0.6378	
Refinement method	Full-matrix least-squares on F^2	
Data / restraints / parameters	4624 / 0 / 161	
Goodness-of-fit on F^2	1.026	
Final R indices [I>2sigma(I)]	R1 = 0.0234, wR2 = 0.0588	
R indices (all data)	R1 = 0.0319, wR2 = 0.0622	
Largest diff. peak and hole	0.681 and -0.405 $e.Å^{-3}$	

Table A.4 Crystal data and structure refinement for **8**.

Empirical formula	C11 H11 N3 O	
Formula weight	201.23	
Temperature	100(2) K	
Wavelength	0.71073 Å	
Crystal system	Triclinic	
Space group	P-1	
Unit cell dimensions	a = 7.7873(5) Å	α = 77.6610(10)°.
	b = 8.1130(6) Å	β = 74.4600(10)°.
	c = 8.8400(6) Å	γ = 68.3980(10)°.
Volume	496.14(6) $Å^3$	
Z	2	
Density (calculated)	1.347 Mg/m^3	
Absorption coefficient	0.091 mm^{-1}	
F(000)	212	
Crystal size	0.25 x 0.22 x 0.20 mm^3	
Theta range for data collection	2.41 to 30.00°.	
Index ranges	-10<=h<=10, -10<=k<=11, -12<=l<=11	
Reflections collected	5729	
Independent reflections	2838 [R(int) = 0.0165]	
Completeness to theta = 30.00°	97.9 %	
Absorption correction	Semi-empirical from equivalents	
Max. and min. transmission	1.000 and 0.798	
Refinement method	Full-matrix least-squares on F^2	
Data / restraints / parameters	2838 / 0 / 142	
Goodness-of-fit on F^2	1.081	
Final R indices [I>2sigma(I)]	R1 = 0.0449, wR2 = 0.1249	
R indices (all data)	R1 = 0.0489, wR2 = 0.1292	
Largest diff. peak and hole	0.476 and -0.232 $e.Å^{-3}$	

Table A.5 Crystal data and structure refinement for **10**.

Empirical formula	C13 H15 N3 O	
Formula weight	229.28	
Temperature	100(2) K	
Wavelength	0.71073 Å	
Crystal system	Triclinic	
Space group	P-1	
Unit cell dimensions	a = 8.0162(4) Å	α = 97.253(2)°.
	b = 8.0603(4) Å	β = 106.060(2)°.
	c = 10.4542(5) Å	γ = 109.335(2)°.
Volume	594.57(5) $Å^3$	
Z	2	
Density (calculated)	1.281 g/cm^3	
Absorption coefficient	0.084 mm^{-1}	
F(000)	244	
Crystal size	0.25 x 0.20 x 0.15 mm^3	
Theta range for data collection	2.09 to 31.00°.	
Index ranges	-11<=h<=11, -11<=k<=11, -14<=l<=15	
Reflections collected	21375	
Independent reflections	3757 [R(int) = 0.0318]	
Completeness to theta = 31.00°	98.9 %	
Absorption correction	None	
Max. and min. transmission	0.9875 and 0.9793	
Refinement method	Full-matrix least-squares on F^2	
Data / restraints / parameters	3757 / 0 / 162	
Goodness-of-fit on F^2	1.083	
Final R indices [I>2sigma(I)]	R1 = 0.0434, wR2 = 0.1205	
R indices (all data)	R1 = 0.0556, wR2 = 0.1299	
Largest diff. peak and hole	0.478 and -0.251 $e.Å^{-3}$	

Table A.6 Crystal data and structure refinement for **12**.

Empirical formula	C13 H14 Br N3 O	
Formula weight	308.18	
Temperature	173(2) K	
Wavelength	0.71073 Å	
Crystal system	Triclinic	
Space group	P-1	
Unit cell dimensions	a = 8.9062(12) Å	α = 73.396(9)°.
	b = 11.6933(18) Å	β = 74.274(9)°.
	c = 14.146(2) Å	γ = 70.553(9)°.
Volume	1305.8(3) $Å^3$	
Z	4	
Density (calculated)	1.568 g/cm^3	
Absorption coefficient	3.140 mm^{-1}	
F(000)	624	
Crystal size	0.35 x 0.25 x 0.08 mm^3	
Theta range for data collection	1.53 to 27.33°.	
Index ranges	-10<=h<=11, -14<=k<=13, -17<=l<=18	
Reflections collected	15905	
Independent reflections	5716 [R(int) = 0.0716]	
Completeness to theta = 27.33°	97.1 %	
Absorption correction	Semi-empirical from equivalents	
Max. and min. transmission	1.000 and 0.144	
Refinement method	Full-matrix least-squares on F^2	
Data / restraints / parameters	5716 / 0 / 329	
Goodness-of-fit on F^2	1.020	
Final R indices [I>2sigma(I)]	R1 = 0.0699, wR2 = 0.1906	
R indices (all data)	R1 = 0.1446, wR2 = 0.2351	
Largest diff. peak and hole	1.254 and -1.006 $e.Å^{-3}$	

Table A.7 Crystal data and structure refinement for **2a**.

Empirical formula	C18 H16 N4 O5	
Formula weight	368.35	
Temperature	100(2) K	
Wavelength	0.71073 Å	
Crystal system	Monoclinic	
Space group	Cc	
Unit cell dimensions	a = 14.485(4) Å	α = 90°.
	b = 4.6366(11) Å	β = 99.831(3)°.
	c = 25.758(6) Å	γ = 90°.
Volume	1704.5(7) $Å^3$	
Z	4	
Density (calculated)	1.435 g/cm^3	
Absorption coefficient	0.107 mm^{-1}	
F(000)	768	
Crystal size	0.36 x 0.34 x 0.09 mm^3	
Theta range for data collection	2.85 to 25.19°.	
Index ranges	-17<=h<=13, -5<=k<=5, -29<=l<=29	
Reflections collected	3961	
Independent reflections	1401 [R(int) = 0.0156]	
Completeness to theta = 25.00°	92.9 %	
Absorption correction	Semi-empirical from equivalents	
Max. and min. transmission	1.000 and 0.646	
Refinement method	Full-matrix least-squares on F^2	
Data / restraints / parameters	1401 / 2 / 253	
Goodness-of-fit on F^2	1.138	
Final R indices [I>2sigma(I)]	R1 = 0.0320, wR2 = 0.0818	
R indices (all data)	R1 = 0.0322, wR2 = 0.0820	
Absolute structure parameter	0.4(12)	
Largest diff. peak and hole	0.212 and -0.271 $e.Å^{-3}$	

Table A.8 Crystal data and structure refinement for **2b**.

Empirical formula	C18 H15 N5 O7	
Formula weight	413.35	
Temperature	100(2) K	
Wavelength	0.71073 Å	
Crystal system	Monoclinic	
Space group	P2(1)/c	
Unit cell dimensions	a = 17.0583(16) Å	α = 90°.
	b = 6.9273(7) Å	β = 112.161(2)°.
	c = 16.3728(15) Å	γ = 90°.
Volume	1791.8(3) $Å^3$	
Z	4	
Density (calculated)	1.532 g/cm^3	
Absorption coefficient	0.121 mm^{-1}	
F(000)	856	
Crystal size	0.34 x 0.26 x 0.22 mm^3	
Theta range for data collection	2.50 to 30.02°.	
Index ranges	-23<=h<=23, -9<=k<=9, -23<=l<=22	
Reflections collected	20001	
Independent reflections	5218 [R(int) = 0.0320]	
Completeness to theta = 30.02°	99.8 %	
Absorption correction	None	
Refinement method	Full-matrix least-squares on F^2	
Data / restraints / parameters	5218 / 0 / 283	
Goodness-of-fit on F^2	1.062	
Final R indices [I>2sigma(I)]	R1 = 0.0434, wR2 = 0.1147	
R indices (all data)	R1 = 0.0492, wR2 = 0.1196	
Largest diff. peak and hole	0.471 and -0.285 $e.Å^{-3}$	

Table A.9 Crystal data and structure refinement for **2c**.

Empirical formula	C18 H16 F N3 O3	
Formula weight	341.34	
Temperature	100(2) K	
Wavelength	0.71073 Å	
Crystal system	Monoclinic	
Space group	P2(1)/n	
Unit cell dimensions	a = 4.3453(7) Å	α = 90°.
	b = 10.8147(17) Å	β = 90.541(2)°.
	c = 34.003(5) Å	γ = 90°.
Volume	1597.8(4) $Å^3$	
Z	4	
Density (calculated)	1.419 g/cm^3	
Absorption coefficient	0.106 mm^{-1}	
F(000)	712	
Crystal size	0.14 x 0.20 x 0.35 mm^3	
Theta range for data collection	1.98 to 26.01°.	
Index ranges	-5<=h<=5, -13<=k<=13, -40<=l<=41	
Reflections collected	9978	
Independent reflections	2909 [R(int) = 0.0362]	
Completeness to theta = 26.01°	92.3 %	
Absorption correction	Semi-empirical from equivalents	
Max. and min. transmission	1.000 and 0.801	
Refinement method	Full-matrix least-squares on F^2	
Data / restraints / parameters	2909 / 0 / 236	
Goodness-of-fit on F^2	1.034	
Final R indices [I>2sigma(I)]	R1 = 0.0407, wR2 = 0.1013	
R indices (all data)	R1 = 0.0485, wR2 = 0.1053	
Largest diff. peak and hole	0.297 and -0.465 $e.Å^{-3}$	

Table A.10 Crystal data and structure refinement for **2d**.

Empirical formula	C18 H16 F N3 O3	
Formula weight	341.34	
Temperature	100(2) K	
Wavelength	0.71073 Å	
Crystal system	Triclinic	
Space group	P-1	
Unit cell dimensions	a = 20.362(3) Å	α = 97.170(3)°.
	b = 21.994(4) Å	β = 115.814(2)°.
	c = 22.540(5) Å	γ = 110.216(2)°.
Volume	8062(3) $Å^3$	
Z	20	
Density (calculated)	1.406 g/cm^3	
Absorption coefficient	0.105 mm^{-1}	
F(000)	3560	
Crystal size	0.48 x 0.15 x 0.12 mm^3	
Theta range for data collection	1.22 to 28.44°.	
Index ranges	-27<=h<=26, -28<=k<=28, -29<=l<=30	
Reflections collected	69882	
Independent reflections	36885 [R(int) = 0.0535]	
Completeness to theta = 28.44°	90.7 %	
Absorption correction	None	
Refinement method	Full-matrix least-squares on F^2	
Data / restraints / parameters	36885 / 0 / 1865	
Goodness-of-fit on F^2	1.078	
Final R indices [I>2sigma(I)]	R1 = 0.1051, wR2 = 0.2598	
R indices (all data)	R1 = 0.2841, wR2 = 0.3387	
Largest diff. peak and hole	1.680 and -1.208 $e.Å^{-3}$	

Table A.11 Crystal data and structure refinement for **2e**.

Empirical formula	C18 H17 N3 O3	
Formula weight	323.35	
Temperature	100(2) K	
Wavelength	0.71073 Å	
Crystal system	Triclinic	
Space group	P-1	
Unit cell dimensions	a = 9.0434(8) Å	α = 101.8070(10)°.
	b = 10.5552(9) Å	β = 102.1260(10)°.
	c = 17.4323(15) Å	γ = 94.3700(10)°.
Volume	1580.1(2) $Å^3$	
Z	4	
Density (calculated)	1.359 g/cm^3	
Absorption coefficient	0.095 mm^{-1}	
F(000)	680	
Crystal size	0.28 x 0.28 x 0.15 mm^3	
Theta range for data collection	1.99 to 28.27°.	
Index ranges	-11<=h<=11, -13<=k<=14, -22<=l<=23	
Reflections collected	14134	
Independent reflections	7283 [R(int) = 0.0270]	
Completeness to theta = 28.27°	93.0 %	
Absorption correction	None	
Refinement method	Full-matrix least-squares on F^2	
Data / restraints / parameters	7283 / 0 / 451	
Goodness-of-fit on F^2	1.058	
Final R indices [I>2sigma(I)]	R1 = 0.0438, wR2 = 0.1121	
R indices (all data)	R1 = 0.0537, wR2 = 0.1184	
Largest diff. peak and hole	0.260 and -0.276 $e.Å^{-3}$	

Table A.12 Crystal data and structure refinement for **2f**.

Empirical formula	C24 H24 N6 O6	
Formula weight	492.49	
Temperature	100(2) K	
Wavelength	0.71073 Å	
Crystal system	Monoclinic	
Space group	P2(1)/n	
Unit cell dimensions	a = 4.2359(8) Å	α = 90°.
	b = 49.029(9) Å	β = 92.780(4)°.
	c = 5.5087(11) Å	γ = 90°.
Volume	1142.7(4) $Å^3$	
Z	2	
Density (calculated)	1.431 Mg/m^3	
Absorption coefficient	0.106 mm^{-1}	
F(000)	516	
Crystal size	0.34 x 0.22 x 0.01 mm^3	
Theta range for data collection	2.49 to 28.39°.	
Index ranges	-5<=h<=5, -63<=k<=64, -4<=l<=6	
Reflections collected	8069	
Independent reflections	2638 [R(int) = 0.0362]	
Completeness to theta = 28.39°	91.5 %	
Absorption correction	None	
Refinement method	Full-matrix least-squares on F^2	
Data / restraints / parameters	2638 / 0 / 172	
Goodness-of-fit on F^2	1.253	
Final R indices [I>2sigma(I)]	R1 = 0.0735, wR2 = 0.1489	
R indices (all data)	R1 = 0.0811, wR2 = 0.1529	
Largest diff. peak and hole	0.434 and -0.310 $e.Å^{-3}$	

Table A.13 Crystal data and structure refinement for **2g**.

Empirical formula	C26 H28 N6 O6	
Formula weight	520.54	
Temperature	173(2) K	
Wavelength	0.71073 Å	
Crystal system	Monoclinic	
Space group	P2(1)/n	
Unit cell dimensions	a = 9.5363(9) Å	α = 90°.
	b = 7.3143(6) Å	β = 96.130(7)°.
	c = 17.6580(15) Å	γ = 90°.
Volume	1224.63(19) $Å^3$	
Z	2	
Density (calculated)	1.412 g/cm^3	
Absorption coefficient	0.103 mm^{-1}	
F(000)	548	
Crystal size	0.40 x 0.35 x 0.25 mm^3	
Theta range for data collection	2.32 to 27.85°.	
Index ranges	-12<=h<=12, -9<=k<=9, -21<=l<=23	
Reflections collected	8075	
Independent reflections	2790 [R(int) = 0.1114]	
Completeness to theta = 27.85°	95.8 %	
Absorption correction	None	
Refinement method	Full-matrix least-squares on F^2	
Data / restraints / parameters	2790 / 0 / 182	
Goodness-of-fit on F^2	1.067	
Final R indices [I>2sigma(I)]	R1 = 0.0639, wR2 = 0.1527	
R indices (all data)	R1 = 0.0816, wR2 = 0.1686	
Extinction coefficient	0.079(10)	
Largest diff. peak and hole	0.496 and -0.354 $e.Å^{-3}$	

Table A.14 Crystal data and structure refinement for **2h**.

Empirical formula	C26 H26 N6 O6	
Formula weight	518.53	
Temperature	173(2) K	
Wavelength	0.71073 Å	
Crystal system	Monoclinic	
Space group	P2(1)/n	
Unit cell dimensions	a = 9.4746(6) Å	α = 90°.
	b = 7.2787(4) Å	β = 94.562(3)°.
	c = 17.6857(12) Å	γ = 90°.
Volume	1215.79(13) $Å^3$	
Z	2	
Density (calculated)	1.416 g/cm^3	
Absorption coefficient	0.103 mm^{-1}	
F(000)	544	
Crystal size	0.40 x 0.35 x 0.25 mm^3	
Theta range for data collection	2.31 to 28.30°.	
Index ranges	-12<=h<=11, -8<=k<=9, -23<=l<=23	
Reflections collected	14011	
Independent reflections	2905 [R(int) = 0.1233]	
Completeness to theta = 28.30°	96.0 %	
Absorption correction	None	
Refinement method	Full-matrix least-squares on F^2	
Data / restraints / parameters	2905 / 0 / 182	
Goodness-of-fit on F^2	1.129	
Final R indices [I>2sigma(I)]	R1 = 0.0557, wR2 = 0.1467	
R indices (all data)	R1 = 0.0667, wR2 = 0.1602	
Extinction coefficient	0.084(10)	
Largest diff. peak and hole	0.458 and -0.318 $e.Å^{-3}$	

Table A.15 Crystal data and structure refinement for **4a**.

Empirical formula	C20 H20 N4 O5	
Formula weight	396.40	
Temperature	120(2) K	
Wavelength	0.71073 Å	
Crystal system	Monoclinic	
Space group	P2(1)/c	
Unit cell dimensions	a = 8.0769(6) Å	α = 90°.
	b = 25.5225(18) Å	β = 98.457(4)°.
	c = 9.1601(6) Å	γ = 90°.
Volume	1867.8(2) $Å^3$	
Z	4	
Density (calculated)	1.410 g/cm^3	
Absorption coefficient	0.104 mm^{-1}	
F(000)	832	
Crystal size	0.20 x 0.20 x 0.08 mm^3	
Theta range for data collection	1.60 to 31.50°.	
Index ranges	-11<=h<=11, -37<=k<=37, -13<=l<=13	
Reflections collected	44009	
Independent reflections	6203 [R(int) = 0.0603]	
Completeness to theta = 31.50°	99.8 %	
Absorption correction	None	
Max. and min. transmission	0.9918 and 0.9796	
Refinement method	Full-matrix least-squares on F^2	
Data / restraints / parameters	6203 / 0 / 273	
Goodness-of-fit on F^2	1.404	
Final R indices [I>2sigma(I)]	R1 = 0.0720, wR2 = 0.2000	
R indices (all data)	R1 = 0.1117, wR2 = 0.2185	
Largest diff. peak and hole	0.472 and -0.427 $e.Å^{-3}$	

Table A.16 Crystal data and structure refinement for **4b**.

Empirical formula	C20 H21 N3 O4	
Formula weight	367.40	
Temperature	120(2) K	
Wavelength	0.71073 Å	
Crystal system	Monoclinic	
Space group	P2(1)/n	
Unit cell dimensions	a = 8.2057(6) Å	α = 90°.
	b = 10.8322(8) Å	β = 90.027(3)°.
	c = 20.4551(14) Å	γ = 90°.
Volume	1818.2(2) $Å^3$	
Z	4	
Density (calculated)	1.342 g/cm^3	
Absorption coefficient	0.095 mm^{-1}	
F(000)	776	
Crystal size	0.30 x 0.25 x 0.20 mm^3	
Theta range for data collection	1.99 to 30.48°.	
Index ranges	-10<=h<=11, -12<=k<=15, -29<=l<=29	
Reflections collected	33960	
Independent reflections	5529 [R(int) = 0.0348]	
Completeness to theta = 30.48°	99.8 %	
Absorption correction	None	
Max. and min. transmission	0.9812 and 0.9721	
Refinement method	Full-matrix least-squares on F^2	
Data / restraints / parameters	5529 / 0 / 258	
Goodness-of-fit on F^2	1.035	
Final R indices [I>2sigma(I)]	R1 = 0.0412, wR2 = 0.1088	
R indices (all data)	R1 = 0.0544, wR2 = 0.1175	
Largest diff. peak and hole	0.362 and -0.240 $e.Å^{-3}$	

Table A.17 Crystal data and structure refinement for **4c**.

Empirical formula	C17 H19 N3 O5	
Formula weight	345.35	
Temperature	100(2) K	
Wavelength	0.71073 Å	
Crystal system	Monoclinic	
Space group	P2(1)/n	
Unit cell dimensions	a = 14.6443(14) Å	α = 90°.
	b = 5.8392(5) Å	β = 99.294(2)°.
	c = 19.4017(18) Å	γ = 90°.
Volume	1637.3(3) $Å^3$	
Z	4	
Density (calculated)	1.401 g/cm^3	
Absorption coefficient	0.105 mm^{-1}	
F(000)	728	
Crystal size	0.36 x 0.34 x 0.14 mm^3	
Theta range for data collection	1.90 to 28.28°.	
Index ranges	-15<=h<=19, -7<=k<=7, -24<=l<=24	
Reflections collected	9283	
Independent reflections	3777 [R(int) = 0.0256]	
Completeness to theta = 28.28°	93.2 %	
Absorption correction	None	
Refinement method	Full-matrix least-squares on F^2	
Data / restraints / parameters	3777 / 0 / 240	
Goodness-of-fit on F^2	1.038	
Final R indices [I>2sigma(I)]	R1 = 0.0440, wR2 = 0.1170	
R indices (all data)	R1 = 0.0519, wR2 = 0.1232	
Largest diff. peak and hole	0.391 and -0.266 $e.Å^{-3}$	

Table A.18 Crystal data and structure refinement for **8a**.

Empirical formula	C15 H17 N3 O6	
Formula weight	335.32	
Temperature	173(2) K	
Wavelength	0.71073 Å	
Crystal system	Monoclinic	
Space group	C2/c	
Unit cell dimensions	a = 21.5505(18) Å	α = 90°.
	b = 5.3999(5) Å	β = 108.270(5)°.
	c = 27.549(2) Å	γ = 90°.
Volume	3044.3(5) $Å^3$	
Z	8	
Density (calculated)	1.463 g/cm^3	
Absorption coefficient	0.115 mm^{-1}	
F(000)	1408	
Crystal size	0.45 x 0.40 x 0.15 mm^3	
Theta range for data collection	1.56 to 28.22°.	
Index ranges	-27<=h<=26, -7<=k<=7, -32<=l<=35	
Reflections collected	10307	
Independent reflections	3538 [R(int) = 0.1314]	
Completeness to theta = 28.22°	94.1 %	
Absorption correction	None	
Refinement method	Full-matrix least-squares on F^2	
Data / restraints / parameters	3538 / 23 / 254	
Goodness-of-fit on F^2	1.042	
Final R indices [I>2sigma(I)]	R1 = 0.0686, wR2 = 0.1719	
R indices (all data)	R1 = 0.0997, wR2 = 0.1893	
Largest diff. peak and hole	0.408 and -0.463 $e.Å^{-3}$	

Table A.19 Crystal data and structure refinement for **8b**.

Empirical formula	C25 H19 N7 O13	
Formula weight	625.47	
Temperature	100(2) K	
Wavelength	0.71073 Å	
Crystal system	Monoclinic	
Space group	C2/c	
Unit cell dimensions	a = 26.096(6) Å	α = 90°.
	b = 17.294(4) Å	β = 118.080(4)°.
	c = 13.247(3) Å	γ = 90°.
Volume	5275(2) $Å^3$	
Z	8	
Density (calculated)	1.575 g/cm^3	
Absorption coefficient	0.130 mm^{-1}	
F(000)	2576	
Crystal size	? x ? x ? mm^3	
Theta range for data collection	2.67 to 27.15°.	
Index ranges	-32<=h<=32, -22<=k<=22, -16<=l<=16	
Reflections collected	24280	
Independent reflections	5515 [R(int) = 0.0696]	
Completeness to theta = 27.15°	94.5 %	
Absorption correction	None	
Refinement method	Full-matrix least-squares on F^2	
Data / restraints / parameters	5515 / 0 / 418	
Goodness-of-fit on F^2	1.006	
Final R indices [I>2sigma(I)]	R1 = 0.0475, wR2 = 0.1015	
R indices (all data)	R1 = 0.1027, wR2 = 0.1231	
Largest diff. peak and hole	0.221 and -0.318 $e.Å^{-3}$	

Table A.20 Crystal data and structure refinement for **15a**.

Empirical formula	C20 H16 N4 O4	
Formula weight	376.37	
Temperature	100(2) K	
Wavelength	0.71073 Å	
Crystal system	Monoclinic	
Space group	P2(1)/c	
Unit cell dimensions	a = 6.9835(4) Å	α = 90°.
	b = 30.8648(16) Å	β = 93.4490(10)°.
	c = 8.0398(4) Å	γ = 90°.
Volume	1729.79(16) $Å^3$	
Z	4	
Density (calculated)	1.445 Mg/m^3	
Absorption coefficient	0.104 mm^{-1}	
F(000)	784	
Crystal size	0.53 x 0.36 x 0.17 mm^3	
Theta range for data collection	2.62 to 28.32°.	
Index ranges	-9<=h<=9, -39<=k<=40, -10<=l<=10	
Reflections collected	13938	
Independent reflections	4014 [R(int) = 0.0231]	
Completeness to theta = 25.00°	99.8 %	
Absorption correction	None	
Refinement method	Full-matrix least-squares on F^2	
Data / restraints / parameters	4014 / 0 / 256	
Goodness-of-fit on F^2	1.050	
Final R indices [I>2sigma(I)]	R1 = 0.0423, wR2 = 0.1059	
R indices (all data)	R1 = 0.0454, wR2 = 0.1081	
Largest diff. peak and hole	0.383 and -0.238 $e.Å^{-3}$	

Table A.21 Crystal data and structure refinement for **15b**.

Empirical formula	C20 H15 N5 O6	
Formula weight	421.37	
Temperature	100(2) K	
Wavelength	0.71073 Å	
Crystal system	Monoclinic	
Space group	P2(1)/n	
Unit cell dimensions	a = 12.2436(14) Å	α = 90°.
	b = 7.3976(8) Å	β = 95.480(2)°.
	c = 20.422(2) Å	γ = 90°.
Volume	1841.2(4) $Å^3$	
Z	4	
Density (calculated)	1.520 g/cm^3	
Absorption coefficient	0.116 mm^{-1}	
F(000)	872	
Crystal size	0.34 x 0.24 x 0.14 mm^3	
Theta range for data collection	2.93 to 30.00°.	
Index ranges	-9<=h<=17, -5<=k<=10, -28<=l<=25	
Reflections collected	10436	
Independent reflections	5160 [R(int) = 0.0363]	
Completeness to theta = 30.00°	95.8 %	
Absorption correction	None	
Refinement method	Full-matrix least-squares on F^2	
Data / restraints / parameters	5160 / 0 / 283	
Goodness-of-fit on F^2	1.082	
Final R indices [I>2sigma(I)]	R1 = 0.0580, wR2 = 0.1453	
R indices (all data)	R1 = 0.0649, wR2 = 0.1510	
Largest diff. peak and hole	0.591 and -0.388 $e.Å^{-3}$	

Table A.22 Crystal data and structure refinement for **15c**.

Empirical formula	C17 H17 N3 O4	
Formula weight	327.34	
Temperature	173(2) K	
Wavelength	0.71073 Å	
Crystal system	Monoclinic	
Space group	C2/c	
Unit cell dimensions	a = 37.956(2) Å	α = 90°.
	b = 4.9029(3) Å	β = 93.700(3)°.
	c = 17.0897(12) Å	γ = 90°.
Volume	3173.6(4) $Å^3$	
Z	8	
Density (calculated)	1.370 g/cm^3	
Absorption coefficient	0.100 mm^{-1}	
F(000)	1376	
Crystal size	0.40 x 0.35 x 0.20 mm^3	
Theta range for data collection	2.15 to 28.30°.	
Index ranges	-49<=h<=50, -6<=k<=6, -21<=l<=21	
Reflections collected	11312	
Independent reflections	3742 [R(int) = 0.1244]	
Completeness to theta = 28.30°	94.5 %	
Absorption correction	None	
Refinement method	Full-matrix least-squares on F^2	
Data / restraints / parameters	3742 / 0 / 223	
Goodness-of-fit on F^2	1.069	
Final R indices [I>2sigma(I)]	R1 = 0.0604, wR2 = 0.1624	
R indices (all data)	R1 = 0.0813, wR2 = 0.1844	
Largest diff. peak and hole	0.366 and -0.269 $e.Å^{-3}$	

Table A.23 Crystal data and structure refinement for **17a**.

Empirical formula	C27 H21 N5 O8	
Formula weight	543.49	
Temperature	100(2) K	
Wavelength	0.71073 Å	
Crystal system	Triclinic	
Space group	P-1	
Unit cell dimensions	a = 8.4037(5) Å	α = 90.0880(10)°.
	b = 10.9449(6) Å	β = 101.5130(10)°.
	c = 13.4142(8) Å	γ = 92.0180(10)°.
Volume	1208.19(12) $Å^3$	
Z	2	
Density (calculated)	1.494 g/cm^3	
Absorption coefficient	0.113 mm^{-1}	
F(000)	564	
Crystal size	0.56 x 0.40 x 0.28 mm^3	
Theta range for data collection	2.41 to 30.05°.	
Index ranges	-11<=h<=11, -15<=k<=15, -18<=l<=18	
Reflections collected	13938	
Independent reflections	6908 [R(int) = 0.0244]	
Completeness to theta = 30.05°	97.4 %	
Absorption correction	None	
Refinement method	Full-matrix least-squares on F^2	
Data / restraints / parameters	6908 / 0 / 367	
Goodness-of-fit on F^2	1.051	
Final R indices [I>2sigma(I)]	R1 = 0.0449, wR2 = 0.1227	
R indices (all data)	R1 = 0.0494, wR2 = 0.1268	
Largest diff. peak and hole	0.480 and -0.367 $e.Å^{-3}$	

Table A.24 Crystal data and structure refinement for **17b**.

Empirical formula	C20 H15 N5 O6	
Formula weight	421.37	
Temperature	173(2) K	
Wavelength	0.71073 Å	
Crystal system	Monoclinic	
Space group	P2(1)/c	
Unit cell dimensions	a = 19.2124(16) Å	α = 90°.
	b = 13.4369(12) Å	β = 104.943(6)°.
	c = 15.1052(14) Å	γ = 90°.
Volume	3767.6(6) $Å^3$	
Z	8	
Density (calculated)	1.486 g/cm^3	
Absorption coefficient	0.113 mm^{-1}	
F(000)	1744	
Crystal size	0.25 x 0.20 x 0.20 mm^3	
Theta range for data collection	1.10 to 28.36°.	
Index ranges	-25<=h<=22, -17<=k<=17, -19<=l<=17	
Reflections collected	26918	
Independent reflections	8695 [R(int) = 0.1702]	
Completeness to theta = 28.36°	92.3 %	
Absorption correction	None	
Refinement method	Full-matrix least-squares on F^2	
Data / restraints / parameters	8695 / 0 / 559	
Goodness-of-fit on F^2	1.066	
Final R indices [I>2sigma(I)]	R1 = 0.1039, wR2 = 0.2468	
R indices (all data)	R1 = 0.2584, wR2 = 0.2952	
Largest diff. peak and hole	1.018 and -0.415 $e.Å^{-3}$	

Table A.25 Crystal data and structure refinement for **20**.

Empirical formula	C14 H16 N6	
Formula weight	268.33	
Temperature	120(2) K	
Wavelength	0.71073 Å	
Crystal system	Monoclinic	
Space group	P2(1)/c	
Unit cell dimensions	a = 15.1130(16) Å	α = 90°.
	b = 3.9871(4) Å	β = 95.549(6)°.
	c = 22.050(2) Å	γ = 90°.
Volume	1322.4(2) $Å^3$	
Z	4	
Density (calculated)	1.348 g/cm^3	
Absorption coefficient	0.087 mm^{-1}	
F(000)	568	
Crystal size	0.25 x 0.10 x 0.05 mm^3	
Theta range for data collection	1.86 to 30.50°.	
Index ranges	-21<=h<=20, -5<=k<=5, -31<=l<=31	
Reflections collected	22961	
Independent reflections	3970 [R(int) = 0.0434]	
Completeness to theta = 30.50°	98.0 %	
Absorption correction	None	
Max. and min. transmission	0.9956 and 0.9785	
Refinement method	Full-matrix least-squares on F^2	
Data / restraints / parameters	3970 / 0 / 185	
Goodness-of-fit on F^2	1.026	
Final R indices [I>2sigma(I)]	R1 = 0.0471, wR2 = 0.1099	
R indices (all data)	R1 = 0.0867, wR2 = 0.1261	
Largest diff. peak and hole	0.295 and -0.253 $e.Å^{-3}$	

Table A.26 Crystal data and structure refinement for **19a**.

Empirical formula	C17 H13 N7 O4	
Formula weight	379.34	
Temperature	133(2) K	
Wavelength	0.71073 Å	
Crystal system	Triclinic	
Space group	P-1	
Unit cell dimensions	a = 3.7754(5) Å	α = 87.131(7)°.
	b = 11.0619(13) Å	β = 89.574(7)°.
	c = 19.509(2) Å	γ = 85.800(7)°.
Volume	811.53(17) $Å^3$	
Z	2	
Density (calculated)	1.552 g/cm^3	
Absorption coefficient	0.116 mm^{-1}	
F(000)	392	
Crystal size	0.30 x 0.16 x 0.08 mm^3	
Theta range for data collection	1.85 to 29.57°.	
Index ranges	-5<=h<=5, -15<=k<=15, -27<=l<=27	
Reflections collected	26179	
Independent reflections	4556 [R(int) = 0.0532]	
Completeness to theta = 29.57°	100.0 %	
Absorption correction	None	
Max. and min. transmission	0.9908 and 0.9660	
Refinement method	Full-matrix least-squares on F^2	
Data / restraints / parameters	4556 / 0 / 256	
Goodness-of-fit on F^2	1.020	
Final R indices [I>2sigma(I)]	R1 = 0.0504, wR2 = 0.1146	
R indices (all data)	R1 = 0.0987, wR2 = 0.1363	
Largest diff. peak and hole	0.247 and -0.300 $e.Å^{-3}$	

Table A.27 Crystal data and structure refinement for **19b**.

Empirical formula	C17 H12 N8 O6	
Formula weight	424.35	
Temperature	173(2) K	
Wavelength	0.71073 Å	
Crystal system	Orthorhombic	
Space group	Pbca	
Unit cell dimensions	a = 19.6259(15) Å	α = 90°.
	b = 14.3503(10) Å	β = 90°.
	c = 37.921(3) Å	γ = 90°.
Volume	10680.0(13) $Å^3$	
Z	24	
Density (calculated)	1.583 g/cm^3	
Absorption coefficient	0.125 mm^{-1}	
F(000)	5232	
Crystal size	0.35 x 0.30 x 0.20 mm^3	
Theta range for data collection	1.07 to 28.38°.	
Index ranges	-24<=h<=26, -18<=k<=19, -50<=l<=50	
Reflections collected	77223	
Independent reflections	12702 [R(int) = 0.1344]	
Completeness to theta = 28.38°	94.9 %	
Absorption correction	None	
Refinement method	Full-matrix least-squares on F^2	
Data / restraints / parameters	12702 / 0 / 847	
Goodness-of-fit on F^2	0.945	
Final R indices [I>2sigma(I)]	R1 = 0.0532, wR2 = 0.1265	
R indices (all data)	R1 = 0.1220, wR2 = 0.1549	
Largest diff. peak and hole	0.295 and -0.285 $e.Å^{-3}$	

Table A.28 Crystal data and structure refinement for **20a**.

Empirical formula	C14 H16 Cl2 Cu N6	
Formula weight	402.77	
Temperature	133(2) K	
Wavelength	0.71073 Å	
Crystal system	Monoclinic	
Space group	P2(1)/c	
Unit cell dimensions	a = 10.6585(6) Å	α = 90°.
	b = 16.5865(9) Å	β = 92.459(3)°.
	c = 18.4152(11) Å	γ = 90°.
Volume	3252.6(3) $Å^3$	
Z	8	
Density (calculated)	1.645 g/cm^3	
Absorption coefficient	1.679 mm^{-1}	
F(000)	1640	
Crystal size	0.25 x 0.15 x 0.10 mm^3	
Theta range for data collection	1.91 to 29.57°.	
Index ranges	-14<=h<=14, -23<=k<=16, -25<=l<=21	
Reflections collected	69657	
Independent reflections	9108 [R(int) = 0.0677]	
Completeness to theta = 29.57°	100.0 %	
Absorption correction	None	
Max. and min. transmission	0.8501 and 0.6790	
Refinement method	Full-matrix least-squares on F^2	
Data / restraints / parameters	9108 / 0 / 423	
Goodness-of-fit on F^2	1.012	
Final R indices [I>2sigma(I)]	R1 = 0.0494, wR2 = 0.1162	
R indices (all data)	R1 = 0.0923, wR2 = 0.1368	
Largest diff. peak and hole	0.588 and -1.623 $e.Å^{-3}$	

Table A.29 Crystal data and structure refinement for **2i**.

Empirical formula	C42 H26 Cu2 F24 N6 O10	
Formula weight	1357.77	
Temperature	100(2) K	
Wavelength	0.71073 Å	
Crystal system	Monoclinic	
Space group	P2(1)/n	
Unit cell dimensions	a = 9.7354(11) Å	α = 90°.
	b = 11.1497(12) Å	β = 96.985(2)°.
	c = 23.870(3) Å	γ = 90°.
Volume	2571.8(5) $Å^3$	
Z	2	
Density (calculated)	1.753 g/cm^3	
Absorption coefficient	0.975 mm^{-1}	
F(000)	1348	
Crystal size	0.41 x 0.13 x 0.13 mm^3	
Theta range for data collection	2.02 to 30.01°.	
Index ranges	-13<=h<=13, -15<=k<=15, -33<=l<=29	
Reflections collected	24508	
Independent reflections	7477 [R(int) = 0.0295]	
Completeness to theta = 30.01°	99.6 %	
Absorption correction	Semi-empirical from equivalents	
Max. and min. transmission	1.000 and 0.672	
Refinement method	Full-matrix least-squares on F^2	
Data / restraints / parameters	7477 / 0 / 385	
Goodness-of-fit on F^2	1.021	
Final R indices [I>2sigma(I)]	R1 = 0.0365, wR2 = 0.0933	
R indices (all data)	R1 = 0.0430, wR2 = 0.0972	
Largest diff. peak and hole	0.620 and -0.279 $e.Å^{-3}$	

Table A.30 Crystal data and structure refinement for **2j**.

Empirical formula	C86 H78 N6 Ni2 O12	
Formula weight	1504.96	
Temperature	100(2) K	
Wavelength	0.71073 Å	
Crystal system	Triclinic	
Space group	P-1	
Unit cell dimensions	a = 9.0170(6) Å	α = 86.3190(10)°.
	b = 12.3493(8) Å	β = 78.0890(10)°.
	c = 17.6357(12) Å	γ = 72.2410(10)°.
Volume	1830.0(2) $Å^3$	
Z	1	
Density (calculated)	1.366 Mg/m^3	
Absorption coefficient	0.584 mm^{-1}	
F(000)	788	
Crystal size	0.38 x 0.24 x 0.16 mm^3	
Theta range for data collection	2.09 to 30.02°.	
Index ranges	-12<=h<=12, -17<=k<=17, -24<=l<=24	
Reflections collected	21060	
Independent reflections	10465 [R(int) = 0.0193]	
Completeness to theta = 30.02°	97.8 %	
Absorption correction	Semi-empirical from equivalents	
Max. and min. transmission	1.000 and 0.811	
Refinement method	Full-matrix least-squares on F^2	
Data / restraints / parameters	10465 / 0 / 481	
Goodness-of-fit on F^2	1.044	
Final R indices [I>2sigma(I)]	R1 = 0.0490, wR2 = 0.1206	
R indices (all data)	R1 = 0.0584, wR2 = 0.1260	
Largest diff. peak and hole	1.129 and -0.284 $e.Å^{-3}$	

Table A.31 Crystal data and structure refinement for **8c**.

Empirical formula	C42 H26 Cu2 F24 N6 O10	
Formula weight	1357.77	
Temperature	100(2) K	
Wavelength	0.71073 Å	
Crystal system	Monoclinic	
Space group	P2(1)/c	
Unit cell dimensions	a = 10.0325(10) Å	α = 90°.
	b = 15.1765(15) Å	β = 99.957(2)°.
	c = 16.6440(16) Å	γ = 90°.
Volume	2496.0(4) $Å^3$	
Z	2	
Density (calculated)	1.807 g/cm^3	
Absorption coefficient	1.005 mm^{-1}	
F(000)	1348	
Crystal size	0.36 x 0.26 x 0.13 mm^3	
Theta range for data collection	2.06 to 30.11°.	
Index ranges	-14<=h<=12, -21<=k<=21, -23<=l<=23	
Reflections collected	28577	
Independent reflections	7318 [R(int) = 0.0302]	
Completeness to theta = 30.11°	99.4 %	
Absorption correction	Semi-empirical from equivalents	
Max. and min. transmission	1.000 and 0.784	
Refinement method	Full-matrix least-squares on F^2	
Data / restraints / parameters	7318 / 0 / 413	
Goodness-of-fit on F^2	1.114	
Final R indices [I>2sigma(I)]	R1 = 0.0356, wR2 = 0.0925	
R indices (all data)	R1 = 0.0417, wR2 = 0.0956	
Largest diff. peak and hole	0.601 and -0.455 $e.Å^{-3}$	

Table A.32 Crystal data and structure refinement for **2k**.

Empirical formula	C34 H40 Cu2 N8 O10	
Formula weight	847.82	
Temperature	173(2) K	
Wavelength	0.71073 Å	
Crystal system	Triclinic	
Space group	P-1	
Unit cell dimensions	a = 7.5896(5) Å	α = 68.531(4)°.
	b = 10.0990(7) Å	β = 82.310(3)°.
	c = 13.3959(8) Å	γ = 72.114(3)°.
Volume	909.07(10) $Å^3$	
Z	1	
Density (calculated)	1.549 g/cm^3	
Absorption coefficient	1.238 mm^{-1}	
F(000)	438	
Crystal size	0.30 x 0.25 x 0.15 mm^3	
Theta range for data collection	1.63 to 28.28°.	
Index ranges	-10<=h<=10, -12<=k<=13, -17<=l<=17	
Reflections collected	14172	
Independent reflections	4271 [R(int) = 0.1187]	
Completeness to theta = 28.28°	94.6 %	
Absorption correction	Semi-empirical from equivalents	
Max. and min. transmission	1.000 and 0.763	
Refinement method	Full-matrix least-squares on F^2	
Data / restraints / parameters	4271 / 0 / 253	
Goodness-of-fit on F^2	1.080	
Final R indices [I>2sigma(I)]	R1 = 0.0529, wR2 = 0.1370	
R indices (all data)	R1 = 0.0600, wR2 = 0.1436	
Largest diff. peak and hole	0.861 and -0.783 $e.Å^{-3}$	

Table A.33 Crystal data and structure refinement for **2l**.

Empirical formula	C50 H38 Cu2 F4 N6 O10	
Formula weight	1085.94	
Temperature	173(2) K	
Wavelength	0.71073 Å	
Crystal system	Monoclinic	
Space group	P2(1)/n	
Unit cell dimensions	a = 10.8218(9) Å	α = 90°.
	b = 19.4000(14) Å	β = 108.346(4)°.
	c = 12.0541(8) Å	γ = 90°.
Volume	2402.0(3) $Å^3$	
Z	2	
Density (calculated)	1.501 g/cm^3	
Absorption coefficient	0.966 mm^{-1}	
F(000)	1108	
Crystal size	0.40 x 0.25 x 0.15 mm^3	
Theta range for data collection	2.07 to 28.33°.	
Index ranges	-14<=h<=14, -23<=k<=25, -15<=l<=14	
Reflections collected	17581	
Independent reflections	5679 [R(int) = 0.1125]	
Completeness to theta = 28.33°	94.8 %	
Absorption correction	None	
Refinement method	Full-matrix least-squares on F^2	
Data / restraints / parameters	5679 / 23 / 353	
Goodness-of-fit on F^2	1.069	
Final R indices [I>2sigma(I)]	R1 = 0.0548, wR2 = 0.1367	
R indices (all data)	R1 = 0.0674, wR2 = 0.1467	
Largest diff. peak and hole	0.436 and -1.095 $e.Å^{-3}$	

Table A.34 Crystal data and structure refinement for **8d**.

Empirical formula	C30 H34 Cu2 N6 O10	
Formula weight	765.71	
Temperature	100(2) K	
Wavelength	0.71073 Å	
Crystal system	Triclinic	
Space group	P-1	
Unit cell dimensions	a = 8.0173(4) Å	α = 110.1640(10)°.
	b = 10.1615(5) Å	β = 109.1250(10)°.
	c = 11.4846(6) Å	γ = 90.5040(10)°.
Volume	821.95(7) $Å^3$	
Z	1	
Density (calculated)	1.547 g/cm^3	
Absorption coefficient	1.359 mm^{-1}	
F(000)	394	
Crystal size	0.38 x 0.30 x 0.07 mm^3	
Theta range for data collection	2.02 to 30.00°.	
Index ranges	-11<=h<=10, -13<=k<=14, -16<=l<=16	
Reflections collected	9572	
Independent reflections	4714 [R(int) = 0.0210]	
Completeness to theta = 30.00°	98.2 %	
Absorption correction	None	
Refinement method	Full-matrix least-squares on F^2	
Data / restraints / parameters	4714 / 0 / 223	
Goodness-of-fit on F^2	1.082	
Final R indices [I>2sigma(I)]	R1 = 0.0304, wR2 = 0.0783	
R indices (all data)	R1 = 0.0325, wR2 = 0.0794	
Largest diff. peak and hole	0.660 and -0.311 $e.Å^{-3}$	

Table A.35 Crystal data and structure refinement for **33**.

Empirical formula	C21 H18 N6	
Formula weight	354.41	
Temperature	120(2) K	
Wavelength	0.71073 Å	
Crystal system	Triclinic	
Space group	P-1	
Unit cell dimensions	a = 9.7801(6) Å	α = 88.323(4)°.
	b = 10.0149(6) Å	β = 63.239(3)°.
	c = 10.7647(6) Å	γ = 83.908(3)°.
Volume	935.92(10) $Å^3$	
Z	2	
Density (calculated)	1.258 g/cm^3	
Absorption coefficient	0.079 mm^{-1}	
F(000)	372	
Crystal size	0.25 x 0.20 x 0.10 mm^3	
Theta range for data collection	2.95 to 32.57°.	
Index ranges	-14<=h<=14, -15<=k<=15, -16<=l<=16	
Reflections collected	39688	
Independent reflections	6760 [R(int) = 0.0597]	
Completeness to theta = 32.57°	99.0 %	
Absorption correction	None	
Max. and min. transmission	0.9921 and 0.9805	
Refinement method	Full-matrix least-squares on F^2	
Data / restraints / parameters	6760 / 0 / 250	
Goodness-of-fit on F^2	0.997	
Final R indices [I>2sigma(I)]	R1 = 0.0495, wR2 = 0.1210	
R indices (all data)	R1 = 0.0942, wR2 = 0.1423	
Largest diff. peak and hole	0.325 and -0.291 $e.Å^{-3}$	

Table A.36 Crystal data and structure refinement for **31a**.

Empirical formula	C21 H17 Cl2 Co N5	
Formula weight	469.23	
Temperature	173(2) K	
Wavelength	0.71073 Å	
Crystal system	Monoclinic	
Space group	P2(1)/c	
Unit cell dimensions	a = 14.0489(19) Å	α = 90°.
	b = 8.2425(11) Å	β = 105.025(7)°.
	c = 18.746(3) Å	γ = 90°.
Volume	2096.6(5) $Å^3$	
Z	4	
Density (calculated)	1.487 g/cm^3	
Absorption coefficient	1.091 mm^{-1}	
F(000)	956	
Crystal size	0.40 x 0.35 x 0.05 mm^3	
Theta range for data collection	1.50 to 28.19°.	
Index ranges	-18<=h<=18, -10<=k<=10, -24<=l<=24	
Reflections collected	15043	
Independent reflections	4843 [R(int) = 0.1432]	
Completeness to theta = 28.19°	93.9 %	
Absorption correction	Semi-empirical from equivalents	
Max. and min. transmission	1.000 and 0.570	
Refinement method	Full-matrix least-squares on F^2	
Data / restraints / parameters	4843 / 0 / 262	
Goodness-of-fit on F^2	0.875	
Final R indices [I>2sigma(I)]	R1 = 0.0555, wR2 = 0.1213	
R indices (all data)	R1 = 0.1131, wR2 = 0.1422	
Largest diff. peak and hole	0.737 and -0.699 $e.Å^{-3}$	

Table A.37 Crystal data and structure refinement for **33a**.

Empirical formula	C27 H27 Ag F6 N9 P	
Formula weight	730.42	
Temperature	120(2) K	
Wavelength	0.71073 Å	
Crystal system	Orthorhombic	
Space group	Pnna	
Unit cell dimensions	a = 14.134(8) Å	α = 90°.
	b = 26.513(15) Å	β = 90°.
	c = 17.588(10) Å	γ = 90°.
Volume	6591(7) $Å^3$	
Z	8	
Density (calculated)	1.472 g/cm^3	
Absorption coefficient	0.726 mm^{-1}	
F(000)	2944	
Crystal size	0.25 x 0.10 x 0.05 mm^3	
Theta range for data collection	1.54 to 29.58°.	
Index ranges	-19<=h<=18, -36<=k<=15, -21<=l<=21	
Reflections collected	26624	
Independent reflections	8521 [R(int) = 0.1291]	
Completeness to theta = 29.58°	91.9 %	
Absorption correction	None	
Max. and min. transmission	0.9646 and 0.8393	
Refinement method	Full-matrix least-squares on F^2	
Data / restraints / parameters	8521 / 63 / 451	
Goodness-of-fit on F^2	1.061	
Final R indices [I>2sigma(I)]	R1 = 0.0968, wR2 = 0.2666	
R indices (all data)	R1 = 0.2391, wR2 = 0.3349	
Largest diff. peak and hole	1.823 and -1.411 $e.Å^{-3}$	

Appendix B - ^{1}H and ^{13}C NMR Data

Figure B.1 ^{1}H NMR of **1**.

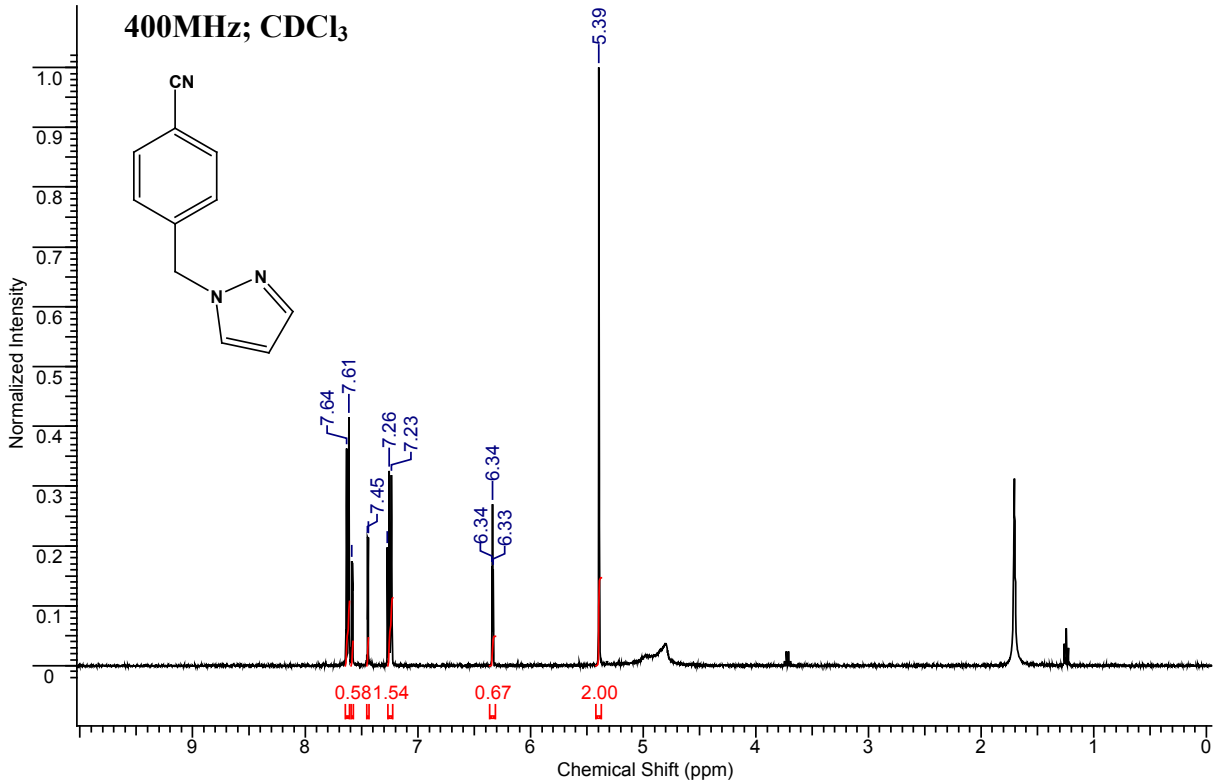

Figure B.2 (a) ^{1}H NMR and (b) ^{13}C NMR of **2**.

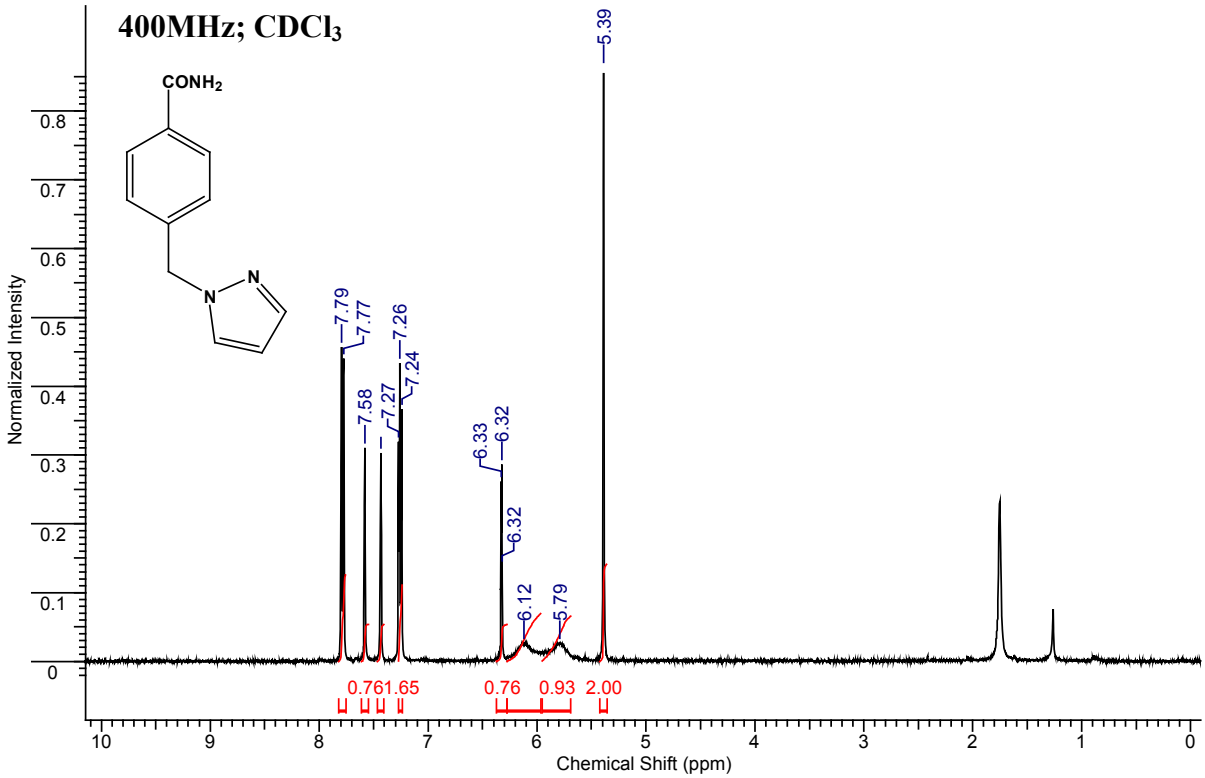

(a)

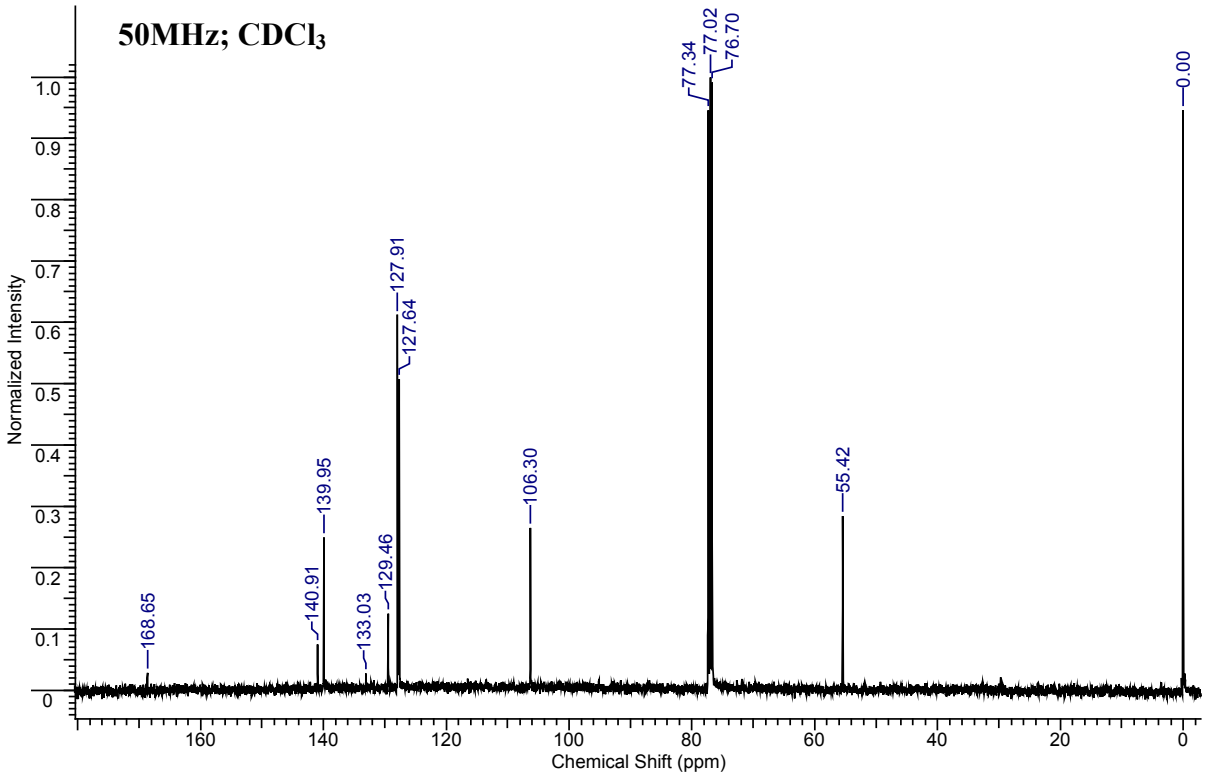

(b)

Figure B.3 ^{1}H NMR of **3**.

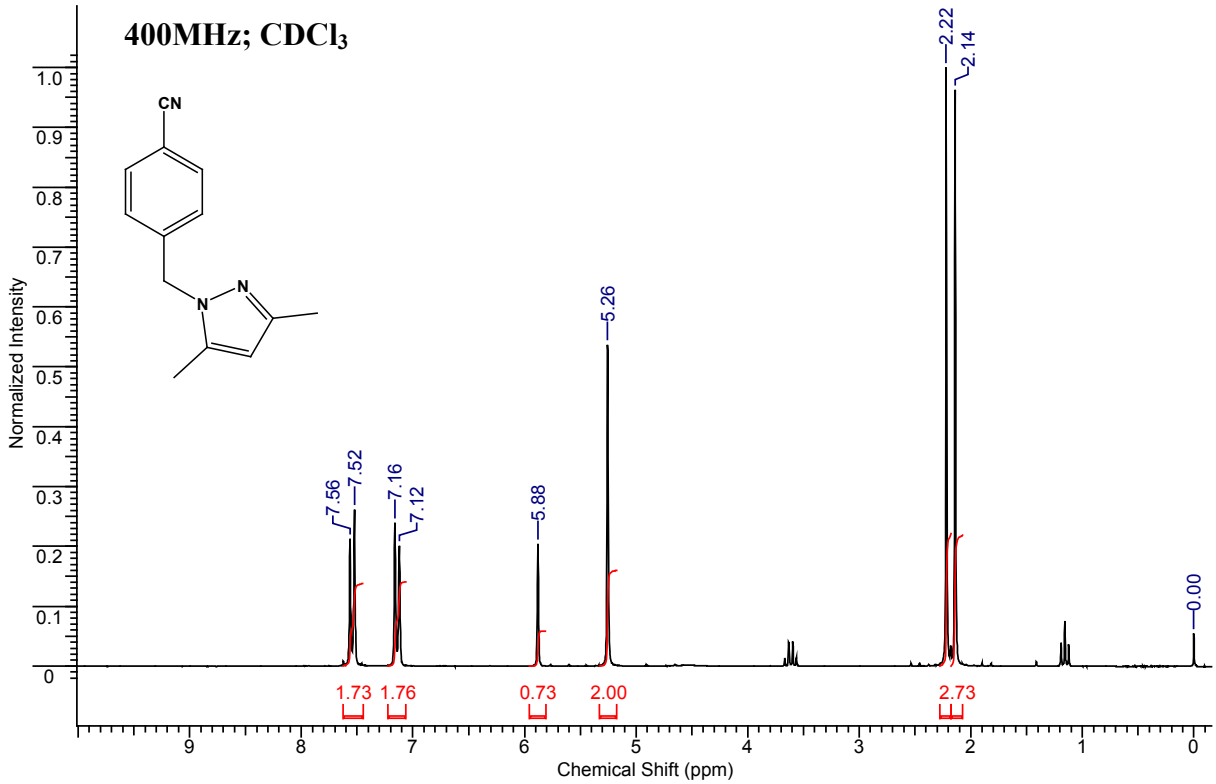

Figure B.4 (a) ^{1}H NMR and (b) ^{13}C NMR of **4**.

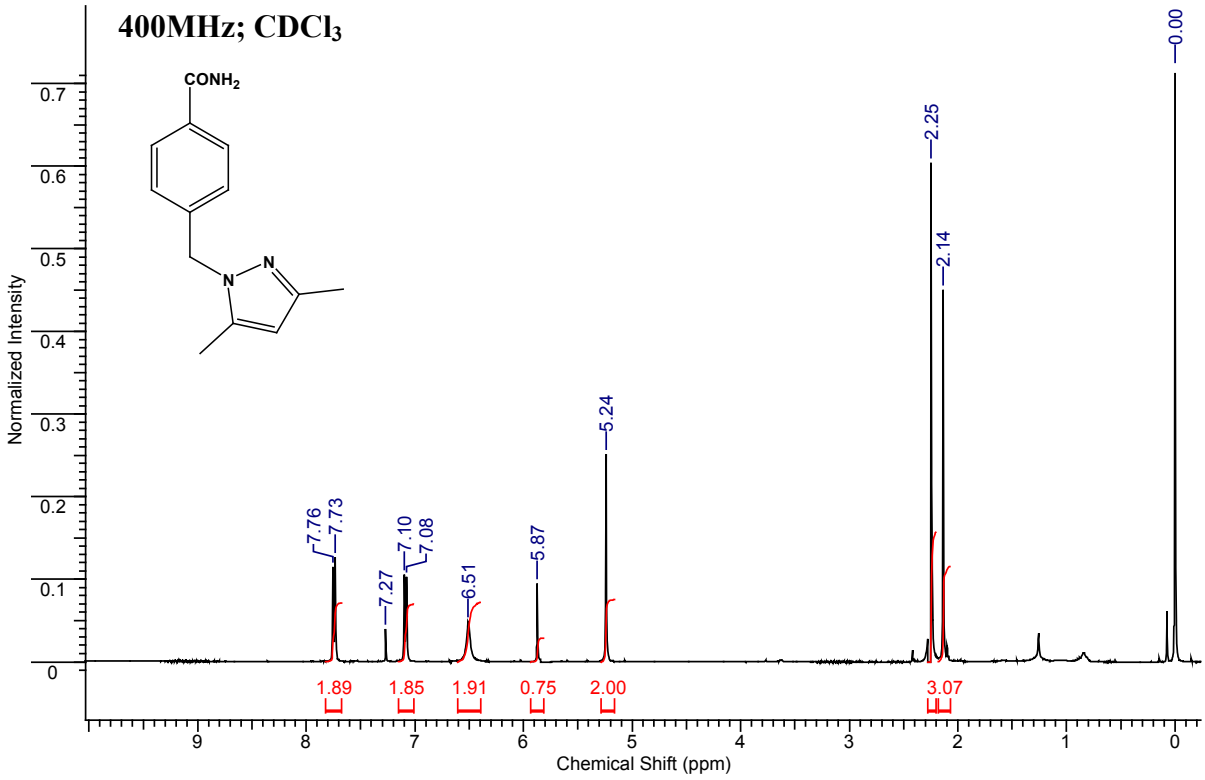

(a)

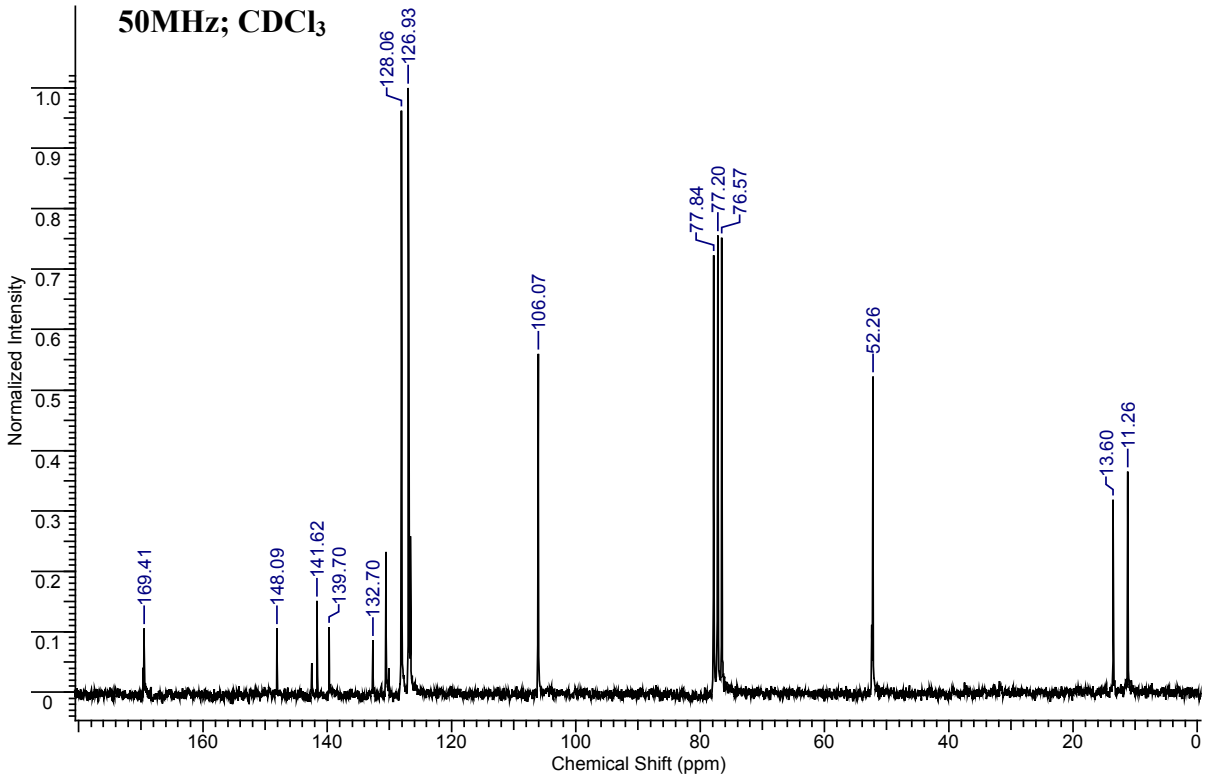

(b)

Figure B.5 ^{1}H NMR of **5**.

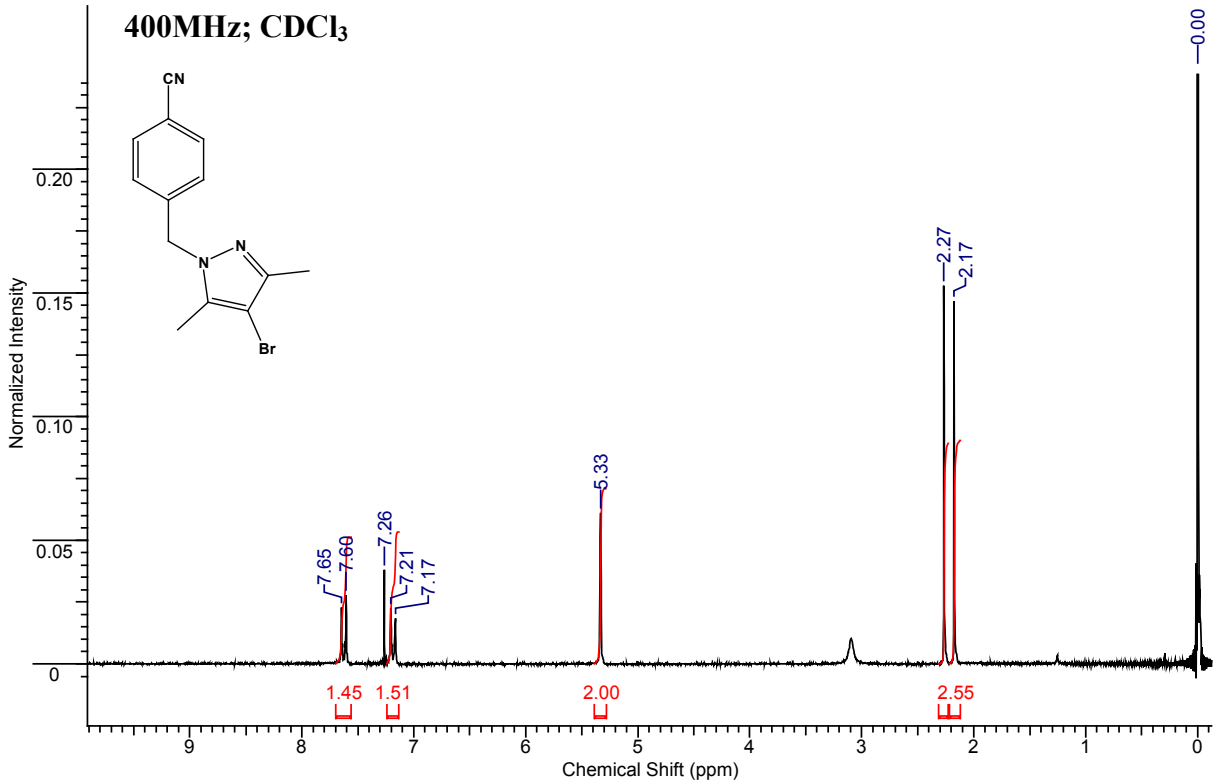

Figure B.6 (a) ^{1}H NMR and (b) ^{13}C NMR of **6**.

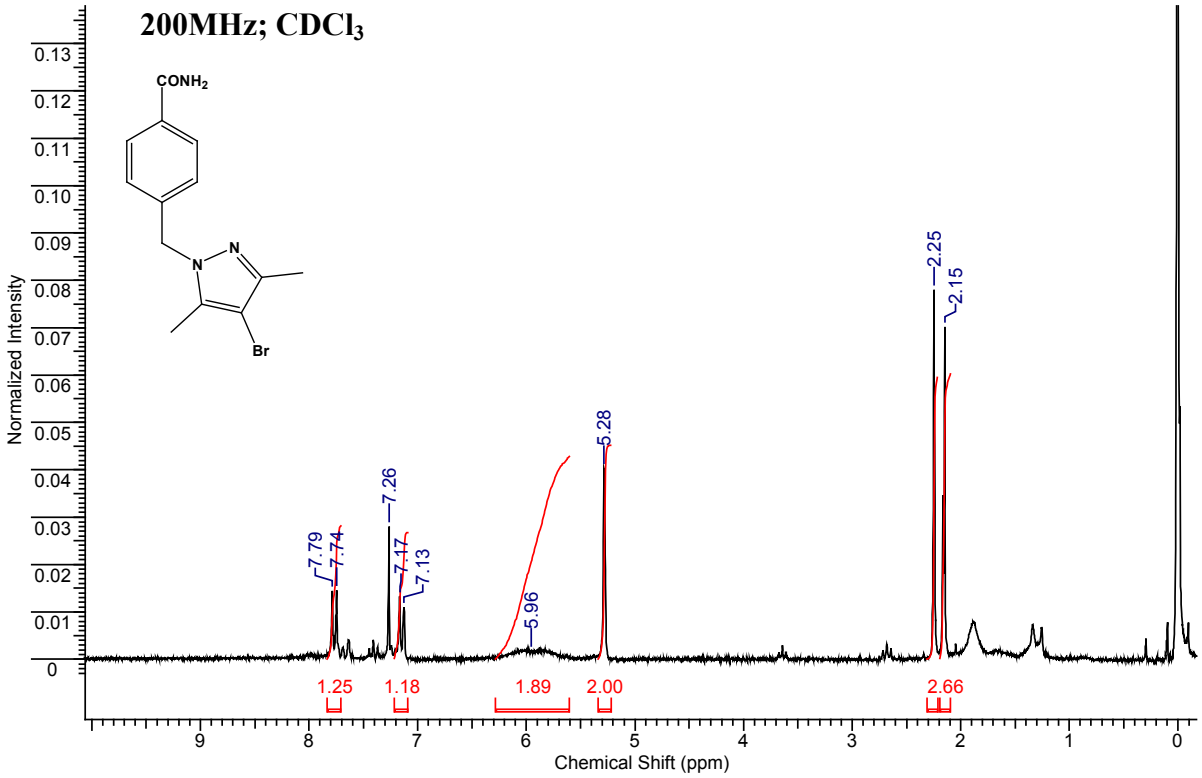

(a)

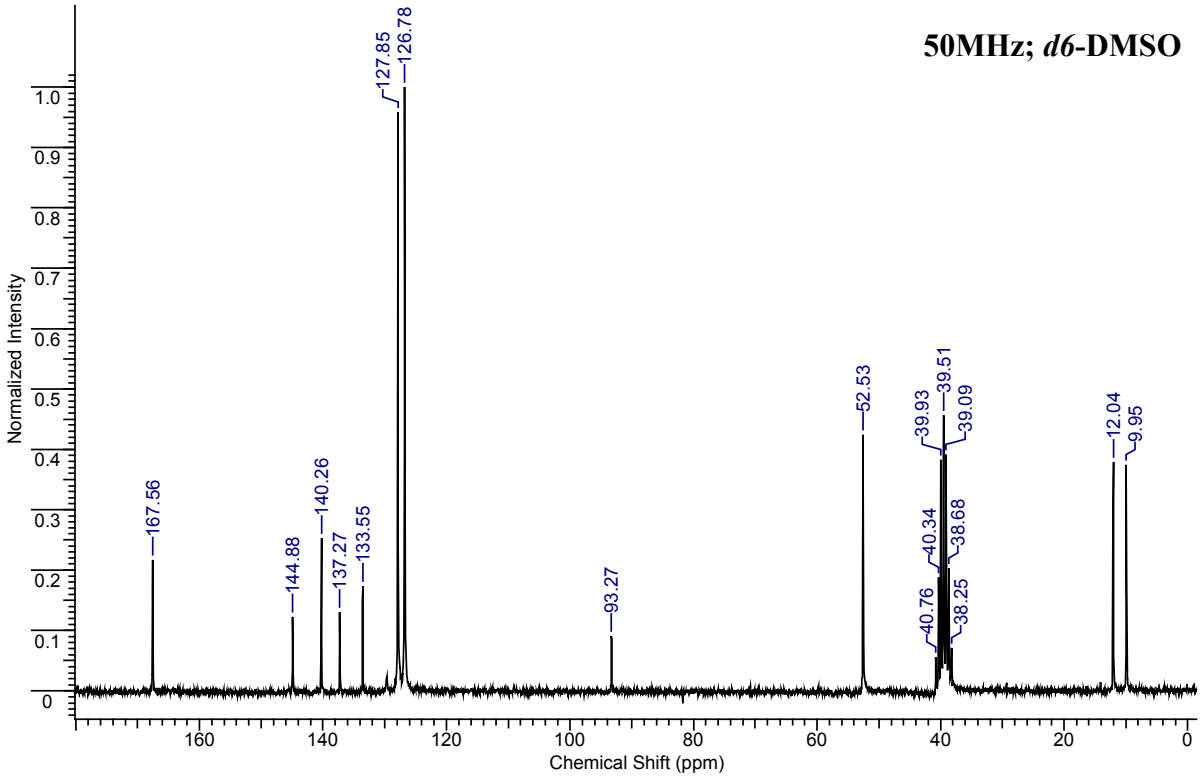

(b)

Figure B.7 ^{1}H NMR of **7**.

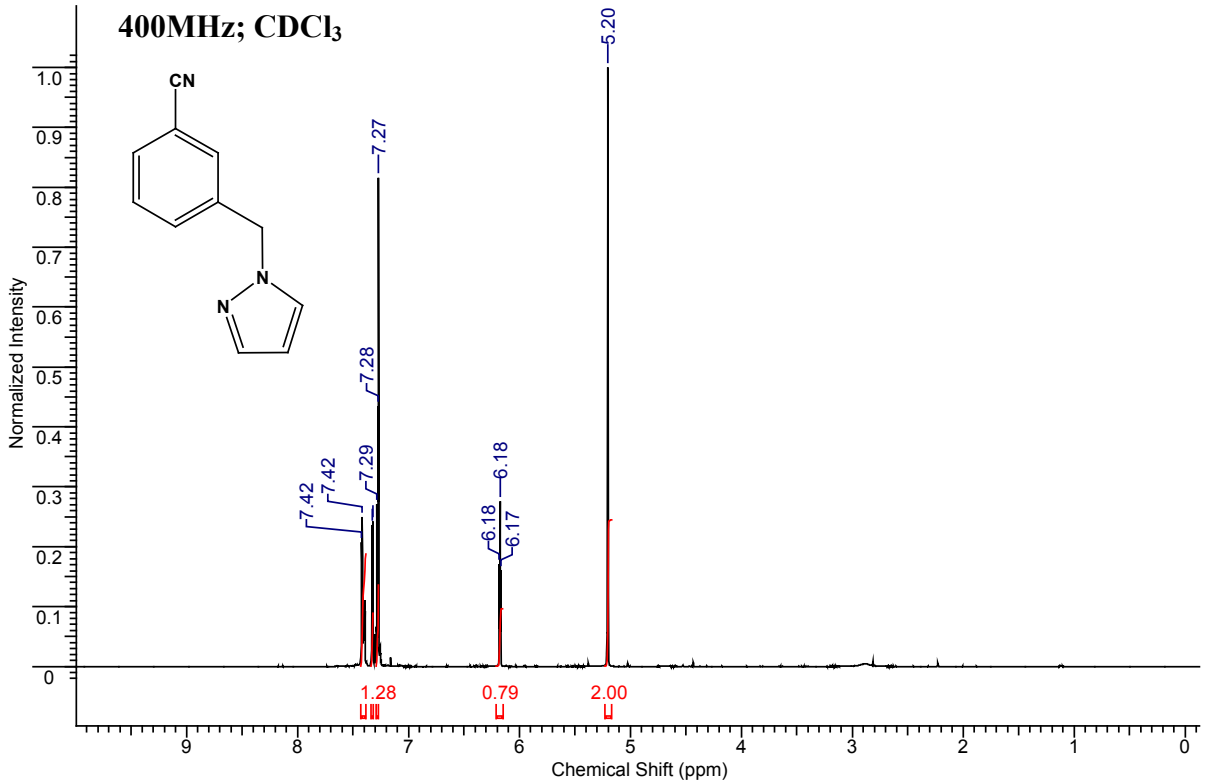

Figure B.8 (a) ^{1}H NMR and (b) ^{13}C NMR of **8**.

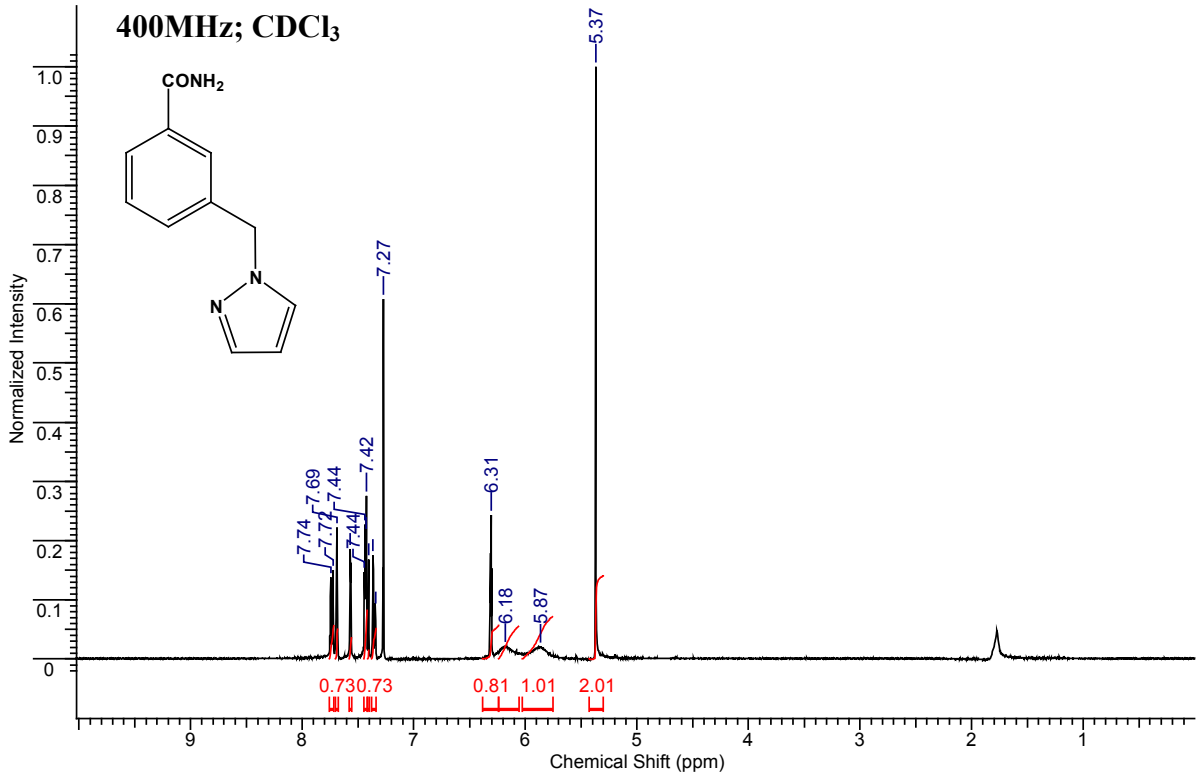

(a)

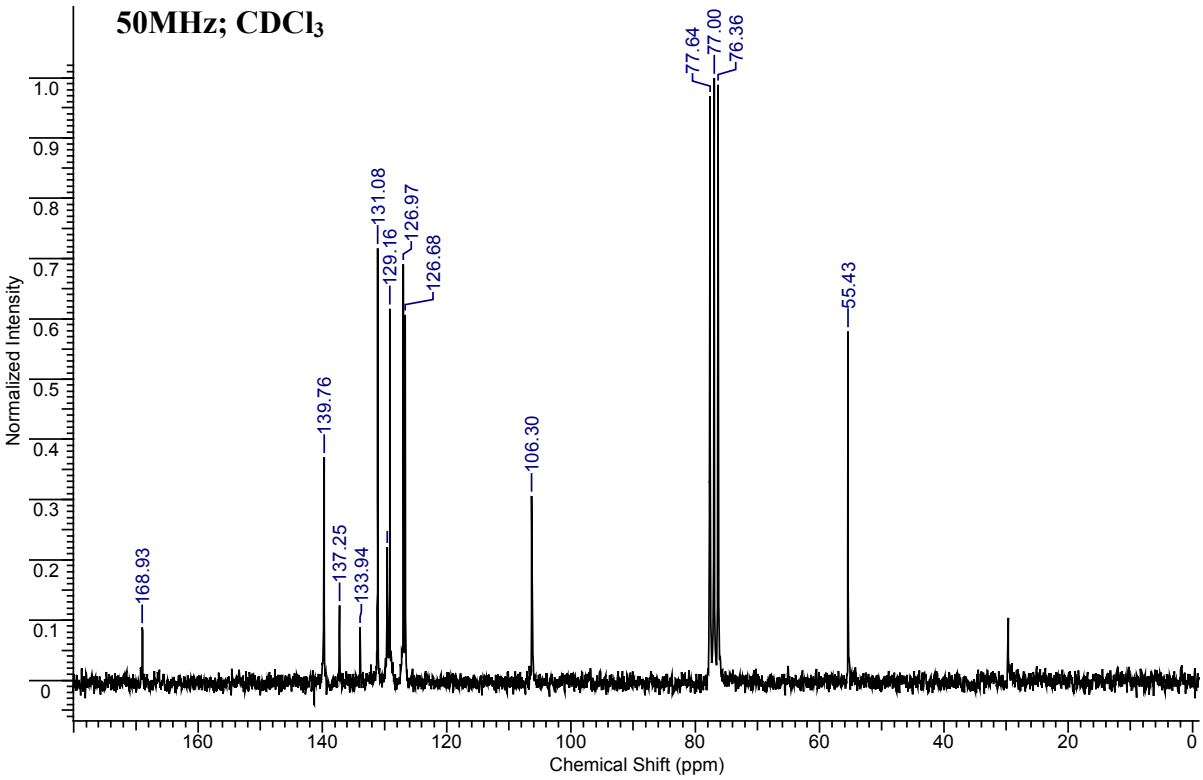

(b)

Figure B.9 ^{1}H NMR of **9**.

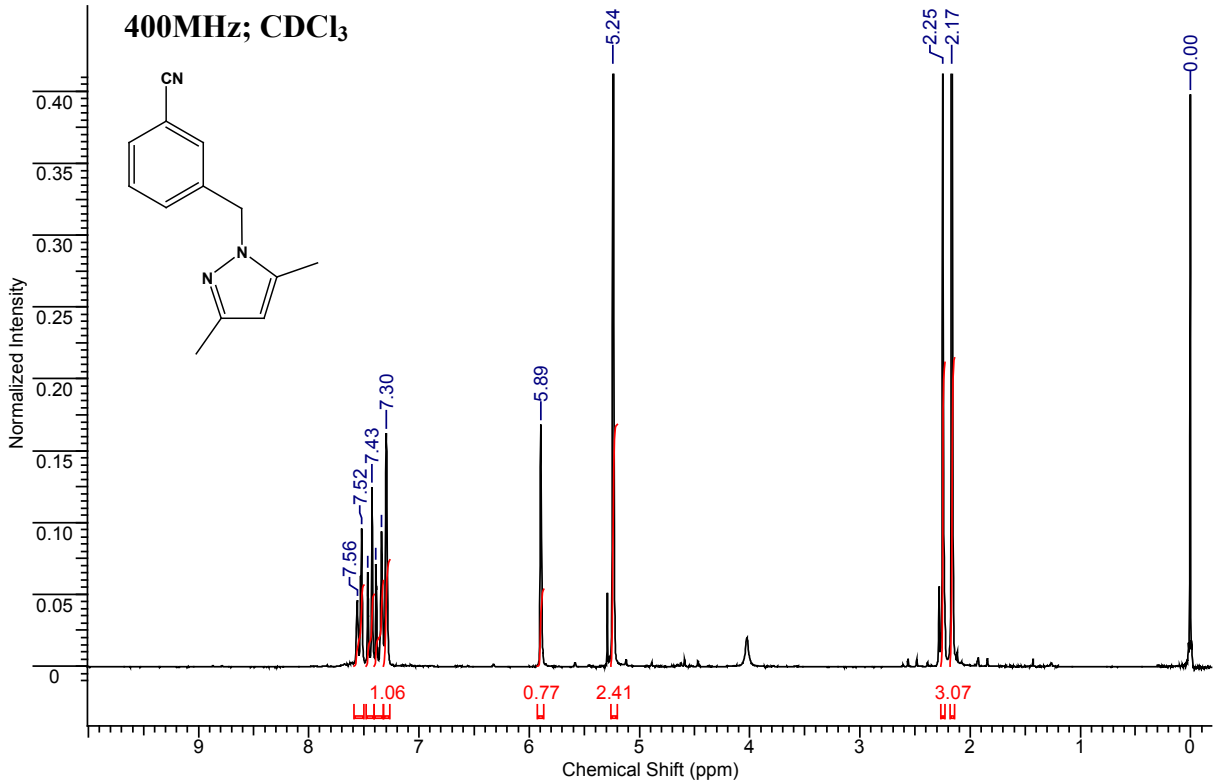

Figure B.10 (a) ^{1}H NMR and (b) ^{13}C NMR of **10**.

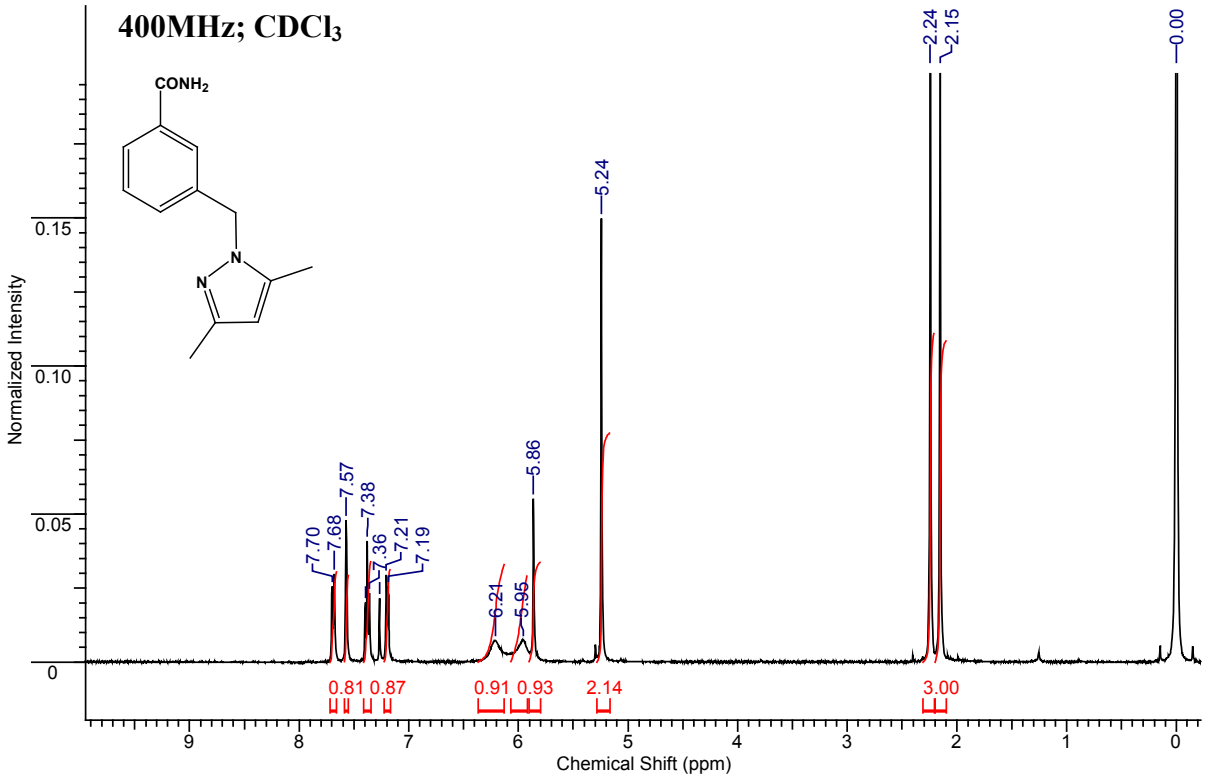

(a)

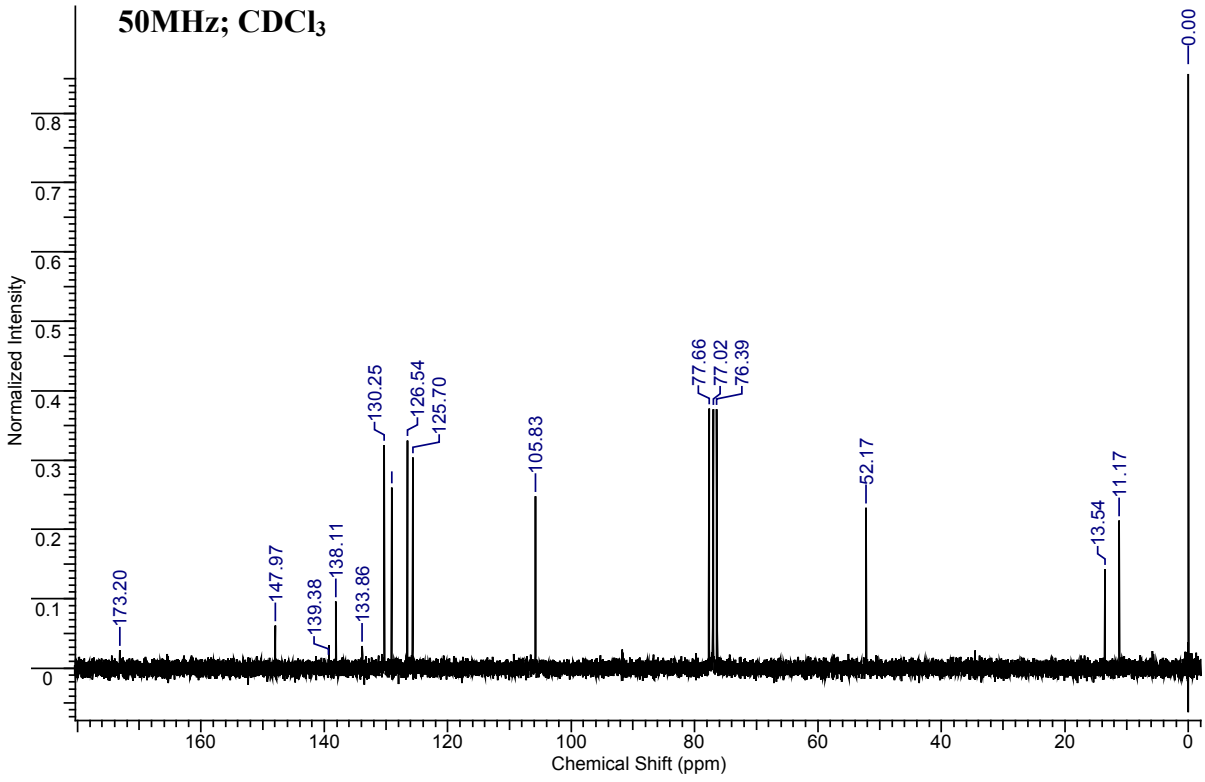

(b)

Figure B.11 ^{1}H NMR of **11**.

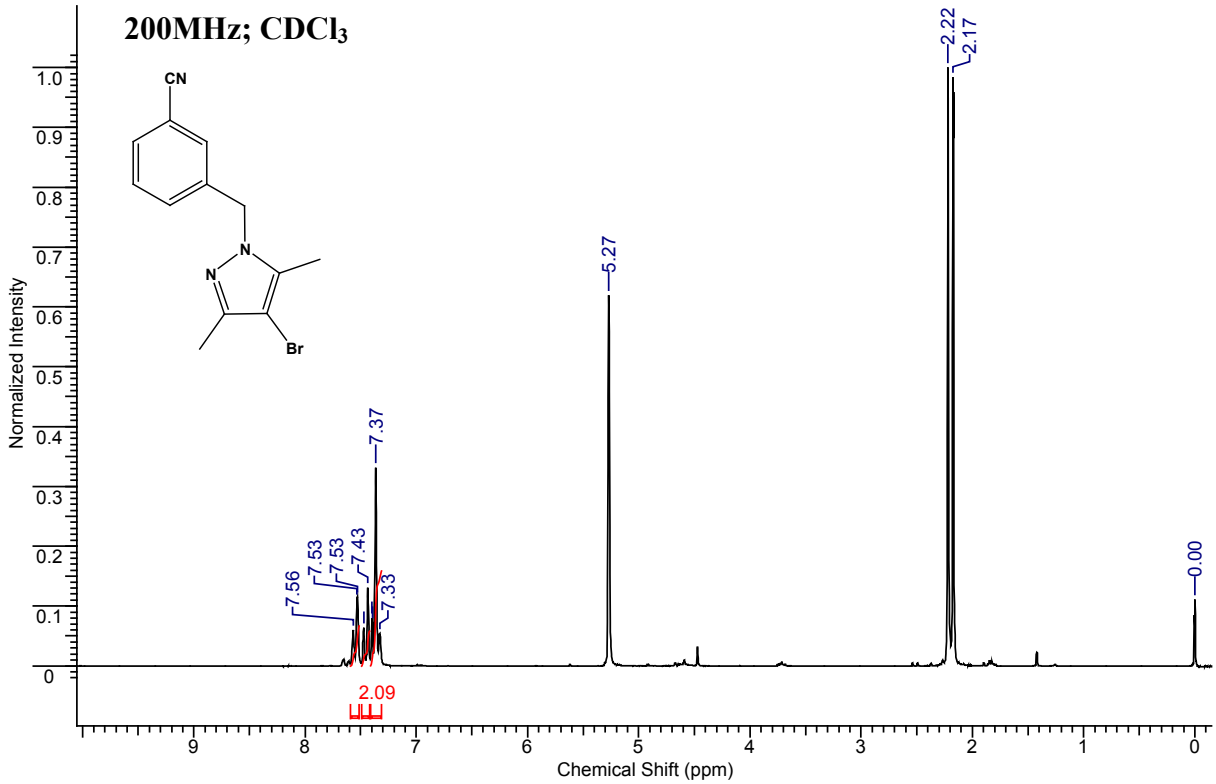

Figure B.12 (a) ^{1}H NMR and (b) ^{13}C NMR of **12**.

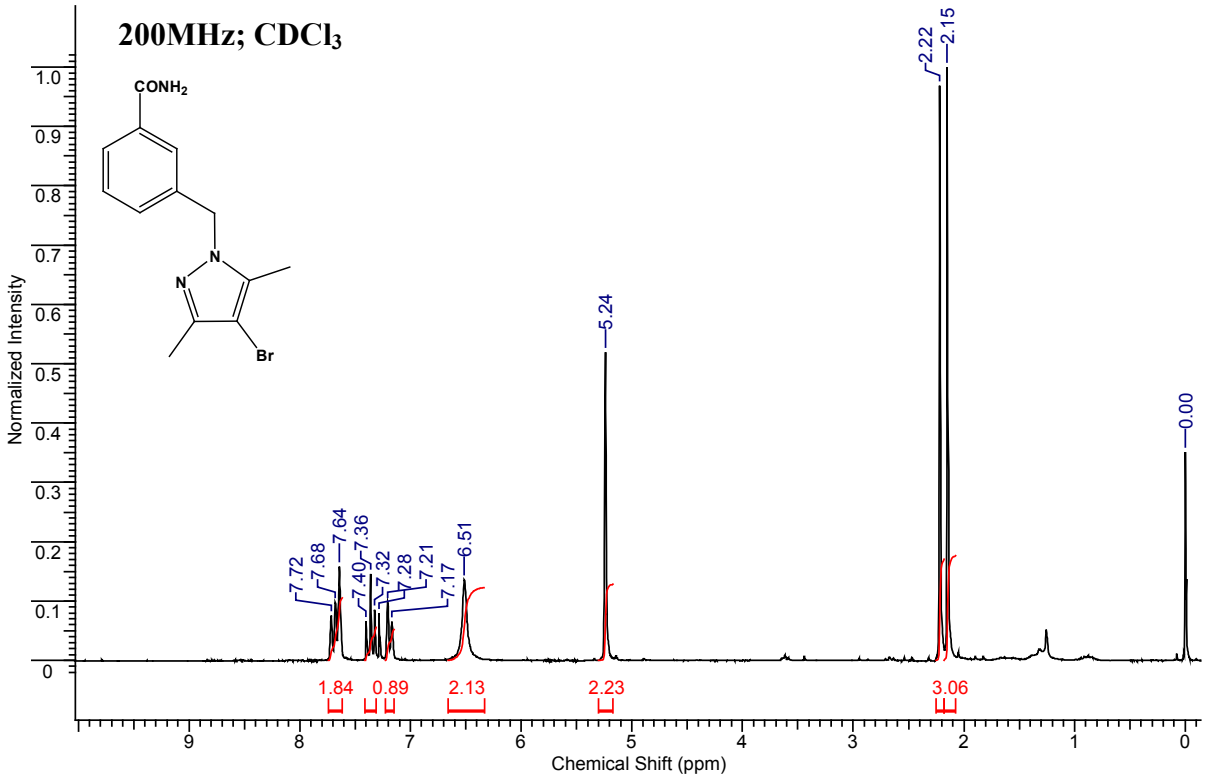

(a)

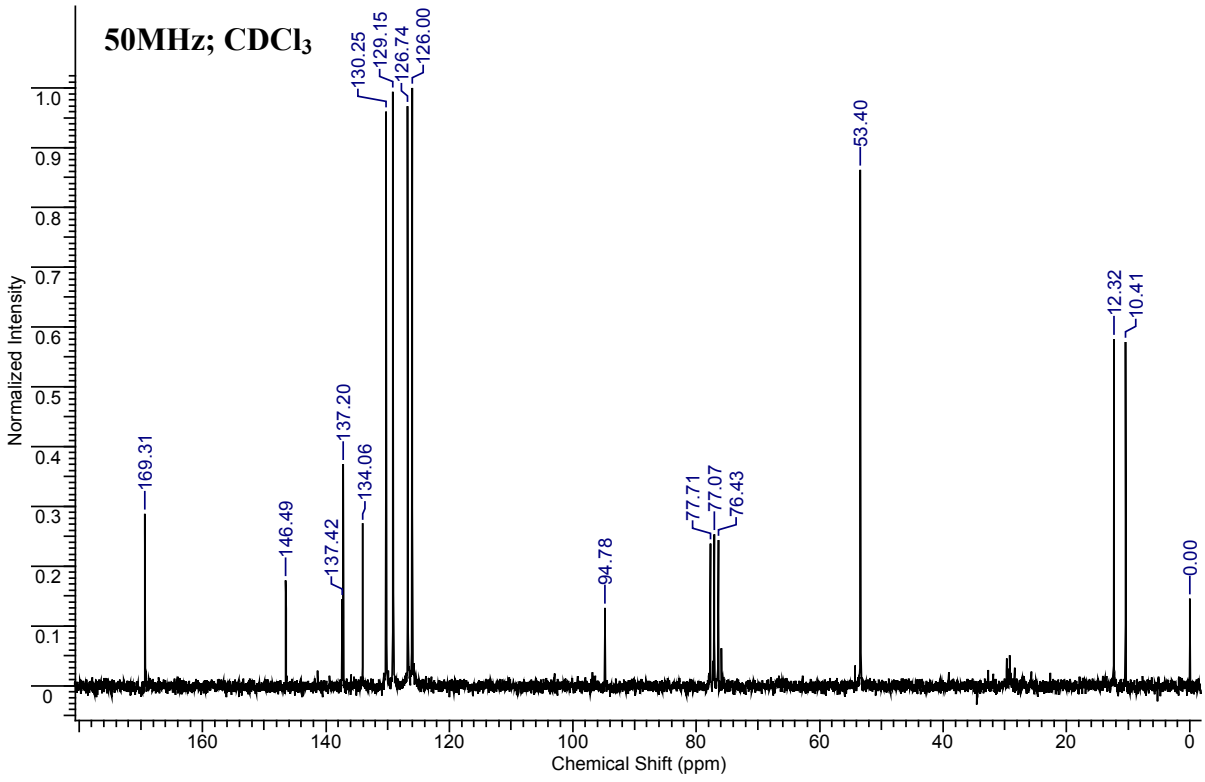

(b)

Figure B.13 (a) ^{1}H NMR and (b) ^{13}C NMR of **13**.

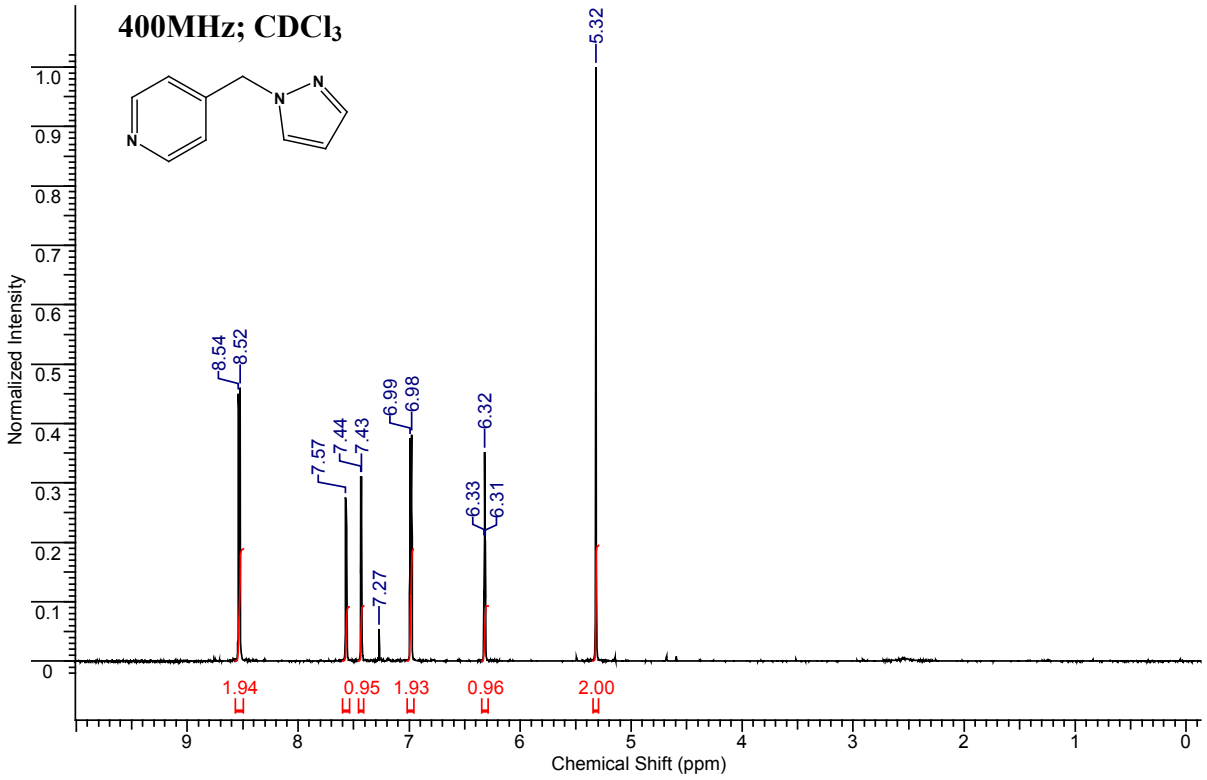

(a)

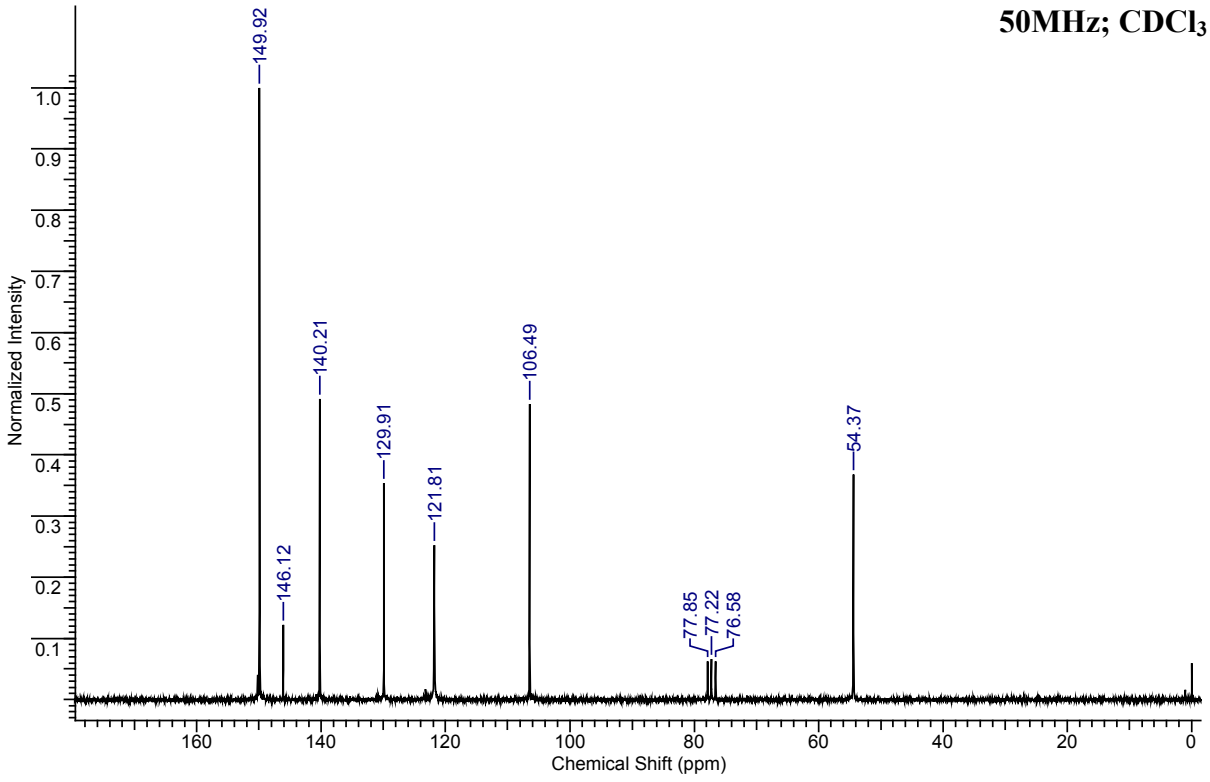

(b)

Figure B.14 (a) ^{1}H NMR and (b) ^{13}C NMR of **14**.

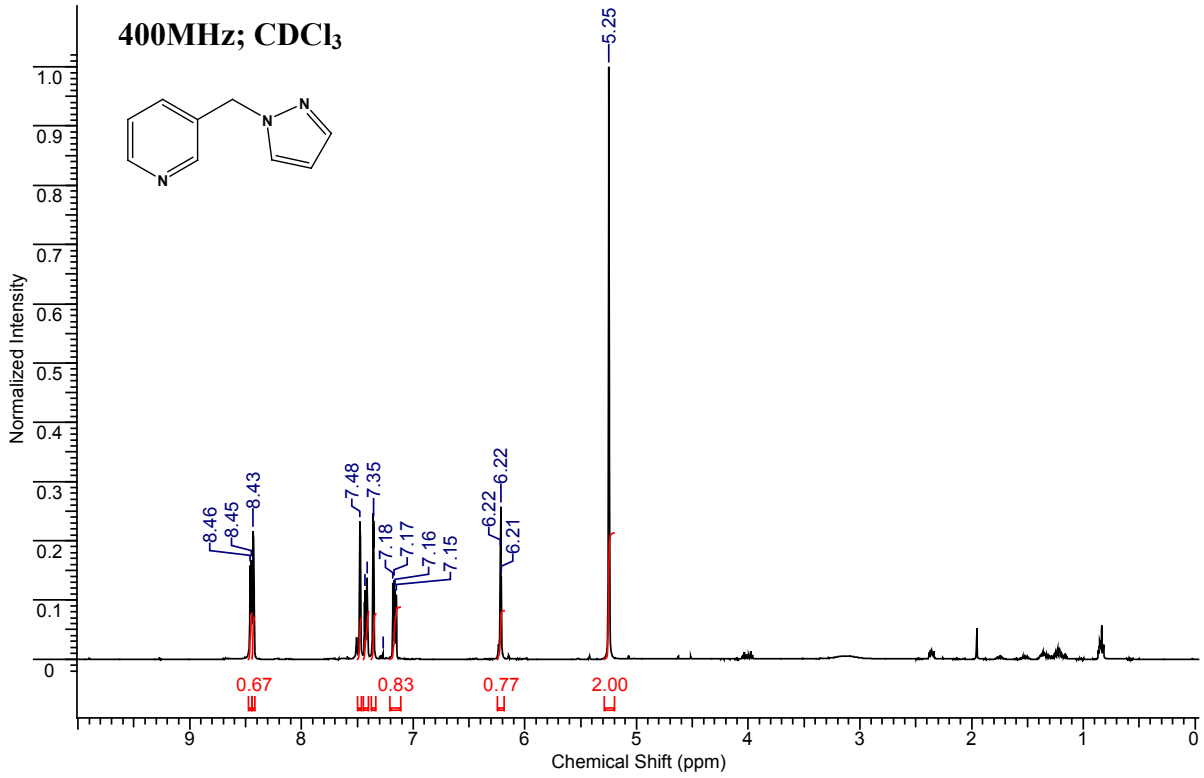

(a)

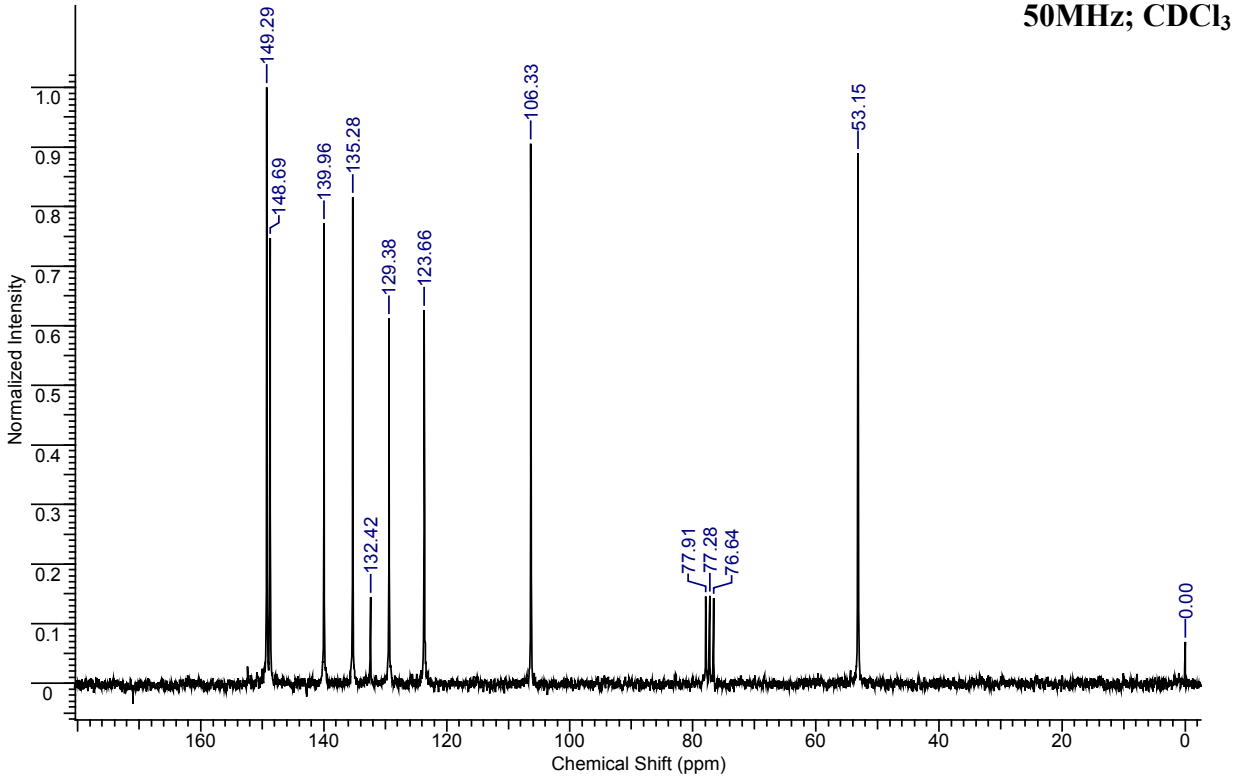

(b)

Figure B.15 (a) ^{1}H NMR and (b) ^{13}C NMR of **15**.

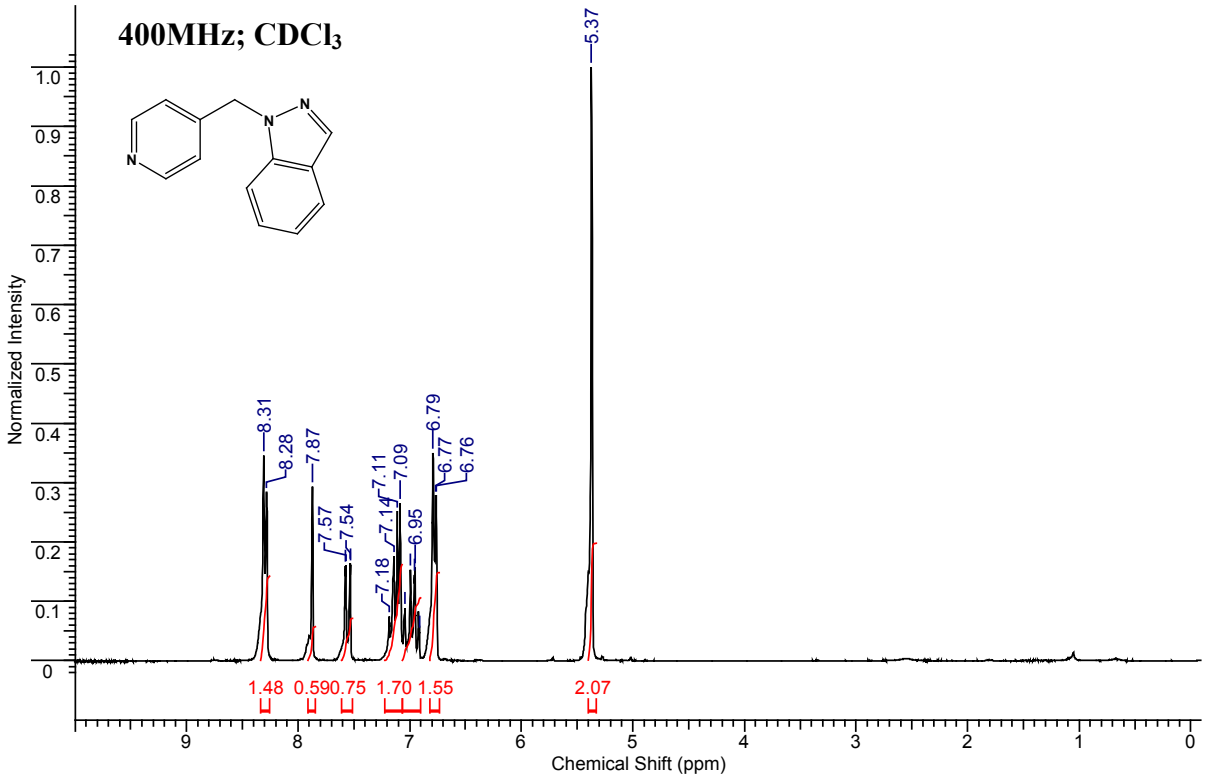

(a)

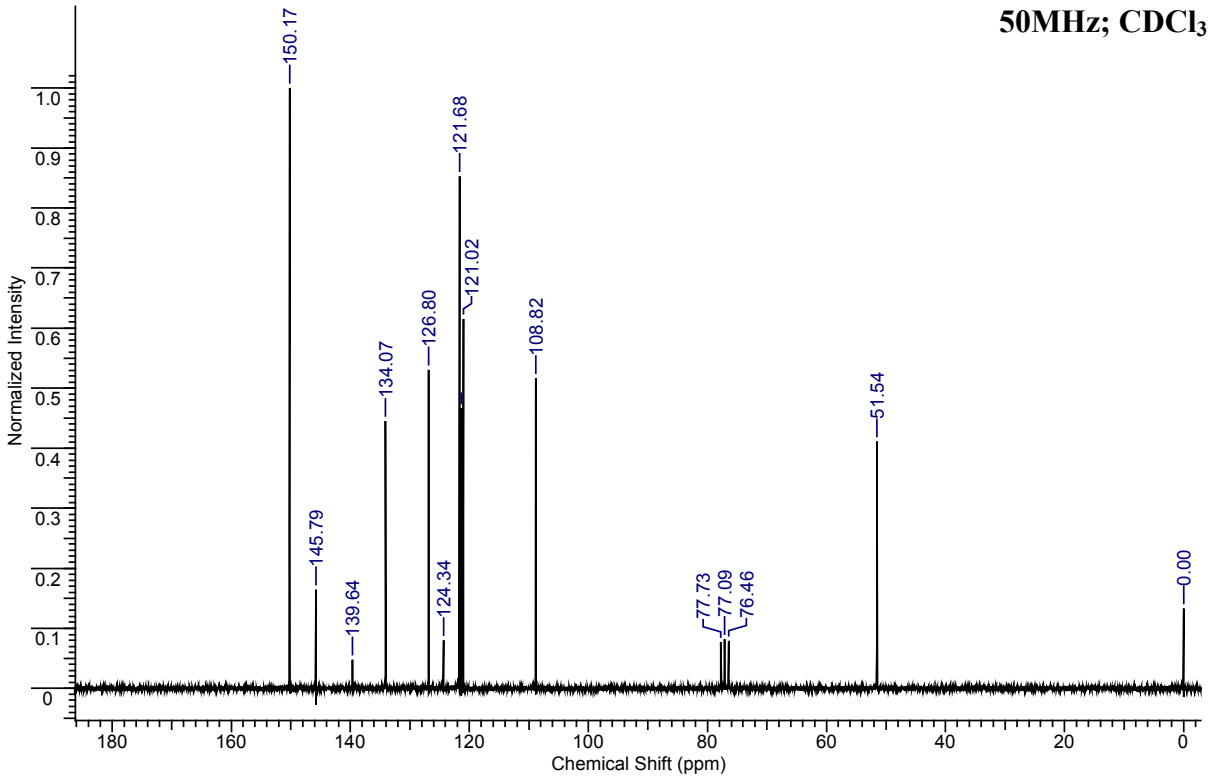

(b)

Figure B.16 (a) ^{1}H NMR and (b) ^{13}C NMR of **16**.

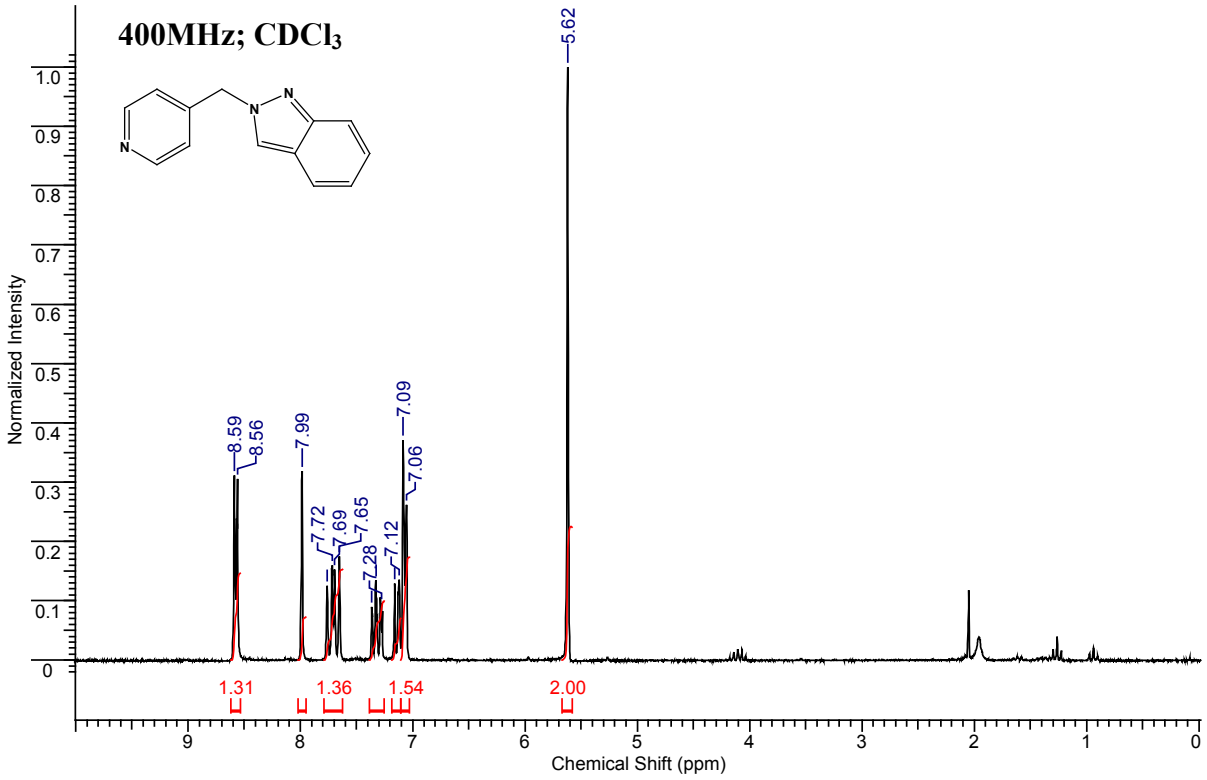

(a)

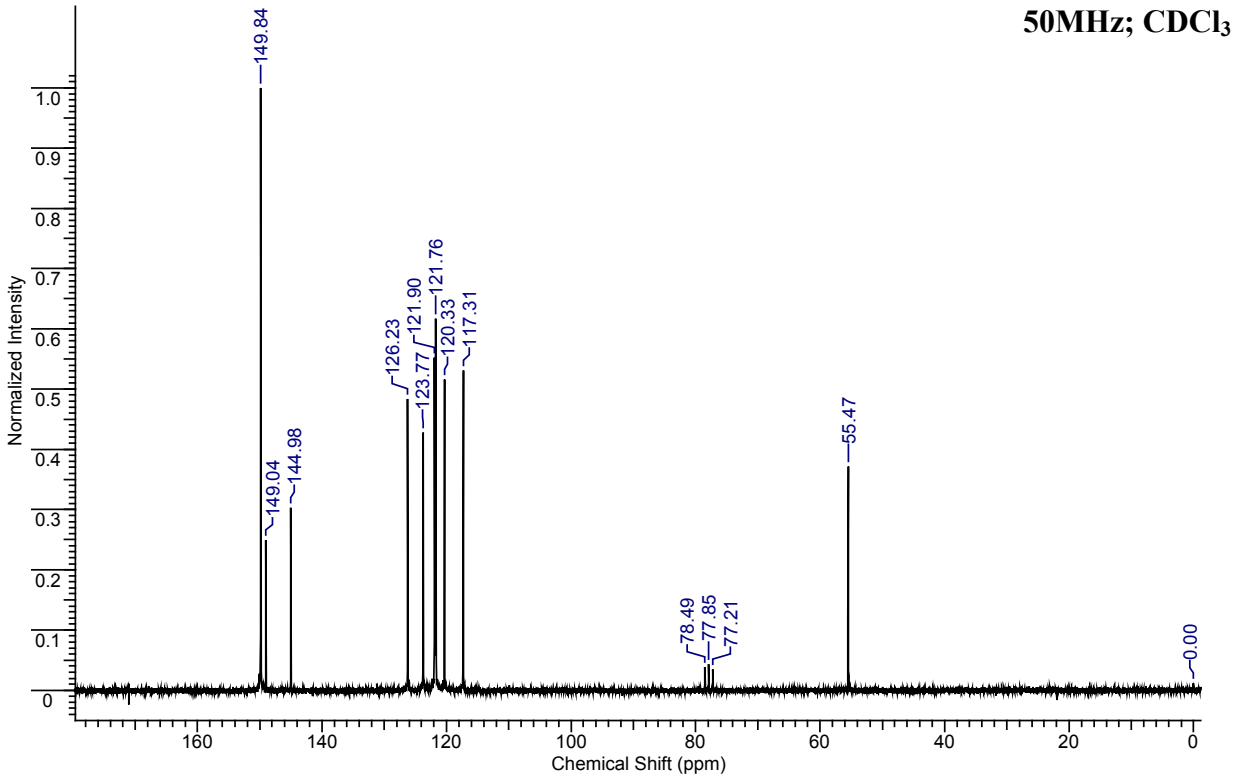

(b)

Figure B.17 (a) ^{1}H NMR and (b) ^{13}C NMR of **17**.

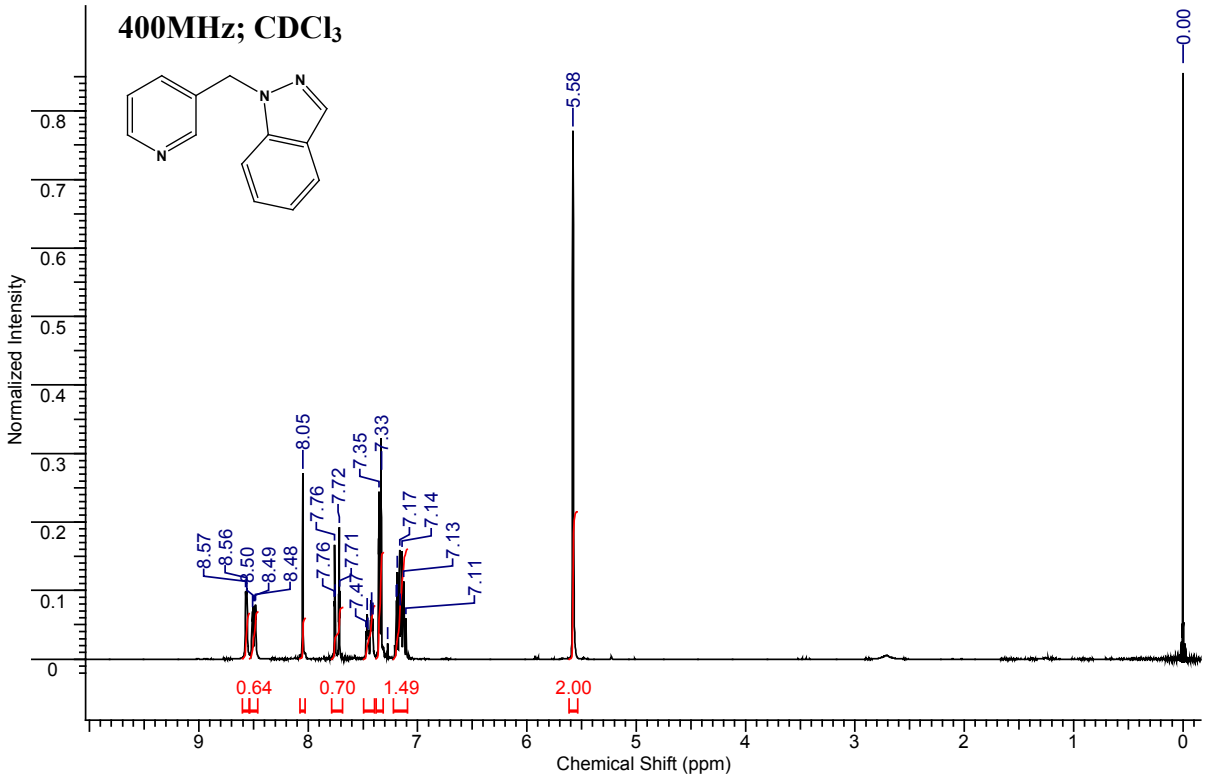

(a)

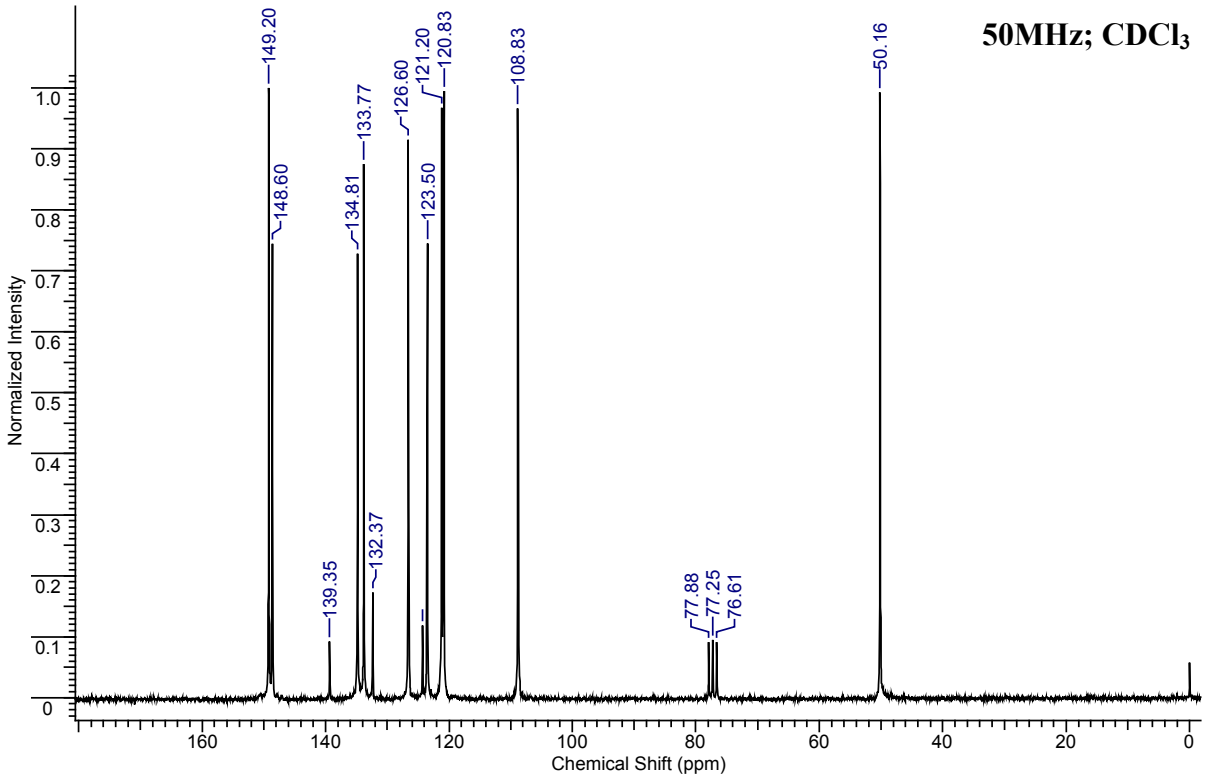

(b)

Figure B.18 (a) ^{1}H NMR and (b) ^{13}C NMR of **18**.

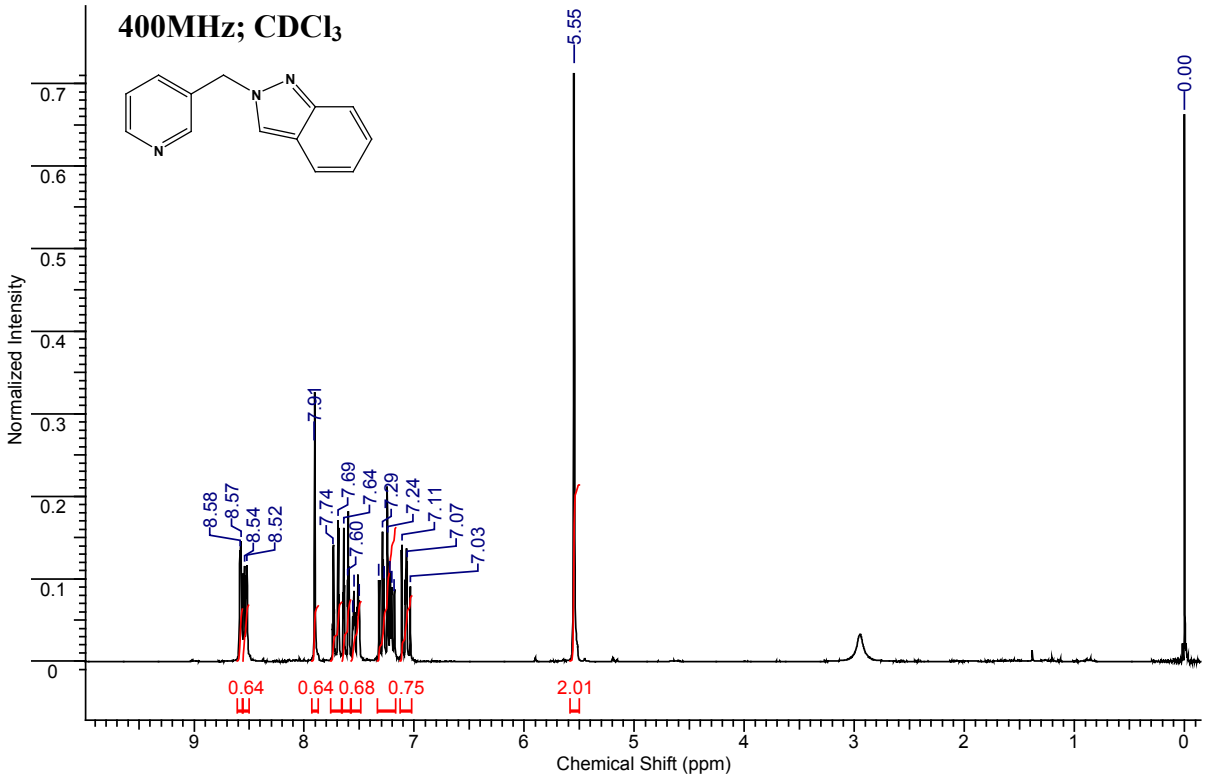

(a)

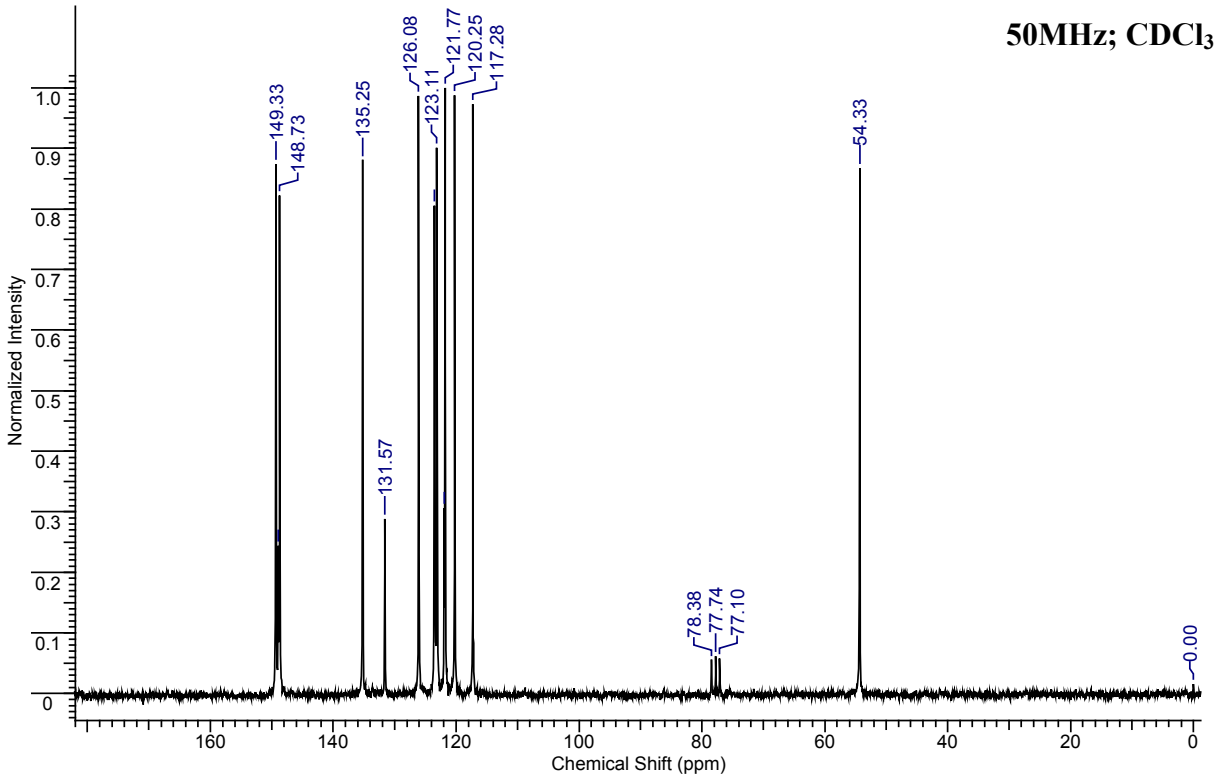

(b)

Figure B.19 (a) ^{1}H NMR and (b) ^{13}C NMR of **19**.

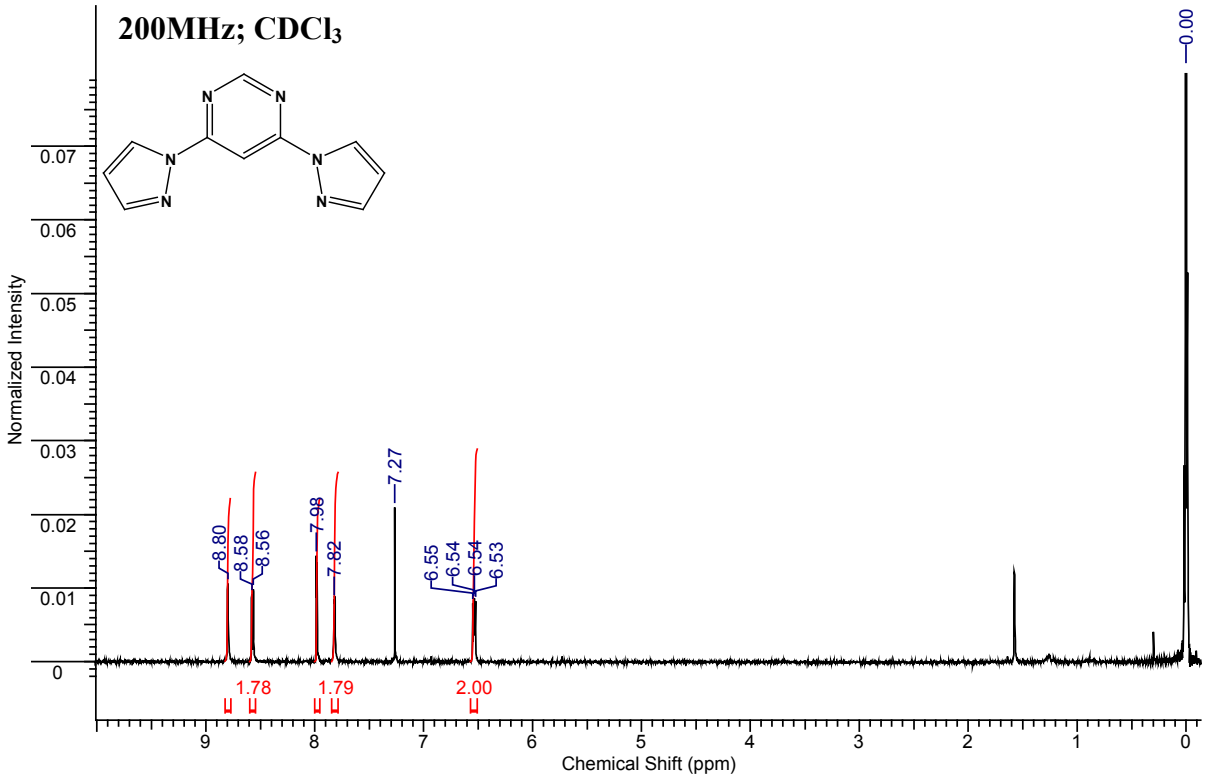

(a)

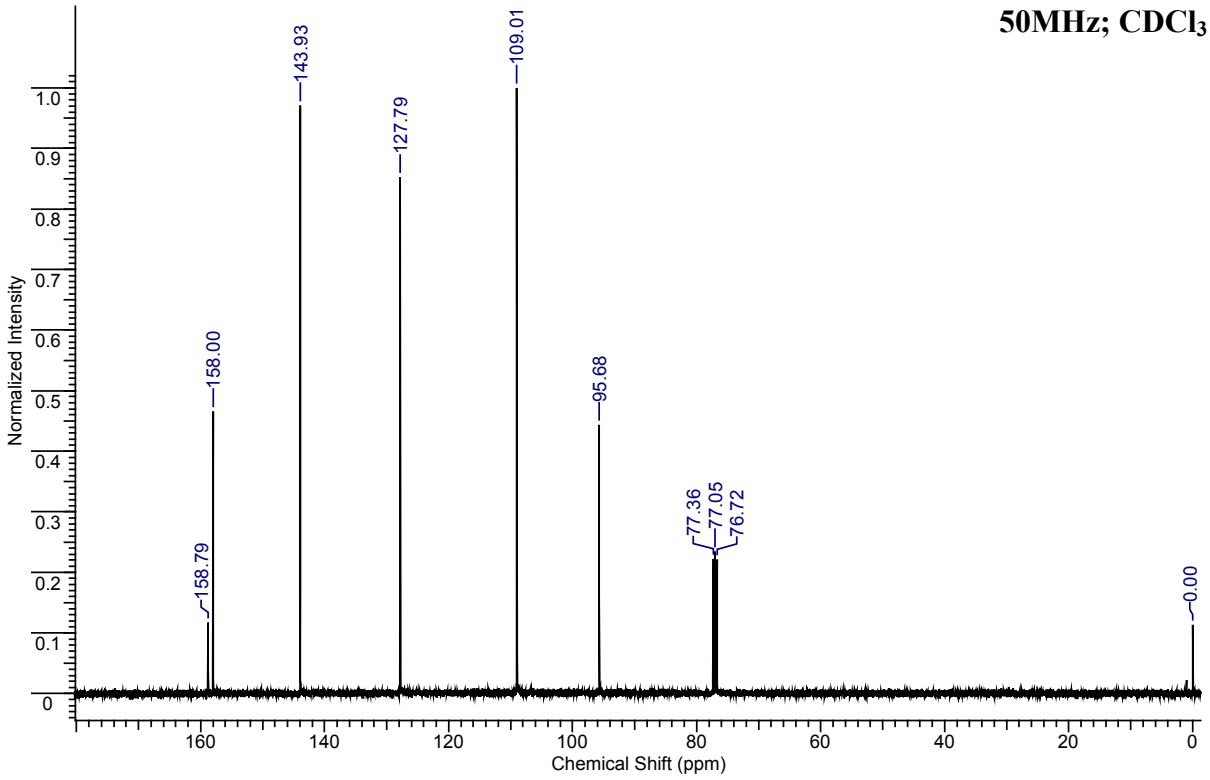

(b)

Figure B.20 (a) ^{1}H NMR and (b) ^{13}C NMR of **20**.

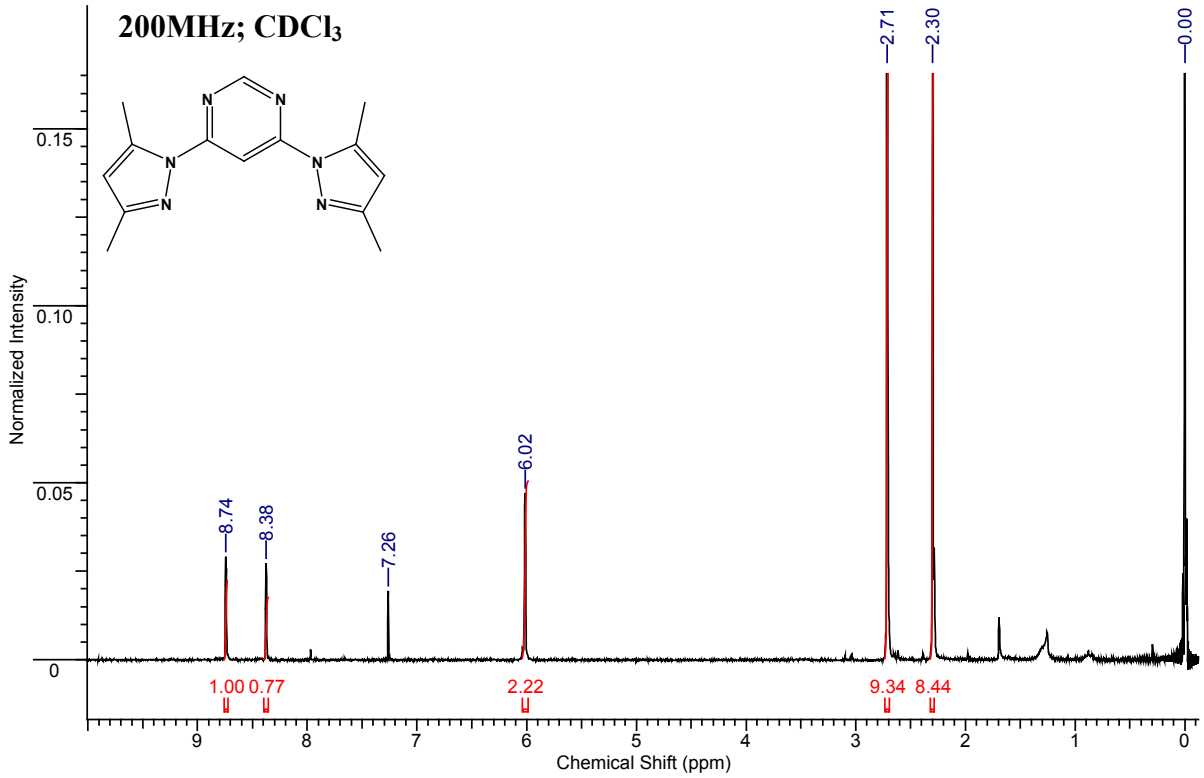

(a)

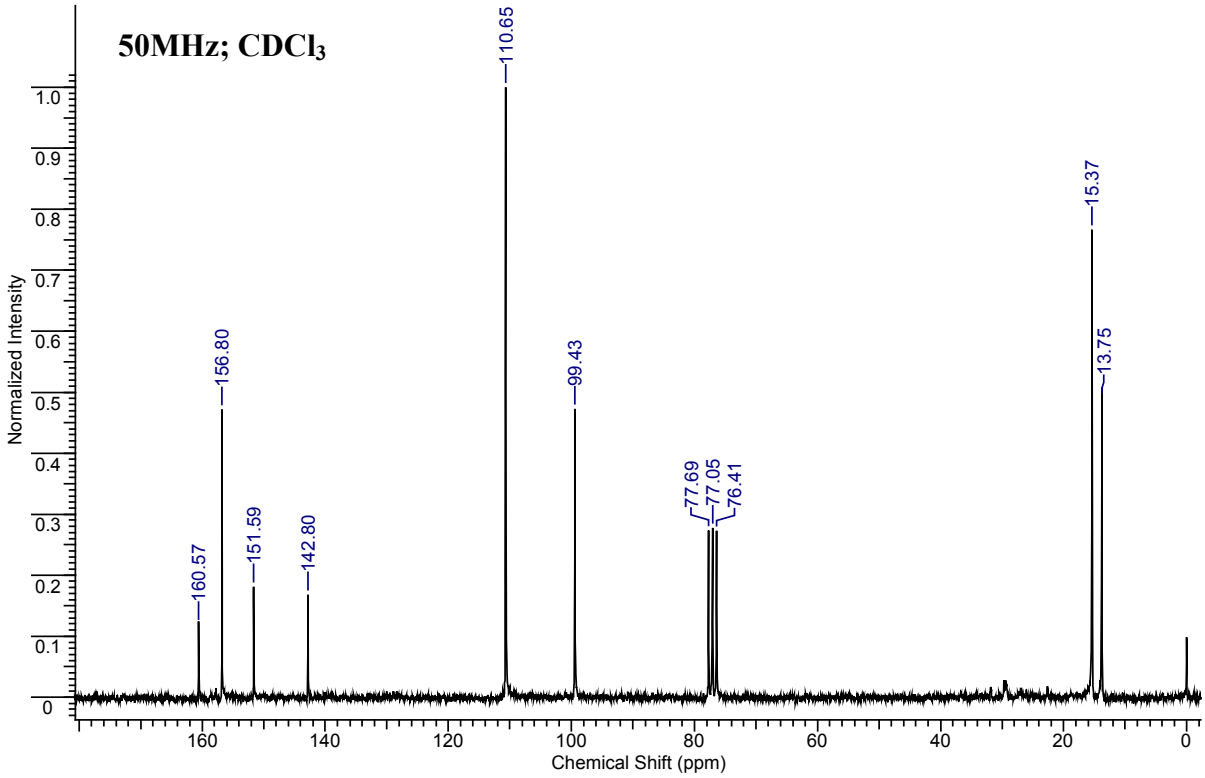

(b)

Figure B.21 (a) ^{1}H NMR and (b) ^{13}C NMR of **21**.

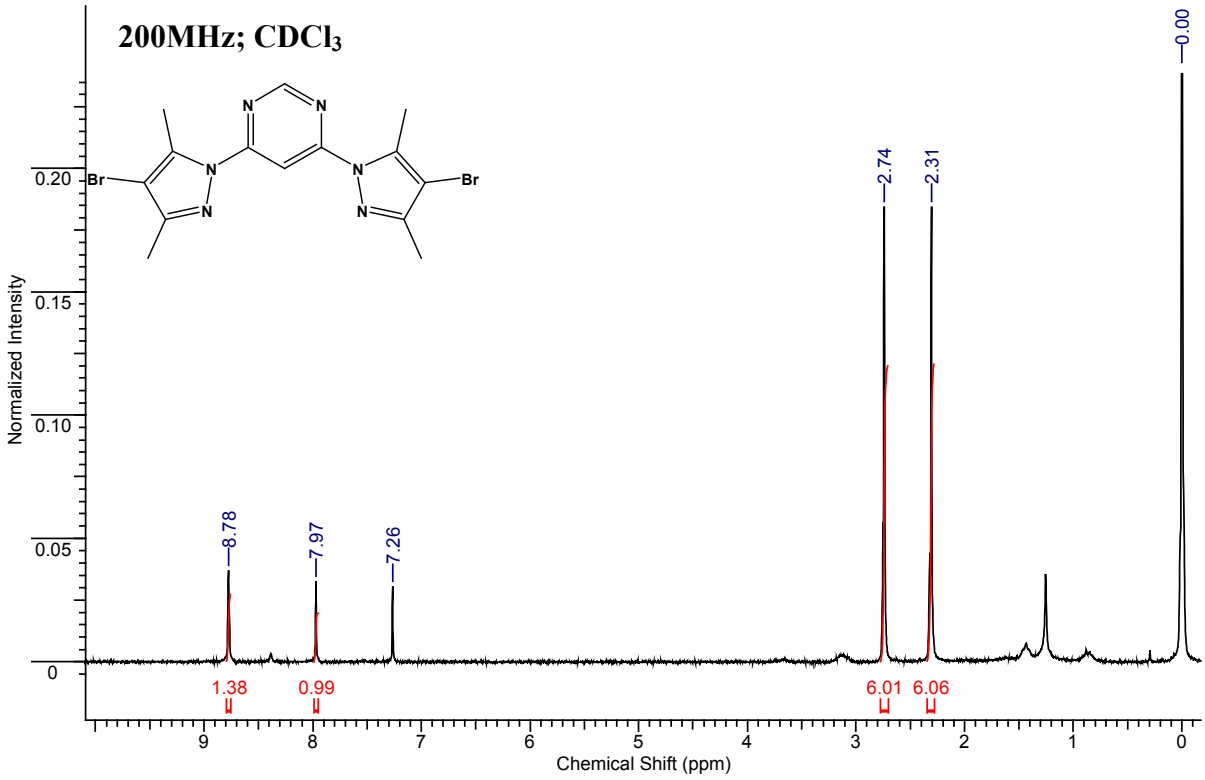

(a)

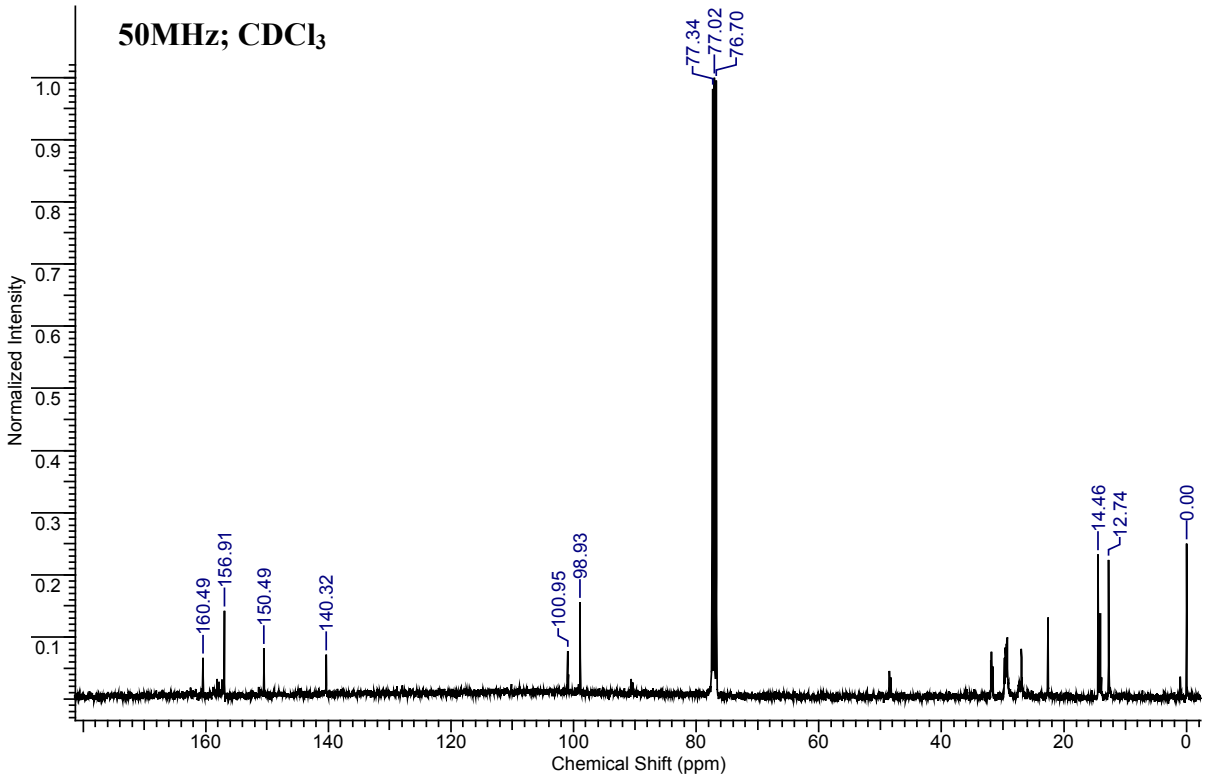

(b)

Figure B.22 (a) ^{1}H NMR and (b) ^{13}C NMR of **22**.

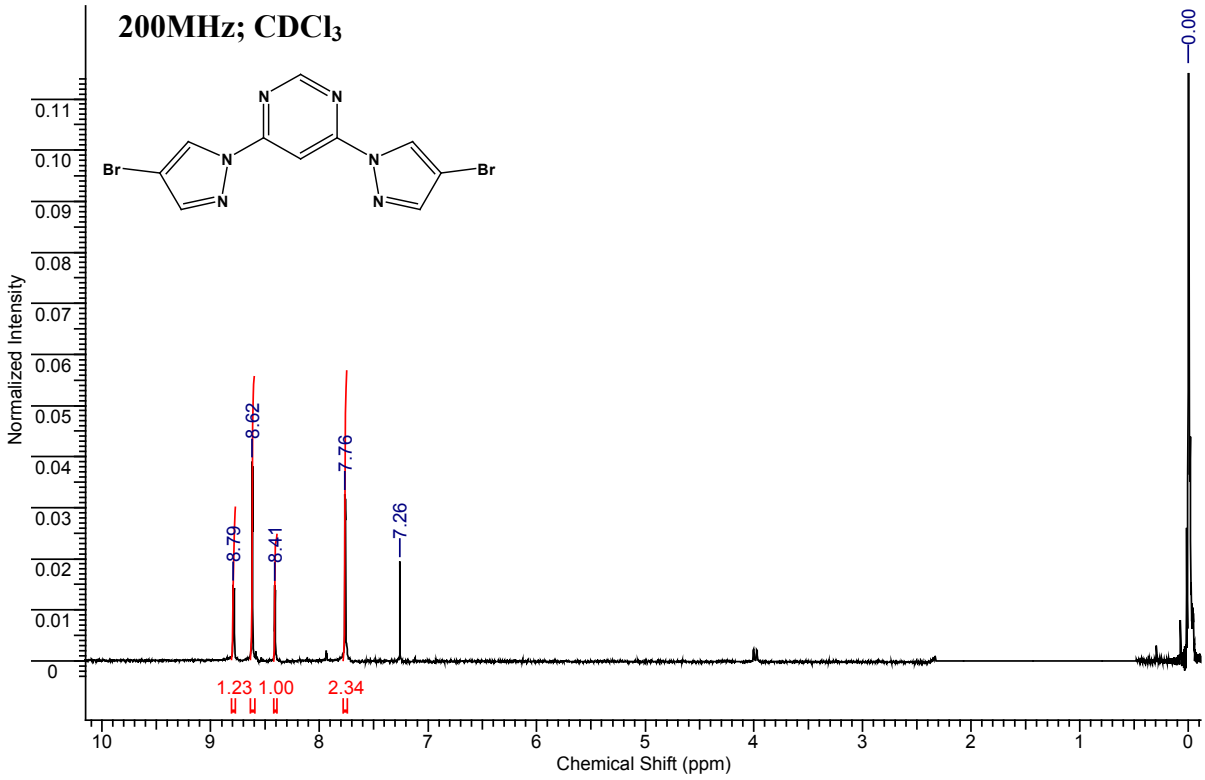

(a)

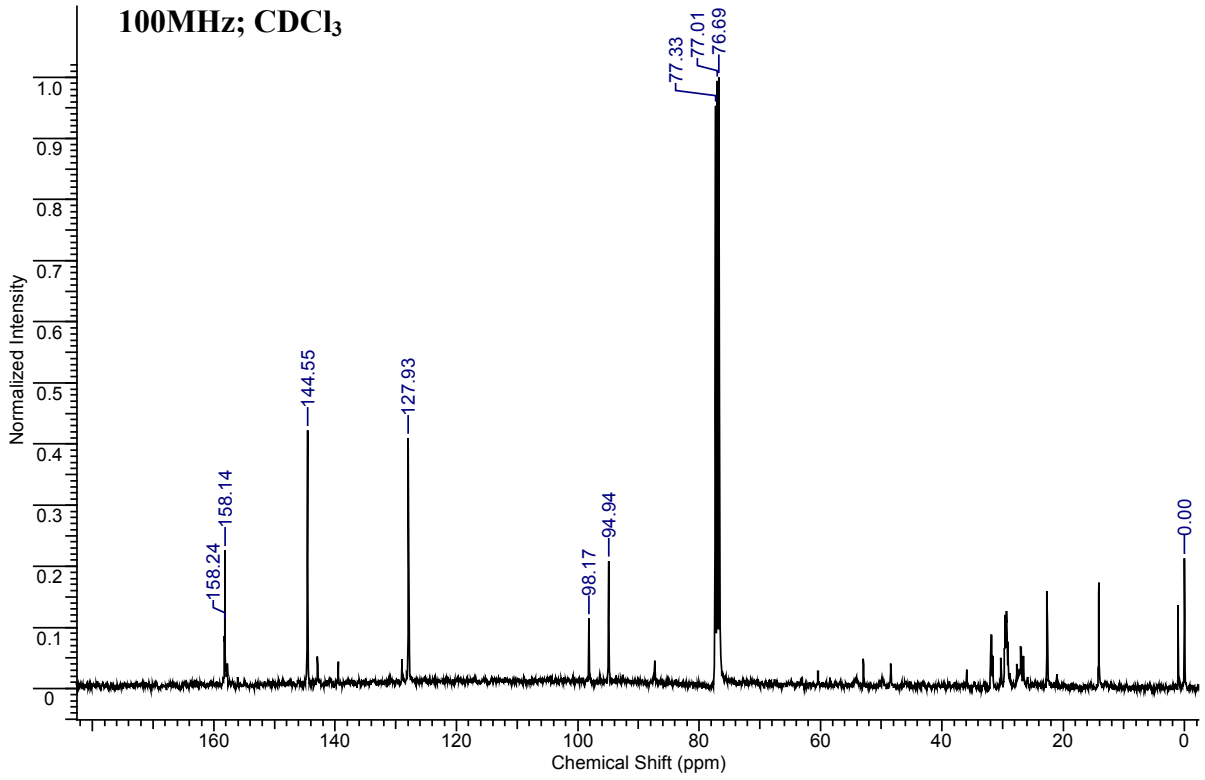

(b)

Figure B.23 (a) ^{1}H NMR and (b) ^{13}C NMR of **23**.

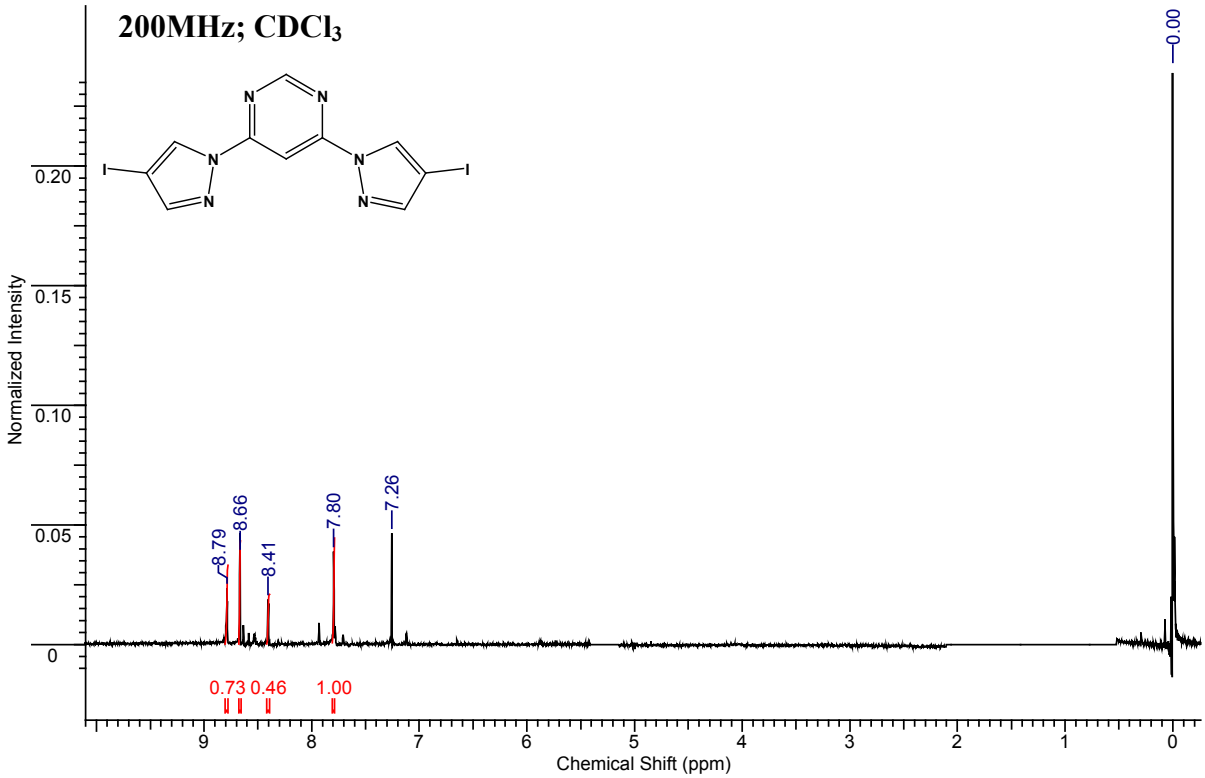

(a)

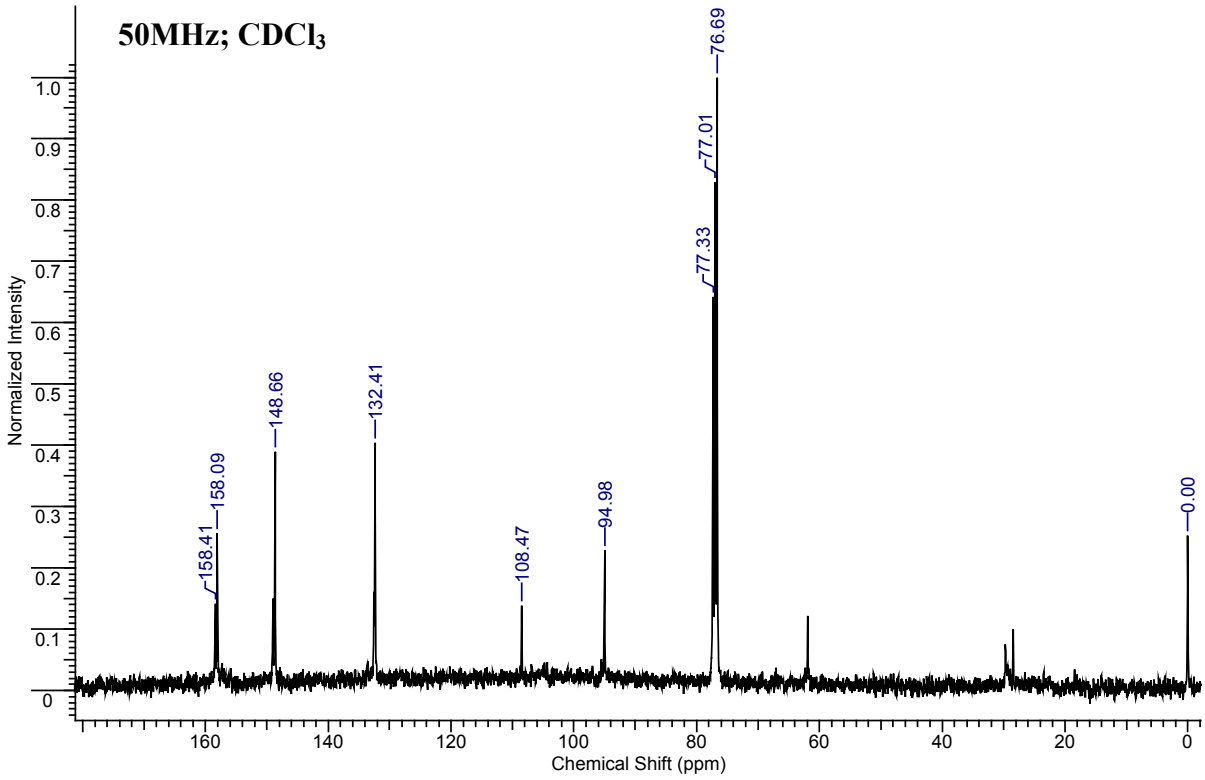

(b)

Figure B.24 ^{1}H NMR of **24**.

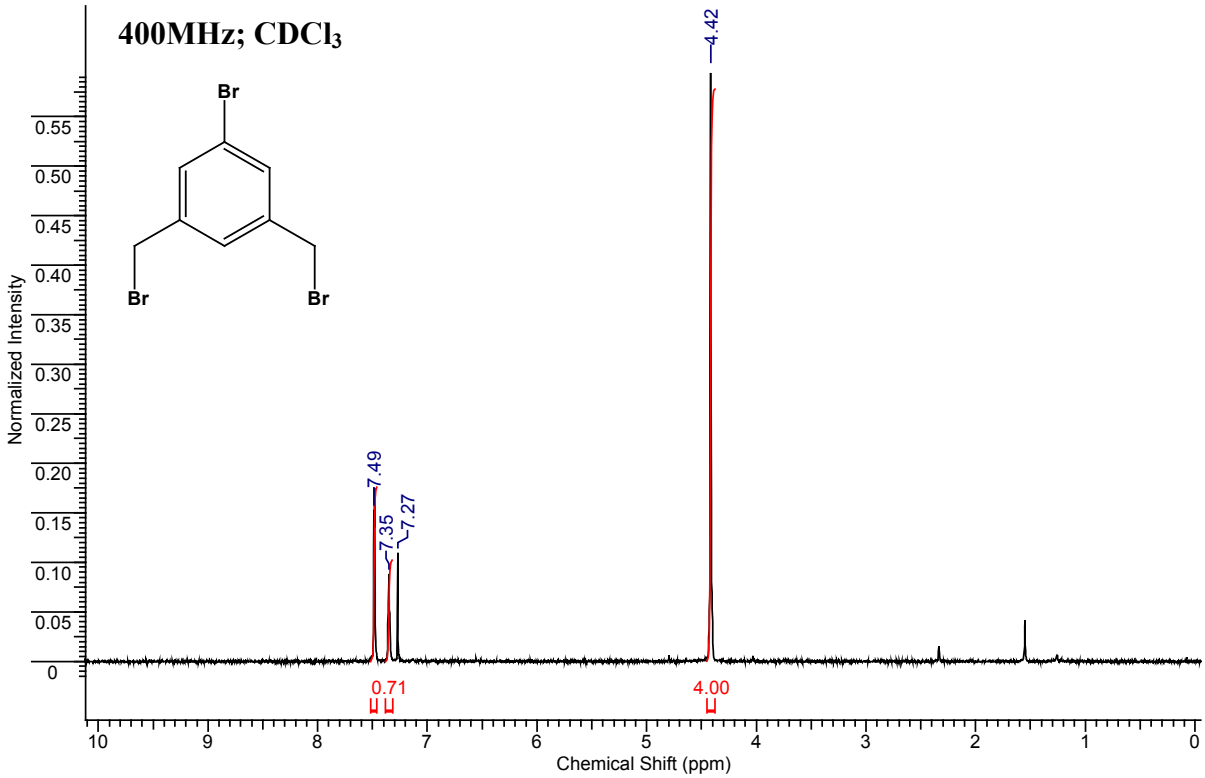

Figure B.25 ^{1}H NMR of **25**.

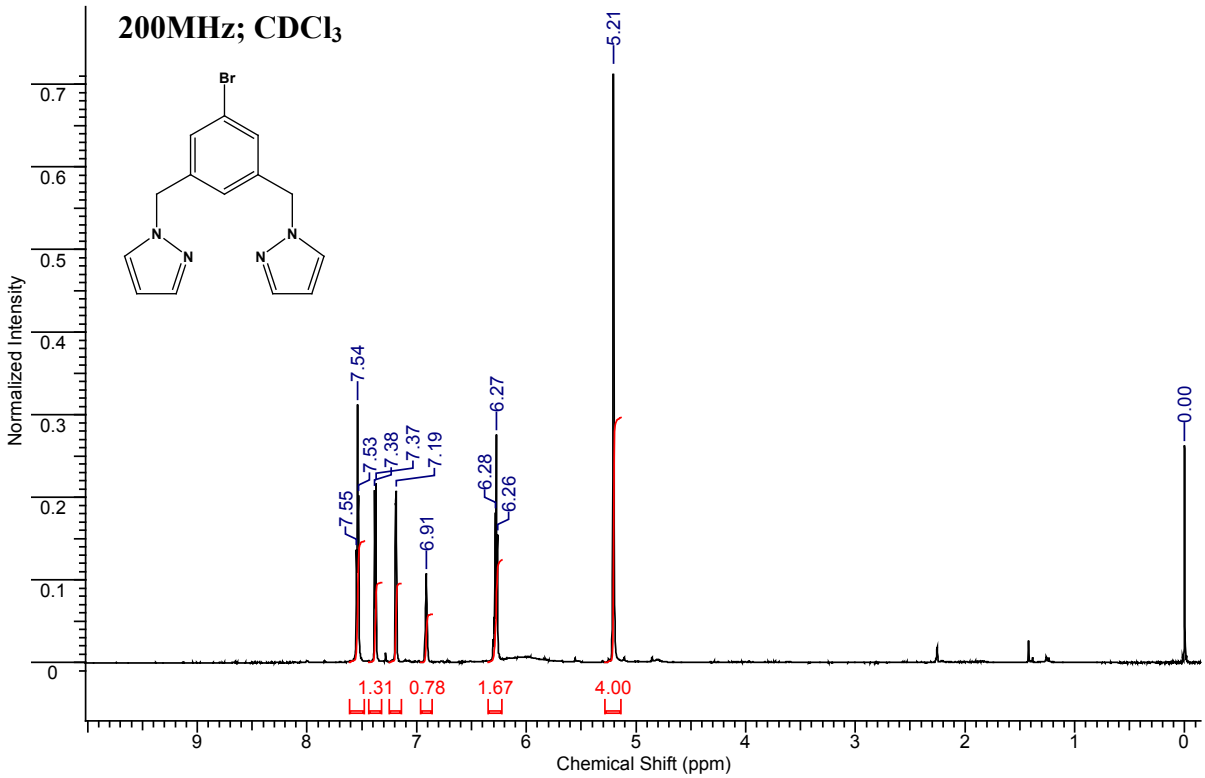

Figure B.26 ^{1}H NMR of **26**.

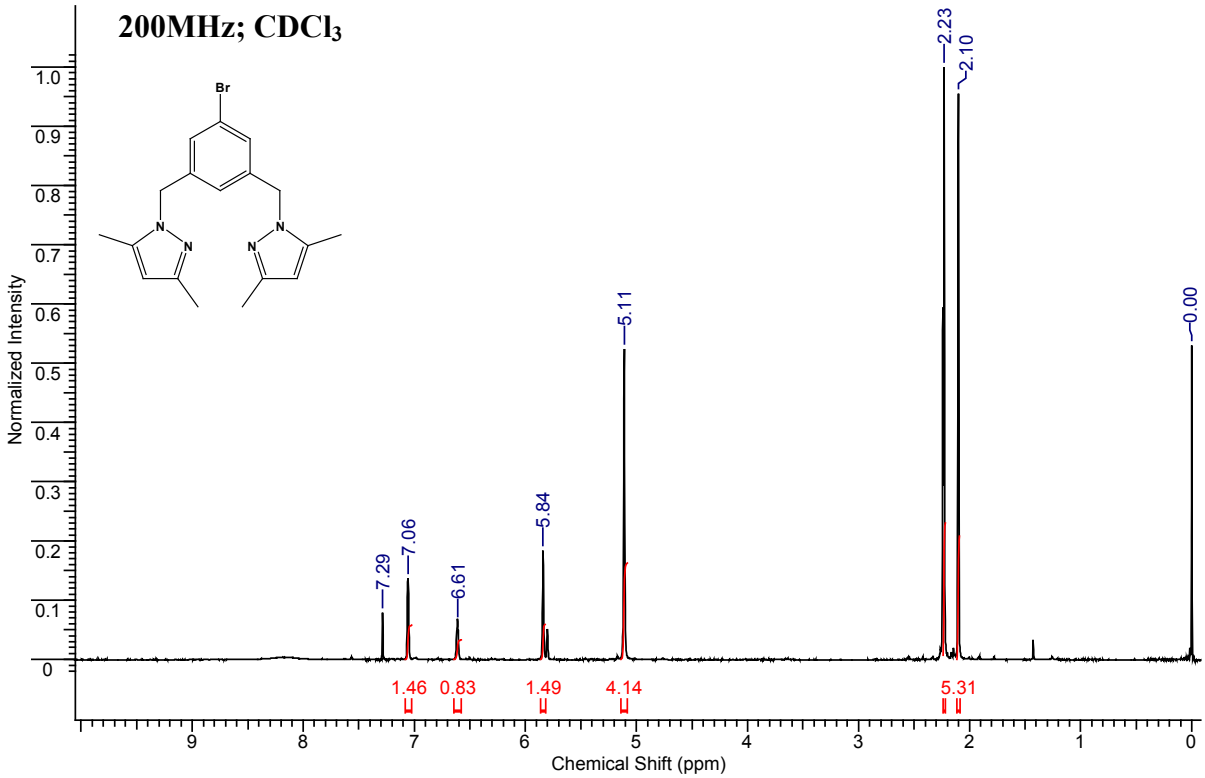

Figure B.27 ^{1}H NMR of **27**.

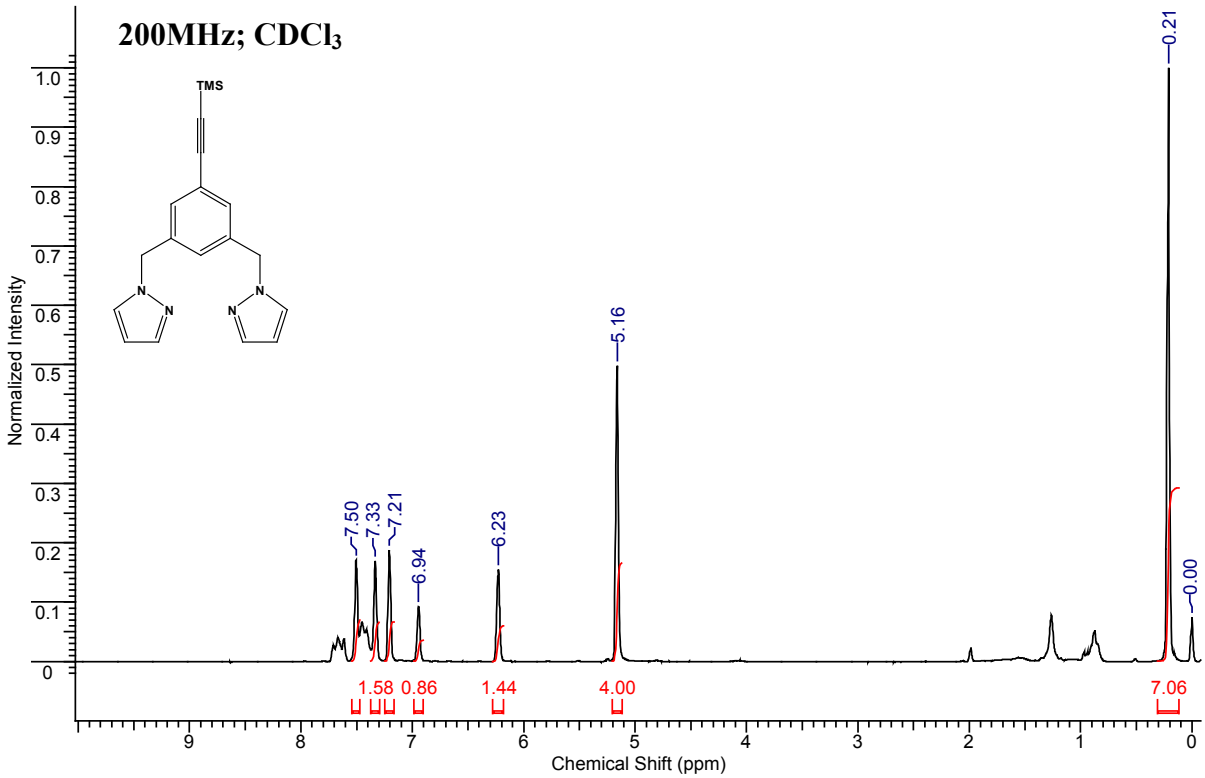

Figure B.28 ^{1}H NMR of **28**.

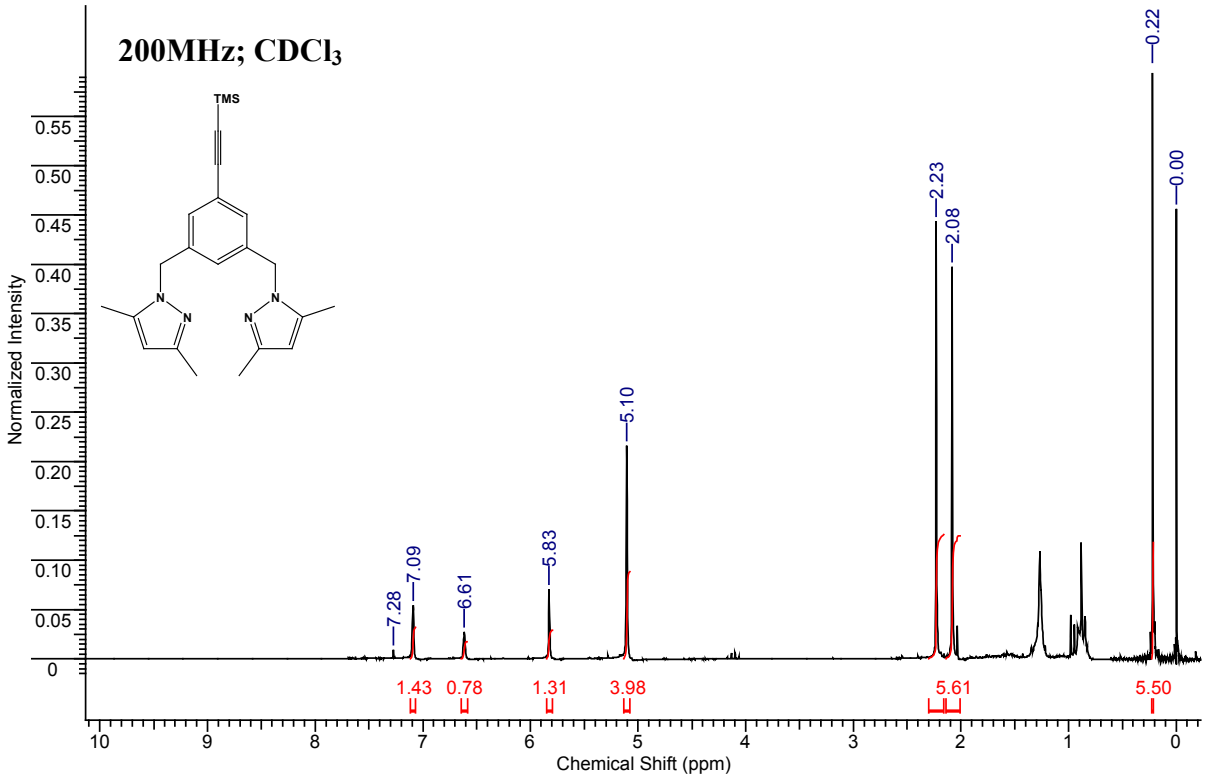

Figure B.29 ^{1}H NMR of **29**.

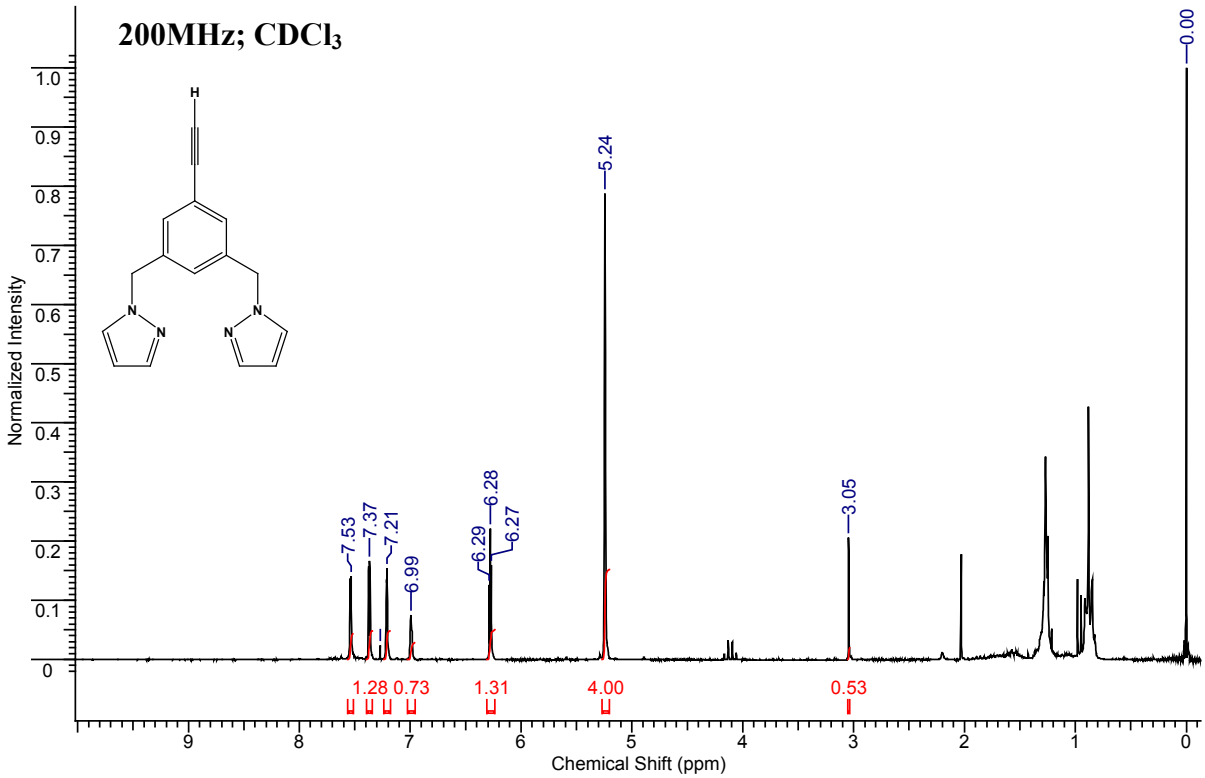

Figure B.30 ^{1}H NMR of **30**.

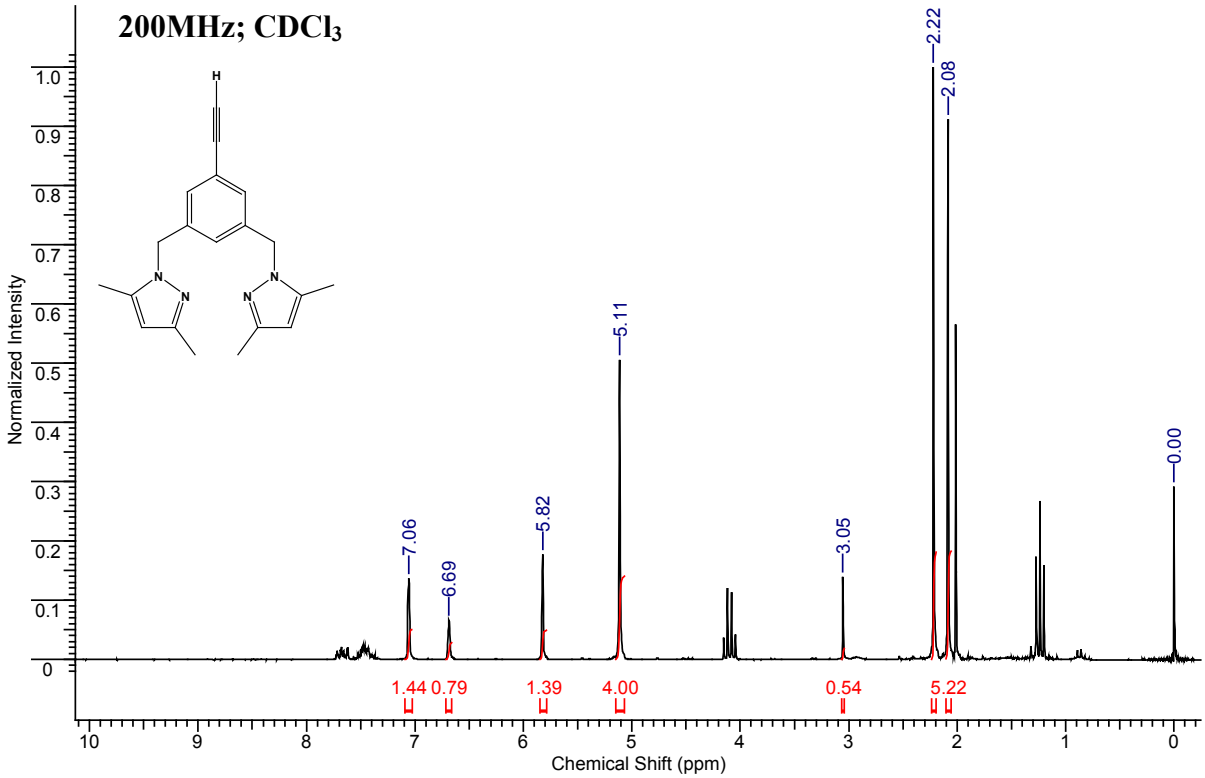

Figure B.31 (a) ^{1}H NMR and (b) ^{13}C NMR of **31**.

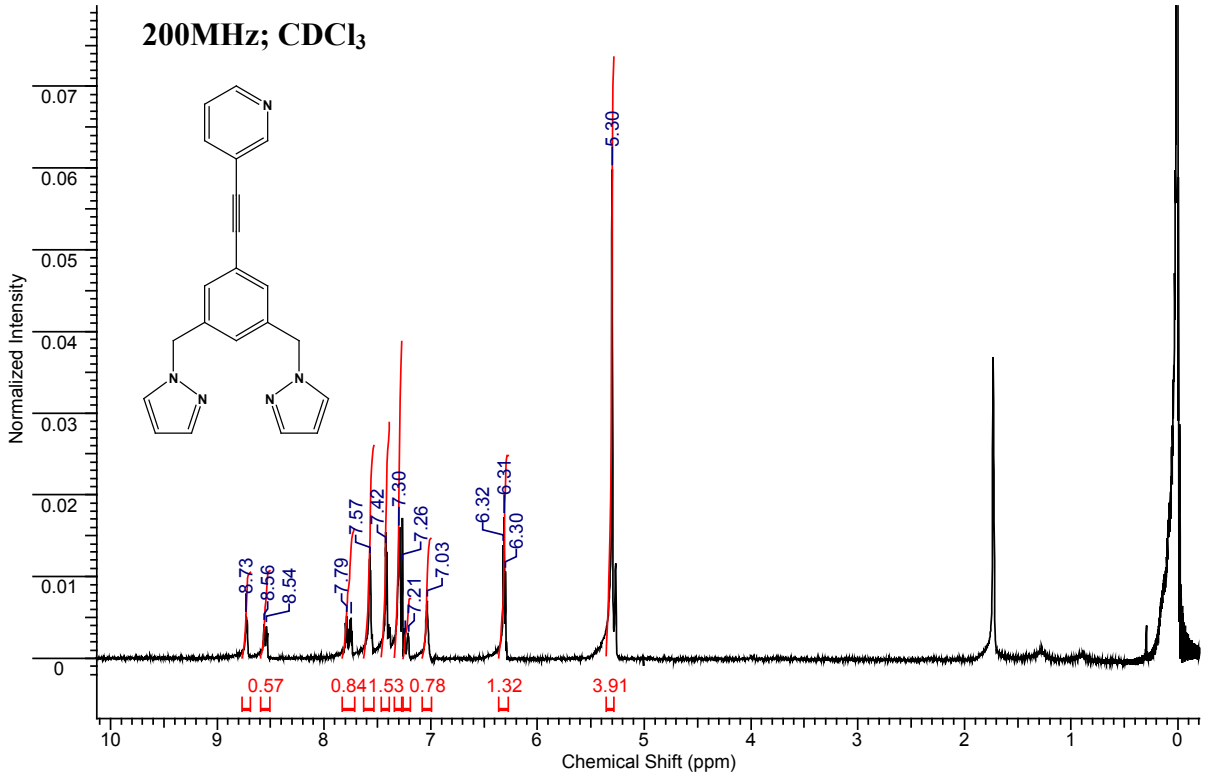

(a)

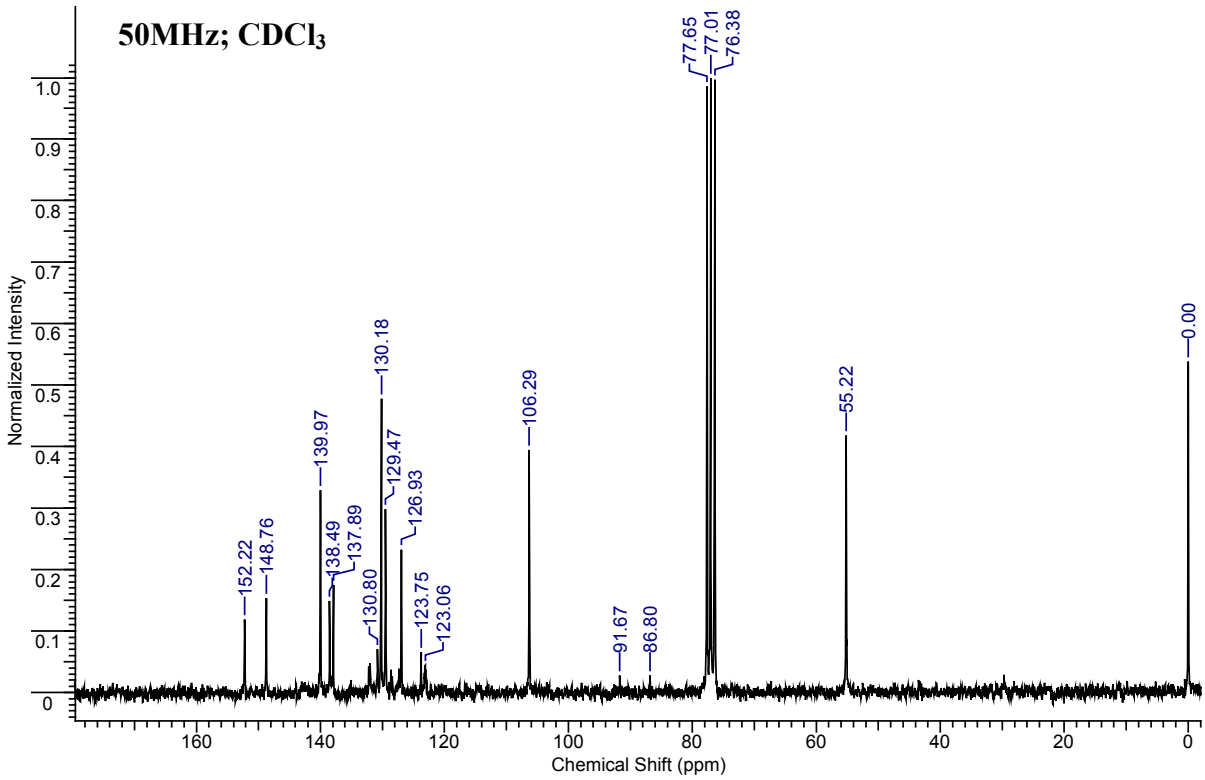

(b)

Figure B.32 (a) ^{1}H NMR and (b) ^{13}C NMR of **32**.

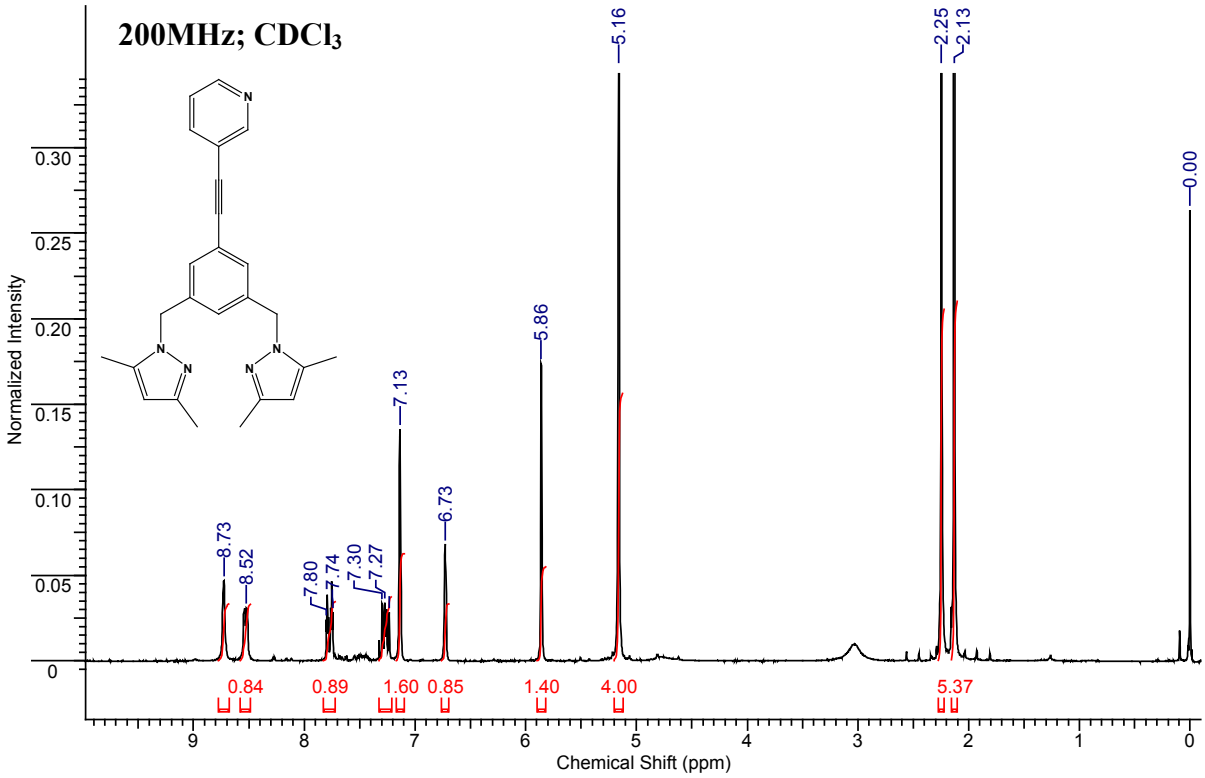

(a)

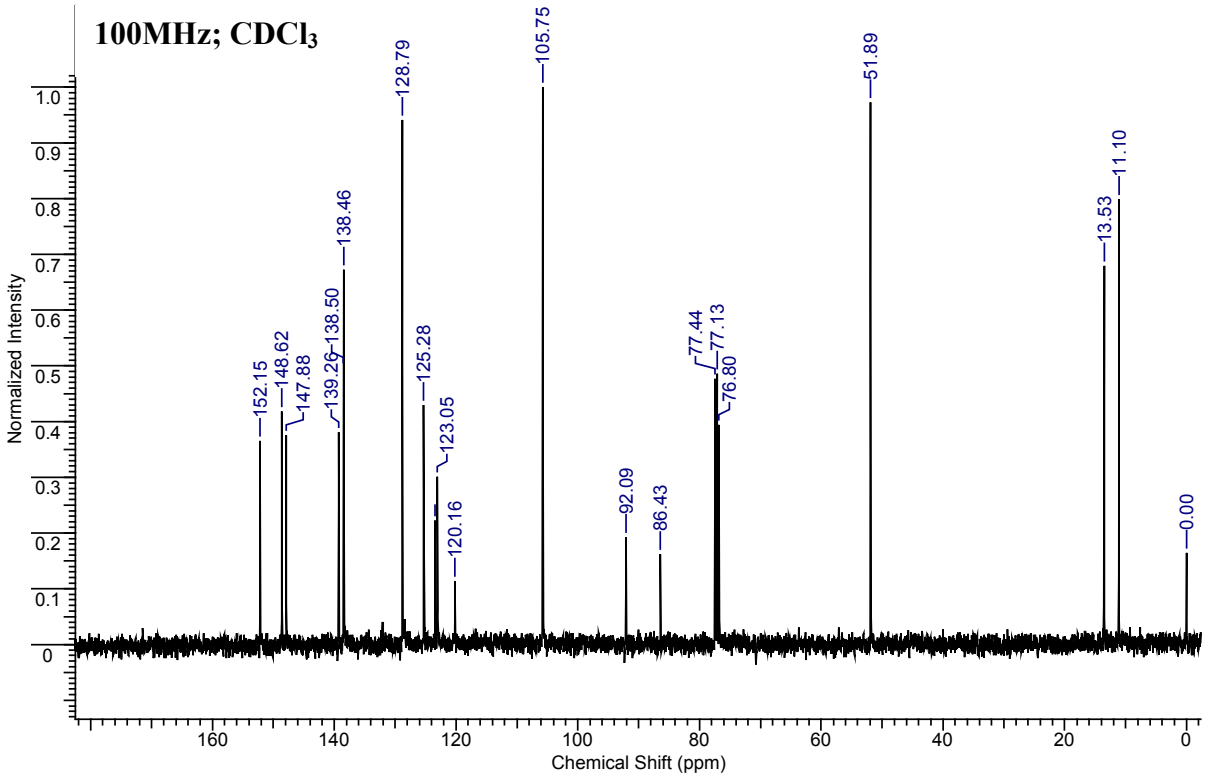

(b)

Figure B.33 (a) ^{1}H NMR and (b) ^{13}C NMR of **33**.

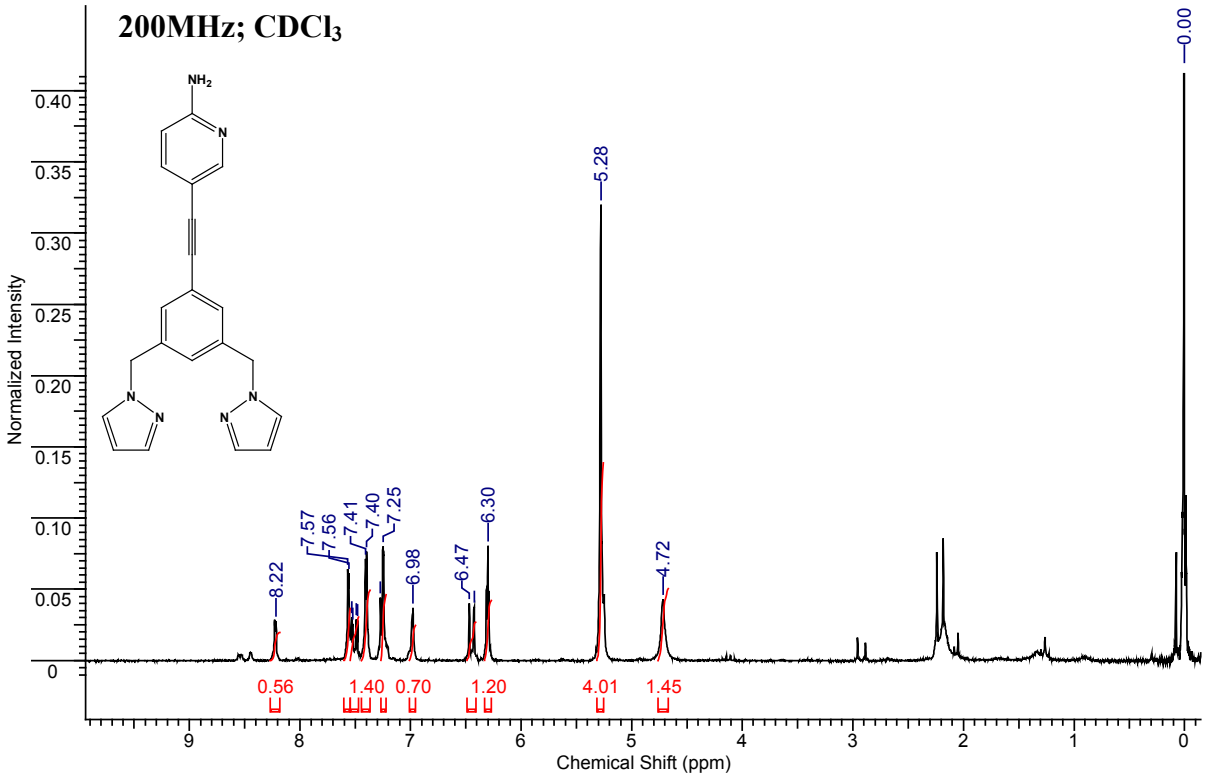

(a)

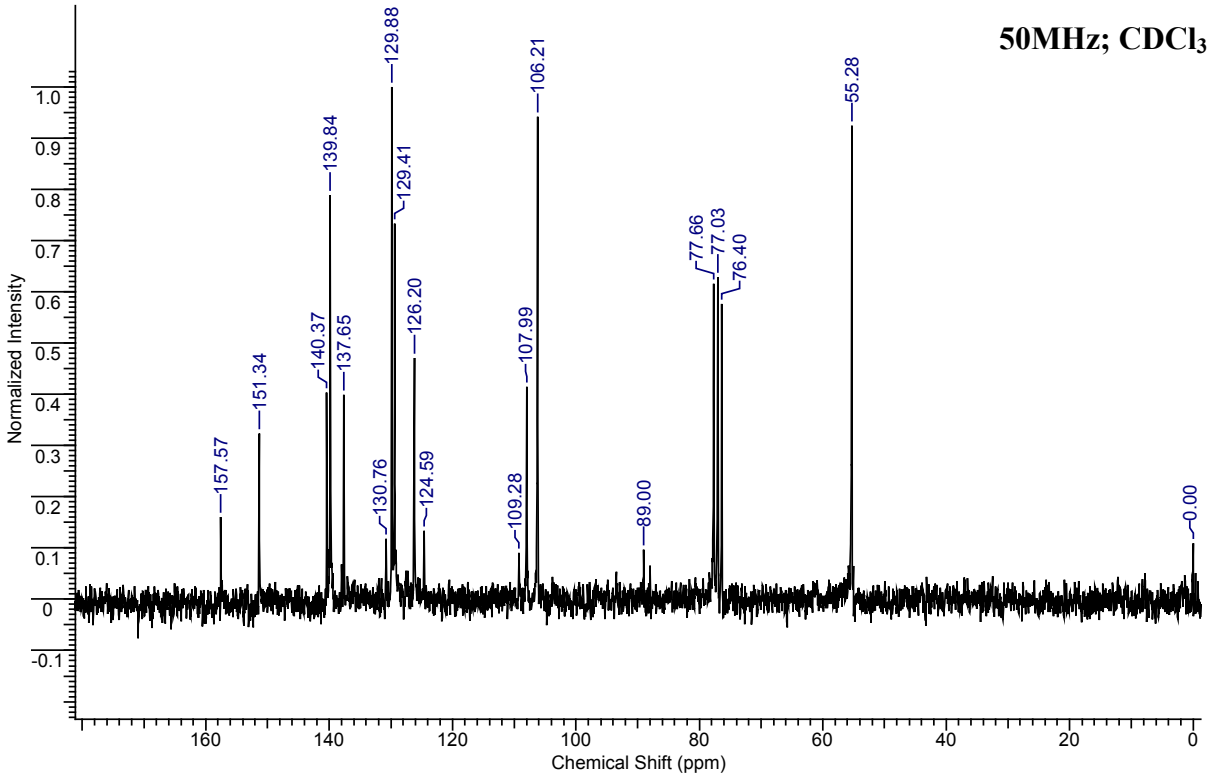

(b)

Figure B.34 (a) ^{1}H NMR and (b) ^{13}C NMR of **34**.

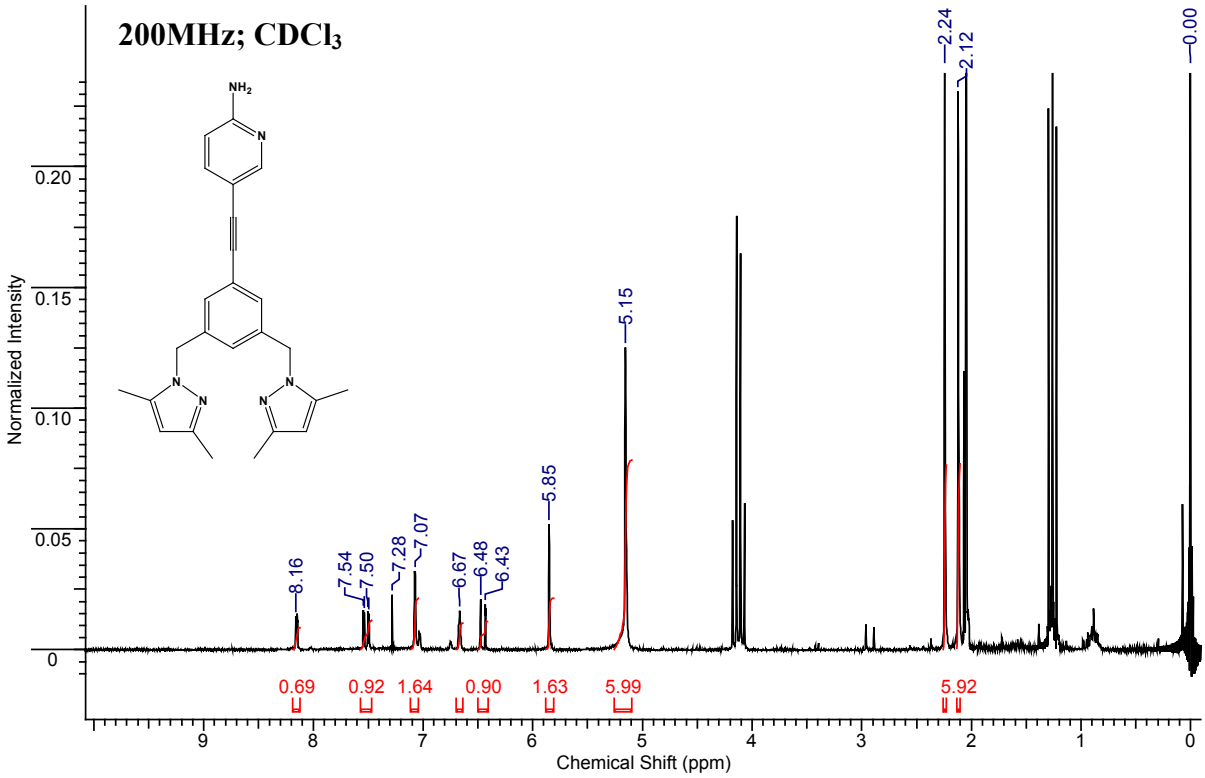

(a)

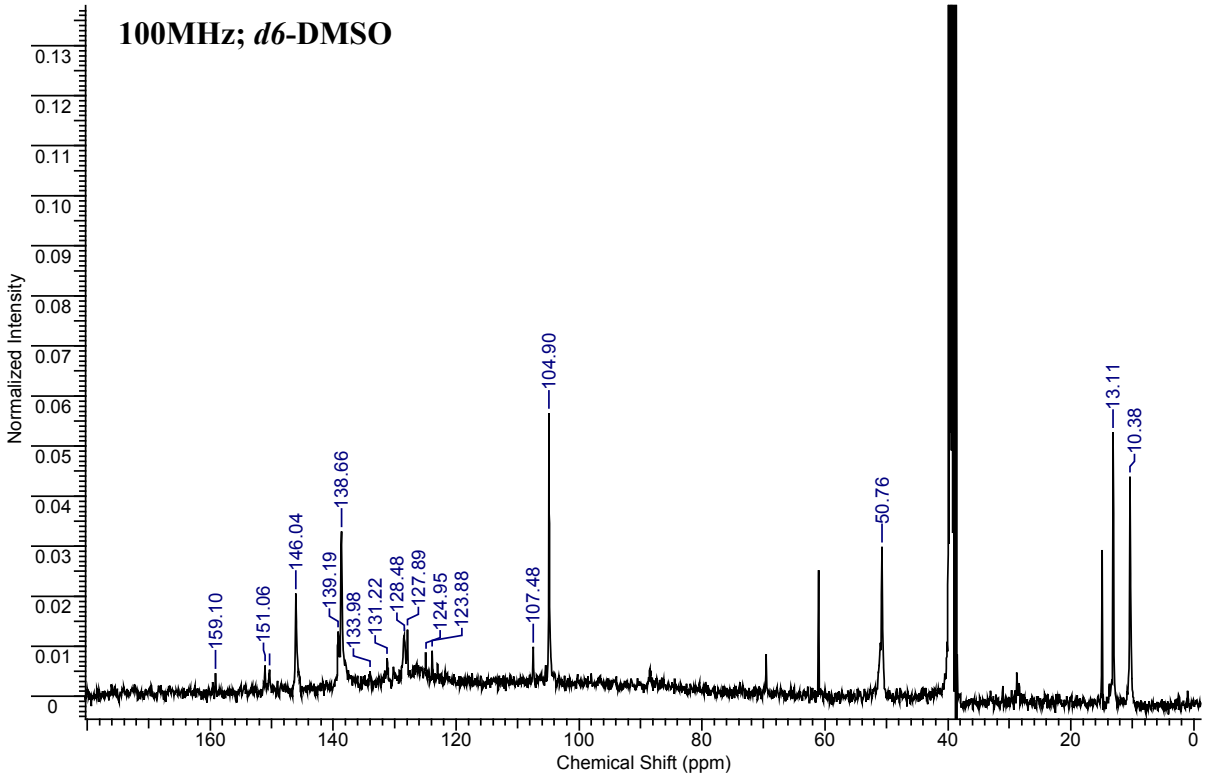

(b)

Figure B.35 ^{1}H NMR of **35**.

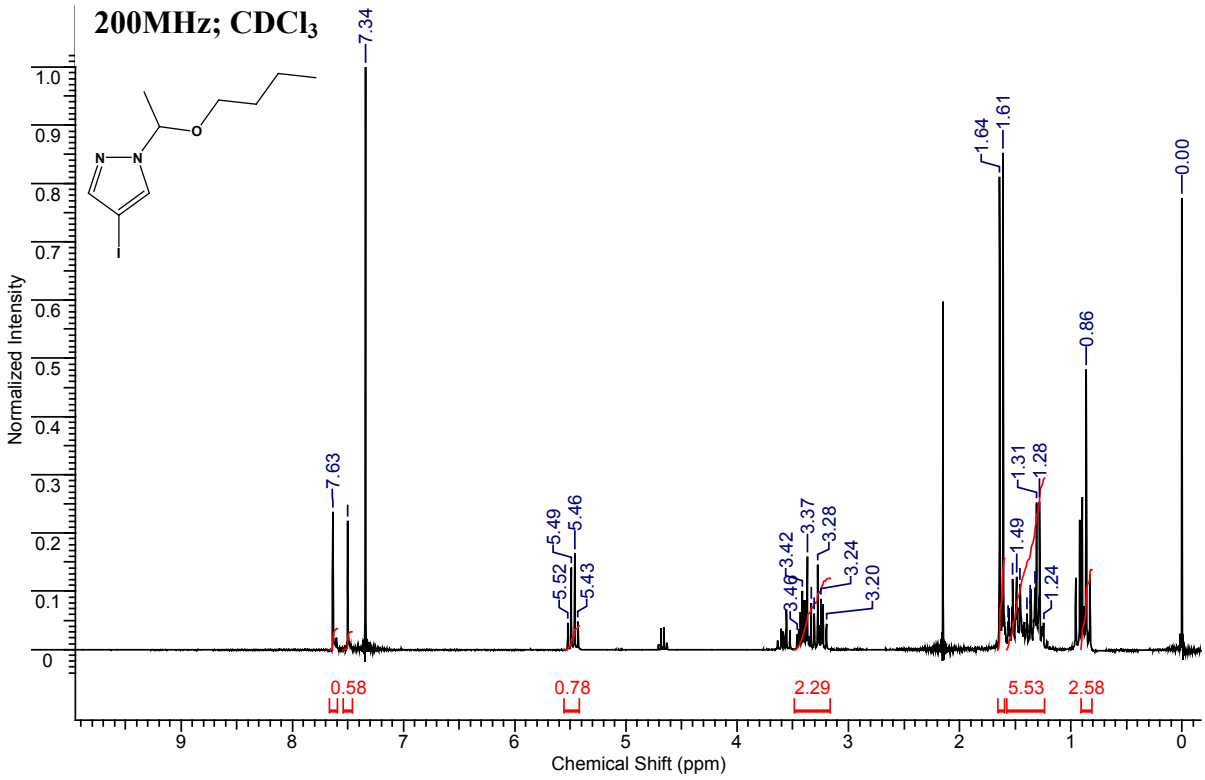

Figure B.36 ^{1}H NMR of **36**.

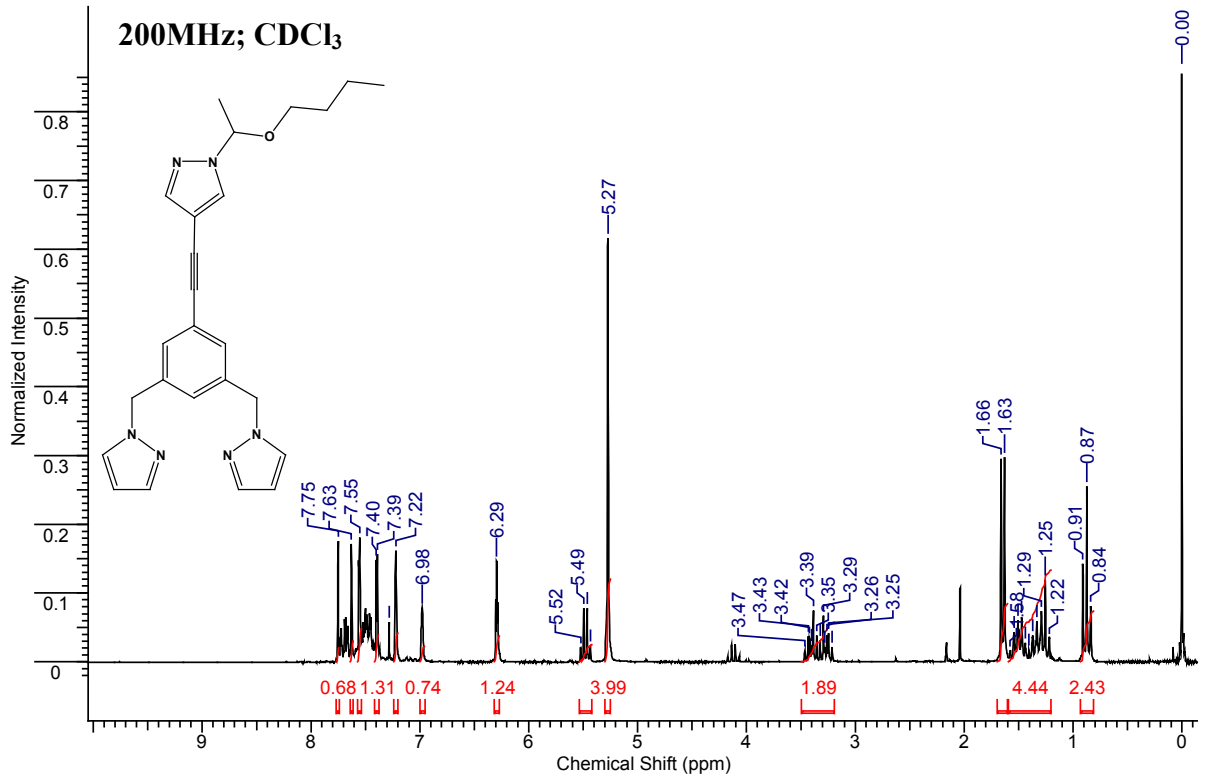

Figure B.37 ^{1}H NMR of **37**.

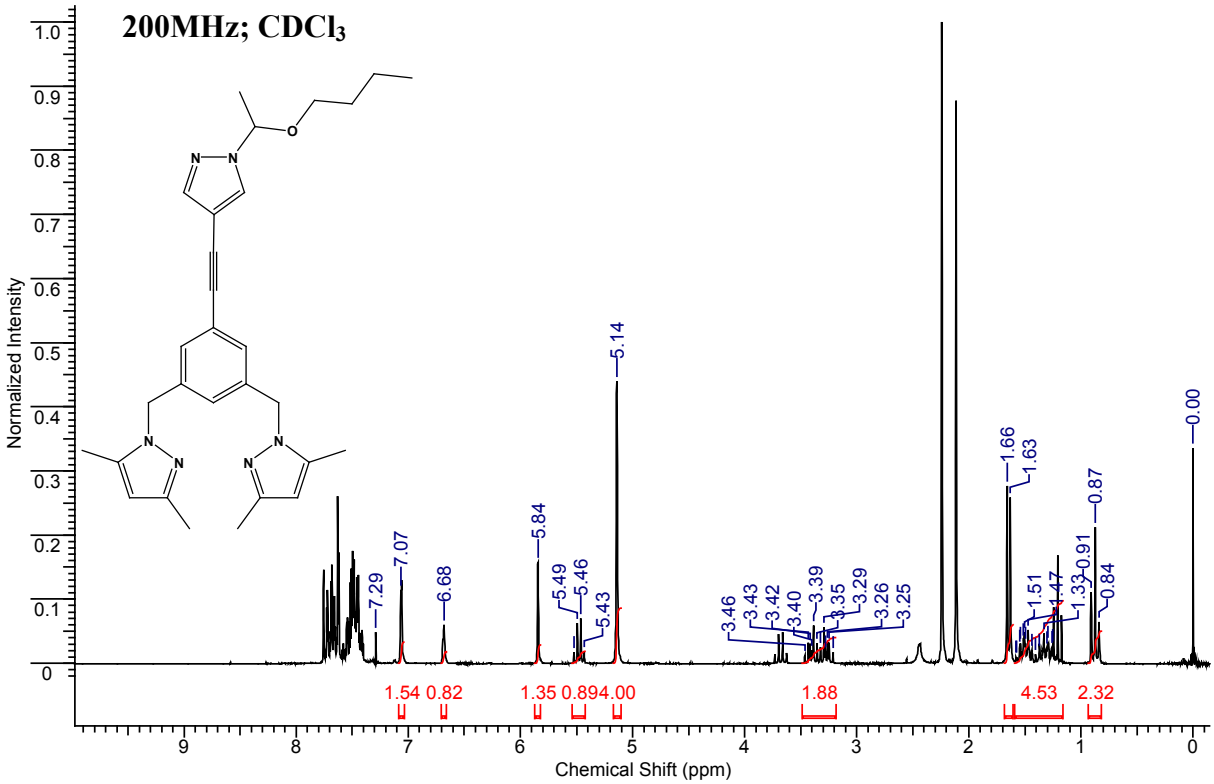

Figure B.38 (a) ^{1}H NMR and (b) ^{13}C NMR of **38**.

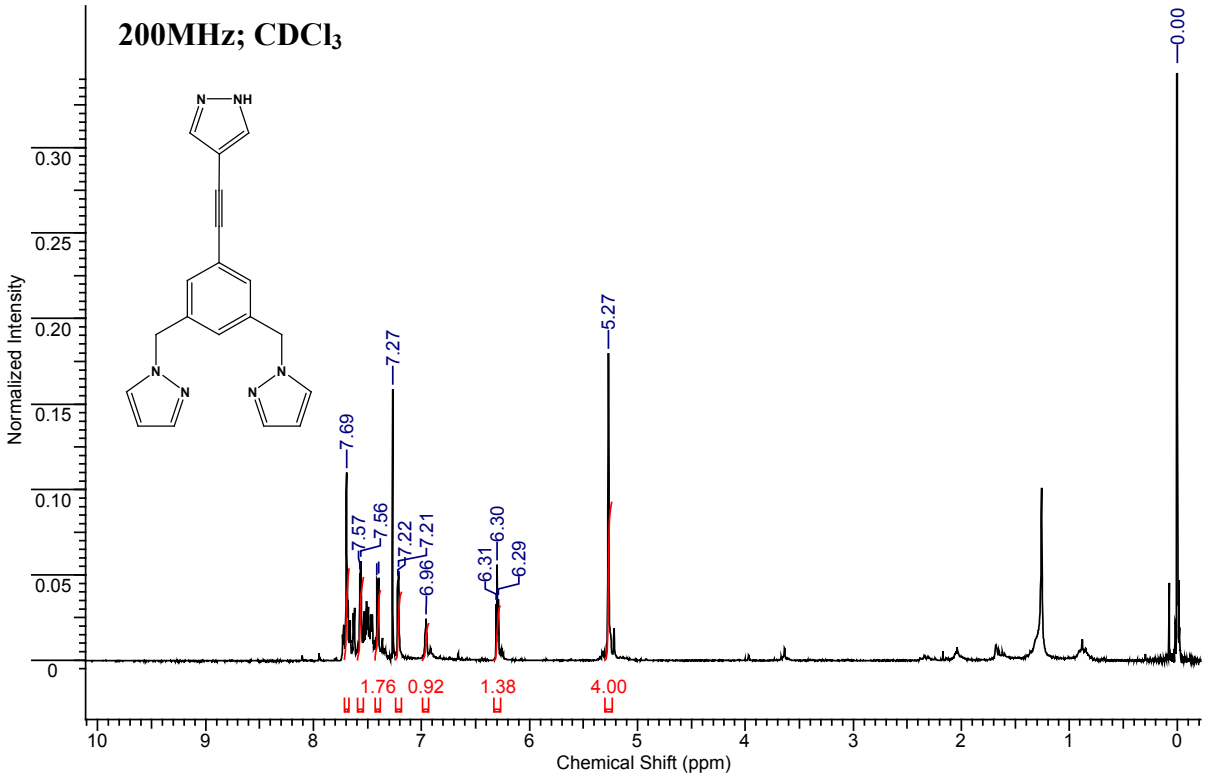

(a)

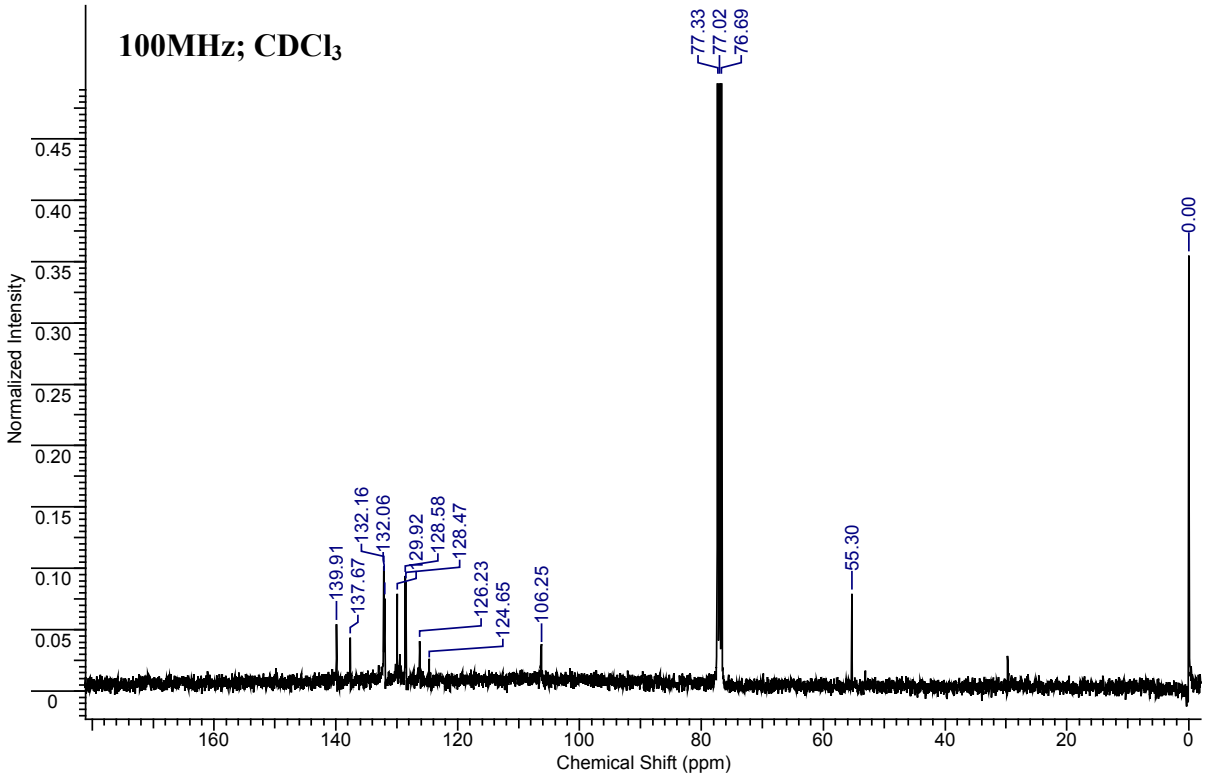

(b)

Figure B.39 (a) ^{1}H NMR and (b) ^{13}C NMR of **39**.

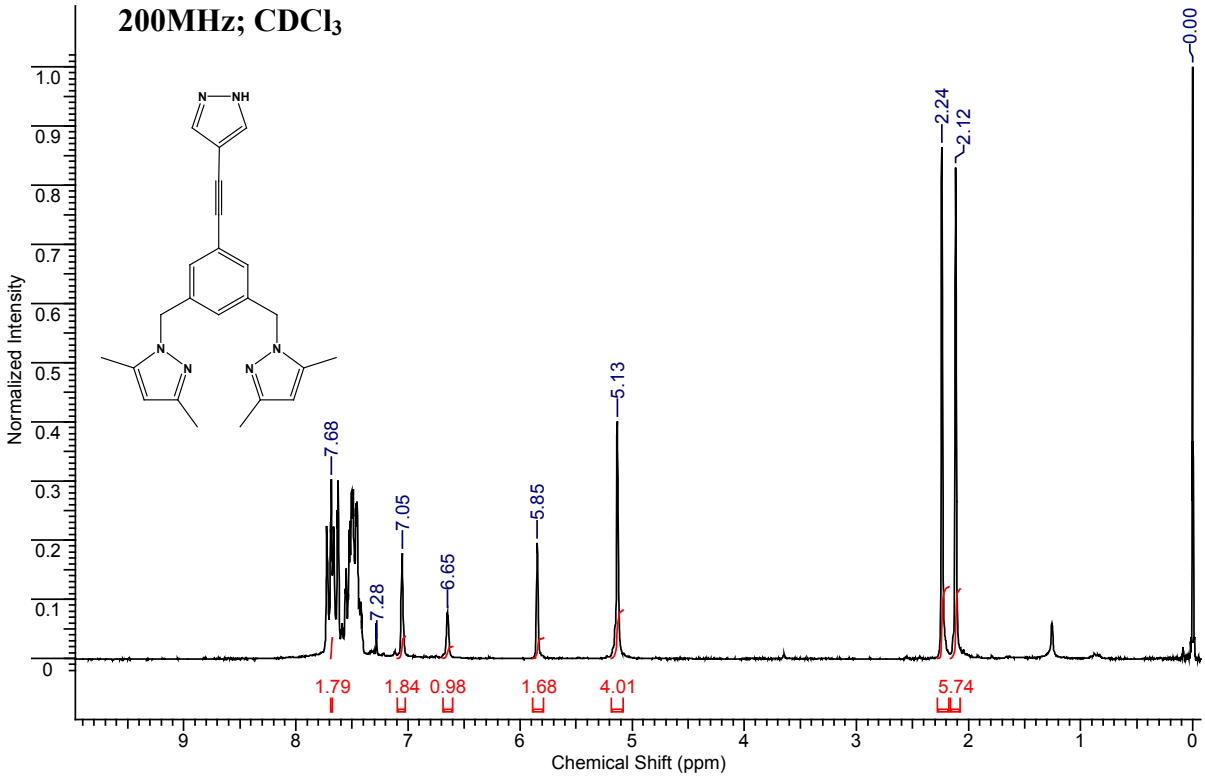

(a)

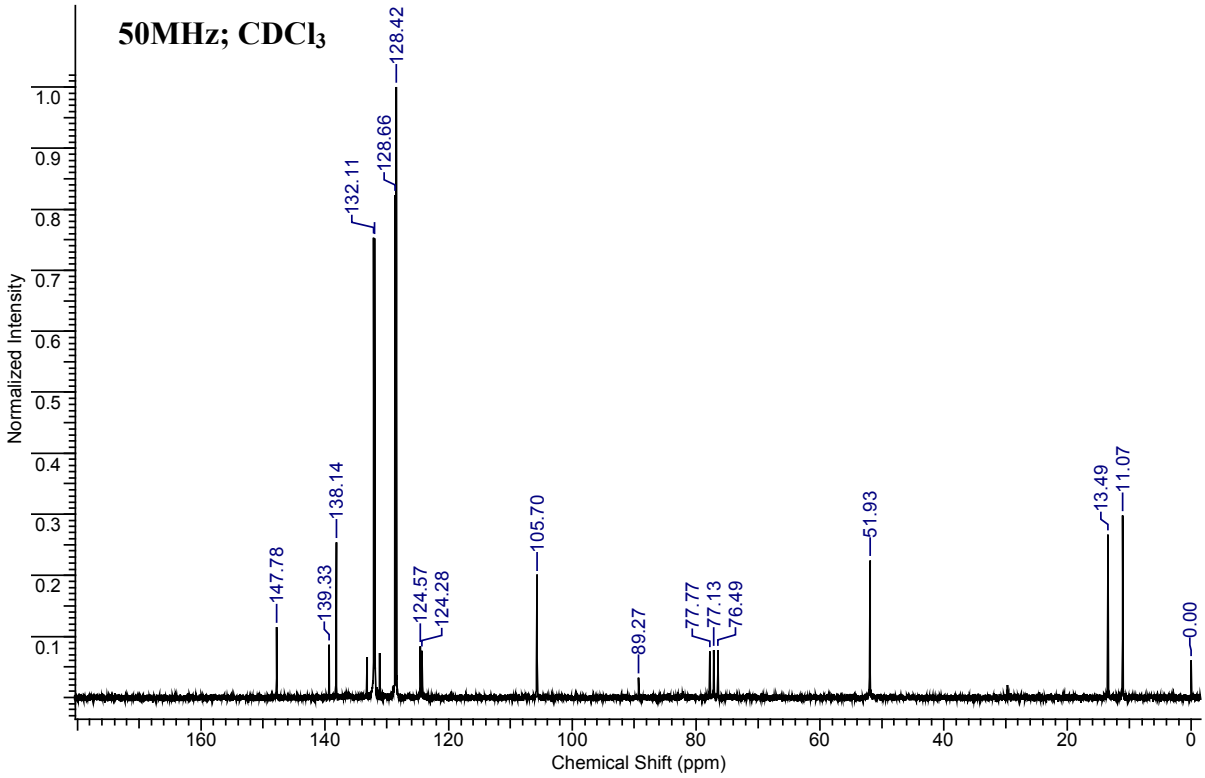

(b)

Figure B.40 ^{1}H NMR of **40**.

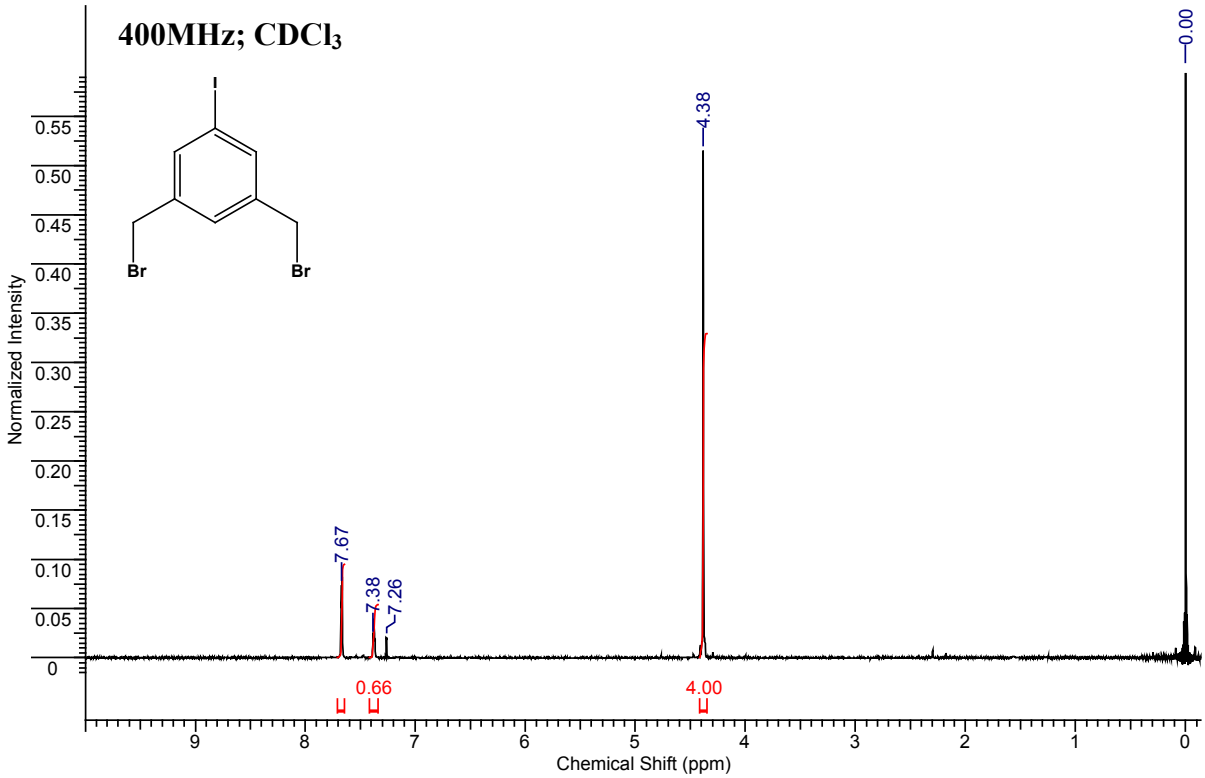

Figure B.41 ^{1}H NMR of **41**.

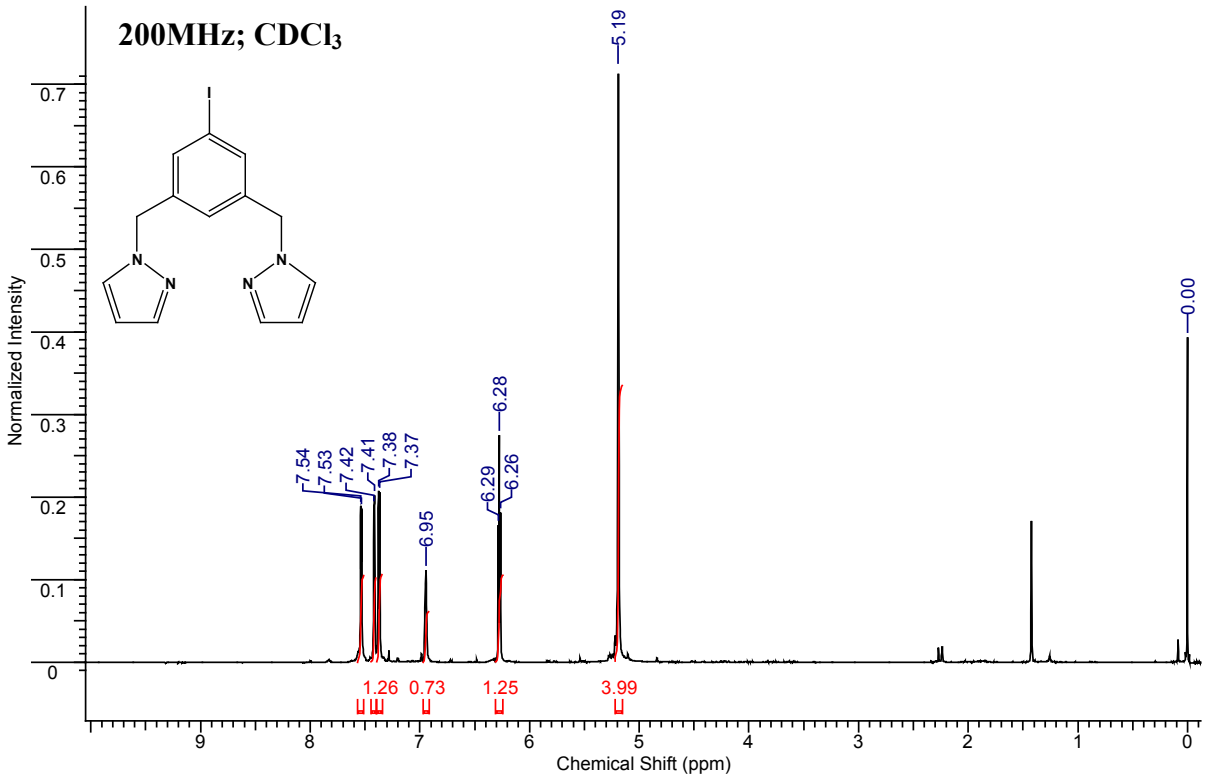

Figure B.42 (a) ^{1}H NMR and (b) ^{13}C NMR of **42**.

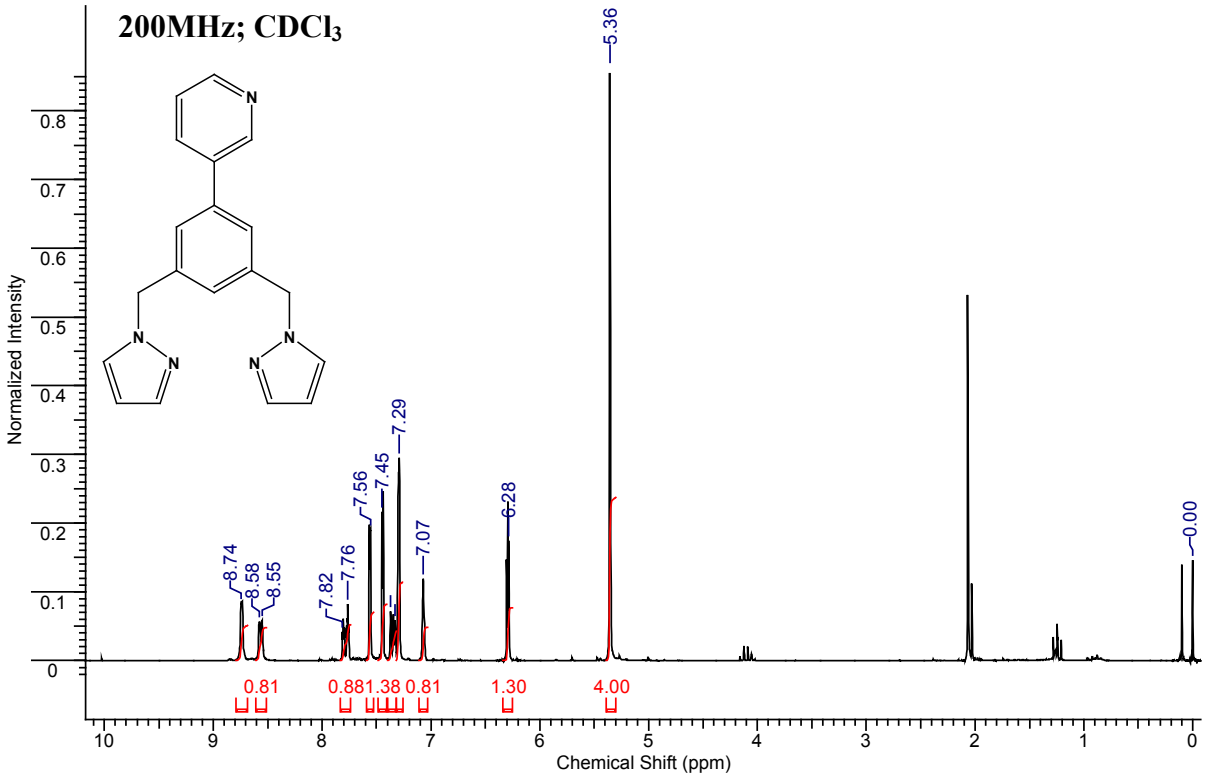

(a)

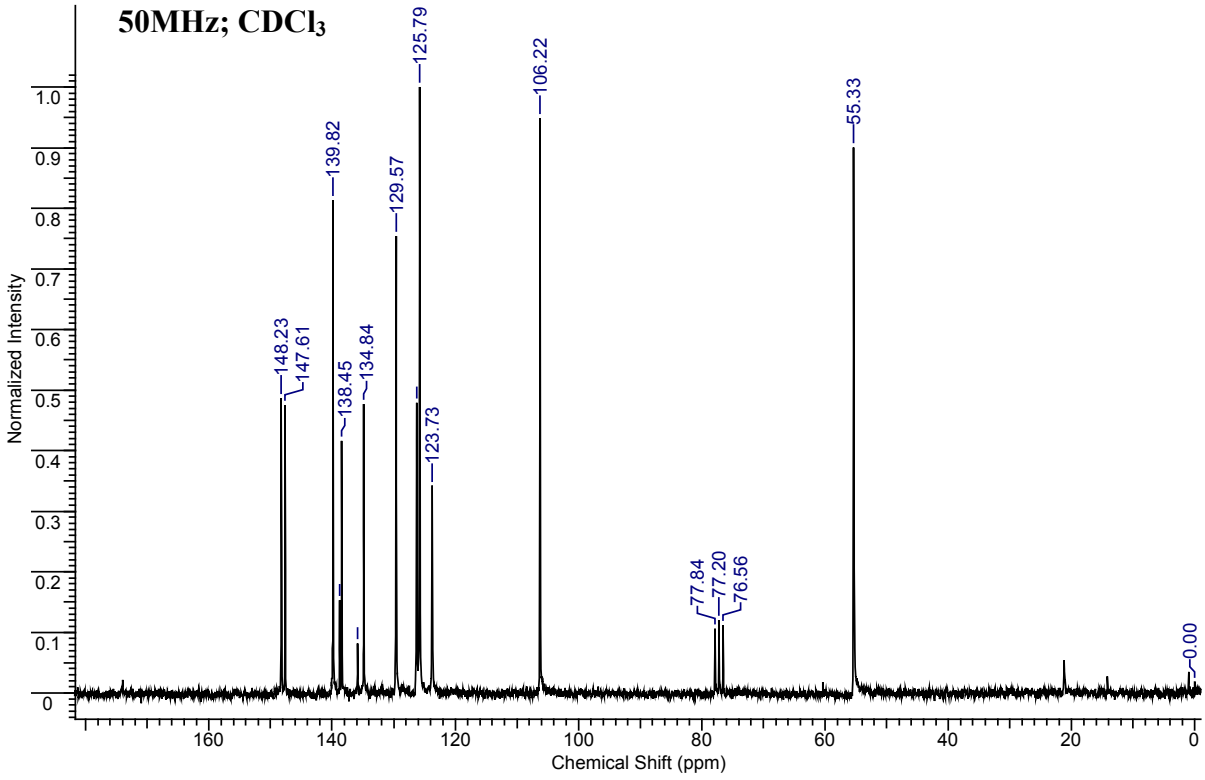

(b)

Figure B.43 ^{1}H NMR of **43**.

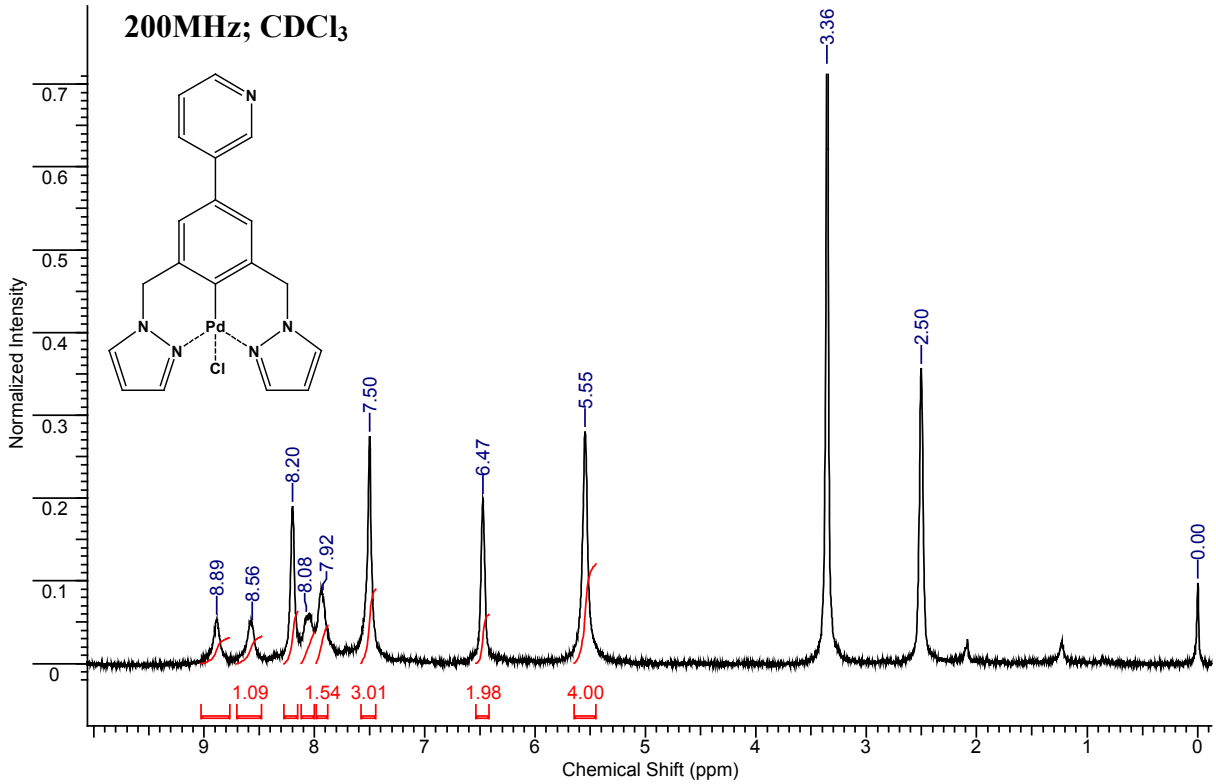

Figure B.44 ^{1}H NMR of **44**.

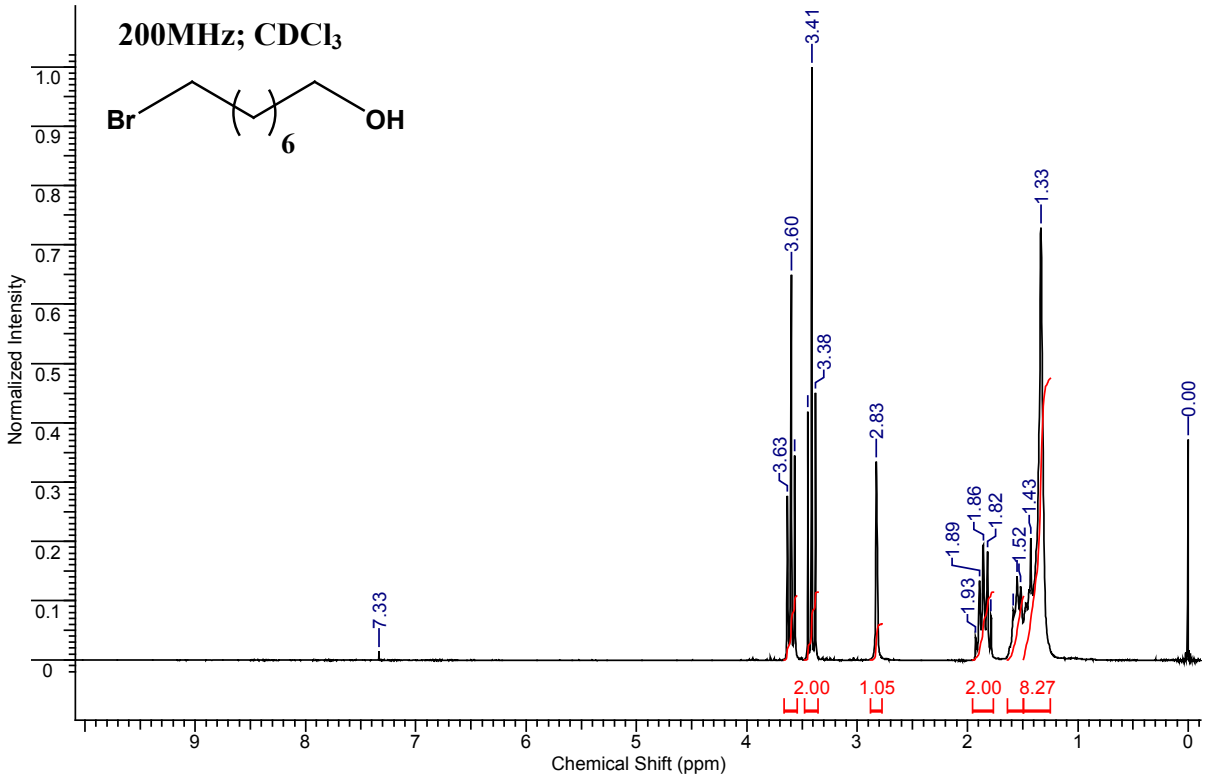

Figure B.45 ^{1}H NMR of **45**.

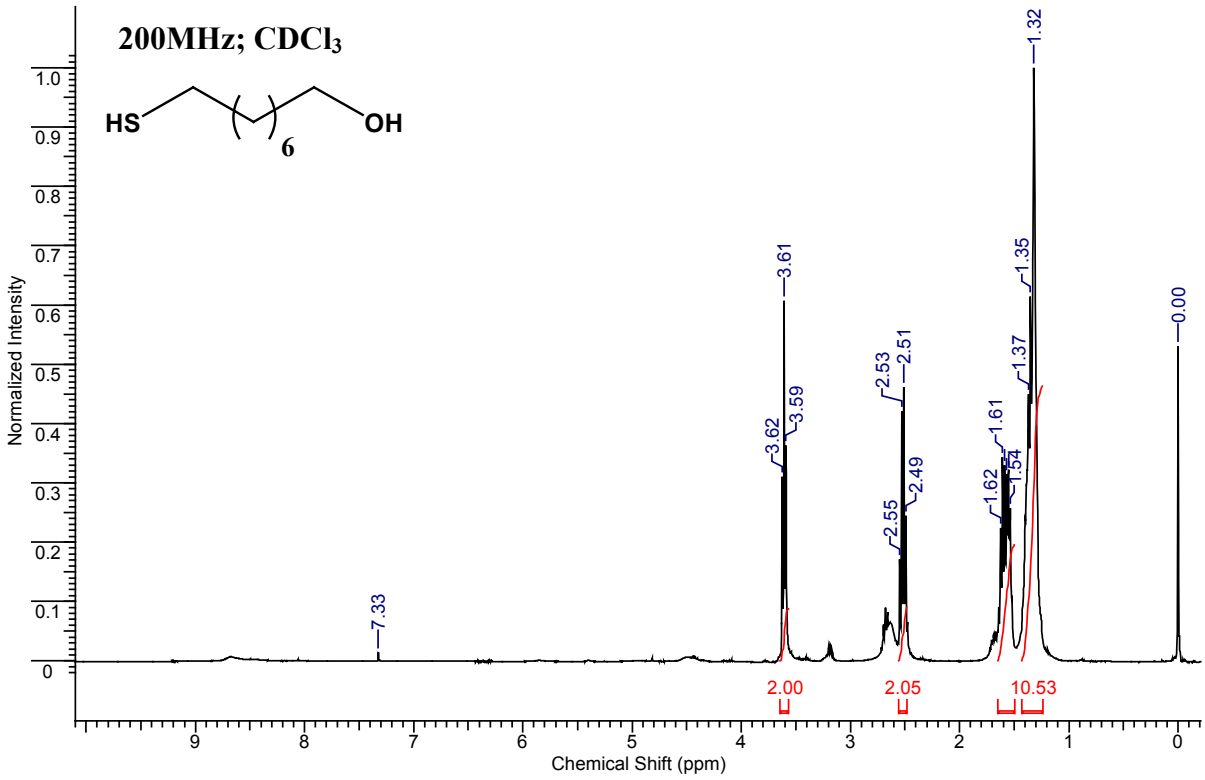

Figure B.46 ^{1}H NMR of **46**.

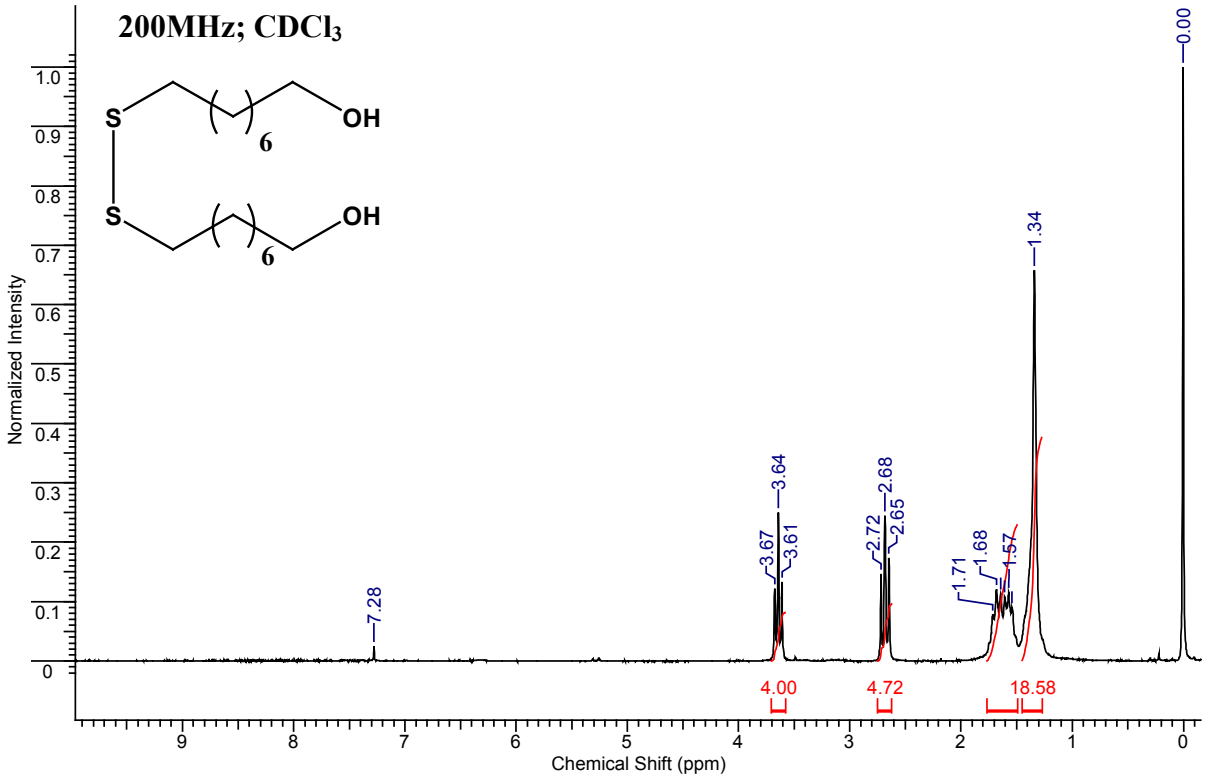

Figure B.47 ^{1}H NMR of **47**.

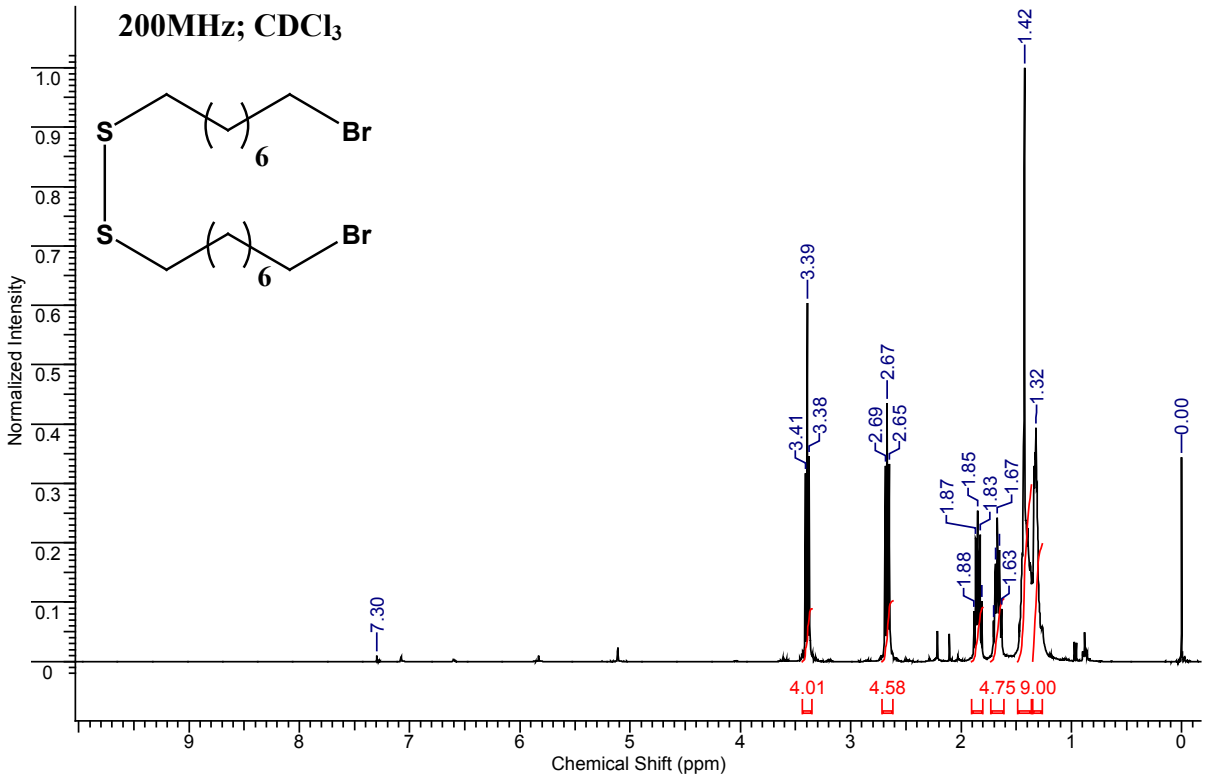

Figure B.48 (a) ^{1}H NMR and (b) ^{13}C NMR of **48**.

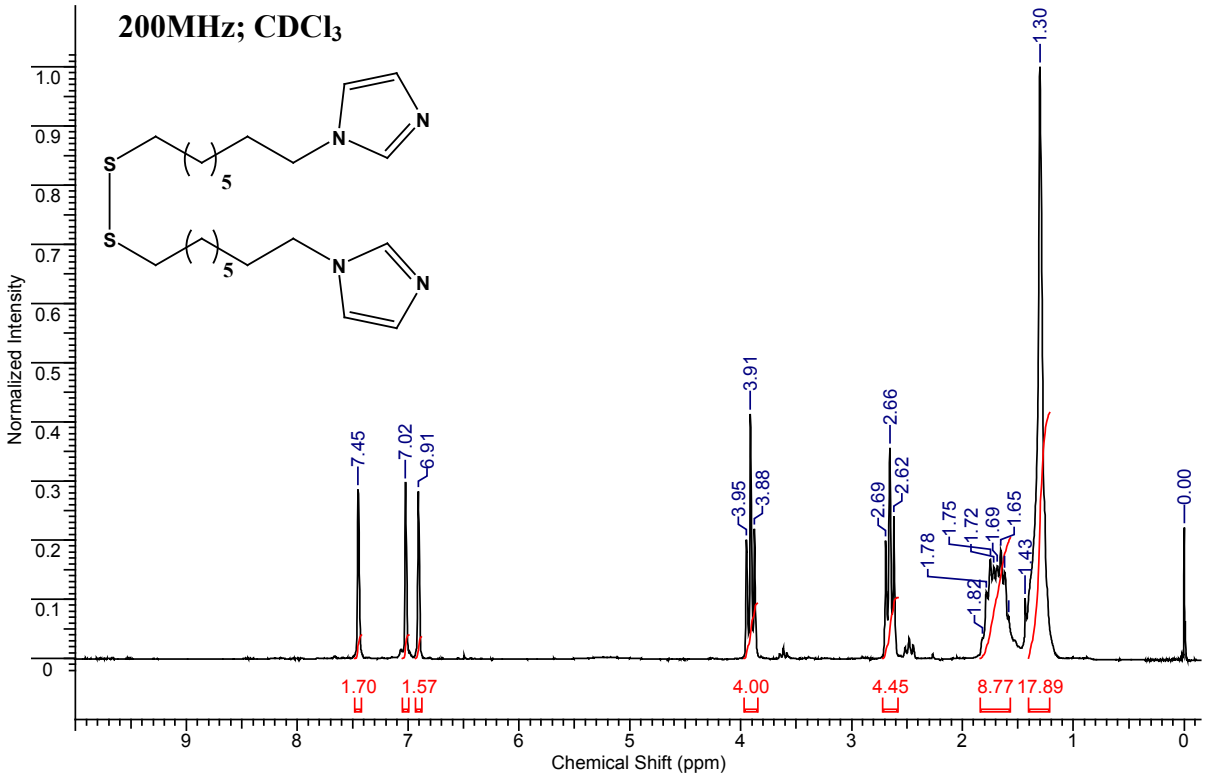

(a)

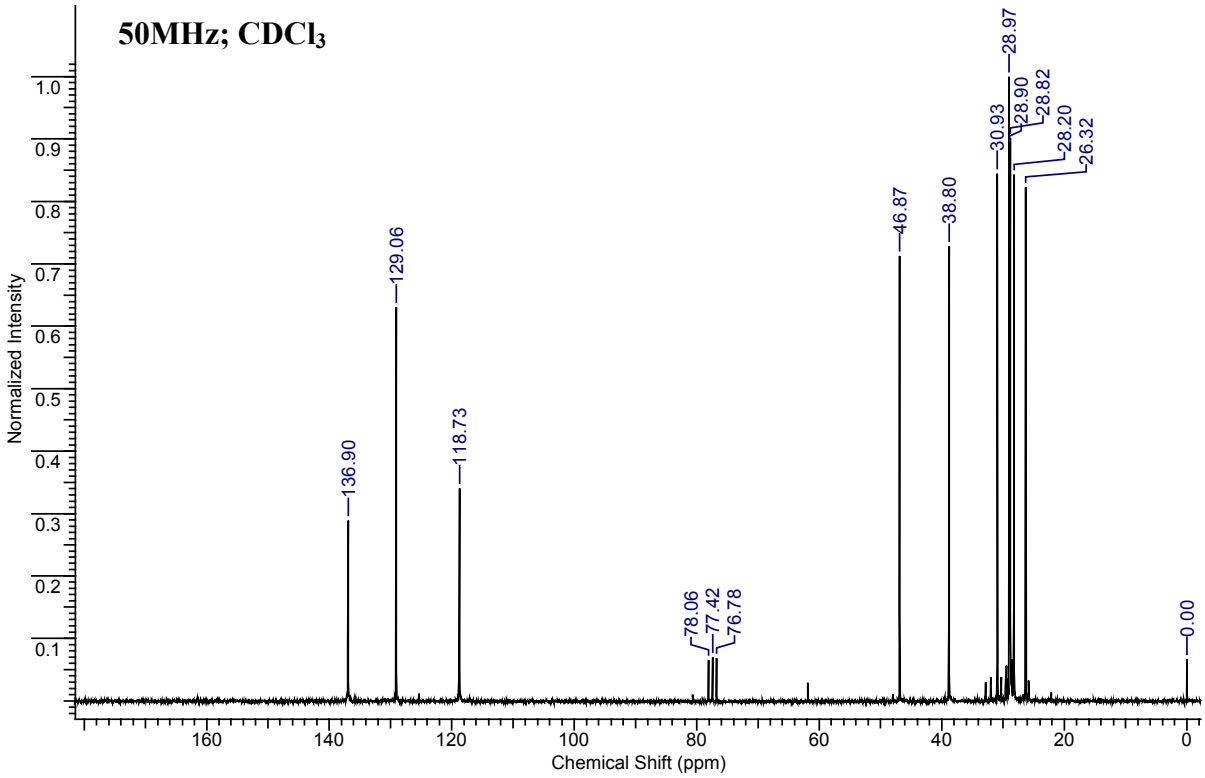

(b)